Advances in Clinical and Experimental Medicine

MONTHLY ISSN 1899-5276 (PRINT) ISSN 2451-2680 (ONLINE) www.advances.umed.wroc.pl

2019, Vol. 28, No. 2 (February)

Impact Factor (IF) – 1.262
Ministry of Science and Higher Education – 15 pts.
Index Copernicus (ICV) – 155.19 pts.

Wroclaw Medical University

Advances
in Clinical and Experimental
Medicine

Advances
in Clinical and Experimental Medicine

ISSN 1899-5276 (PRINT) ISSN 2451-2680 (ONLINE) www.advances.umed.wroc.pl

MONTHLY 2019
Vol. 28, No. 2
(February)

Advances in Clinical and Experimental Medicine is a peer-reviewed open access journal published by Wroclaw Medical University. Its abbreviated title is Adv Clin Exp Med. Journal publishes original papers and reviews encompassing all aspects of medicine, including molecular biology, biochemistry, genetics, biotechnology, and other areas. It is published monthly, one volume per year.

Editorial Office
ul. Marcinkowskiego 2–6
50-368 Wrocław, Poland
Tel.: +48 71 784 12 05
E-mail: redakcja@umed.wroc.pl

Publisher
Wroclaw Medical University
Wybrzeże L. Pasteura 1
50-367 Wrocław, Poland

Online edition is the original version of the journal

Editorial Policy

Advances in Clinical and Experimental Medicine (Adv Clin Exp Med) is an independent multidisciplinary forum for exchange of scientific and clinical information, publishing original research and news encompassing all aspects of medicine, including molecular biology, biochemistry, genetics, biotechnology and other areas. During the review process, the Editorial Board conforms to the "Uniform Requirements for Manuscripts Submitted to Biomedical Journals: Writing and Editing for Biomedical Publication" approved by the International Committee of Medical Journal Editors (www.ICMJE.org/). The journal publishes (in English only) original papers and reviews. Short works considered original, novel and significant are given priority. Experimental studies must include a statement that the experimental protocol and informed consent procedure were in compliance with the Helsinki Convention and were approved by an ethics committee.

For all subscription-related queries please contact our Editorial Office:
redakcja@umed.wroc.pl

For more information visit the journal's website:
www.advances.umed.wroc.pl

Pursuant to the ordinance No. 134/XV R/2017 of the Rector of Wroclaw Medical University (as of December 28, 2017) from January 1, 2018 authors are required to pay a fee amounting to 700 euros for each manuscript accepted for publication in the journal Advances in Clinical and Experimental Medicine.

„Podniesienie poziomu naukowego i poziomu umiędzynarodowienia wydawanych czasopism naukowych oraz upowszechniania informacji o wynikach badań naukowych lub prac rozwojowych – zadanie finansowane w ramach umowy 784/p-DUN/2017 ze środków Ministra Nauki i Szkolnictwa Wyższego przeznaczonych na działalność upowszechniającą naukę".

Indexed in: MEDLINE, Science Citation Index Expanded, Journal Citation Reports/Science Edition, Scopus,
EMBASE/Excerpta Medica, Ulrich's™ International Periodicals Directory, Index Copernicus

Typographic design: Monika Kolęda, Piotr Gil
DTP: Wydawnictwo UMW
Cover: Monika Kolęda
Printing and binding: EXDRUK

Advances
in Clinical and Experimental Medicine

MONTHLY 2019, Vol. 28, No. 2 (February)

ISSN 1899-5276 (PRINT)
ISSN 2451-2680 (ONLINE)
www.advances.umed.wroc.pl

Contents

Original papers

Reviews

Anti-neoplastic effects of aprotinin on human breast cancer cell lines: In vitro study

Saeed Soleyman-Jahi[1–3,A–F], Fatemeh Sadeghi[1,2,B–F], Ziba Afshari[1,A,B,E,F], Tahereh Barati[4,B,E,F], Sevil Ghasemi[1,A,D–F], Samad Muhammadnejad[5,A,C,E,F], Saeid Amanpour[4,A,E,F], Kazem Zendehdel[1,A,C,E,F]

[1] Cancer Research Center, Cancer Institute of Iran, Tehran University of Medical Sciences, Iran
[2] Cancer Immunology Project (CIP), Universal Scientific Education and Research Network (USERN), Tehran, Iran
[3] Division of Gastroentrology, Department of Internal Medicine, Washington University, St. Louis, USA
[4] Cancer Models Research Center, Cancer Institute of Iran, Tehran University of Medical Sciences, Iran
[5] Research Center for Molecular and Cellular Imaging, Tehran University of Medical Sciences, Iran

A – research concept and design; B – collection and/or assembly of data; C – data analysis and interpretation; D – writing the article; E – critical revision of the article; F – final approval of the article

Advances in Clinical and Experimental Medicine, ISSN 1899-5276 (print), ISSN 2451-2680 (online) *Adv Clin Exp Med*. 2019;28(2):151–157

Address for correspondence
Kazem Zendehdel
E-mail: kzendeh@tums.ac.ir

Funding sources
None declared

Conflict of interest
None declared

Acknowledgements
We thank Ms Mahnaz Haddadi for her consults and assistance in laboratory procedures.

Received on August 10, 2017
Reviewed on November 17, 2017
Accepted on April 6, 2018

Published online on November 5, 2018

Cite as
Soleyman-Jahi S, Sadeghi F, Afshari Z, et al. Anti-neoplastic effects of aprotinin on human breast cancer cell lines: In vitro study. *Adv Clin Exp Med*. 2019;28(2):151–157. doi:10.17219/acem/89770

DOI
10.17219/acem/89770

Abstract

Background. Aprotinin is a nonspecific serine protease inhibitor, which can inhibit plasminogen-plasmin system and matrix metalloproteinases. Aprotinin has been investigated as an antitumor agent. However, its antineoplastic effects on breast cancer (BC) have not been investigated yet.

Objectives. The objective of this study was to assess the inhibitory effects of aprotinin on human BC cell lines. We assessed the effects of aprotinin on local invasion and survival of human BC cell lines MDA-MB-231, SK-BR-3 and MCF-7 in vitro.

Material and methods. CHEMICON cell invasion assay kit was used to assess local invasion, and (3-(4,5-dimethylthiazol-2-yl)-2,5-diphenyltetrazolium bromide) tetrazolium reduction (MTT) assay was used to determine the antiproliferative activity of aprotinin. Human dermal fibroblast (HDF-1) cell line was used as control normal cells.

Results. Cancer cell lines showed more invasion characteristics compared to HDF-1. Aprotinin significantly decreased the invasiveness of MDA-MB-231 in concentrations of 1 trypsin inhibitor unit (TIU)/mL, 1.3 TIU/mL and 1.7 TIU/mL in comparison with the untreated group (analysis of variance (ANOVA) $p < 0.001$). Treatment of SK-BR-3 with 1.3 TIU/mL aprotinin caused no significant reduction in invasiveness ($p = 0.06$). Treatment with different concentrations of aprotinin significantly decreased the surviving fraction and inhibited the growth of all cell lines tested in this study (analysis of variance (ANOVA) $p < 0.001$). Compared to cancer cell lines, normal HDF-1 cell line showed less sensitivity to antiproliferative effects of aprotinin, both in low and high doses.

Conclusions. Aprotinin significantly inhibited the growth of human breast cancer cell lines MDA-MB-231, SK-BR-3 and MCF-7, and normal fibroblast cell line HDF-1. The growth inhibitory effect was more dominant in cancer cell lines. Inhibition of local invasion by aprotinin was significant only in the case of MDA-MB-231. Future molecular studies could shed more light on mechanisms underlying antineoplastic effects of aprotinin and its potential therapeutic effects.

Key words: breast cancer, in vitro, cell proliferation, aprotinin, neoplasm invasion

Introduction

Tumor cells proceed along distinct steps to detach from their primary location, metastasize to a distant site and form a metastatic lesion. Invasion through extracellular matrix (ECM), intravasation into circulation, survival in circulation, and extravasation into the distant site are some important steps of this process.[1,2] Metastasizing tumor cells require lytic substances to degrade the matrix and membranes on their way toward the distant site.[3]

Proteolytic enzymes of the plasminogen-plasmin system play a pivotal role in the local invasion and metastasis of cancer cells.[4] Plasminogen activator (PA) is a serine protease which is highly active in many types of primary tumor cells. The 2 main types of PA are the urokinase-type (uPA) and the tissue-type (t-PA). These enzymes activate plasminogen to plasmin, which is a strong proteolytic enzyme capable of digesting proteins of extracellular connective tissue matrix. Expression of uPA, its receptor (uPAR) and its inhibitor (uPAI) are reported to be involved in tumor invasion, tumor cell proliferation, metastasis, and tissue remodeling.[3,4] Plasmin can also indirectly contribute to the spread of tumor cells by activating matrix metalloproteinases (MMPs).[4] Matrix metalloproteinases are a group of endogenous metal ion-dependent proteolytic enzymes that can degrade most ECM components and regulate the activity of enzymes, chemokines and cellular receptors. These inherent properties enable MMPs to affect both the invasion and proliferation of cancer cells.[5]

Many clinical studies have demonstrated that the expression of uPA and uPAR has notable prognostic effects in many types of cancers, such as colon,[6] rectum,[7] stomach,[8] and ovary[9] cancers. There is overwhelming evidence supports of uPA-plasmin system contribution to the invasion and metastasis of breast cancer (BC).[10,11] Similarly, overexpression of MMPs have been associated with poor prognosis in many types of cancers, such as breast,[12] colon,[13] stomach,[14] and ovary cancers. Therefore, blockade of these proteolytic enzyme cascades could be a promising target for cancer therapy.[15]

Aprotinin is a nonspecific serine protease inhibitor. Besides reversible inhibition of kallikrein, uPA and many other serine proteases, aprotinin has antifibrinolytic and anti-inflammatory properties.[16,17] Recent studies have shown that a high dose of aprotinin can suppress the release of proinflammatory cytokines[17] and decrease the capacity of leukocytes to pass through vascular wall.[18] Historically, aprotinin has been used to reduce blood loss and the need for perioperative blood transfusion in many types of major surgeries. However, controversies have recently been raised regarding this indication of aprotinin.[16]

Aprotinin has also been investigated as an antitumor agent. Its capability to inhibit important proteolytic enzymes in the process of cancer invasion and metastasis, such as uPA-plasmin system, suggests notable antitumor potential of aprotinin. However, in vitro and in vivo studies investigating the antitumor activities of aprotinin are limited in number and have reported different results, based on the type of cancer model investigated.[19–21] Despite the significant role of both uPA-plasmin system and MMPs in the progression and prognosis of BC, antitumor effects of aprotinin on this type of cancer have not been investigated. In this in vitro study, we aimed to investigate the effects of aprotinin treatment on human BC cell lines.

Material and methods

Effects of aprotinin treatment on survival and invasion of human BC cell lines MDA-MB-231, MCF-7 and SK-BR-3, and normal human dermal (HDF-1) cell line as control, were investigated in this study.

MTT assay

The antiproliferative activity of aprotinin was assessed by (3-(4,5-dimethylthiazol-2-yl)-2,5-diphenyltetrazolium bromide) (MTT) assay (Sigma-Aldrich, Steinheim, Germany) in accordance with the standard protocol.[22] In brief, all cell lines were seeded into 96-well cell culture plate with different cell densities. The plates were treated with increasing concentrations of aprotinin (0.4, 0.7, 1, 1.3, and 1.5 trypsin inhibitor unit (TIU)/mL) in triplicate for 72 h. Then, aprotinin was removed and the plates were fed daily with a fresh medium for 3 days. After that, the culture medium was replaced by fresh media and 50 µL of MTT (5 mg/mL). After 4 h of incubation, 200 µL of dimethyl sulfoxide (DMSO) and 25 µL of glycine buffer was added to each well, and absorbance was immediately recorded at 570 nm using enzyme-linked immunosorbent assay (ELISA) reader (Stat Fax 3200; Awareness Technology, Palm City, USA).

Invasion assay

To determine the effect of aprotinin on the local invasion of tumor cells, we performed the invasion assay using a 24-well trans-well chamber (CHEMICON Cell Invasion Assay Kit; Merck Millipore, Billerica, USA). In brief, after performing baseline invasion assays of untreated cell lines, MDA-MB-231 cell line was treated with 5 increasing concentrations of aprotinin, from 0.4 TIU/mL to 1.7 TIU/mL. After each treatment, a repeat invasion assay was performed on the corresponding cell culture. Based on the results obtained from MDA-MB-231 cell line treatment, SK-BR-3 BC cell line was treated with 1.3 TIU/mL concentration of aprotinin, followed by a repeat post-treatment invasion assay. The invasion capabilities of treated cells in duplicate wells were compared with duplicate control untreated wells. The HDF-1 normal fibroblast cell line was considered as a negative control in all procedures. We used invert microscopy for a qualitative assessment

of the invasion process and obtained photographic images of invading cells at the bottom of each invasion well. The optical absorbance of each test was measured by an ELISA reader at 570 nm wavelength.

Statistical analysis

We used mean post-treatment survival fractions given by MTT assay as a measure of survival, and mean optical densities after invasion assay as a measure of local invasion. Analysis of variance (ANOVA) test was used to compare the mean values among different cell lines. Paired t-test or repeated measure ANOVA were used to compare mean values of the same group across different concentrations of treatment when 2 or more than 2 concentrations were used, respectively. Linear regression analysis was used to investigate the correlation between aprotinin dose and response parameters. A p-value <0.05 was considered statistically significant. The statistical analyses were conducted using SPSS for Windows v. 22.0 software (IBM Corp., Armonk, USA) and GraphPad Prism v. 7 (GraphPad Software, La Jolla, USA).

Results

MTT assay

Treatment with different concentrations of aprotinin significantly decreased the surviving fraction and inhibited the growth of both normal and BC cell lines ($p < 0.001$) tested in this study (Table 1). Higher doses of aprotinin treatment were associated with a correspondingly further drop in the percentage of survival fraction (Fig. 1).

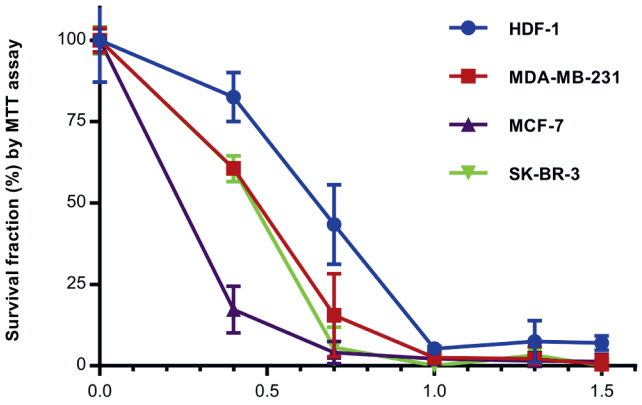

Fig. 1. Growth inhibitory effects of aprotinin on normal fibroblast and breast cancer (BC) cell lines. The figure illustrates the survival fraction of study cell lines when treated by different doses of aprotinin. By increasing the dose of aprotinin, the survival fraction decreased in both normal human fibroblast cell line (HDF-1) and human BC cell lines (MDA-MB-231, MCF-7 and SK-BR-3). The HDF-1 cell line showed significantly less sensitivity to growth inhibitory effects of aprotinin, compared to cancer cell lines

The majority of growth inhibitory effects was achieved by the application of 1 TIU/mL of aprotinin. Compared to tumor cell lines, normal fibroblast cell line HDF-1 showed less sensitivity to growth inhibitory effects of aprotinin at 0.4 TIU/mL ($p < 0.001$), 0.7 TIU/mL ($p = 0.003$) and 1.5 TIU/mL ($p = 0.02$) concentrations of aprotinin. Compared to other BC cell lines, MCF-7 cell line showed higher sensitivity to growth inhibitory effects of aprotinin at a concentration of 0.4 TIU/mL ($p < 0.001$).

Invasion assay

As expected, cancer cell lines demonstrated significantly higher degrees ($p < 0.05$) of invasion compared

Table 1. Assessment of cell growth by MTT assay for normal and human breast cancer (BC) cell lines treated with different concentrations of aprotinin

Aprotinin concentration [TIU]	Mean/SD	Survival fraction [%]				p-value
		HDF-1	MDA-MB-231	MCF-7	SK-BR-3	
0	mean	100	100	100	100	>0.99
	SD	12.88	3.78	3.57	4.19	
0.4	mean	82.56	60.60	17.32	60.58	<0.001
	SD	7.56	1.47	7.18	4.02	
0.7	mean	43.37	15.57	4.10	5.60	0.003
	SD	12.25	12.75	3.39	6.28	
1	mean	5.30	2.49	2.11	0	0.31
	SD	2.00	3.33	3.92	3.35	
1.3	mean	7.45	2.19	1.52	3.25	0.42
	SD	6.45	3.77	2.71	4.22	
1.5	mean	6.98	0.51	1.36	0	0.02
	SD	2.20	2.92	2.31	1.12	
p-value		<0.001	<0.001	<0.001	<0.001	–

HDF-1 – human normal dermal fibroblast cell line; MDAMB-231, MCF-7 and SK-BR-3 – human breast cancer cell lines; TIU – trypsin inhibiting unit; SD – standard deviation.

to HDF-1 normal cell line as a negative control (Table 2). Compared to untreated MDA-MB-231 cells, treatment of these BC cells with 1 TIU/mL (p = 0.01), 1.3 TIU/mL (p = 0.01) or 1.7 TIU/mL (p = 0.005), concentrations of aprotinin significantly decreased the degree of invasion (Table 2, Fig. 2,3).

Treatment of SK-BR-3 cells with 1.3 TIU/mL dose of aprotinin reduced the mean values of optical absorbance obtained for invasion solution (Fig. 4); however, the reduction was not statistically significant (p = 0.06).

Table 2. Quantitative results of invasion by measuring optical absorbance of solutions prepared form invasion kit wells

Cell line	Optical density				p-value
	experiment 1	experiment 2	mean	SD	
HDF					
untreated	0.63	0.53	0.58	0.07	–
SK-BR3					0.06
untreated	1.82	1.86	1.84	0.03	
treated (1.3 TIU)	1.52	1.66	1.59	0.09	
MDA-MB 231					
untreated	1.91	1.96	1.93	0.03	–
treated					
0.4 TIU	1.87	1.93	1.90	0.04	0.99
0.7 TIU	1.78	1.88	1.83	0.07	0.69
1 TIU	1.48	1.62	1.55*	0.10	0.01
1.3 TIU	1.52	1.64	1.58*	0.08	0.01
1.7 TIU	1.46	1.54	1.50*	0.06	0.005

HDF – human dermal fibroblast; SD – standard deviation; TIU – trypsin inhibiting unit; NS – not significant; * p-value <0.05 for post-hoc comparisons of corresponding group with untreated group.

Discussion

In this study, we found that aprotinin could significantly inhibit the local invasion of human BC cell line MDA-MB-231, an aggressive type of breast adenocarcinoma, in a concentration-dependent manner. In contrast, it showed a nonsignificant trend of inhibitory effect on local invasion of less aggressive type of BC cell line, SK-BR-3. In addition, aprotinin significantly decreased the survival fraction and inhibited the growth of normal human fibroblast cell line, HDF-1, and human BC cell lines MCF-7, MDA-MB-231 and SK-BR-3. However, normal fibroblast cells were less sensitive to growth-inhibitory effects of aprotinin compared to tumor cells.

A number of in vitro and in vivo studies have investigated the effects of aprotinin treatment on the local invasion of human cancer. In vitro studies reported that aprotinin could substantially reduce the local invasion of prostate cancer through a different mechanism. In a study conducted by Gao et al., aprotinin decreased the invasion of DU145 human prostate cancer cell line through the inhibition of tissue kallikrein.[20] Tissue kallikreins are a subgroup of serine proteases that can promote cancer cell migration and invasion. Likewise, Bekes et al. demonstrated that the administration of aprotinin can have antitumor effects by reducing the local invasion and distant metastasis of PChi/diss, which is a highly metastatic type of PC-3 human prostate carcinoma cell line.[19] They reported a different mechanism for this observation. In their experiments, aprotinin attenuated tumor cell line invasion via inhibition of plasmin,[19] which is an activator of pro-urokinase-type plasminogen activator (pro-uPA). Pro-uPA is a serine protease pro-enzyme that, after converting to its activated form, uPA, contributes to the degradation of extracellular matrix and possibly tumor cell migration and proliferation. Similarly, in this study, we observed that aprotinin decreased the local invasion of MDA-MB-231 human BC cell line when used in concentrations of 1 TIU/mL or higher. To date, this is the first experiment that investigates the inhibitory effects of aprotinin on human BC invasion.

It is postulated that anti-invasion effects of aprotinin on MDA-MB-231 BC cell line could be mediated by the inhibition of uPAR/uPA pathway. Previous studies have

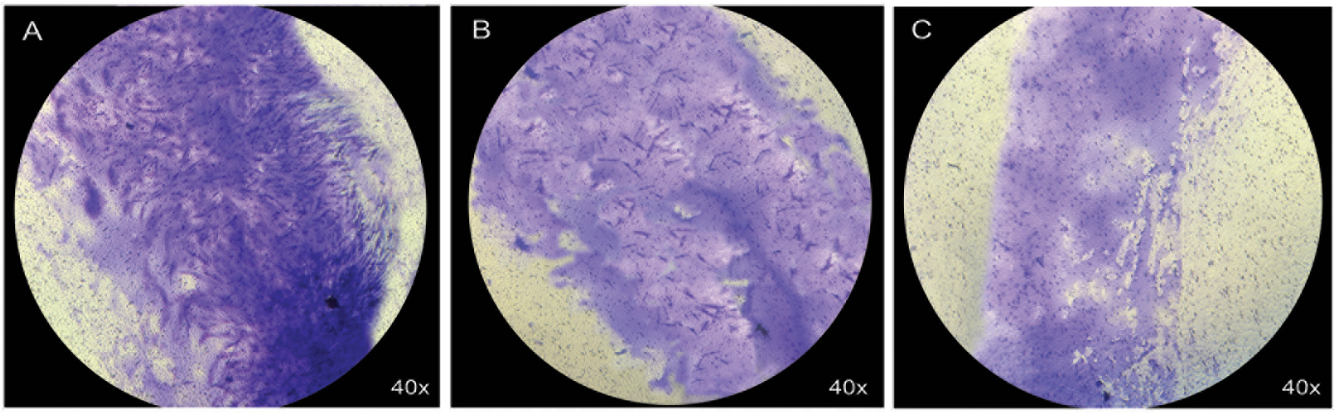

Fig. 2. Inhibitory effects of aprotinin on local invasion of MDA-MB-231 cell line. These series of images taken using invert microscope illustrate effects of treatment with increasing doses of aprotinin on local invasion of MDA-MB-231 human breast cancer (BC) cell line. Compared to untreated cells (A), treatment with 1.0 (B) and 1.5 (C) TIU/mL of aprotinin resulted in significantly (p < 0.001) more profound inhibition of local invasion in a step-wise manner. The magnification scale is ×40

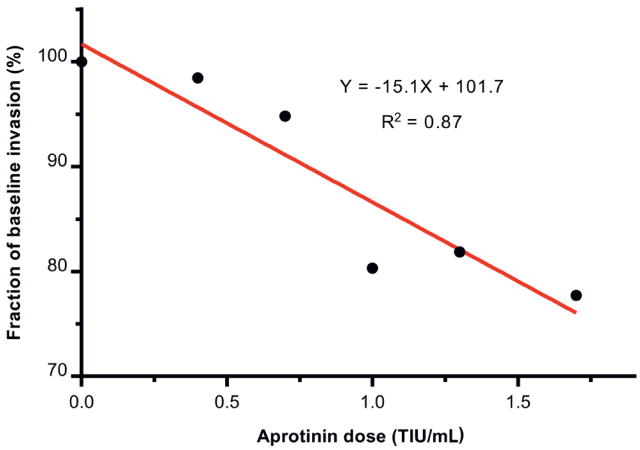

Fig. 3. Linear regression analysis of aprotinin dosage vs inhibition of local invasion in MDA-MB-231 cell line. Each circular dot in this scatterplot corresponds to fraction of base-line (in untreated cells) local invasion detected in MDA-MB-231 cell lines treated with increasing dose of aprotinin. The trend-line and linear regression equation generated imply significant (slope = –15.1, p = 0.007) and robust (R^2 = 0.87) inverse association between dose of aprotinin used and fraction of baseline local invasion observed. Each 1 TIU/mL increments in dose of aprotinin resulted in almost 15% inhibition of local invasion

demonstrated that uPAR/uPA pathway is overexpressed endogenously in MDA-MB-231 cell line.[23] Breast cancer cells that express higher amounts of uPA have a greater proteolytic capacity at the cell surface–ECM interface, which gives them higher invasion potentials. Aprotinin can both reduce cell-surface binding to plasminogen and prevent the conversion of pro-uPA to the active uPA form.[24] Therefore, it could be expected that aprotinin can attenuate invasive potentials of MDA-MB-231 cell line.

On the other hand, studies have demonstrated no inhibitory effects of aprotinin on melanoma[25] and thyroid cancers.[26] Prange et al. found that aprotinin had no anti-invasive effect on Melanom-5 and Melanom-57/12 cell lines.[25] Likewise, aprotinin, even in high doses, had no effect on EGF-stimulated invasion of thyroid cancer.[26] The authors proved that serine proteases, such as plasmin, had less prominent effects in cancer models used in their study.

We observed the antiproliferative effects of aprotinin on both normal and tumor cell lines. Normal human fibroblast cell line HDF-1 demonstrated less sensitivity to growth-inhibitory effects of both lower and higher doses of aprotinin, compared to tumor cell lines. Among 3 human BC cell lines investigated, MCF-7 showed slightly higher sensitivity to antiproliferative effects of low-dose aprotinin. Similar antiproliferative effects of aprotinin were seen on 3-methyl cholanthrene-induced squamous cell carcinoma in a murine model; mice treated with aprotinin had significantly smaller tumors and longer survival compared with control.[27] Furthermore, aprotinin treatment could inhibit tumor growth in Lewis lung carcinoma, Hepatoma-22 cell[28] and Walker-0256 carcinosarcoma[29] model systems in mice. Therefore, the majority of current literature indicates antiproliferative effects of aprotinin on both normal and tumor cell lines, with varying degrees.

To date, few studies have reported the inhibitory effects of aprotinin on both the survival and local invasion of cancer. As seen in our study, Latner et al. showed that aprotinin treatment reduced both tumor growth and invasion when administered to hamsters bearing a highly invasive fibrosarcoma, or to mice bearing a similar malignant mammary carcinoma. Aprotinin also increased tumor necrosis.[30] The authors attributed this effect to the enhancement of the host's immunological system by aprotinin against the tumor cells.[30] In addition to this mechanism, the antiproliferative role of aprotinin could be mediated by its downstream inhibitory effects on MMPs, in a similar way to mechanism underlying its anti-invasive role. Matrix metalloproteinases generally increase cell proliferation by modulating cell surface receptors as well as extracellular cytokines and apoptotic ligands.[5] Therefore, the inhibition of MMPs by aprotinin could expectedly alter cellular proliferation. Finally, the inhibitory effect of aprotinin on the local invasion could occur, at least in part, due to its inhibitory effects on survival. However, distinct independent mechanisms should coexist for anti-invasive effects. It is inferred from our observation that despite similar inhibitory effects of aprotinin on the survival of MDA-MB-231 and SK-BR-3 cell lines, the inhibition of the local invasion was more dominant in MDA-MB-231.

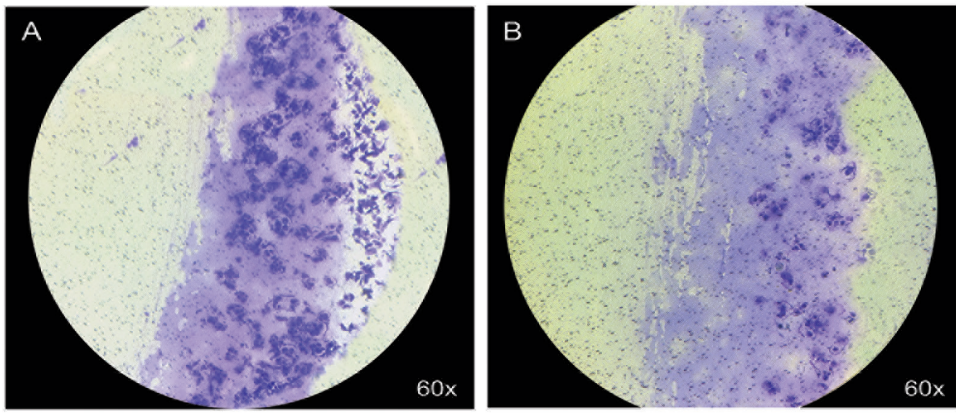

Fig. 4. Effects of aprotinin treatment on local invasion of SK-BR-3 cell line. This panel of images taken using invert microscope illustrates effects of aprotinin treatment on local invasion of SK-BR-3 human breast cancer (BC) cell line. Compared to untreated cells (A), treatment of SK-BR-3 cells with 1.3 (B) TIU/mL of aprotinin resulted in insignificant (p = 0.06) inhibition of local invasion. The magnification scale is ×60

Further studies utilizing in-depth and comprehensive molecular and genetic assessments are needed to provide mechanistic insights on how aprotinin inhibits the survival and invasion of BC cells. These assessments could include the expression of MMPs and uPA/uPAR system, and overexpression/silencing of other potential molecules. Furthermore, examining the type of cell death

(e.g., necrosis, apoptosis, autophagy, or necroptosis) induced by aprotinin in cancer cell lines studied in this study could shed further light on the mechanism of inhibitory effects of aprotinin.

In contrast to local antiproliferative and anti-invasive effects, aprotinin treatment could increase the survival of metastatic cancer cells in some in vivo studies. This was attributed to its antifibrinolytic effects.[31,32] The spread of metastatic cells through the vasculature of secondary tissue is enhanced by the association of these cells with microthrombi. Aprotinin and other antifibrinolytic agents could enhance the association between metastatic cancer cells and microthrombi, resulting in increased survival of these cells. Therefore, it could be inferred that aprotinin would be more beneficial in the early stages of cancer, before metastasis occurs. Furthermore, it seems mandatory to individually investigate the summary effects of aprotinin on each specific type of cancer by weighing local antiproliferative and anti-invasion effects against the potential harmful effects attributable to improving the survival of metastatic cells.

Beneficial effects of aprotinin in cancer patients have also been reported in clinical studies. Aprotinin administration could increase the post-pneumectomy survival of patients with mesothelioma, whether due to its anti-inflammatory, antiserine protease, or anti-angiogenesis effects.[33] This beneficial role of aprotinin in survival was independent from its positive effects attributable to reducing bleeding. Such clinical evidence further supports potential indications of aprotinin as an antitumor drug. Similar to other recently introduced agents with potential antitumor effects,[34,35] aprotinin could be considered as an adjunct therapy to complement current chemotherapeutic regimens. In addition to enhancing the efficacy, this combination could decrease the dose of chemotherapeutic drugs needed and limit exposure to their numerous unfavorable toxic effects.[36]

Clinical studies have reported some adverse effects of systemic administration of aprotinin. High doses of aprotinin resulted in allergic and anaphylactic reactions, as well as immunoglobulin G (IgG) formation in 50% of patients receiving aprotinin in the context of cardiac operations.[37,38] In addition, systemic administration of aprotinin could increase the risk of renal failure, myocardial infarction, stroke, and encephalopathy.[39] Therefore, if confirmed by future experimental and clinical studies as promising anticancer drug, it would be safer to consider aprotinin as a local agent. For example, tissue-engineering techniques could be exploited to develop scaffolds that locally release aprotinin in a specific timely manner. Surgeons could use these scaffolds to invest the resection site of primary tumor bulk (e.g., after mastectomy) in order to locally inhibit the proliferation and invasion of remaining tumoral cells in the resection margin. An almost similar method of anticancer drug delivery is currently used in the treatment of glioblastoma multiform.[40]

The MTT assay used in this study is a simple, rapid and reproducible method to investigate cytotoxicity of anticancer agents.[41,42] Its results have high correlation with more labour-intensive and time-consuming method, clonogenic assay.[43] Longer recovery phase used in this study could diminish the limitation of MTT assay in differentiating the reduction in cellular metabolic activity from the reduction in number of cells.

We investigated 3 human BC cell lines in this study. Selection of these cell lines was carried out in order to include different subtypes of human BC cell lines with respect to the expression of estrogen receptor (ER), progesterone receptor (PR) and HER2. MCF7 is positive for ER and PR and negative for HER2. SK-BR3 is negative for ER and PR and positive for HER2. MDA-MB-231 is negative for all 3. Future studies could consider other BC cell lines to investigate whether current findings could be generalized to other types of BC cell lines. Furthermore, we used HDF-1 as a control group in this study. It is a non-transformed, non-malignant normal human fibroblast cell line with high sensitivity to cytotoxic agents. Although findings on this cell line could be extrapolated to other normal cell lines, using purely normal human breast cell line as a control could have provided more robust evidence in this topic. Finally, in vitro behavior of aprotinin may not be a precise predictor of its behavior in in vivo or in situ settings. Animal model and clinical studies, if indicated after further confirmatory in vitro studies, could provide more robust evidence.

In conclusion, our study showed that aprotinin significantly inhibited the growth of normal fibroblast and BC cell lines. Compared to normal cell line, tumor cell lines showed higher sensitivity to antiproliferative effects of both low- and high-dose aprotinin. Furthermore, aprotinin administration at doses equal to or above 1 TIU/mL, significantly inhibited the local invasion of MDA-MB-231 BC cell line. Our findings encourage further confirmatory in vitro studies to be conducted with a more comprehensive mechanistic approach. They can determine if investigations of aprotinin as anticancer drug could advance to in vivo or clinical studies.

References

1. Chaffer CL, Weinberg RA. A perspective on cancer cell metastasis. *Science*. 2011;331(6024):1559–1564.
2. Fidler IJ. The pathogenesis of cancer metastasis: The "seed and soil" hypothesis revisited. *Nat Rev Cancer*. 2003;3(6):453–458.
3. Andreasen PA, Kjøller L, Christensen L, Duffy MJ. The urokinase-type plasminogen activator system in cancer metastasis: A review. *Int J Cancer*. 1997;72(1):1–22.
4. Dass K, Ahmad A, Azmi AS, Sarkar SH, Sarkar FH. Evolving role of uPA/uPAR system in human cancers. *Cancer Treat Rev*. 2008;34(2):122–136.
5. Hadler-Olsen E, Winberg JO, Uhlin-Hansen L. Matrix metalloproteinases in cancer: Their value as diagnostic and prognostic markers and therapeutic targets. *Tumour Biol*. 2013;34(4):2041–2051.
6. Halamkova J, Kiss I, Pavlovsky Z, et al. Clinical relevance of uPA, uPAR, PAI 1 and PAI 2 tissue expression and plasma PAI 1 level in colorectal carcinoma patients. *Hepatogastroenterology*. 2011;58(112):1918–1925.
7. Razik E, Kobierzycki C, Grzegrzółka J, et al. Plasminogen activation system in rectal adenocarcinoma. *Anticancer Res*. 2015;35(11):6009–6015.

8. Brungs D, Chen J, Aghmesheh M, et al. The urokinase plasminogen activation system in gastroesophageal cancer: A systematic review and meta-analysis. *Oncotarget*. 2017;8(14):23099–23109.
9. Kuhn W, Schmalfeldt B, Reuning U, et al. Prognostic significance of urokinase (uPA) and its inhibitor PAI-1 for survival in advanced ovarian carcinoma stage FIGO IIIc. *Br J Cancer*. 1999;79(11–12):1746–1751.
10. Tang L, Han X. The urokinase plasminogen activator system in breast cancer invasion and metastasis. *Biomed Pharmacother*. 2013;67(2):179–182.
11. Hildenbrand R, Schaaf A. The urokinase-system in tumor tissue stroma of the breast and breast cancer cell invasion. *Int J Oncol*. 2009;34(1):15–23.
12. Ren F, Tang R, Zhang X, et al. Overexpression of MMP family members functions as prognostic biomarker for breast cancer patients: A systematic review and meta-analysis. *PloS One*. 2015;10(8):e0135544.
13. Sun DW, Zhang YY, Qi Y, Zhou XT, Lv GY. Prognostic significance of MMP-7 expression in colorectal cancer: A meta-analysis. *Cancer Epidemiol*. 2015;39(2):135–142.
14. Soleyman-Jahi S, Nedjat S, Abdirad A, Hoorshad N, Heidari R, Zendehdel K. Prognostic significance of matrix metalloproteinase-7 in gastric cancer survival: A meta-analysis. *PloS One*. 2014;10(4):e0122316.
15. Mueller J, Gaertner FC, Blechert B, Janssen K-P, Essler M. Targeting of tumor blood vessels: A phage-displayed tumor-homing peptide specifically binds to matrix metalloproteinase-2-processed collagen IV and blocks angiogenesis in vivo. *Mol Cancer Res*. 2009;7(7):1078–1085.
16. Royston D. The current place of aprotinin in the management of bleeding. *Anaesthesia*. 2015;70(Suppl 1):46–49,e17.
17. Day JR, Landis RC, Taylor KM. Aprotinin and the protease-activated receptor 1 thrombin receptor: Antithrombosis, inflammation, and stroke reduction. *Semin Cardiothorac Vasc Anesth*. 2006;10(2):132–142.
18. Asimakopoulos G, Lidington EA, Mason J, Haskard DO, Taylor KM, Landis RC. Effect of aprotinin on endothelial cell activation. *J Thorac Cardiovasc Surg*. 2001;122(1):123–128.
19. Bekes EM, Deryugina EI, Kupriyanova TA, et al. Activation of pro-uPA is critical for initial escape from the primary tumor and hematogenous dissemination of human carcinoma cells. *Neoplasia*. 2011;13(9):806–821.
20. Gao L, Smith RS, Chen LM, Chai KX, Chao L, Chao J. Tissue kallikrein promotes prostate cancer cell migration and invasion via a protease-activated receptor-1-dependent signaling pathway. *Biol Chem*. 2010;391(7):803–812.
21. Prange E, Schroyens W, Pralle H. The influence of the protease inhibitor aprotinin on tumor invasion of three cell lines in vitro. *Clin Exp Metastasis*. 1988;6(2):107–113.
22. Plumb JA, Milroy R, Kaye SB. Effects of the pH dependence of 3-(4, 5-dimethylthiazol-2-yl)-2, 5-diphenyltetrazolium bromide-formazan absorption on chemosensitivity determined by a novel tetrazolium-based assay. *Cancer Res*. 1989;49(16):4435–4440.
23. Stillfried GE, Saunders DN, Ranson M. Plasminogen binding and activation at the breast cancer cell surface: The integral role of urokinase activity. *Breast Cancer Res*. 2007;9(1):R14.
24. Blouse GE, Bøtkjær KA, Deryugina E, et al. A novel mode of intervention with serine protease activity targeting zymogen activation. *J Biol Chem*. 2009;284(7):4647–4657.
25. Prange E, Schroyens W, Pralle H. The influence of the protease inhibitor aprotinin on tumor invasion of three cell lines in vitro. *Clin Exp Metastasis*. 1988;6(2):107–113.
26. Yeh MW, Rougier JP, Park JW, et al. Differentiated thyroid cancer cell invasion is regulated through epidermal growth factor receptor-dependent activation of matrix metalloproteinase (MMP)-2/gelatinase A. *Endocr Relat Cancer*. 2006;13(4):1173–1183.
27. Ohkoshi M. Effect of aprotinin on growth of 3-methylcholanthrene-induced squamous cell carcinoma in mice. *Gan*. 1980;71(2):246–250.
28. Lage A, Diaz JW, Gonzalez I. Effect of proteinase inhibitor in experimental tumors. *Neoplasma*. 1977;25(2):257–259.
29. Thomson AW, Pugh-Humphreys RG, Horne CH, Tweedle DJ. Aprotinin and growth of Walker 256 carcinosarcoma in the rat. *Br J Cancer*. 1977;35(4):454–460.
30. Latner AL, Longstaff E, Turner GA. Anti-tumor activity of aprotinin. *Br J Cancer*. 1974;30(1):60–67.
31. Kristensen P, Pyke C, Lund LR, Andreasen PA, Danø K. Plasminogen activator inhibitor-type 1 in Lewis lung carcinoma. *Histochemistry*. 1990;93(6):559–566.
32. Turner GA, Weiss L. Analysis of aprotinin-induced enhancement of metastasis of Lewis lung tumors in mice. *Cancer Res*. 1981;41(7):2576–2580.
33. Naqvi SH, Naqvi SH, Bandukda MY, Naqvi SM. Present status and upcoming prospects of hedgehog pathway inhibitors in small cell lung cancer therapy. *Infect Agent Cancer*. 2013;8(1):17.
34. Soleyman-Jahi S, Abdirad A, Fallah AA, et al. Prognostic significance of preoperative and postoperative plasma levels of ghrelin in gastric cancer: 3-year survival study. *Clin Transl Gastroenterol*. 2017;8(1):e209.
35. Soleyman-Jahi S, Zendehdel K, Akbarzadeh K, Haddadi M, Amanpour S, Muhammadnejad S. In vitro assessment of antineoplastic effects of deuterium depleted water. *Asian Pac J Cancer Prev*. 2014;15(5):2179–2183.
36. Mahmoodi M, Soleyman-Jahi S, Zendehdel K, et al. Chromosomal aberrations, sister chromatid exchanges, and micronuclei in lymphocytes of oncology department personnel handling anti-neoplastic drugs. *Drug Chem Toxicol*. 2017;40(2):235–240.
37. Dietrich W, Spath P, Ebell A, Richter JA. Prevalence of anaphylactic reactions to aprotinin: Analysis of two hundred forty-eight reexposures to aprotinin in heart operations. *J Thorac Cardiovasc Surg*. 1997;113(1):194–201.
38. Dietrich W, Späth P, Zühlsdorf M, et al. Anaphylactic reactions to aprotinin reexposure in cardiac surgery: Relation to antiaprotinin immunoglobulin G and E antibodies. *Anesthesiology*. 2001;95(1):64–71.
39. Martin K, Wiesner G, Breuer T, Lange R, Tassani P. The risks of aprotinin and tranexamic acid in cardiac surgery: A one-year follow-up of 1188 consecutive patients. *Anesth Analg*. 2008;107(6):1783–1790.
40. Bastiancich C, Danhier P, Préat V, Danhier F. Anticancer drug-loaded hydrogels as drug delivery systems for the local treatment of glioblastoma. *J Control Release*. 2016;243:29–42.
41. Sieuwerts AM, Klijn JGM, Peters HA, Foekens JA. The MTT tetrazolium salt assay scrutinized: How to use this assay reliably to measure metabolic activity of cell cultures in vitro for the assessment of growth characteristics, IC50-values and cell survival. *Eur J Clin Chem Clin Biochem*. 1995;33(11):813–824.
42. van Meerloo J, Kaspers GJL, Cloos J. Cell sensitivity assays: The MTT assay. *Methods Mol Biol*. 2011;731:237–245.
43. Perez RP, Godwin AK, Handel LM, Hamilton TC. A comparison of clonogenic, microtetrazolium and sulforhodamine B assays for determination of cisplatin cytotoxicity in human ovarian carcinoma cell lines. *Eur J Cancer*. 1993;29A(3):395–399.

A quantitative method for measuring the transfection efficiency of CD19-directed chimeric antigen receptor in target cells

Na Fang[B,C], Niannian Zhong[C], Tingxuan Gu[B], Yahui Wang[B], Xiangqian Guo[E], Shaoping Ji[A,D,F]

Department of Biochemistry and Molecular Biology, Medical School, Henan University, Kaifeng, China

A – research concept and design; B – collection and/or assembly of data; C – data analysis and interpretation;
D – writing the article; E – critical revision of the article; F – final approval of the article

Advances in Clinical and Experimental Medicine, ISSN 1899-5276 (print), ISSN 2451-2680 (online) *Adv Clin Exp Med*. 2019;28(2):159–164

Address for correspondence
Shaoping Ji
E-mail: shaopingji@henu.edu.cn

Funding sources
National Natural Science Foundation of China (No. 31371386); Program for Excellent Talents in Henan Province (No. 124200510010); Program for Researchers in the Educational System in Henan Province (No.17A310004).

Conflict of interest
None declared

Received on January 6, 2017
Reviewed on February 17, 2017
Accepted on May 5, 2018

Published online on December 5, 2018

Abstract

Background. Adoptive cell therapy (ACT) based on chimeric antigen receptors (CARs) expressed on the surface of T cells shows a remarkable clinical outcome, particularly for B-cell malignancies. However, toxicity and side effects of CD19-redirected CAR T cells have been observed concurrently in most cases due to cytokine release and tumor cell lysis. Therefore, strictly controlling the amount of valid T cells re-transfused to patients seems to be an important step in reducing toxicity and side effects of CAR T cells. Transfection efficiency via lentiviral particles varies widely in different cases.

Objectives. The aim of this study was to accurately calculate and control the number of valid CAR T cells through ACT because the restriction antibiotics gene or the fluorescence gene are not suitable for tracking or screening for valid transfected T cells.

Material and methods. We expressed and purified a GFP-CD19 fusion protein as a probe to measure the expression efficiency of CD19-redirected CAR on the cell surface in adherent and suspension cell lines.

Results. We can precisely calculate the transfected efficiency of lentiviral particles by counting the number of GFP-labeled cells under a microscope, as well as calculate the percentage by comparing the number of GFP-labeled cells to total cells.

Conclusions. We propose a method to control the number of valid cells in ACT and to reduce toxicity and side effects in clinical use – a convenient technique for monitoring the dosage of CAR T cells for patients.

Key words: immunotherapy, CAR-T, CD19, examination, B-cell malignancy

Cite as
Fang N, Zhong N, Gu T, Wang Y, Guo X, Ji S. A quantitative method for measuring the transfection efficiency of CD19-directed chimeric antigen receptor in target cells. *Adv Clin Exp Med*. 2019;28(2):159–164. doi:10.17219/acem/90772

DOI
10.17219/acem/90772

Introduction

Chimeric antigen receptors (CARs) were engineered by Gross et al.,[1] who first generated and expressed the chimeric T-cell receptor (TCR), which is composed of the TCR constant domains and variable domains of the antibody, and these chimeric genes are non-MHC-restricted. A specific single chain fragment variable (scFv) from anti-tumor-associated antigen (TAA) antibody was fused to T-cell activation-related domains and was expressed on membrane of the cells.[2] As a result, the T cells display tumor-targeted cytotoxic activity and the ability to proliferate sustainably. Subsequently, a CD19-redirected CAR T cell targeted against B-cell malignancies was developed and clinically tested, and it demonstrated remarkable effectiveness both in children and adult patients.[3,4] Chimeric antigen receptor T-cell therapy provides a novel treatment choice for blood cancer patients, particularly for relapsed and refractory leukemia.

CD19 is a specifically expressed antigen in the B lymphocyte lineage, maintaining an upregulated expression during the early B-lineage cells to the mature B cell differentiation until final downregulation during terminal differentiation cells, and that CD19 has become a chimeric immunotarget for malignant B cells, including acute lymphoblastic leukemia (ALL) and non-Hodgkin's lymphomas (NHL).[5] In addition, another publication revealed an essential role for CD19 in promoting early B-cell activation events in response to membrane-bound ligand stimulation.[6] Therefore, CD19 chimeric antigen receptor therapy in oncology has progressed remarkably in recent years, especially for refractory/relapsed hematological malignancies.[3,4,7–9] Furthermore, a recently modified CAR based on cancer-associated Tn-Glycoform has revealed the effect of CAR T cells on solid cancer.[10] In clinical studies, T cells were collected from a patient with leukapheresis and then isolated and activated with antibodies[11] which induced T cell activation and proliferation, thereby making the cells more likely to be responsible for viral transduction. These transduced cells can be expanded to the required quantity. Quality control and assurance assays are necessary before the prepared T cells can be re-transfused to patients.[12]

However, there are many challenges and considerations. For instance, if the dose of infused CAR T cells is insufficient, the expected result may not be achieved; on the other hand, an over-infused dose may cause toxicities mediated by CAR T cells, such as cytokine release syndrome (CRS).[13] An effective method for examining and quantifying the transduced cells could help to accurately control the amount of infused CAR T cells administered to the patient, and could therefore lead to a more effective treatment. Flow cytometry (FCM) is a good choice, but a new set of detection apparatus must be used for each individual patient to protect against cross-infection. The cost of the FCM detection method can be prohibitive.

Green/red fluorescent protein (GFP) has been a useful tool for intracellular study since it was discovered[14] and it is used as a marker for gene expression.[15] These non-invasive and visualization proteins can serve as a marker for quantifying the number of interest infected T cells when administered clinically[16] or can be used to determine the ratio of infected cells to total cells. In addition, an antibiotic-resistance gene used in a recombinant vector is another method of screening for infected cells or valid cells with removing the uninfected cells. However, both approaches have employed exotic genes/proteins which are immunogenic molecules and pose a potential hazard to patients in clinical use. In this study, we fused GFP to CD19 as a fusion protein, expressed it in *Escherichia coli* and purified it as a probe, so as to examine the infection efficiency of the CD19-directed chimeric antigen receptor on the surface of T cells based antigen–antibody interactions. Positive cells are marked with the GFP-CD19 fusion protein, due to the CD19-directed CAR being expressed on the surface of the infected cells. Valid CAR T cells can be calculated by counting the number of positive cells. Using this method, the number of valid cells can be accurately calculated before being re-transfused to patients.

Material and methods

Cloning of target genes

The CD19 gene and the GFP gene were amplified with polymerase chain reaction (PCR) from cDNA (GeneChem, Shanghai, China) and pET-28b-EGFP plasmid (Dingguo Changsheng, Beijing, China), respectively. The specific DNA primers for CD19 with restriction sites BamHI (upstream) and HindIII (TaKaRa, Osaka, Japan) (downstream) were 5'- AGGATCCGAGGAACCTCTAGTGGTGAAGG-3' (up) and 5'- CAAGCTTTCACCTGGTGCTCCAGGTGCCC-3' (down). The specific DNA primers for GFP were 5'- GCATATGGTGAGCAAGGGCGAGGAG-3' (up) and 5'-AGGATCCCTTGTACAGCTCGTCCATGCC-3' (down) with restriction sites NdeI and BamHI (TaKaRa) upstream and downstream, respectively. The PCR products were analyzed in 1.0% agarose gel and purified.

Plasmid construction

The target DNA was isolated through electrophoresis in 1.0% agarose gel. In brief, the gels with DNA fragments were excised and purified with a Gel Extraction Kit (Lifefeng, Shanghai, China). These fragments were inserted into pGEM T-Easy plasmid (Promega, Madison, USA) using T/A cloning. The ligation products were transformed into Top10 competent *E. coli* cells. Following a heat shock, the transformed cells were recovered in super optimal broth with catabolite repression (super optimal catabolite repression (SOC) medium, 2% tryptone, 0.5% yeast extract,

0.05% sodium chloride (NaCl), 2.5mM potassium chloride (KCl), 10mM magnesium chloride ($MgCl_2$), and 20mM glucose) at 37°C for 45 min. Recombinant colonies were cultured in agar plates (1% tryptone, 0.5% yeast extract, 1% NaCl, and 1.5% agar). Notably, the ligation product should be incubated at 70°C for 5 min to inactivate the ligase before the transformation. The recombinant plasmids were extracted from the bacteria and identified using endonuclease analysis. The CD19-T vector recombinant plasmid was identified by BamHI and HindIII, and the GFP-T vector by NdeI and BamHI. The inserted sequences were verified through DNA sequencing (Sangon Biotech, Shanghai, China).

Subsequently, the verified CD19-T vector recombinant plasmid and pCold TF plasmid which contained CspA promoter (a cold promoter, used to induce expression at low temperatures) and an ampicillin-resistance gene were digested by BamHI and HindIII, respectively. Electrophoresis with 1.0% agarose gel was performed. The target CD19 gene fragment and the linearized pCold TF plasmid in the gels were purified and ligated with T4 DNA ligase. The ligation products were transformed into Top10 competent *E. coli* cells, which were then cultured in agar plates and SOC medium with ampicillin. The reconstructed CD19-pCold TF plasmid was extracted from the bacteria and identified by BamHI and HindIII. Finally, the GFP-T vector recombinant plasmid and this CD19-pCold TF plasmid were digested by NdeI and BamHI, respectively. The GFP gene fragment and CD19-pCold TF plasmid vector were purified and the GFP-CD19-pCold TF recombinant plasmid was constructed through ligation and identified with NdeI and HindIII.

Construction of CD19-CAR lentiviral vector and packaging of lentivirus

The CD19-CAR lentiviral expression plasmid was constructed and the insert included the Kozak sequence, the IL-2 signaling peptide, scFv antibody, Fc hinge, CD28 transmembrane domain, 4-1 BB signaling domain, and CD3 zeta. The scFv antibody fragment is a gift from our colleague Dr. Jianghai Liu (Sichuan University, Chengdu, China), and the rest of the insert was a gift from Dr. Guo's lab (University of Saskatchewan, Saskatoon, Canada). The whole insert was inserted into lentiviral expression vector pCDH-EF1 (no fluorescence). The recombinant vector was identified with XbaI and SalI and verified through sequencing. The lentiviral particles were purchased from Shanghai GenePharma Co. Ltd (Shanghai, China). The final virus titer was 1×10^8 TU/mL.

Protein GFP-CD19 expression

The GFP-CD19-pCold TF recombinant plasmid was transformed into BL21(DE3) competent *E. coli* bacteria for expression.[17] After overnight incubation in agar plates, single colonies were picked from the plates and placed into lysogeny (LB) broth with ampicillin to grow overnight at 37°C in a shaker.

This cultured medium was transferred into fresh LB (1:200) with ampicillin in a flask to culture for about 2 h until its OD 600 value was 0.5. The culture was cooled at room temperature. When the temperature of the broth dropped to 15°C, isopropyl-β-D-thiogalactopyranoside (IPTG; Solarbio, Beijing, China) was added into the culture. The final concentration of IPTG in the culture was 0.5mM and the bacteria were cultured at 15°C for additional 4 h. Cells were harvested using centrifugation at 4000 g at room temperature for 10 min and they appeared to be green under visible light. The harvested cells were stored at –80°C or used immediately.

Protein purification

The cell pellet harvested from 100 mL of the culture described above was re-suspended in 25 mL of phosphate-buffered saline (PBS; 137mM NaCl, 2.7mM KCl, 10mM disodium phosphate (Na_2HPO_4) and 2mM monopotassium phosphate (KH_2PO_4 at a pH of 7.0) with 1mM of phenylmethylsulfonyl fluoride (PMSF) and 0.5% Triton X-100 (0.5%) on ice. The sample was frozen at –80°C for 30 min and were taken out. After thawing out, it was sonicated at 85 W for 6 s, followed by 7 s on ice in order to shear the DNA for lower viscosity. Sonication and icing were repeated 5–7 times in all samples until the solution was clear. The cell debris was centrifuged at 12,000 g for 10 min at 4°C. The supernatant was then transferred to a new tube. Then, sodium dodecyl sulfate–polyacrylamide gel electrophoresis (SDS-PAGE) for the supernatant was performed to figure out the solubility of the protein. The rest of the supernatant was stored at –20°C or on ice for the following step.

Ni-NTA-agarose purification was prepared and 4 mL of Ni-NTA resin (beads) was pipetted into a 10 mL purification column. The resin was washed using 5 column volume (CV) of deionized water and then 5 CV of PBS (pH 7.0) for equilibrium. Twenty-five milliliters of the supernatant was slowly added into the column for binding. The protein in the column was washed with 5 CV of PBS (pH 7.0) and 3 CV of wash buffer (PBS pH 7.0 buffer containing 20mM imidazole) successively, and eluted with PBS (pH 7.0) with 250mM of imidazole into a new tube. The resin was again washed with PBS (pH 7.0) with 800mM of imidazole (3 CV). Finally, the column was washed with PBS (pH 7.0) 5–8 times, with sterile deionized water 3–5 times and washed again with 20 mL of 20% ethanol; then it was filled with 20% alcohol and stored at 4°C. The eluted protein was confirmed using SDS-PAGE analysis. The 250mM of imidazole was centrifuged at 4500 g for 50 min at 4°C in an ultrafiltration centrifuge tube (Merck Millipore, Billerica, USA), in order to remove small molecular substances and to concentrate the purified protein. This step was repeated and the protein was concentrated to 2.0 μg/mL.

Infection of 3 cell lines

The lentiviral vector was packaged for CD19-CAR expression and the titer was 1×10^8 TU/mL (GenePharma). First, the HEK 293 cells (5×10^4/mL) were seeded in 6 of the wells (500 µL each) of a 24-well plate. After the seeded cells were cultured for 12 h, the media were replaced with infection mix. Three of the wells had 490 µL of complete medium, 10 µL of lentivirus and 0.5 µL of polybrene added, with a working concentration of 5 µg/mL for each one. The other 3 control wells had only 500 µL of complete medium added. Daudi cells and Jurkat cells were infected through the same process as the HEK 293 cells, but the method of treating the cells was different. The cells were cultured at 37°C in 5% CO_2 for 72 h. Then, 5 µL of the GFP-CD19 fusion protein was added to each culture (0.2–2.0 µg/mL). Subsequently, the cells were cultured under the same conditions for another 6 h, the media were replaced by PBS and the cells were observed with fluorescence microscope and quantified using cell counting in each chamber.

Results

Plasmid construction

The CD19 gene (coding sequence; 1671bp) and the GFP gene (717bp) were acquired through PCR from commercial cDNA and pET28b-GFP plasmid, respectively, and were identified with 1% agarose gel electrophoresis, as shown in Fig. 1. Then, the target genes were ligated into T vector. The CD19 gene was identified by BamHI and HindIII. A 1671bp fragment can be seen in Fig. 2A. Similarly, the GFP gene was identified by NdeI and BamHI. A 717bp gene fragment shows correctly in Fig. 2B. Furthermore, the sequencing results of the constructed T vector plasmids were also correct. The CD19 gene was cut and then ligated to pCold TF vector. The recombinant plasmid was identified by BamHI and HindIII. A 1671bp gene fragment and a 5769bp gene fragment can be seen in Fig. 3A. The GFP gene was ligated to this recombinant plasmid and identified by NdeI and BamHI. The 2388bp gene fragment of the CD19-GFP gene and a 5769bp gene fragment of linearized pCold TF plasmid visible in Fig. 3B indicate that the recombinant plasmid was constructed successfully.

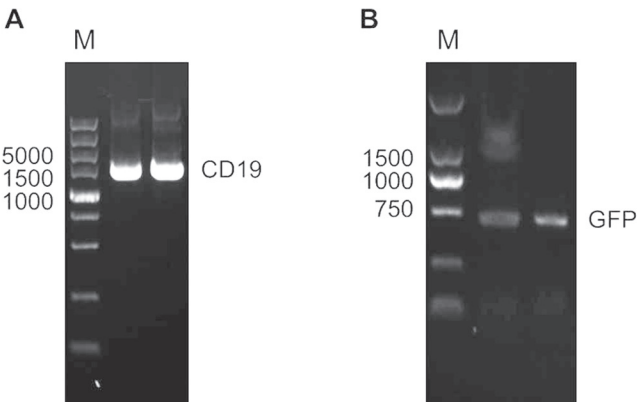

Fig. 1. Polymerase chain reaction (PCR) results of CD19. The 2 lanes are the CD19 encoding region (A); the GFP gene (B) is amplified as shown in both lanes

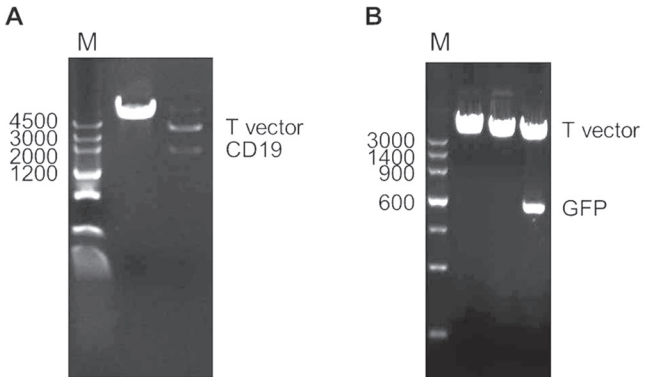

Fig. 2. Identification of the CD19-T vector plasmid (A) through digestion with EcoRI in the right lane. The GFP-T vector plasmid (B) was identified with EcoRI and the right lane is a positive clone. Both vectors were verified with sequencing

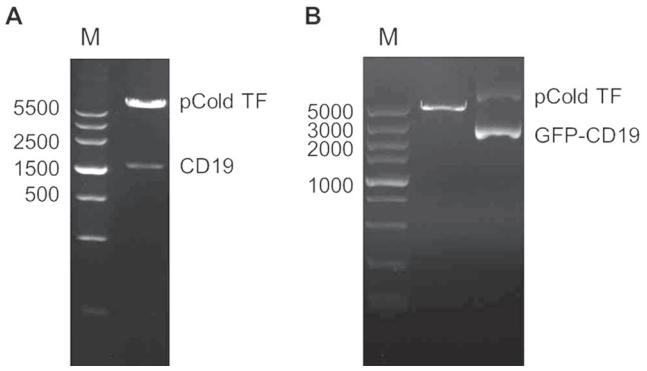

Fig. 3. Identification of the recombinant plasmids CD19-pCold TF (A) and CD19-GFP-pCold TF (B). Correct bands were cut out from both recombinant vectors, indicating that the vectors are correct

Expression and purification of the CD19-GFP fusion protein

The CD19-GFP fusion protein induced by IPTG was expressed in BL21 *E. coli* bacteria and collected. It was purified using Ni-NTA-agarose purification and concentrated using protein concentrators. The expression and purification results were confirmed using SDS-PAGE (Fig. 4).

Quantitative analysis of infected efficiency

The CD19-CAR was transduced by lentiviral vector into HEK 293 cells. There was no green or red fluorescence particles visible in the cells which were infected by the lentivirus. Expression of GFP can be detected under a microscope due to the specificity of CAR T cells. The images captured

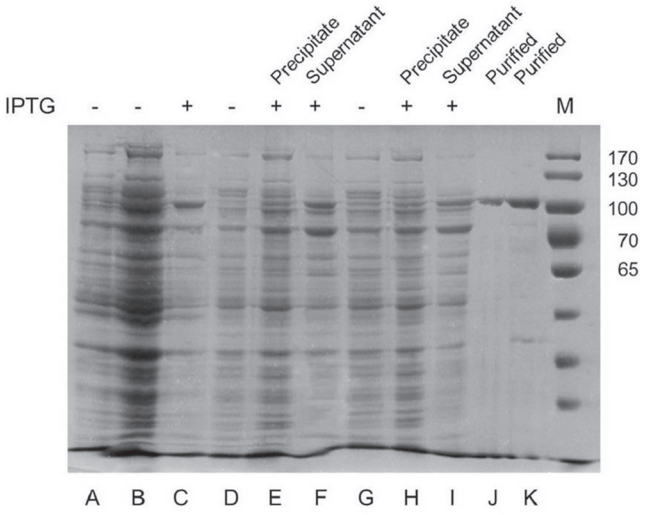

Fig. 4. Expression and purification of the CD19-GFP fusion protein (A, B, D, and G); protein expression of bacteria before IPTG induction (C); protein expression of bacteria after IPTG induction (E and H); the precipitate of protein expression of the bacteria after IPTG induction (F and I); the supernatant of protein expression of bacteria after IPTG induction (J and K); the target protein purified using the Ni-NTA-agarose purification system

under a fluorescent microscope and shown in Fig. 5 prove that the fusion proteins were targeted to HEK 293 cells, Daudi cells and Jurkat cells. Moreover, the expression rate of CAR in transduced Daudi cells was 42% while it was 76% in the Jurkat cells.

Discussion

CD19 mainly expresses on B-lineage cells, which makes it a specific antigen for immunotherapy.[18] CD19-directed CAR T cells against B-cell malignancies provides a novel and effective treatment for patients, particularly for those with relapsed and refractory B-lineage leukemia.[19–22] Except engineered T cell, CD19-redirected NK92 cells also show a promising result against B-lineage leukemia.[23] In addition, CD19-redirected T memory stem cells represent a potential method for the treatment of B-lineage leukemia.[24] In the process of engineering therapeutic cells, another vector, apart from the lentiviral vector, is also employed to mediate the expression of CAR.[25]

Toxicity and the side effects of CD19-directed CAR T cells are increasingly drawing attention to this immunotherapy. The main mechanism of the toxicity and side effects could be attributed to cytokine release, tumor cell lysis, B-cell aplasia, and macrophage-activation syndrome.[26,27] Although most mild toxicity and side effects are reversible, some severe toxicities need medical treatment. A low dose of engineered cells may not trigger a response of antitumor activity, and an extra dose of immunotherapeutic cells may lead to severe toxicity and side effects. Therefore, administering the appropriate amount of engineered T cells to patients may be the first step in controlling the occurrence of toxicity and side effects.

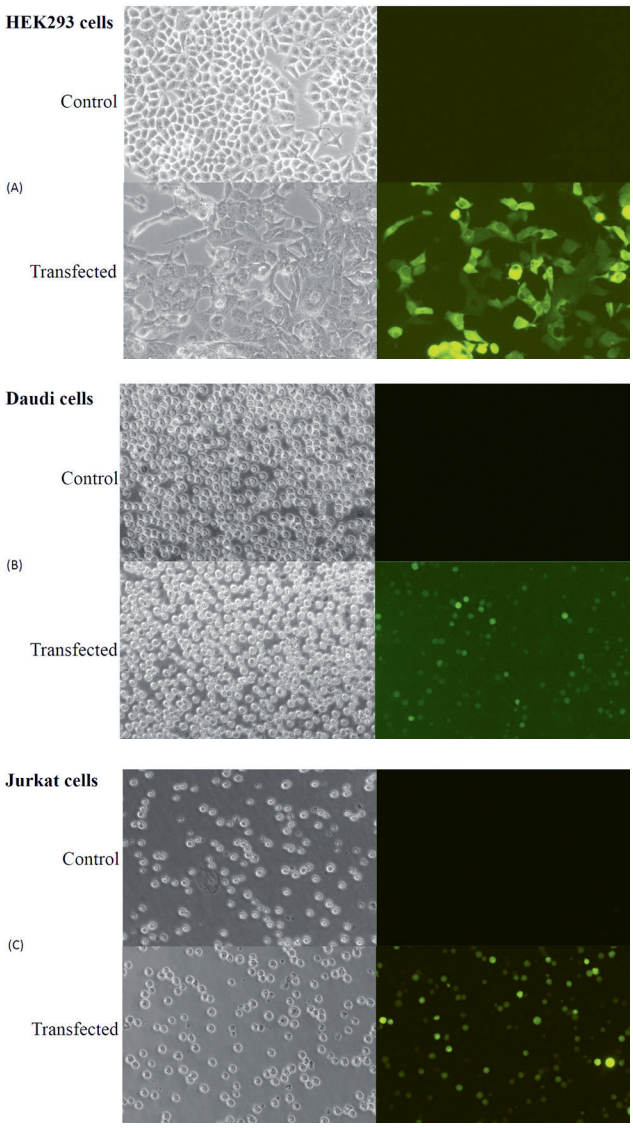

Fig. 5. GFP-expressing cells under a microscope (×100 magnification). Bright field images and cell fluorescence images of HEK 293 cells. Control – HEK 293 cells without infection (A). Bright field images and cell fluorescence images of Daudi cells. Control – Daudi cells without infection (B). Bright field images and cell fluorescence images of Jurkat cells. Control – Jurkat cells without infection (C)

It is widely accepted that a correct dosage of CAR T cells is required for each re-transfusion to patients,[12,19] so the infection efficiency and the number of valid CAR T cells is accurately calculated before re-transfusion. Due to the alteration of infection efficiency, valid CAR T cells cannot be estimated from the total number of infused cells. In order to track infection efficiency or to screen for valid infected cells by removing uninfected cells, a fluorescence protein gene and a resistant gene are commonly used in molecular manipulation. Valid cells can be counted and calculated before re-transfusion by the former method, and valid cells can be gathered by removing uninfected cells via the latter one. Both methods can provide us with an approach using which we can accurately control the infusion dosage of CAR T cells rather than the number of total cultured cells.

Unfortunately, both proteins are derived from exotic genes and their products carry immunogenicity to acceptors,[28] leading to impairment when these proteins are infused into patients along with CAR T cells. On the other hand, if flow cytometry is employed with an immunofluorescence antibody, it will increase the cost of treatment because each sorting process requires a new set of sorting apparatus. In addition, the application of an immunofluorescence antibody may become a new immunogen, leading to new barriers in the application.

A safe and simple approach is needed in order to quickly determine the infection efficiency and to calculate the number of valid engineered cells in the application. In this study, we fused CD19 to GFP and expressed it in *E. coli* under a regular molecular biological process. The fusion protein solubility was optimized at 15°C and was purified with Ni-NTA agarose beads.[29] After the target cells (including adherent and suspension cell lines) were infected with lentiviral particles, the purified fusion protein was directly added to the culture medium and left to culture for 6 h. GFP could be directly observed under a microscope and the infected cells (expressing CD-19 CAR) could be determined from other cells (data not shown). The results would become clearer than before when the cultured medium (including CD19-GFP) was removed by washing the cells with a regular culture medium.

Because CD19-GFP (as an antigen) can be recognized by CAR expressed on the surface of the target cells, the fusion protein serves as a probe to visualize the CAR-expressing cells. The non-specific binding of CD19-GFP to other proteins is negligible when a fluorescence microscope is used. The ratio of fluorescence cells to total cells can be calculated by determining the number of cells in fluorescence fractions and the number of total cells. In clinical use, the number of valid cells can be accurately administrated to patients. This method provides a novel approach to administrating a dose of CAR T cells in clinical practice using vectors free of the antibiotic-resistance gene and the fluorescence protein gene.

References

1. Gross G, Waks T, Eshhar Z. Expression of immunoglobulin-T-cell receptor chimeric molecules as functional receptors with antibody-type specificity. *Proc Natl Acad Sci U S A*. 1989;86(24):10024–10028.
2. Huston JS, Levinson D, Mudgett-Hunter M, et al. Protein engineering of antibody binding sites: Recovery of specific activity in an anti-digoxin single-chain Fv analogue produced in *Escherichia coli*. *Proc Natl Acad Sci U S A*. 1988;85(16):5879–5883.
3. Porter DL, Levine BL, Kalos M, Bagg A, June CH. Chimeric antigen receptor-modified T cells in chronic lymphoid leukemia. *N Engl J Med*. 2011;365(8):725–733.
4. Grupp SA, Kalos M, Barrett D, et al. Chimeric antigen receptor-modified T cells for acute lymphoid leukemia. *N Engl J Med*. 2013;368(16):1509–1518.
5. Scheuermann RH, Racila E. CD19 antigen in leukemia and lymphoma diagnosis and immunotherapy. *Leuk Lymphoma*. 1995;18(5–6):385–397.
6. Depoil D, Fleire S, Treanor BL, et al. CD19 is essential for B cell activation by promoting B cell receptor-antigen microcluster formation in response to membrane-bound ligand. *Nat Immunol*. 2008;9(1):63–72.
7. Brentjens RJ, Davila ML, Riviere I, et al. CD19-targeted T cells rapidly induce molecular remissions in adults with chemotherapy-refractory acute lymphoblastic leukemia. *Sci Transl Med*. 2013;5(177):177ra38.
8. Kalos M, Levine BL, Porter DL, et al. T cells with chimeric antigen receptors have potent antitumor effects and can establish memory in patients with advanced leukemia. *Sci Transl Med*. 2011;3(95):95ra73.
9. Kochenderfer JN, Wilson WH, Janik JE, et al. Eradication of B-lineage cells and regression of lymphoma in a patient treated with autologous T cells genetically engineered to recognize CD19. *Blood*. 2010;116(20):4099–4102.
10. Posey AD Jr, Schwab RD, Boesteanu AC, et al. Engineered CAR T cells targeting the cancer-associated Tn-glycoform of the membrane mucin MUC1 control adenocarcinoma. *Immunity*. 2016;44(6):1444–1454.
11. Wang X, Riviere I. Manufacture of tumor- and virus-specific T lymphocytes for adoptive cell therapies. *Cancer Gene Ther*. 2015;22(2):85–94.
12. Davila ML, Sadelain M. Biology and clinical application of CAR T cells for B cell malignancies. *Int J Hematol*. 2016;104(1):6–17.
13. Kochenderfer JN, Dudley ME, Feldman SA, et al. B-cell depletion and remissions of malignancy along with cytokine-associated toxicity in a clinical trial of anti-CD19 chimeric-antigen-receptor-transduced T cells. *Blood*. 2012;119(12):2709–2720.
14. Johnson FH, Shimomura O, Saiga Y. Action of cyanide on Cypridina luciferin. *J Cell Comp Physiol*. 1962;59:265–272.
15. Chalfie M, Tu Y, Euskirchen G, Ward WW, Prasher DC. Green fluorescent protein as a marker for gene expression. *Science*. 1994;263(5148):802–805.
16. Arun KH, Kaul CL, Ramarao P. Green fluorescent proteins in receptor research: An emerging tool for drug discovery. *J Pharmacol Toxicol Methods*. 2005;51(1):1–23.
17. Subedi GP, Satoh T, Hanashima S, et al. Overproduction of anti-Tn antibody MLS128 single-chain Fv fragment in *Escherichia coli* cytoplasm using a novel pCold-PDI vector. *Protein Expr Purif*. 2012;82(1):197–204.
18. Turtle CJ, Riddell SR, Maloney DG. CD19-Targeted chimeric antigen receptor-modified T-cell immunotherapy for B-cell malignancies. *Clin Pharmacol Ther*. 2016;100(3):252–258.
19. Onea AS, Jazirehi AR. CD19 chimeric antigen receptor (CD19 CAR)-redirected adoptive T-cell immunotherapy for the treatment of relapsed or refractory B-cell Non-Hodgkin's Lymphomas. *Am J Cancer Res*. 2016;6(2):403–424.
20. Sadelain M, Brentjens R, Riviere I, Park J. CD19 CAR therapy for acute lymphoblastic leukemia. *Am Soc Clin Oncol Educ Book*. 2015:e360–363.
21. Sadelain M. CAR therapy: The CD19 paradigm. *J Clin Invest*. 2015;125(9):3392–3400.
22. Miller BC, Maus MV. CD19-targeted CAR T cells: A new tool in the fight against B cell malignancies. *Oncol Res Treat*. 2015;38(12):683–690.
23. Romanski A, Uherek C, Bug G, et al. CD19-CAR engineered NK-92 cells are sufficient to overcome NK cell resistance in B-cell malignancies. *J Cell Mol Med*. 2016;20(7):1287–1294.
24. Sabatino M, Hu J, Sommariva M, et al. Generation of clinical-grade CD19-specific CAR-modified $CD8^+$ memory stem cells for the treatment of human B-cell malignancies. *Blood*. 2016;128(4):519–528.
25. Kebriaei P, Singh H, Huls MH, et al. Phase I trials using Sleeping Beauty to generate CD19-specific CAR T cells. *J Clin Invest*. 2016;126(9):3363–3376.
26. Ruella M, Barrett DM, Kenderian SS, et al. Dual CD19 and CD123 targeting prevents antigen-loss relapses after CD19-directed immunotherapies. *J Clin Invest*. 2016;126(10):3814–3826.
27. Wang L, Ma N, Okamoto S, et al. Efficient tumor regression by adoptively transferred CEA-specific CAR-T cells associated with symptoms of mild cytokine release syndrome. *Oncoimmunology*. 2016;5(9):e1211218.
28. Ansari AM, Ahmed AK, Matsangos AE, et al. Cellular GFP toxicity and immunogenicity: Potential confounders in in vivo cell tracking experiments. *Stem Cell Rev*. 2016;12(5):553–559.
29. Jawale CV, Lee JH. Development of a biosafety enhanced and immunogenic *Salmonella enteritidis* ghost using an antibiotic resistance gene free plasmid carrying a bacteriophage lysis system. *PLoS One*. 2013;8(10):e78193.

Expression of mucins MUC5AC and MUC19 on the ocular surface in dry eye syndrome model of ovariectomized female rabbits

Guoxing Li[1,A,B], Peirong Lu[2,B,C], Huiyang Song[1,B,C], Qinxiang Zheng[1,D,E], Kaihui Nan[1,D–F]

[1] Eye Hospital, Wenzhou Medical University, China
[2] Department of Ophthalmology, The First Affiliated Hospital of Soochow University, Suzhou, China

A – research concept and design; B – collection and/or assembly of data; C – data analysis and interpretation;
D – writing the article; E – critical revision of the article; F – final approval of the article

Advances in Clinical and Experimental Medicine, ISSN 1899–5276 (print), ISSN 2451–2680 (online) *Adv Clin Exp Med*. 2019;28(2):165–169

Address for correspondence
Kaihui Nan
E-mail: nankh@eye.ac.cn

Funding sources
This research was supported with grants from the Natural Science Foundation of Zhejiang Province, China (No. LY17H120003).

Conflict of interest
None declared

Received on February 18, 2017
Revised on March 15, 2017
Accepted on September 26, 2017

Published online on January 14, 2019

Cite as
Li G, Lu P, Song H, Zheng Q, Nan K. Expression of mucins MUC5AC and MUC19 on the ocular surface in dry eye syndrome model of ovariectomized female rabbits. *Adv Clin Exp Med*. 2019;28(2):165–169. doi:10.17219/acem/78021

Abstract

Background. Dry eye syndrome (DES) is a common symptom of tear film instability and ocular surface damage due to an abnormal quality and quantity of tears, including the sensation of foreign objects and blurred vision. Among all factors for tear film stability, MUC5AC and MUC19 are very important; the levels of both mucins are associated with the pathogenesis of DES.

Objectives. The aim of this study was to explore the expression of MUC5AC and MUC19 on the ocular surface in a DES model of ovariectomized female rabbits.

Material and methods. Healthy female New Zealand white rabbits ($n = 18$; age: 1 year, weight: 2.5 $\pm$0.6 kg) were randomly assigned to a test group and a control group. The DES model was constructed in ovariectomized female rabbits. Indicators of ocular surface injury, such as Schirmer's test, corneal fluorescence staining, a conjunctival imprinting cytology test, and the expression of MUC5AC and MUC19 in conjunctival tissues were evaluated with immunohistochemistry in week 1, week 2 and week 4.

Results. Both the length of soaked test paper and the total scores of corneal fluorescence staining at all time-points were significantly lower in the test group than in the control group, and they decreased over time ($p < 0.05$). The grades of imprinted cells at all time-points were significantly higher in the test group than in the control group, and they increased over time ($p < 0.05$). The percentage of goblet cells was significantly lower in the test group than in the control group, and it decreased over time ($p < 0.05$). The percentages of cells with a positive expression of MUC5AC and MUC19 at all time-points were significantly lower in the test group than in the control group, and they decreased over time ($p < 0.05$).

Conclusions. The pathogenesis of DES is associated with an increased grade of imprinted cells, decreased goblet cells, and a decreased expression of MUC5AC and MUC19.

Key words: dry eye syndrome model, ovariectomized female rabbits, MUC5AC, MUC19

DOI
10.17219/acem/78021

Introduction

Dry eye syndrome (DES) is a common symptom of tear film instability and ocular surface damage due to an abnormal quality and quantity of tears, including the sensation of foreign objects and blurred vision. The prevalence of DES is high in menopausal women, approx. 30–65%.[1] The decrease of sex hormones may be the most important reason for the significant increase in DES prevalence in perimenopausal women, which is difficult to treat.[2] The symptomatic treatment includes artificial tear replacement and extended ocular retention of tears, which can only increase tearing passively.[3] Recently, autologous submandibular gland transplantation has been somewhat effective, but there may be serious traumatic injury and physiological differences in the liquids secreted by the submandibular and lacrimal glands.[4] Aragona et al. found that oral pilocarpine hydrochloride could increase the number of goblet cells on the ocular surface and promote the secretion of tearing in patients with Sjögren's syndrome.[5] Kojima et al. reported that autoserum could significantly improve tear film stability and the scores of fluorescein staining and rose bengal (RB) staining on the ocular surface.[6] In addition, the immunosuppressant ciclosporin A could also promote the apoptosis of lymphocytes in the lacrimal glands and conjunctivae, and reverse the inflammation on the ocular surface and in the lacrimal glands; however, the local stimulation caused by ciclosporin A limited this application.[7] Several studies suggested that hormone replacement therapy (HRT) could improve tear function and conjunctival goblet cells[8]; however, since HRT may increase the risk of DES[9] and may induce the pathogenesis of endometrial carcinoma and mammary cancer as well as androphany and hirsutism,[10] its use was controversial. It was reported that increased tear osmotic pressure and inflammation were the pathological changes in the progress of DES, and tear film instability was the key factor in the pathological damage of DES and that mucin was one of the necessary active components in tear film.[11] A change in the quantity and structure of mucin was the intermediate process and one of the results of DES pathogenesis.[12] Among all factors for tear film stability, MUC5AC and MUC19 were very important: the levels of both mucins were associated with the pathogenesis of DES.[13,14] Thus, this study aimed to analyze the effect of the expression of MUC5AC and MUC19 on the ocular surface in DES patients, and to provide targets for clinical treatment.

Material and methods

Material

This study was in accordance with ethical standards and was approved by the Wenzhou Medical University (China). Healthy female New Zealand white rabbits (n = 18; age: 1 year, weight: 2.5 ±0.6 kg) were purchased from the Shanghai Sangon Experimental Animal Center. These rabbits were fed regularly and were acclimated for 1 week before the experiment. The construction of the DES model of ovariectomized female rabbit consisted of the following: the rabbit was fasted for 12 h; general anesthesia was performed by the administration of ketamine hydrochloride 50 mg/kg (i.m.); the outer thigh of the hind legs was disinfected with iodophor; the rabbit was placed in the dorsal position and the limbs were fixed; the abdominal cavity was opened through abdominal incision; the bilateral ovarium was resected with an aseptic technique. If the time to tear film rupture (the break-up time (BUT) value) was less than or equal to half the time for normal eyes, the DES model was successfully constructed.

Methods

The rabbits were randomly assigned to a test group or a control group. Three rabbits in each group at week 1, week 2 and week 4 were selected; the indicators of ocular surface injury, such as Schirmer's test, corneal fluorescence staining, a conjunctival imprinting cytology test, and the expression of MUC5AC and MUC19 in conjunctival tissues, were evaluated by immunohistochemistry. Schirmer's test consists of placing the Schirmer's test paper in the outer 1/3 boundary of the conjunctival sac in conscious rabbits and suspending the remaining part outside of the conjunctival sac. The paper was retrieved after 5 min and placed at room temperature for 30 min. The length of soaked test paper was measured with a vernier caliper under microscopy. The procedure for corneal fluorescence staining was as follows: 1% fluorescein sodium was dropped into the conjunctival sac with a glass rod; after 1 min, the cornea was exposed with a slit lamp and the fluorescent staining of the cornea was detected by cobalt blue light under microscopy; the cornea was divided into 4 quadrants and the intensity of fluorescent staining in each quadrant was graded on a scale from 0 to 3. The total score was 0–3 points, i.e., 0 points – no staining; 1 point – disperse and focal staining; 2 points – a cluster of focal staining; 3 points – patchy staining. The procedure for a conjunctival imprinting cytology test was as follows: cellulose filter paper was cut to a size of 5 mm × 5 mm and was immersed in distilled water overnight; it was then placed on the bulbar conjunctiva, pressed for 10 min and removed; cellulose filter paper was fixed in neutral formaldehyde solution for 10–20 min and stained with the periodic acid–Schiff (PAS) method; the imprinted cells were then observed under light microscopy. Nelson grading criteria (1989) were applied. Squamous metaplasia was graded on a scale of 0–3: 0 points – normal; 1 point – mild; 2 points – moderate; 3 points – severe. Goblet cells were counted by randomly selecting 5 fields (left, right, upper, lower, and central) under light microscopy (×200) and calculating the percentage of goblet cells.

The immunohistochemistry testing (Strept Avidin-Biotin Complex (SABC)) was done as follows: anesthesia of the ocular surface was performed with a 0.5 % Benoxil solution; a cellulose acetate membrane (5 mm × 7 mm) was pressed onto the bulbar conjunctiva 2 mm posterior from the temporal limbus for 50 s; the membrane was then taken and dried; firstly, the membrane was incubated with mouse anti-rabbit MUC5AC and MUC19 mAb (Jiangsu Biyuntian Technology Co., Ltd., Nantong, China), 1:2,000, at 4°C overnight and was washed 3 times with phosphate-buffered saline (PBS) for 5 min; the membrane was then incubated with secondary antibody donkey anti-mouse IgG (Jiangsu Biyuntian Technology Co., Ltd.), 1:500, at room temperature for 20 min and was washed 3 times with PBS for 5 min; next, the membrane was incubated with horseradish peroxidase-labeled streptavidin at room temperature for 20 min and was washed 3 times with PBS for 5 min; 3,3'-diaminobenzidine (DAB) was added for color development; the membrane was re-stained with hematoxylin, differentiated with hydrochloric acid alcohol, treated with ammonia water, and washed with distilled water. Five fields were randomly selected under light microscopy (×200) to calculate the percentage of positively-stained cells. Phosphate-buffered solution was used instead of the first antibody as a negative control.

Statistical analysis

SPSS v. 20.0 software (IBM, Inc., Armonk, USA) was used for the statistical analysis. The data is presented as mean and standard deviation (SD). Student's t-test was used for comparison between the 2 independent groups. The one-way analysis of variance (ANOVA) followed by Tukey's post hoc test was used to analyze differences among 3 or more independent groups. Probability value of $p < 0.05$ was considered a significant difference.

Results

Schirmer's test

As shown in Table 1, the length of soaked test paper at all time-points was significantly shorter in the test group than in the control group, and it decreased over time ($p < 0.05$).

Corneal fluorescence staining

As shown in Table 2, the total scores of corneal fluorescence staining at all time-points were significantly lower in the test group than in the control group, and they decreased over time ($p < 0.05$).

Conjunctival imprinting cytology test

As shown in Table 3, the grades of imprinted cells at all time-points were significantly higher in the test group than in the control group, and they increased over time ($p < 0.05$). The percentage of goblet cells was significantly lower in the test group than in the control group, and it decreased over time ($p < 0.05$).

Table 1. Schirmer's test results [cm]

Group	Week 1	Week 2	Week 4	F	p-value
Control group	8.2 ±1.3	8.3 ±1.4	7.8 ±1.5	0.132	0.869
Test group	6.4 ±1.2	5.2 ±1.3	3.9 ±1.4	5.624	0.021
t	3.965	4.527	5.327	–	–
p	0.035	0.029	0.024	–	–

t, p – Student's t-test; F, p-value – one-way analysis of variance (ANOVA), followed by Tukey's post hoc test.

Table 2. Corneal fluorescence staining

Group	Week 1	Week 2	Week 4	F	p-value
Control group	10.5 ±2.3	10.3 ±2.4	10.4 ±2.6	0.096	0.952
Test group	7.8 ±1.5	5.9 ±1.3	4.1 ±1.4	5.432	0.024
t	3.857	4.628	5.714	–	–
p	0.036	0.026	0.017	–	–

Table 3. Conjunctival imprinting cytology test

Group	Grade of imprinted cells					Percentage of goblet cells				
	week 1	week 2	week 4	F	p-value	week 1	week 2	week 4	F	p-value
Control group	0.8 ±0.2	1.2 ±0.3	1.0 ±0.4	0.241	0.758	42.5 ±6.5	43.6 ±7.2	44.8 ±7.9	0.326	0.721
Test group	1.5 ±0.3	1.8 ±0.4	2.3 ±0.5	5.327	0.028	35.4 ±10.2	31.2 ±11.3	25.6 ±12.2	5.764	0.013
t	3.625	4.721	5.285	–	–	4.325	4.869	5.326	–	–
p	0.039	0.025	0.017	–	–	0.032	0.027	0.021	–	–

Table 4. The percentages of cells with positive expression of MUC5AC and MUC19

Group	MUC5AC					MUC19				
	week 1	week 2	week 4	F	p-value	week 1	week 2	week 4	F	p-value
Control group	35.9 ±12.3	36.7 ±13.4	34.8 ±15.2	0.165	0.825	41.2 ±13.6	38.9 ±14.2	37.5 ±15.7	0.215	0.832
Test group	29.5 ±12.6	26.3 ±11.4	21.2 ±12.3	5.217	0.026	30.5 ±12.5	27.6 ±11.7	23.4 ±12.3	5.525	0.016
t	3.654	3.987	4.432	–	–	4.127	4.659	4.897	–	–
p	0.038	0.035	0.028	–	–	0.036	0.033	0.028	–	–

The expression of MUC5AC and MUC19

As shown in Table 4, the percentages of cells with a positive expression of MUC5AC and MUC19 at all time-points were significantly lower in the test group than in the control group, and they decreased over time ($p < 0.05$).

Discussion

Proteins are the final effectors of genes and they directly reflect the complexity and diversity of biological activities. Mucin is produced in the conjunctiva and apparatus lacrimalis, and is connected to the oligosaccharide side chain through hydrophilic oxygen. Glycosylation provides an electrical charge to mucin, which forms a hydrogen bond with H_2O; thus, highly hydrophilic gel is formed to prevent dryness on the ocular surface. The level of mucin on the ocular surface can be used to evaluate the function of the tear film. MUC5AC is the mucin formed by high-molecular-weight gel and secreted by conjunctival goblet cells. Zhao et al. reported that the level of MUC5AC was significantly lower in patients with DES than in the normal population.[15] Corrales et al. reported that the level of MUC5AC was significantly lower in patients with DES and was associated with the degree of corneal fluorescence staining.[16] Zhang et al. found that the expression of MUC5AC was positively associated with the time to tear film rupture.[17] MUC19 was highly expressed in normal tear gland tissues, conjunctival goblet cells and corneal and conjunctival epithelial cells, yet the expression of MUC19 was significantly decreased in patients with DES; the decrease was similar to that of MUC5AC.[18]

Watanabe reported that changes in the expression levels of both the transmembrane mucin MUC5AC produced in corneal and conjunctival epithelial cells and the secretory gel-like mucin MUC19 produced in goblet cells could directly impact the stability of tear film.[19] Moreover, the stability of tear film was also dependent on the normal functioning of the neural reflex system, which controls the secretion of the tear gland and the eyelid movement of blinking, namely the first branch of the trigeminal nerve and the facial nerve. The neurons containing vasoactive intestinal peptides (VIPs) were distributed around conjunctival goblet cells; both in vitro and in vivo studies confirmed that VIPs could promote the secretion of mucin in conjunctival goblet cells. In contrast, when the number and function of conjunctival goblet cells were abnormal, the secretion of mucin in tears was abnormal as well, and tear film was less stable. As a result, the production of tears on the ocular surface became abnormal, leading to eye discomfort and decreased vision.

This study showed that both the length of soaked test paper and the total scores of corneal fluorescence staining at all time-points were significantly lower in the test group than in the control group, and that they decreased over time ($p < 0.05$); the grades of imprinted cells at all time-points were significantly higher in the test group than in the control group, and they increased over time ($p < 0.05$); the percentage of goblet cells was significantly lower in the test group than in the control group, and it decreased over time ($p < 0.05$); the percentages of cells with a positive expression of MUC5AC and MUC19 at all time-points were significantly lower in the test group than in the control group, and they decreased over time ($p < 0.05$). These results indicated that the pathogenesis of DES was associated with a greater number of imprinted cells, fewer goblet cells and a decreased expression of MUC5AC and MUC19.

Etiological treatment may be the best treatment of diseases. It has been reported that both the immediate and persistent effects of acupuncture were better than that of artificial tears in the treatment of DES.[20] Acupuncture was characterized by little to no trauma, and it could promote the active secretion of tears from the tear glands, which might increase the level of VIPs in the tear glands and the expression of MUC5AC and MUC19.

References

1. Wan KH, Chen LJ, Young AL. Depression and anxiety in dry eye disease: A systematic review and meta-analysis. *Eye (Lond)*. 2016;30(12):1558–1567.
2. Sriprasert I, Warren DW, Mircheff AK, et al. Dry eye in postmenopausal women: A hormonal disorder. *Menopause*. 2016;23(3):343–351.
3. Ching-Li T, Ya-Jung H, Chen ZY, et al. Synergistic effect of artificial tears containing epigallocatechin gallate and hyaluronic acid for the treatment of rabbits with dry eye syndrome. *PLoS One*. 2016;11(6):e0157982.
4. Yu GY, Zhu ZH, Mao C, et al. Microvascular autologous submandibular gland transfer in severe cases of keratoconjunctivitis sicca. *Maxillofac Plast Reconstruct Surg*. 2015;33:235–239.
5. Aragona P, Pietro RD, Spinella R, et al. Conjunctival epithelium improvement after systemic pilocarpine in patients with Sjogren's syndrome. *Brit J Ophthalmol*. 2006;90:166–170.
6. Kojima T, Ishida R, Dogru M, et al. The effect of autologous serum eyedrops in the treatment of severe dry eye disease: A prospective randomized case-control study. *Am J Ophthalmol*. 2005;139:242–246.

7. Yavuz B, Pehlivan SB, Kaffashi A, et al. In vivo tissue distribution and efficacy studies for cyclosporin A loaded nano-decorated subconjunctival implants. *Drug Deliv.* 2016;23(9):3279–3284.
8. Feng Y, Feng G, Peng S, et al. The effect of hormone replacement therapy on dry eye syndrome evaluated with Schirmer test and break-up time. *J Ophthalmol*. 2015;2015:420302.
9. Feng Y, Feng G, Peng S, et al. The effects of hormone replacement therapy on dry eye syndromes evaluated by Schirmer test depend on patient age. *Cont Lens Anterior Eye*. 2015;39:124–127.
10. Erdem U, Ozdegirmenci O, Sobaci E, et al. Dry eye in post-menopausal women using hormone replacement therapy. *Maturitas*. 2007;56: 257–262.
11. Ablamowicz AF, Nichols JJ. Ocular surface membrane-associated mucins. *Ocul Surf*. 2016;14:331–341.
12. Uchino Y, Uchino M, Yokoi N, et al. Impact of cigarette smoking on tear function and correlation between conjunctival goblet cells and tear MUC5AC concentration in office workers. *Sci Rep*. 2016;6. Article number: 27699.
13. Coursey TG, Henriksson JT, Barbosa FL, et al. Interferon-γ-induced unfolded protein response in conjunctival goblet cells as a cause of mucin deficiency in Sjögren syndrome. *Am J Pathol*. 2016;186: 1547–1558.
14. Lin H, Qu Y, Geng Z, et al. Air exposure induced characteristics of dry eye in conjunctival tissue culture. *PLoS One*. 2014;9:e87368.
15. Zhao H, Jumblatt JE, Wood TO, et al. Quantification of MUC5AC protein in human tears. *Cornea*. 2001;20:873–877.
16. Corrales RM, Narayanan S, Fernández I, et al. Ocular mucin gene expression levels as biomarkers for the diagnosis of dry eye syndrome. *Invest Ophthalmol Vis Sci*. 2011;52:8363–8369.
17. Zhang J, Yan X, Li H. Analysis of the correlations of mucins, inflammatory markers, and clinical tests in dry eye. *Cornea*. 2013;32:928–932.
18. Yu DF, Chen Y, Han JM, et al. MUC19 expression in human ocular surface and lacrimal gland and its alteration in Sjögren syndrome patients. *Exp Eye Res*. 2008;86:403–411.
19. Watanabe H. Significance of mucin on the ocular surface. *Cornea*. 2002;21:17–22.
20. Yang L, Yang Z, Yu H, et al. Acupuncture therapy is more effective than artificial tears for dry eye syndrome: Evidence based on a meta-analysis. *Evid Based Complement Alternat Med*. 2015;2015:143858.

Effects of puerarin on spatial learning and memory function in mice with acute alcohol consumption: An evaluation based upon firing rate and oxygen saturation analysis

Weitao Li[A,D,F], Yan Zhang[B], Yanbai Xue[B,C], Hejuan Yu[B,C], Yameng Zhang[B], Ling Tao[E], Yamin Yang[D,E], Zhiyu Qian[A,F]

Department of Biomedical Engineering, College of Automation Engineering, Nanjing University of Aeronautics and Astronautics, China

A – research concept and design; B – collection and/or assembly of data; C – data analysis and interpretation;
D – writing the article; E – critical revision of the article; F – final approval of the article

Advances in Clinical and Experimental Medicine, ISSN 1899–5276 (print), ISSN 2451–2680 (online) *Adv Clin Exp Med*. 2019;28(2):171–178

Address for correspondence
Weitao Li
E-mail: liweitao@nuaa.edu.cn

Funding sources
National Natural Science Foundation of China (81727804 and 81601532), Jiangsu Science and Technology Support Plan (Social Development) (BE2016759), Natural Science Foundation of Jiangsu Province (BK20160814), and Scientific Research Foundation of Nanjing University of Aeronautics and Astronautics (YAH16009).

Conflict of interest
None declared

Received on April 27, 2017
Reviewed on August 18, 2017
Accepted on December 21, 2017

Published online on October 9, 2018

Abstract

Background. Ethanol is associated with various medical comorbidities affecting the brain and central nervous system.

Objectives. The use of puerarin in treating alcohol-induced memory disorders is systematically evaluated in this study based upon an analysis of the firing rate and oxygen saturation (SO_2).

Material and methods. A multi-channel data acquisition system and near-infrared spectroscopy (NIRS) were combined to obtain the electroneurophysiological signals and SO_2 in the hippocampus of mice from the Institute of Cancer Research (ICR) after ethanol injection. A T-maze test was performed to study the alteration of spatial memory function. Ethanol was administered intraperitoneally (i.p.) in 2 dosages (1.5 g/kg and 0.5 g/kg). To investigate the effects of puerarin against acute ethanol-induced memory impairment, the same parameters corresponding to electroneurophysiological signals, SO_2 and behavior performance in mice were also recorded upon the supplementation of puerarin in 2 dosages (25 mg/kg and 50 mg/kg).

Results. An inhibited firing rate and decreased SO_2 were found in mice treated with an ethanol dose of 1.5 g/kg, which resulted in a low correct choice rate in the T-maze test, while an opposite trend appeared in mice which had been administered a moderate ethanol dose (0.5 g/kg). The trend of SO_2 was positively correlated with that of the firing rate. A decreased firing rate and SO_2 were accompanied by a decrease in the correct choice rate. With the supplementation of puerarin, a significant increase in the mean firing rate and SO_2, as well as an improved correct choice rate, can be found in mice injected with excessive ethanol.

Conclusions. The electroneurophysiological signals and NIRS were combined for the first time to prove that an excessive intake of ethanol can inhibit the spatial learning and memory function of mice. The supplementation of puerarin can suppress these adverse effects induced by ethanol at a high dosage, as evidenced by the increased firing rate and SO_2.

Key words: spatial memory, near-infrared spectroscopy, hippocampal neuron, microelectrode

Cite as
Li W, Zhang Y, Xue Y, et al. Effects of puerarin on spatial learning and memory function in mice with acute alcohol consumption: An evaluation based upon firing rate and oxygen saturation analysis. *Adv Clin Exp Med*. 2019;28(2):171–178. doi:10.17219/acem/81520

DOI
10.17219/acem/81520

Introduction

Alcohol abuse and alcoholism are serious public health problems throughout the world. Ethanol is associated with various medical comorbidities affecting numerous body systems, such as the brain and central nervous system.[1] The hippocampus, which is closely related to learning and memory function, can especially be affected by ethanol.[2,3] Thus, developing suitable medications and evaluating their use in the treatment of alcohol-induced disorders remains a challenging goal in alcohol-related research.

As a Chinese medicinal herb, *Puerariae radix* has been proven to reduce alcohol consumption in both humans and animals.[4,5] Puerarin is one of the main effective components of *Puerariae radix*.[6] It has been found that puerarin can inhibit oxidative stress induced by acute alcoholism.[7] Several studies have reported that the supplementation of a *Puerariae radix*-ethanol extract can inhibit lipid peroxidation in the liver and enhance the antioxidative defense competence of rats.[8] In addition, many studies have indicated that puerarin may ameliorate hippocampal neuronal death induced by oxygen/glucose deprivation in vitro and may improve the learning-memory ability after global cerebral ischemia and reperfusion in rats.[4,9]

Mounting evidence suggests that alcohol affects brain function by interacting with multiple neurotransmitter systems in the hippocampus.[10] It has been shown that the effects of ethanol on brain function are related to altered hippocampal physiology. However, the way the neurotransmitter systems are affected following medication (e.g., puerarin) for acute alcoholism, and how these changes in neurotransmission contribute to the protective effects of such medication, are poorly understood.

Electrophysiological technology using a microelectrode array can provide an important basis for the study of brain neural activities.[11,12] This technology could obtain high-resolution temporal and spatial response patterns of information in neural networks.[13] In addition, the distribution and change of blood oxygen in the cerebral cortex could be another indicator for understanding the activity of the brain under the influence of alcohol.[14] By using near-infrared spectroscopy (NIRS) noninvasively, oxygen saturation (SO_2) can be measured simultaneously while acquiring hippocampal neurophysiological data.

In this study, in order to investigate the effects of puerarin on the memory system of mice following acute alcohol consumption, microelectrodes and NIRS were combined in order to obtain the neurophysiological signals and SO_2 in the hippocampus, and a T-maze test was performed to evaluate the functioning of spatial memory. This research presents a novel approach to evaluating the protective effects of puerarin against acute ethanol-induced memory impairment in mice.

Material and methods

Animal preparation

The Institute of Cancer Research (ICR) male mice (~32 g) were purchased from the Qinglongshan Animal Experiment Center (Nanjing, China). After individualization (postnatal day 36), mice were housed in cages at a constant temperature (25 ±1°C) and controlled illumination (12-h light/dark cycle) and humidity (55 ±10%) for 7 days. Food and water were available ad libitum. All animal experimental procedures were conducted in accordance with the guidelines of the protocols approved by the Institution Animal Care and Use Committee at Nanjing University of Aeronautics and Astronautics, China.

The 9-week-old mice were randomly assigned to 8 groups and each group consisted of 8 mice. According to previous studies, the effective doses of puerarin mostly ranged from 25 to 100 mg/kg.[8] Therefore, in this study, dosages of 25 and 50 mg/kg of puerarin were chosen and all medications were injected intraperitoneally (ip.). For clarification, the groups of our experimental design are listed in Table 1. As control groups, the mice in groups G1 and G2 were injected with saline (1.5 g/kg) and puerarin (50 mg/kg), respectively. Groups G3–G5 and groups G6–G8 were defined as high-ethanol-dose groups and low-ethanol-dose groups, respectively. Groups G3 and G6 were injected with ethanol alone at different concentrations. Groups G4 and G5 were administered puerarin in doses of 25 and 50 mg/kg, respectively, 20 min after the injection of ethanol (1.5 g/kg). In groups G7 and G8, puerarin was administered in doses of 25 and 50 mg/kg, respectively, after the injection of ethanol at a lower dose (0.5 g/kg).

The mice were anesthetized by an initial injection i.p. of 5% chloral hydrate (~400 mg/kg). Then, the mice were placed in a stereotaxic frame with a skull-reduced flat orientation. An incision was made in the skin and a bur hole was drilled over the right side of the hippocampus after cleaning the skull surface. The center of the hole was roughly 1.8 mm posterior to the bregma and 1.5 mm lateral to the midline. Afterwards, the mice were implanted with a 2 × 4 nickel 14-cadmium microelectrode array (diameter:

Table 1. Groups of experimental design

Groups	Doses [g/kg b.w.]	Number of animals
G1	saline (1.5)	8
G2	puerarin (0.05)	8
G3	ethanol (1.5)	8
G4	ethanol (1.5) and puerarin (0.025)	8
G5	ethanol (1.5) and puerarin (0.05)	8
G6	ethanol (0.5)	8
G7	ethanol (0.5) and puerarin (0.025)	8
G8	ethanol (0.5) and puerarin (0.05)	8

~33 μm, impedance: <1 MΩ), targeting the hippocampal region (1–2 mm in depth). In addition, the NIRS probe was inserted in the adjacent region of the hippocampus.

Electrophysiological signal recording

After the mice awoke from anesthesia, 8-channel local field potentials (LFPs) and spikes were recorded simultaneously using a Cerebus Multi-Channel Acquisition System (Cyberkinetics, Foxborough, USA). The LFP data was amplified (gain: 5000), filtered (0.3–500 Hz) and sampled at 2 kHz. Spikes (high pass filter: 250–7500 Hz, sampled at 30 kHz) with a root mean square exceeding 5.0 were stored with the time stamps per channel. As shown in Fig. 1A, the system consists of an amplifier power supply, a neural signal amplifier, a processor, and a computer system. The location of the 8-channel microelectrode in the hippocampus of the brain is illustrated in Fig. 1C. The procedure of ethanol and puerarin injection and measurement is shown in the upper row of Fig. 1D, and the dash circles indicate the location of the hole in the skull.

Prior to any intraperitoneal injection, a 5-min baseline of a spontaneous neural electrophysiological signal was first recorded. Neural activity recording started upon the injection of ethanol and continued for 80 min. Four spontaneous electrophysiological signals at a bin width of 5 min were stored with a time interval of 20 min.

Spike recording and data analysis

Spike acquisition and collection was carried out with a Cerebus system (Blackrock Microsystems LLC, Salt Lake City, USA). To obtain a spike signal, the wide-band electrophysiological signals were filtered at 0.25–5 kHz. The power (root mean square) of the filtered signal in a sliding window of 0.2 ms was calculated for spike detection. Spikes with a power of more than 5 times the standard deviation (SD) from the baseline mean were extracted. The spike waveforms were reconstructed to 30 kHz based on the sampling theorem. The units were then identified and de-noised by clustering software Wave_Clus (University of Leicester, UK). The sorting neuron firing rate was obtained at a bin width of 10 s.

Oxygen saturation measurement

Along with electrophysiological signal recording, SO_2 in the hippocampus of the mice was simultaneously measured using a customized NIRS monitoring system developed by our lab. The schematic design of the NIRS system is shown in Fig. 1B. The system consists of an integrated double optical fiber probe (diameter: 200 um), a halogen light source (HL2000-HP-FHSA; Ocean Optics, Largo, USA), a fiber optic spectrometer (USB2000; Ocean Optics), and a computer with custom monitoring software (Laboratory of Biomedical Photonics, Nanjing University of Aeronautics and Astronautics, China).[15,16] The SO_2 value of the NIRS monitoring system was validated by an ISS Oximeter (96208; ISS, Champaign, USA).[17] Then, this device was utilized to monitor changes in SO_2 before and after the injection of alcohol and puerarin in mice, starting from 10 min before ethanol injection. We recorded NIRS signals in the hippocampus for a total duration of 90 min. Oxygen saturation data acquisition lasted for 80 min post-ethanol administration and 60 min post-puerarin injection.

T-maze test

In order to investigate the effects of ethanol consumption with or without puerarin injection on spatial working memory, a T-maze test was performed in mice. The mice were maintained on a restricted diet and kept at 85% of free-feeding body weight during the behavioral testing in order to maintain the appetitive motivation. The mice first received a 5-min training session to adapt to the T-maze prior to testing. This training session was carried out 2 times per day for 3 consecutive days by placing 4 grain pellets (45 mg) in the 2 arms of the T-maze. Then, a forced choice training of left-right discrimination was performed 8 times per day for 2 consecutive days. In the study, the arm on the right side of the T-maze was set as the correct one. With the addition of reward pellets in the right arm, the mice were trained to retrieve their spatial working memory and to choose the right direction in the T-maze test. The forced choice training was repeated until the mice achieved a correct choice rate of at least 15/16 for 2 consecutive days. Qualified mice were then administered ethanol and puerarin under various conditions, and the correct choice rate was recorded.

Statistical analysis

Statistical analysis was performed using SPSS software (SPSS Statistics v. 19.0, IBM Corp., Armonk, USA) by one-way analysis of variance (ANOVA) test and subsequent Dunnett's post-hoc test. Differences were considered to be statistically significant at $p < 0.05$.

Results

In consideration of the physiological variation of different mice, we normalized the mean firing rate between 0 and 1 in different experiments. As shown in Fig. 2A, the mean firing rate decreased immediately after acute ethanol administration at a dosage of 1.5 g/kg (G3), continued declining and reached its lowest point at 20 min post-injection. It then gradually recovered and returned to its normal level by the 80 min mark. However, with a lower dosage of ethanol of 0.5 g/kg (G6), the mean firing rate of neurons remained steady and caused a slight increase at 20 min post-injection. The effects of puerarin (G2) by itself on the mean firing rate were also studied,

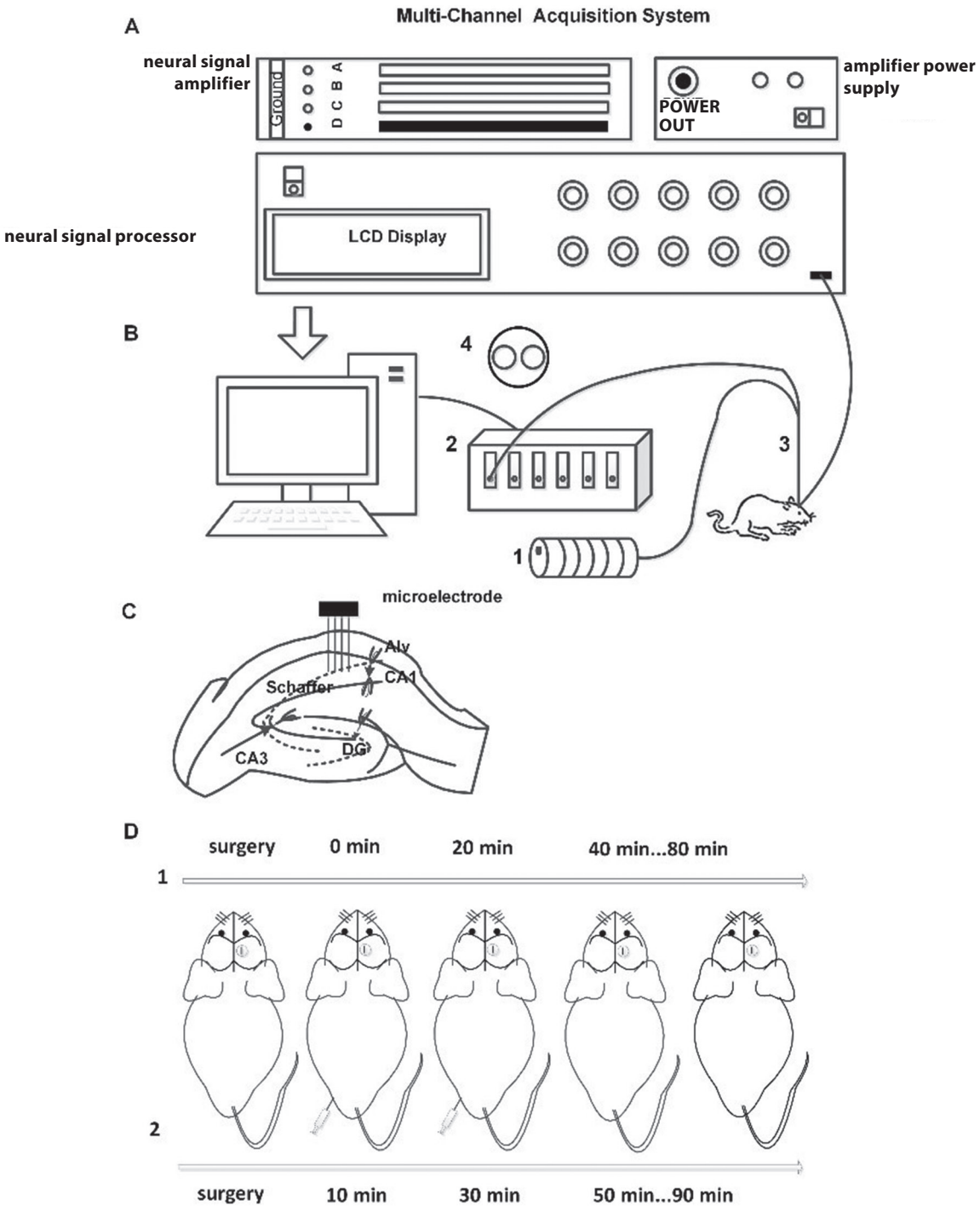

Fig. 1. Experimental setup of electrophysiological signal and SO_2 recording

A – schematic diagram of multi-channel data acquisition system; B – schematic illustration of near-infrared spectroscopy (NIRS) monitoring system for oxygen saturation (SO_2) consisting of: 1 – halogen light source; 2 – fiber optic spectrometer; and 3 – optical fiber probe; C – the location of the microelectrode in the hippocampus of mice; D – experiment procedure including: 1 – electrophysiological experiment and 2 – NIRS experiment (the dashed circles present the location of the hole in the skull).

and it is suggested that puerarin alone may also alter the mean firing rate with a decreasing tendency.

After ethanol exposure, with the supplementation of puerarin, significant changes in the mean firing rate of neurons in the hippocampal region were found. As shown in Fig. 2B and 2C, in the mice injected with ethanol in a higher dosage (G4 and G5), a higher mean firing rate was observed with the involvement of puerarin. In addition, a higher dose of puerarin (50 mg/kg) caused a higher mean firing rate. However, as to the mice injected with ethanol in a lower dosage (G7 and G8), the mean firing rate was lower with the combination of puerarin. The effects of puerarin are also dose-dependent, with the higher dosage of puerarin (50 mg/kg) causing a significantly lower mean firing rate.

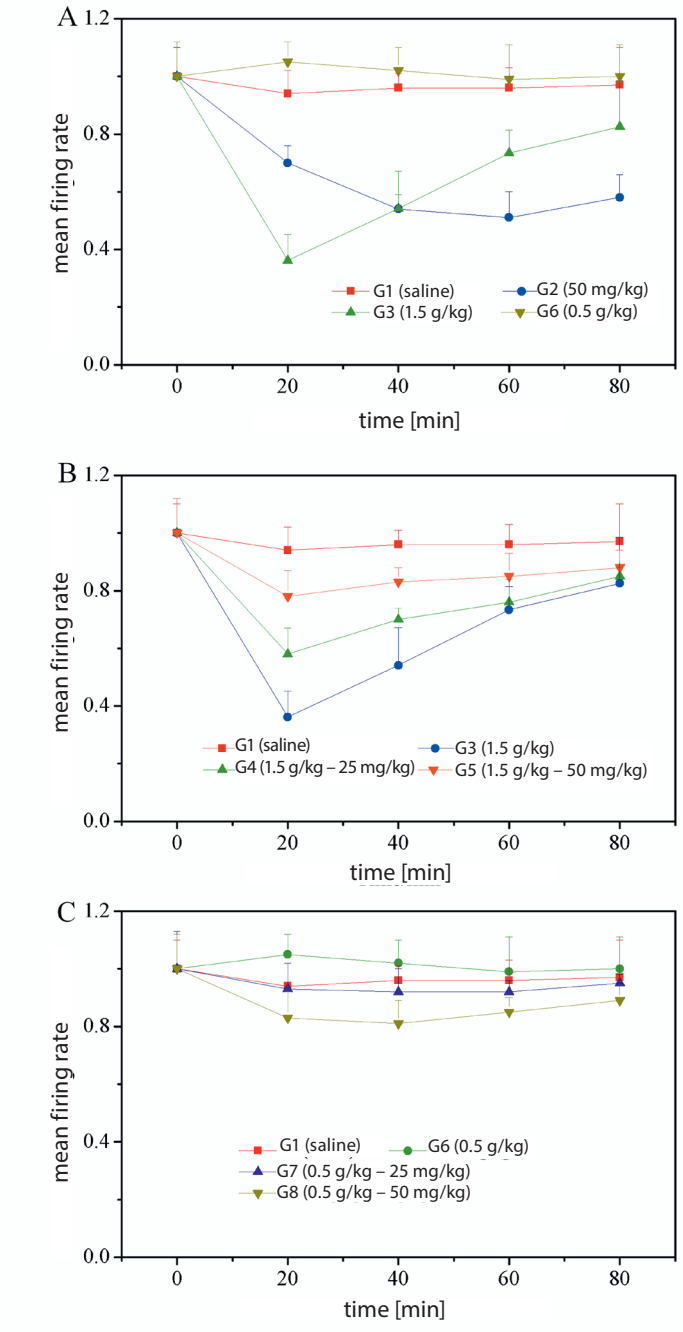

Fig. 2. Mean firing rate

A – mice injected with ethanol in higher (1.5 g/kg) and lower (0.5 g/kg) dosages; B – mice injected with a combination of ethanol in a higher dosage (1.5 g/kg) and puerarin (25 and 50 mg/kg); C – mice injected with a combination of ethanol in a lower dosage (0.5 g/kg) and puerarin (25 and 50 mg/kg); mice injected with saline (1.5 g/kg) were used as the control group; the mean firing rate of mice injected only with puerarin (50 mg/kg) is also presented.

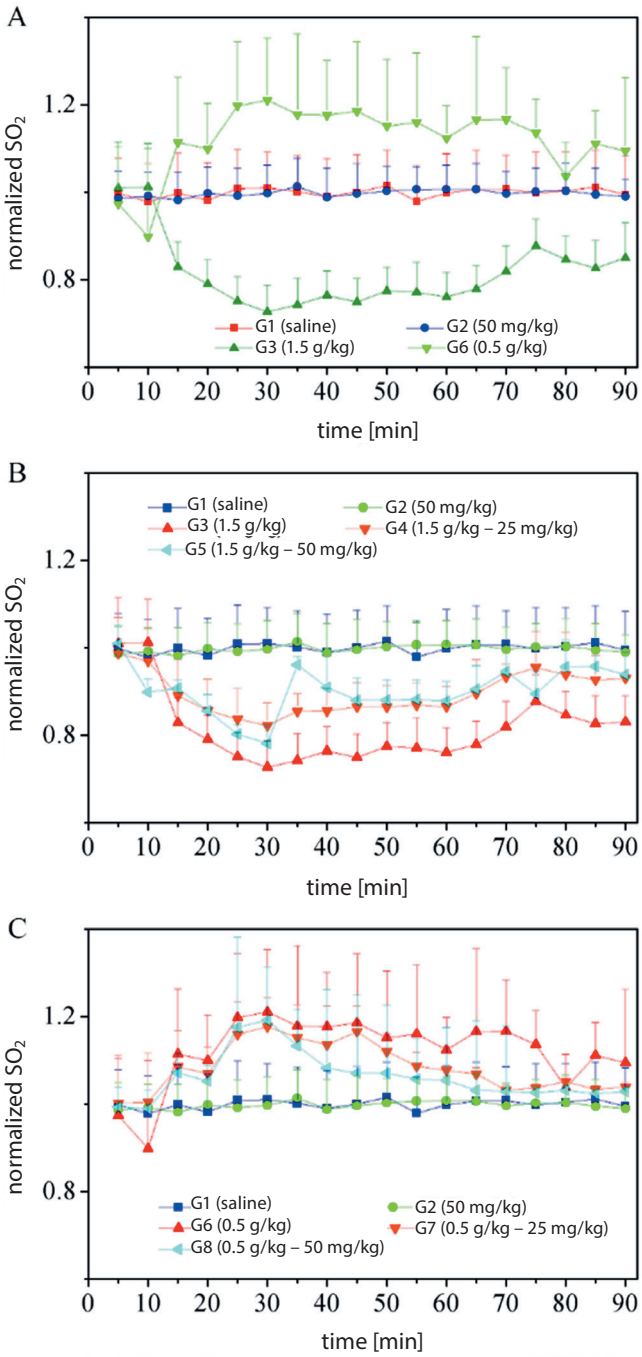

Fig. 3. Normalized oxygen saturation (SO_2)

A – mice injected with ethanol in higher (1.5 g/kg) and lower (0.5 g/kg) dosages; B – mice injected with a combination of ethanol in a higher dosage (1.5 g/kg) and puerarin (25 and 50 mg/kg); C – mice injected with a combination of ethanol in a lower dosage (0.5 g/kg) and puerarin (25 and 50 mg/kg); mice injected with saline (1.5 g/kg) were used as the control group; the normalized SO_2 of mice injected only with puerarin (50 mg/kg) is also presented; in each group, data at 10-minute intervals was collected for a baseline, and puerarin at various concentrations was injected 20 min after ethanol administration.

To investigate the effects of puerarin on mice following acute alcohol consumption, SO_2 was measured after various treatments. Considering the individual differences, SO_2 data was normalized to the SO_2 value at the 1st sampling time-point. As shown in Fig. 3A, the normalized SO_2 in G3, which was injected with ethanol in a higher dosage (1.5 g/kg), was significantly lower ($p < 0.05$) than that of G1 (saline), while SO_2 showed a significant increase ($p < 0.05$) in mice from G6, injected with ethanol in a lower dosage (0.5 g/kg). Similar to the negative control group, puerarin by itself showed no obvious changes in SO_2 in mice. In Fig. 3B, under ethanol consumption in a higher dosage (1.5 g/kg), the SO_2 level increased significantly with the supplementation of puerarin in both dosages (25 mg/kg

and 50 mg/kg). Meanwhile, SO_2 recovered more quickly in the group treated with puerarin in a higher dosage (G5) 10 min after injection.

In Fig. 3C, the SO_2 value in G6 is higher than that of G1. Then, with the supplementation of puerarin in various dosages (G7 and G8), the SO_2 value decreased obviously. The tendency of SO_2 in Fig. 3C is opposite to that presented in Fig. 3B.

To evaluate the effects on the spatial memory of mice after ethanol and puerarin administration, a T-maze test was performed; the results are presented in Fig. 4. The correct choice rate of mice in G1 (saline injection, 1.5 g/kg) did not show an obvious change during the entire time period, while in mice treated with puerarin (G2), the correct choice rate decreased in the first 60 min, and then increased gradually, as shown in Fig. 4A.

As shown in Fig. 4B, following ethanol consumption, a higher dosage of puerarin (G5; 50 mg/kg) resulted in a significant increase in the correct choice rate in mice compared to the ethanol group (G3), while the correct choice rate in mice treated with a lower dosage of puerarin (G4; 25 mg/kg) was remarkably lower than that of G5. This indicates that, under excessive ethanol consumption, puerarin can resolve the deficit of spatial learning and memory function.

In Fig. 4C, interestingly, the correct choice rate of mice in the ethanol group of the lower dosage (G6; 0.5 g/kg) was consistent with that of the saline group, while the injection of puerarin in ethanol-treated mice led to a decrease in the correct choice rate. This suggests that, in contrary to the above-mentioned results, under excessive alcohol exposure, ethanol in low doses could result in neuronal excitation and an opposite response to puerarin.

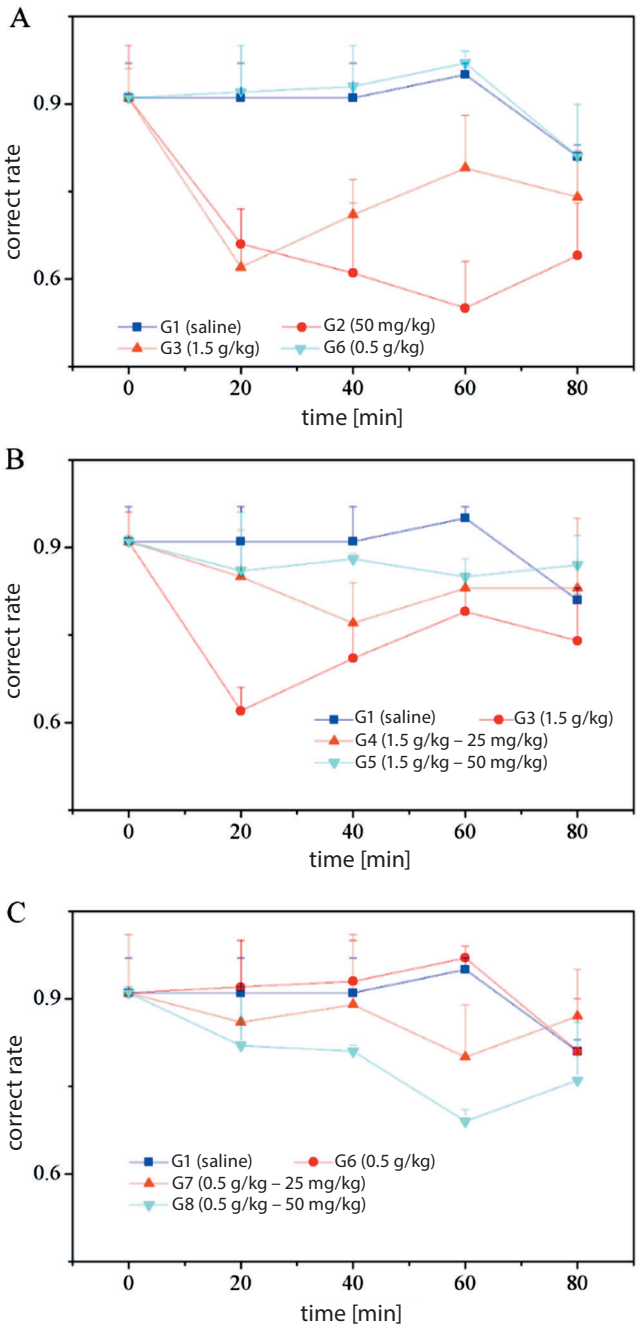

Fig. 4. The average correct choice rate of mice in a T-maze test

A – after ethanol injection alone; B – after ethanol injection in a higher dosage (1.5 g/kg), followed by puerarin injection (25 and 50 mg/kg); C – after ethanol injection in a lower dosage (0.5 g/kg), followed by puerarin injection (25 and 50 mg/kg); mice injected with saline (1.5 g/kg) were used as the control group; the average correct choice rate of mice injected only with puerarin (50 mg/kg) is also presented.

Discussion and conclusions

In our study, electrophysiological signals and SO_2 in the hippocampal region of mice were first obtained in vivo before and after the administration of ethanol. As in the case of our previous results, an ethanol dosage of 1.5 g/kg inhibited the firing rate of neurons. By inhibiting the function of glutamate receptors and/or altering the balance between inhibitory and excitatory neurotransmission, acute alcohol consumption can cause cognitive impairment in certain brain areas, such as the hippocampus, amygdale and striatum.[18] Interestingly, however, ethanol at a lower dosage (0.5 g/kg) resulted in the opposite tendency. This suggests that the inhibitory effects of ethanol on the brain are highly dependent on the dose of ethanol applied.

In addition to electrophysiological changes, a lot of evidence suggested that alcohol could decrease the affinity of hemoglobin to oxygen, resulting in lower SO_2 levels. Alcohol ingestion was reported to increase the incidence of arterial oxygen desaturation and disordered breathing during sleep.[19] Therefore, SO_2 could be another indicator which reveals the effects of ethanol on the brain and could be used to evaluate the effectiveness of medications in treating alcoholism. By integrating NIRS with an electrophysiological signal recording system, the SO_2 values in the hippocampus of mice under various treatments were obtained simultaneously. We found that changes of SO_2 were positively correlated with the firing rate. The decrease

in SO_2 was accompanied by a decline in the firing rate of mice injected with ethanol in higher dosages. Interestingly, similar dose-dependence was also found in SO_2 results, with higher SO_2 appearing in the lower-dosage ethanol group. Indeed, previous experiments have found that ethanol in a moderate dosage of 0.2 g/kg and 0.5 g/kg could somehow increase the activity of superoxide dismutase (SOD) and decrease the content of malondialdehyde (MDA), thus resulting in an increase of the neuron firing rate and SO_2 level.[20] In contrast, an excessive intake of ethanol caused a significantly greater reduction in SO_2 together with an obvious decrease in the firing rate.

In order to assess the effects of ethanol on spatial learning and memory function, we performed a T-maze test on mice under various treatments. Consistent with previous reports, we indeed found that the spatial memory function of mice could be impaired by excessive ethanol injection. Similar decreasing trends in both behavior performance and spike recording were observed in mice exposed to ethanol in a higher dosage (1.5 g/kg). The most significant spatial memory dysfunction appeared at the time-point when firing rates changed most drastically. In addition, the present study also provides direct evidence for the association between the impairment of spatial memory function and the changes of electrophysiological signals and SO_2. The results of the T-maze test show the same tendency regarding the firing rate and SO_2. These findings are consistent with previous results, suggesting that behavioral disorders and hippocampal dysfunctions would appear upon excessive intake of ethanol, while a moderate dosage of ethanol would not impair spatial memory in mice.[21]

Based on many years of clinical experience, *Puerariae radix* as a Chinese herbal medicine has been widely used to cure alcoholism.[22,23] Puerarin extracted from *Puerariae radix* is one of the main effective components which can suppress the severity of alcohol withdrawal symptoms. Previous studies have suggested that puerarin could reduce the ethanol concentration in the blood of Sprague Dawley® (SD) rats with acute ethanol intoxication.[24] The pharmacological function of puerarin also includes its vasodilative effects, which thereby increase oxygen supply to brain tissues. In our study, the protective effects of puerarin in ethanol-induced brain impairment were investigated by monitoring the typical changes of electrophysiological and SO_2 levels, and analyzing behavior performance during treatment. Puerarin had a significant antagonistic effect on the decreased firing rate, SO_2 level and correct choice rate upon acute high-dosage ethanol consumption. Previous studies have found that puerarin has strong antioxidant effects.[25,26] Indeed, in the present study, we found that oxygen desaturation induced by excessive ethanol consumption could be alleviated with the addition of puerarin. It indicated that ethanol-induced brain impairment could be suppressed by treatment with puerarin, as evidenced by the increased firing rate and SO_2 level, and improved behavior performance. Besides, the dose-dependent effects of puerarin on the firing rate and SO_2 are also consistent with previous in vitro findings, showing that cell viability was recovered dose-dependently with puerarin in ethanol-treated cells.

In conclusion, electrophysiological signal analysis and NIRS were combined for the first time to prove that the impairment of spatial learning and memory of mice induced by ethanol is dose-dependent. An excessive consumption of ethanol is required to cause detrimental effects on the spatial memory of mice by modulating electrophysiological transmission and SO_2 in brain tissue. Our research showed that puerarin could inhibit ethanol-induced brain impairment by ameliorating oxidative reactions in vivo against the adverse effect of ethanol injection. These findings highlight the significance of our study in providing an innovative approach to evaluate the use of the medication in the treatment of alcohol-induced brain disorders.

References

1. Constant A, Sherlaw W, Kovess-Masfety V. Seeking mental health care from private health practitioners among individuals with alcohol dependence/abuse results from a study in the French general population. *Alcohol*. 2017;59:1–6.
2. Wimmer, GE, Shohamy D. Preference by association: How memory mechanisms in the hippocampus bias decisions. *Science*. 2012; 338(6104):270–273.
3. Elibol-Can B, Kilic E, Yuruker S, Jakubowska-Dogru E. Investigation into the effects of prenatal alcohol exposure on postnatal spine development and expression of synaptophysin and PSD95 in rat hippocampus. *Int J Dev Neurosci*. 2014;33:106–114.
4. Zou, Y, Hong B, Fan L, Zhou L, Liu Y, Wu Q. Protective effect of puerarin against beta-amyloid-induced oxidative stress in neuronal cultures from rat hippocampus: Involvement of the gsk-3β/nrf2 signaling pathway. *Free Radic Res*. 2013;47(1):55–63.
5. Zhang R, Hu Y, Yuan J, Wu D. Effects of puerariae radix extract on the increasing intestinal permeability in rat with alcohol-induced liver injury. *J Ethnopharmacol*. 2009;126(2):207–214.
6. Liu CM, Ma JQ, Sun YZ. Puerarin protects rat kidney from lead-induced apoptosis by modulating the pi3k/akt/enos pathway. *Toxicol Appl Pharmacol*. 2012;258(3):330–342.
7. Zhao SS, Yang WN, Jin H, Ma KG, Feng GF. Puerarin attenuates learning and memory impairments and inhibits oxidative stress in STZ-induced SAD mice. *Neurotoxicology*. 2015;51:166–171.
8. Lee O. Effects of supplementation of puerariae radix ethanol extract on the antioxidative defense system in rats. *Korean J Nutr*. 2004;37: 872–880.
9. Wu HQ, Guo HN, Wang HQ, Chang MZ, Zhang GL, Zhao YX. Protective effects and mechanism of puerarin on learning-memory disorder after global cerebral ischemia-reperfusion injury in rats. *Chin J Integr Med*. 2009;15(1):54–59.
10. Jonsson S, Ericson M, Söderpalm B. Modest long-term ethanol consumption affects expression of neurotransmitter receptor genes in the rat nucleus accumbens. *Alcohol Clin Exp Res*. 2014;38(3):722–729.
11. Shahidi S, Zargooshnia S, Asl SS, Komaki A, Sarihi A. Influence of N-acetyl cysteine on beta-amyloid-induced Alzheimer's disease in a rat model: A behavioral and electrophysiological study. *Brain Res Bull*. 2017;131:142–149.
12. Horvath G, Petrovszki Z, Kekesi G, et al. Electrophysiological alterations in a complex rat model of schizophrenia. *Behav Brain Res*. 2016;307:65–72.
13. Chernov MM, Chen G, Torre-Healy LA, Friedman RM, Roe AW. Microelectrode array stimulation combined with intrinsic optical imaging: A novel tool for functional brain mapping. *J Neurosci Meth*. 2016;263:7–14.

14. Migliorini R, Moore EM, Glass L, et al. Anterior cingulate cortex surface area relates to behavioral inhibition in adolescents with and without heavy prenatal alcohol exposure. *Behav Brain Res*. 2015;292:26–35.
15. Qian Z, Victor SS, Gu Y, Giller CA, Liu H. "Look-ahead distance" of a fiber probe used to assist neurosurgery: Phantom and Monte Carlo study. *Opt Express*. 2003;11:1844–1855.
16. Li W, Qian Z, Li T. Method to improve the performance of reflectance diffuse optical imaging based on polygonal optical fibers arrangement. *Chin Opt Lett*. 2009;7:852–856.
17. Yubing L, Hongke W, Yangyang L, Weitao L, Zhiyu Q. Monte Carlo and phantom study in the brain edema models. *J Innov Opt Health Sci*. 2017;10(3):1–11.
18. Matthews DB, Simson PE, Best PJ. Ethanol alters spatial processing of hippocampal place cells: A mechanism for impaired navigation when intoxicated. *Alcohol Clin Exp Res*. 1996;20(2):404–407.
19. Carole W, Sherry L, Taasan VC, Block AJ, Boysen PG, Wynne JW. Alcohol increases sleep apnea and oxygen desaturation in asymptomatic men. *Am J Med*. 1981;71(2):240–245.
20. Zhao SM, Huang JJ, Huang LJ, Xian-Jiao HE, Jin L. Effects of different dose alcohol on the sod activity and mda content in rabbits. *Journal of Youjiang Medical College for Nationalities*. 2000;22(05):689-690.
21. Novier A, Van Skike CE, Chin VS, Diazgranados JL, Matthews DB. Low and moderate doses of acute ethanol do not impair spatial cognition but facilitate accelerating rotarod performance in adolescent and adult rats. *Neurosci Lett*. 2012;512(1):38–42.
22. Liu Y, Yang Y, Sun M. Highly specific noninvasive photoacoustic and positron emission tomography of brain plaque with functionalized croconium dye labeled by a radiotracer. *Chem Sci*. 2017;8(4):2710–2716.
23. Nie L, Guo Z, Wang LV. Photoacoustic tomography of monkey brain using virtual point ultrasonic transducers. *J Biomed Opt*. 2011;16(7):076005.
24. Barry DI, Hemmingsen R. Cerebral blood flow autoregulation during acute ethanol intoxication in the rat. *Acta Pharmacol Toxicol (Copenh)*. 1984;54(3):227–232.
25. Ronis MJ, Hennings L, Stewart B, Basnakian AG, Apostolov EO, Albano E. Effects of long-term ethanol administration in a rat total enteral nutrition model of alcoholic liver disease. *Am J Physiol Gastrointest Liver Physiol*. 2011;300(1):109–119.
26. Noh BK. Restoration of autophagy by puerarin in ethanol-treated hepatocytes via the activation of AMP-activated protein kinase. *Biochem Biophys Res Commun*. 2011;414(2):361–366.

The importance of the Wnt/β-catenin pathway and LRP5 protein in bone metabolism of postmenopausal women

Adam Kamiński[1,A,B,F], Monika Karasiewicz[2,B–E], Anna Bogacz[3,4,B–E], Karolina Dziekan[3,B,C], Agnieszka Seremak-Mrozikiewicz[5,6,A,F], Bogusław Czerny[3,7,B,E]

[1] Department of Orthopedics and Traumatology, Independent Public Clinical Hospital No. 1, Pomeranian Medical University in Szczecin, Poland
[2] Laboratory of International Health, Department of Preventive Medicine, Poznan University of Medical Sciences, Poland
[3] Department of Stem Cells and Regenerative Medicine, Institute of Natural Fibres and Medicinal Plants, Plewiska, Poland
[4] Department of Histocompatibility with Laboratory of Genetic Diagnostics, Regional Blood Center, Poznań, Poland
[5] Division of Perinatology and Women's Diseases, Poznan University of Medical Sciences, Poland
[6] Department of Pharmacology and Phytochemistry, Institute of Natural Fibres and Medicinal Plants, Plewiska, Poland
[7] Department of General Pharmacology and Pharmacoeconomics, Pomeranian Medical University, Szczecin, Poland

A – research concept and design; B – collection and/or assembly of data; C – data analysis and interpretation;
D – writing the article; E – critical revision of the article; F – final approval of the article

Advances in Clinical and Experimental Medicine, ISSN 1899–5276 (print), ISSN 2451–2680 (online) *Adv Clin Exp Med*. 2019;28(2):179–184

Address for correspondence
Monika Karasiewicz
E-mail: karasiewicz.m@wp.pl

Funding sources
None declared

Conflict of interest
None declared

Received on January 16, 2017
Reviewed on February 12, 2017
Accepted on November 8, 2017

Published online on July 2, 2018

Abstract

Background. Postmenopausal osteoporosis is the most common metabolic bone disease among women. The Wnt signaling pathway has been known to be the critical regulator of osteoblastogenesis. Alterations in this mechanism may have consequences for bone remodeling in humans.

Objectives. The aim of the study was to evaluate the frequency of genotypes and alleles of single nucleotide polymorphism (SNP) rs4988321 and rs312009 of *LRP5* in Polish postmenopausal women with osteopenia (n = 109) and osteoporosis (n = 333). Potential correlations between genetic polymorphisms, bone mineral density (BMD), risk for bone fractures, and other clinical parameters were analyzed.

Material and methods. Genomic DNA was extracted from the blood samples and the sequence polymorphisms of *LRP5* gene were detected using real-time polymerase chain reaction (RT-PCR) methods with melting curve analysis. We also calculated the odds ratio (OR) for the *LRP5* genotypes and the alleles. Then, we evaluated the effect of the *LRP5* polymorphism on T-score, Z-score, L2L4AM, L2L4YA, L2L4BMD, body mass index (BMI), and other clinical parameters.

Results. No statistically significant differences in the distribution of *LRP5* rs312009 genotypes between the groups were observed. Furthermore, our findings indicate that there is no correlation between *LRP5* genotypes and the clinical characteristics of women with osteopenia/osteoporosis. In contrast, there was an increased value of OR in heterozygotes for rs4988321, both in patients with osteopenia (OR = 1.47) and in those with osteoporosis (OR = 1.33). In our study, we were not able to calculate the OR parameter for the AA genotype due to its low prevalence in the population.

Conclusions. Our results suggest that the Val667Met *LRP5* (rs312009) polymorphism may contribute to an elevated risk for fractures in postmenopausal Polish women.

Key words: bone mineral density, LRP5, postmenopausal women, osteoporosis

Cite as
Kamiński A, Karasiewicz M, Bogacz A, Dziekan K, Seremak-Mrozikiewicz A, Czerny B. The importance of the Wnt/β-catenin pathway and LRP5 protein in bone metabolism of postmenopausal women. *Adv Clin Exp Med*. 2019;28(2):179–184. doi:10.17219/acem/79969

DOI
10.17219/acem/79969

Introduction

Osteoporosis is typically manifested by disturbances in the microstructure of bone tissue and increased susceptibility to bone fracture due to reduced bone mass. Due to its high incidence among patients over 50 years of age and the considerable costs of treatment, osteoporosis continues to be one of the greatest health challenges of an aging society. Osteoporotic fractures, which constitute the main consequences of the asymptomatic course of the disease, usually lead to long-term disability and even death. Over the last decade, studies on candidate genes, family analysis and genome-wide association studies (GWAS) resulted in the identification of numerous genetic loci related to osteoporosis. Genetic factors are believed to constitute 50–80% of individual differences in bone mineral density (BMD).[1] Studies on the background of skeletal dysplasias with decreased bone mass, e.g., brittle bone disease and the osteoporosis-pseudoglioma syndrome, pointed to the role of the Wnt/β-catenin pathway – including low-density lipoprotein receptor-related protein 5 (LRP5) and WNT1 – in the regulation of bone tissue homeostasis.[2–4]

The Wnt signaling pathway increases the activity and differentiation of bone marrow stem cells and stimulates the osteoblast lines, with a simultaneous decrease toward chondrogenic and adipogenic cell lines. Activation of that pathway inhibits the apoptosis of mature osteoblasts, thus extending their resilience.[5] Additionally, the Wnt/β-catenin pathway decreases osteoclast differentiation by stimulating the synthesis and secretion of osteoprotegerin, which regulates bone resorption by inhibiting osteoclast differentiation into mature forms.[6] The canonical Wnt signaling pathway plays an essential role in the regulatory processes of bone formation, so its disturbed activity may result in grave consequences for bone metabolism.[7–10] In short, LRP-5 and LRP-6 proteins, which belong to the low-density lipoprotein-receptor-related proteins (LDL) receptor family, function in this pathway as 1-domain co-receptors which, together with Fzd 7-domain endothelial receptor, facilitate the binding of the Wnt glycoproteins and the activation of cell response through β-catenin and Tcf/Lef factor-dependent transcription. The details of the Wnt signaling pathway have already been described.[11,12] The Wnt/β-catenin pathway is subject to antagonist regulation, sclerostin, Dkk1 and Dkk2, and Wnt modulator of surface ectoderm (Wise), for example, which – by binding to PRP5 – block access for the Wnt proteins and inhibit the classic signaling pathway, thus inhibiting osteoblastogenesis, induced via the Wnt/β-catenin pathway. The *LRP5* gene is expressed in the osteoblasts, and in vitro and in vivo studies have confirmed that its deletion inhibited osteoblast function, causing serious anomalies in bone phenotype.[7–9] This protein, via the Wnt pathway, influences the bone mass. The connection between the sequence polymorphism of that gene and bone mineral density (BMD) has been extensively studied.[13]

The review of the latest literature reports revealed that single nucleotide polymorphism (SNP) changes in genes encoding the LRP family proteins may also affect bone phenotype and, at the same time, present a risk for osteoporosis.[14] Studies on the phenotype–genotype relationship regarding osteoporosis seem to be crucial for early diagnosis and the development of treatment for postmenopausal osteoporosis, osteoarthritis, rheumatoid arthritis, and rare bone diseases.

Objectives

The aim of the study was to evaluate the frequency of the genotypes and alleles of SNP rs4988321 and rs312009 of *LRP5* in Polish postmenopausal women with osteopenia (n = 109) and osteoporosis (n = 333). The potential correlations between genetic polymorphisms, BMD, risk for bone fractures, and other clinical parameters were analyzed.

Material and methods

Patients

The study included 109 unrelated postmenopausal Caucasian women with osteopenia (mean age: 53.24 ±8.12 years) and 333 patients with osteoporosis (mean age: 56.06 ±8.83 years). The control group consisted of 233 postmenopausal women with normal T-scores (mean age: 53.38 ±8.2 years) recruited from the patients of the same hospital. Blood samples were collected at the Department of Orthopedics and Traumatology, Pomeranian Medical University in Szczecin, Poland. Bone densitometry was performed at the Laboratory of Densitometry, Clinical Hospital No. 1, Pomeranian Medical University in Szczecin, Poland, to determine the BMD values, T-scores and Z-scores. Bone mineral density was detected in the lumbar spine from L2 to L4 vertebrae using the dual energy X-ray absorptiometry (DEXA) method. Densitometry was performed using a Lunar DPX 100 camera (Lunar Corp., Madison, USA). A normal BMD value by DEXA is between one standard deviation (SD) from the mean with respect to the age of peak bone mass (–1 <T-score > 1). Based on these measurements, the women were classified into the following groups: osteopenia (–2.5 <T-score ≤1), osteoporosis (T-score ≤2.5) and normal T-score (T-score ≥1). The ratio of the average BMD in relation to the mean value for young adults (YA) and in comparison to age (age-matched – AM) was also evaluated. Furthermore, height and weight were measured and the body mass index (BMI) was calculated. During an interview with each patient, data on disease manifestation, drug use, age at 1st and last menstruation, gravidity, and birth weight were collected. The inclusion criteria for the genetic research were as follows: menopause at least 1 year before participation in the study, and no

hormone replacement therapy (HRT) or drugs taken affecting bone mass (selective estrogen receptor modulators (SERMs), calcitonin, bisphosphonates, heparin, steroids, thyroid hormones, antiepileptic drugs, GnRH analogues, or tibolone). The study excluded patients with endocrine and metabolic disorders, hematological diseases, kidney disease, cancer, and autoimmune and connective tissue disease, as well as who had undergone bilateral ovariectomy. Written informed consent was obtained from each patient. The Pomeranian Medical University Ethics Committee approved the study (approval No. KB-0012/100/15).

Genetic analysis

Genetic polymorphisms were determined at the Department of Stem Cell and Regenerative Medicine at the Institute of Natural Fibers and Medicinal Plants in Poznań, Poland. Genomic DNA was obtained from 5 mL of whole blood using a Qiagen DNA isolation kit (Qiagen, Hilden, Germany), according to the manufacturer's protocol. DNA concentration was measured using a DeNovix DS-11 Spectrophotometer (DeNovix Inc., Wilmington, USA). A LightCycler FastStart DNA Master HybProbe (Roche Diagnostics, Risch-Rotkreuz, Switzerland) assay and a LightCycler® 480 instrument for *LRP5* gene genotyping were used. The *LRP5* gene polymorphisms were performed using a LightSNiP LRP5 (TIBMolbiol, Berlin, Germany), which contained the primers and probes specific for the amplified fragment. Polymerase chain reaction (PCR) was performed in 10 µL of reaction mixture, according to the manufacturer's protocol, under the following conditions: initial denaturation at 95°C for 10 min, 35 cycles (denaturation at 95°C for 10 s, annealing at 60°C for 10 s, elongation for 15 s at 72°C, and melting for 30 s at 95°C and 40°C for 120 s). Polymorphism *LRP5* gene sequences were observed as different melting curves of PCR products. SPSS Statistics v. 17.0 for Windows (IBM Corp., Armonk, USA) was used for statistical analysis. We used the Hardy-Weinberg equation to calculate the expected genotype frequencies for each polymorphism, which were compared with the observed values using χ^2 test. The expected results are presented with 95% confidence intervals (CI). We also calculated the odds ratio (OR) for the genotypes and the alleles. Then, we evaluated the effect of the *LRP5* polymorphism on T-score, Z-score, L2L4AM, L2L4YA, L2L4BMD, BMI, and other clinical parameters. A correlation analysis between genotypes and clinical parameters using one-way analysis of variance (ANOVA) test was performed. A p-value <0.05 was considered statistically significant.

Results

The distribution of genotype frequency is consistent with the Hardy-Weinberg equation, both for *LRP5* rs312009 (Tables 1–3) and rs4988321 (Table 3, 4). The χ^2 test found no statistically significant differences between the values obtained for the rs312009 (p = 0.334) and rs4988321

Table 1. Frequency of the genotype and allele of the *LRP5* rs312009 polymorphism in women with osteopenia and the controls

Genotype/ allele	Osteopenia		Controls		OR	95% CI	p-value
	observed value n [%]	expected value [%]	observed value n [%]	expected value [%]			
CC	76 (69.7)	68.9	141 (60.5)	61.6	1.50	0.90–2.53	0.06
CT	29 (26.6)	28.2	84 (36.1)	33.8	0.64	0.37–1.09	0.05
TT	4 (3.7)	2.9	8 (3.4)	4.6	1.09	0.23–4.11	0.57
Total	109 (100)	100	233 (100)	100	–	–	–
C	181 (83)	–	366 (78.5)	–	1.34	0.87–2.09	0.10
T	37 (17)	–	100 (21.5)	–	0.75	0.48–1.15	0.10
Total	218 (100)	–	466 (100)	–	–	–	–

OR – odds ratio; CI – confidence interval.

Table 2. Frequency of the genotype and allele of the *LRP5* rs312009 polymorphism in women with osteoporosis and the controls

Genotype/ allele	Osteoporosis		Controls		OR	95% CI	p-value
	observed value n [%]	expected value [%]	observed value n [%]	expected value [%]			
CC	196 (58.9)	59.6	141 (60.5)	61.6	0.93	0.65–1.33	0.38
CT	122 (36.6)	35.2	84 (36.1)	33.8	1.02	0.71–1.48	0.48
TT	15 (4.5)	5.2	8 (3.4)	4.6	1.33	0.52–3.68	0.34
Total	333 (100)	100	233 (100)	100	–	–	–
C	514 (77.2)	–	366 (78.5)	–	0.92	0.69–1.24	0.32
T	152 (22.8)	–	100 (21.5)	–	1.08	0.81–1.46	0.32
Total	666 (100)	–	466 (100)	–	–	–	–

OR – odds ratio; CI – confidence interval.

Table 3. Frequency of the genotype and allele of the *LRP5* rs4988321 polymorphism in women with osteopenia and the controls

Genotype/ allele	Osteopenia		Controls		OR	95% CI	p-value
	observed value n [%]	expected value [%]	observed value n [%]	expected value [%]			
GG	98 (89.9)	89.3	1,218 (93.6)	93.7	0.61	0.25–1.54	0.17
GA	10 (9.2)	10.4	15 (6.4)	6.2	1.47	0.57–3.63	0.24
AA	1 (0.9)	0.3	0	0.1	–	–	–
Total	109 (100)	100	233 (100)	100	–	–	–
G	206 (94.5)	–	451 (96.8)	–	0.57	0.24–1.36	0.11
A	12 (5.5)	–	15 (3.2)	–	1.75	0.73–4.09	0.11
Total	218 (100)	–	466 (100)	–	–	–	–

OR – odds ratio; CI – confidence interval.

Table 4. Frequency of the genotype and allele of the *LRP5* rs4988321 polymorphism in women with osteoporosis and the controls

Genotype/ allele	Osteoporosis		Controls		OR	95% CI	p-value
	observed value n [%]	expected value [%]	observed value n [%]	expected value [%]			
GG	305 (91.6)	91.8	218 (93.6)	93.7	0.75	0.36–1.49	0.24
GA	28 (8.4)	8.0	15 (6.4)	6.2	1.33	0.67–2.75	0.24
AA	0	0.2	0	0.1	–	–	–
Total	333 (100)	100	233 (100)	100	–	–	–
G	638 (95.8)	–	451 (96.8)	–	0.76	0.37–1.49	0.25
A	28 (4.2)	–	15 (3.2)	–	1.32	0.67–2.69	0.25
Total	666 (100)	–	466 (100)	–	–	–	–

OR – odds ratio; CI – confidence interval.

(p = 0.179) study groups. An analysis of genotype frequency for the *LRP5* rs312009 polymorphism in women with osteopenia and osteoporosis and the controls revealed no statistically significant differences. No statistically significant differences were noted for allele frequency either (Tables 1, 2).

Increased OR values in heterozygotes for rs4988321 were noted in women with both osteopenia (OR = 1.47, 95% CI = 0.57–3.63, p = 0.24) and osteoporosis (OR = 1.33, 95% CI = 0.67–2.75, p = 0.24). In light of the sample size of our study, the OR for the AA genotype could not be established due to its relatively low incidence in the population. Increased OR values for the A allele were found in women with osteopenia (OR = 1.75, 95% CI = 0.73–4.09, p = 0.11) and osteoporosis (OR = 1.32, 95% CI = 0.67–2.69, p = 0.25) (Tables 3, 4). The genotype analysis for both *LRP5* polymorphisms revealed no statistically significant correlations in clinical features between the groups of women. Furthermore, characteristics of the study population (perimenopausal women with osteopenia, osteoporosis and normal T-scores) are presented in Table 5.

Discussion

The analyses of the genetic background of osteoporosis have indicated a relationship between a mutation in the 11q12-13 locus, the same one where the *LRP5* gene is located, and the incidence of osteoporosis-pseudoglioma syndrome (OPPG), autosomal dominant phenotype of high bone mass (HBM) and autosomal dominant osteoporosis type I.[15] Polymorphic variants, including Val667Met, have been suggested as being associated with BMD and the risk for fracture of various intensity and effect in different populations, which was confirmed by numerous multicenter studies.[14] The aim of our study was to evaluate the frequency of the polymorphisms in the *LRP5* gene in Polish postmenopausal women with osteopenia, osteoporosis, and normal T-scores, as well as to assess a possible relationship between genotypes and BMD values and other clinical features.

An analysis of genotype and allele frequency for the *LRP5* rs312009 polymorphism in women with osteopenia and osteoporosis and healthy controls revealed no statistically significant differences. An earlier study by Agueda et al. postulated a link between BMD of the lumbar region of the spine and SNP *LRP5* rs312009.[16] A nucleotide change (SNP rs312009) was proved to be located in the LRP5 5' region at the RUNX2 binding site. The rs312009-dependent variability was experimentally confirmed in 2 osteoblastic cell lines, with higher transcription activity in the T allele as compared to the C allele. In vitro studies found the mRNA LRP5 value to be RUNX2-dependent, thus proving a link between 2 bone-regulating systems – the RUNX2 transcription-factor cascade and the Wnt signaling pathway.[17] Panach et al. found significantly lower L2–L4 BMD values in women with the CC genotype, and elevated risk for osteoporosis as compared to TT and CT.[18]

Table 5. Characteristics of the study population (perimenopausal women with osteopenia, osteoporosis and normal T-scores)

Parameter		p-value	Mean	SEM	95% CI	
					lower limit	upper limit
T-score	osteopenia	<0.001[b]	–1.9072	0.05627	–1.9072	–1.7530
	osteoporosis		–3.1640		–3.2757	–3.0522
	controls		0.0779	0.11321	–0.1482	0.3040
	total		–1.8138	0.08072	–1.9727	–1.6549
Z-score	osteopenia	0.117[a]	–0.8448	0.08470	–1.0143	–0.6754
	osteoporosis	<0.001[b]	–3.5691	1.94626	–7.4572	0.3190
	controls		0.6425	0.19620	0.2423	1.0427
	total		–1.6696	0.81499	–3.2794	–0.0597
Weight [kg]	osteopenia	0.026[a]	65.1721	0.99502	63.2022	67.1420
	osteoporosis	0.001[b]	61.2088	0.93755	59.3462	63.0714
	controls		68.7273	1.49288	65.7458	71.7088
	total		64.7204	0.65801	63.4251	66.0157
Height [cm]	osteopenia	0.08[a]	162.6311	0.45083	161.7386	163.5237
	osteoporosis	0.01[b]	160.2527	0.52869	159.2024	161.3031
	controls		163.0758	0.73612	161.6056	164.5459
	total		161.9606	0.32149	161.3277	162.5934
BMI	osteopenia	0.04[a]	24.6445	0.35747	23.9368	25.3522
	osteoporosis	0.04[b]	23.7879	0.31784	23.1564	24.4193
	controls		25.8802	0.55665	24.7685	26.9919
	total		24.6574	0.23299	24.1988	25.1161
Age [years]	osteopenia	0.54[a]	53.2377	0.73506	51.7825	54.6930
	osteoporosis	0.014[b]	56.0643	0.74650	54.5883	57.5403
	controls		53.3788	1.01176	51.3582	55.3994
	total		54.4726	0.47138	53.5452	55.3999
Birth weight [g]	osteopenia	0.026[a]	3,226.7857	77.68484	3,067.3896	3,386.1818
	osteoporosis	0.005[b]	3,141.2500	134.07981	2,855.4656	3,427.0344
	controls		3,628.9474	110.29173	3,397.2330	3,860.6617
	total		3,326.3492	63.20235	3,200.0095	3,452.6889
Years of reproduction	osteopenia	0.724[a]	36.2000	0.63682	34.9257	37.4743
	osteoporosis	0.528[b]	35.6154	0.62160	34.3736	36.8572
	controls		36.3750	0.94586	34.4459	38.3041
	total		35.9936	0.40144	35.2007	36.7866
Age of first menstruation	osteopenia	0.636[a]	13.1167	0.30908	12.4982	13.7351
	osteoporosis	0.754[b]	12.9385	0.26843	12.4022	13.4747
	controls		13.3750	0.33224	12.6974	14.0526
	total		13.0955	0.17517	12.7495	13.4416
Age of last menstruation	osteopenia	0.069[a]	49.2099	0.49588	48.2230	50.1967
	osteoporosis	0.058[b]	48.1585	0.54804	47.0681	49.2490
	controls		50.1707	0.68512	48.7860	51.5554
	total		48.9804	0.32876	48.3322	49.6286
Number of pregnancies	osteopenia	0.869[a]	1.8852	0.09821	1.6908	2.0797
	osteoporosis	0.902[b]	1.9560	0.13525	1.6873	2.2247
	controls		1.9394	0.14940	1.6410	2.2378
	total		1.9211	0.07075	1.7819	2.0604
Years after menopause	osteopenia	0.854[a]	7.1833	0.77769	5.6272	8.7395
	osteoporosis	0.001[b]	10.6308	0.71305	9.2063	12.0553
	controls		7.0313	0.98832	5.0156	9.0469
	total		8.5796	0.48209	7.6273	9.5319
BMD L2–L4 [g/cm^2]	osteopenia	0.986[a]	0.9674	0.02003	0.9276	1.0072
	osteoporosis	0.944[b]	0.9752	0.01495	0.9456	1.0048
	controls		0.9694	0.02186	0.9254	1.0133
	total		0.9713	0.01066	0.9503	0.9923
BMD L2–L4 YA [%]	osteopenia	0.965[a]	80.9022	1.71939	77.4868	84.3175
	osteoporosis	0.982[b]	81.2783	1.24077	78.8203	83.7362
	controls		81.0204	1.77293	77.4557	84.5851
	total		81.0938	0.89537	79.3305	82.8570
BMD L2–L4 AM [%]	osteopenia	0.989[a]	89.1304	1.82717	85.5010	92.7599
	osteoporosis	0.968[b]	89.5043	1.23064	87.0665	91.9422
	controls		89.7755	1.93765	85.8796	93.6714
	total		89.4219	0.93156	87.5873	91.2564

CI – confidence interval; ANOVA – analysis of variance; BMD – bone mineral density; BMI – body mass index; SEM – standard error of the mean; [a] comparison between the groups with osteopenia and normal T-scores (one-way ANOVA); [b] comparison between the groups with osteoporosis and normal T-scores (one-way ANOVA).

In our study, we detected higher OR values in heterozygotes for rs4988321 SNP in women with both osteopenia (OR = 1.47, 95% CI = 0.57–3.63, p = 0.24) and osteoporosis (OR = 1.33, 95% CI = 0.67–2.75, p = 0.24). We were not able to determine the OR for the AA genotype in our groups due to its low incidence in the population. Elevated OR values for the A allele were found in women with osteopenia (OR = 1.75, 95% CI = 0.73–4.09, p = 0.11) and osteoporosis (OR = 1.32, 95% CI = 0.67–2.69, p = 0.25), which is consistent with the results of the study by van Meurs et al., who demonstrated the rs4988321 *LRP5* polymorphism (Val667Met) to be associated with vertebral fractures and lowered BMD values, with the OR for fracture estimated at 1.26 (95% CI = 1.08–1.47).[14] The rs4988321(A) allele was associated with a reduced BMD of the lumbar vertebrae ($p = 3.3 \times 10^{-8}$) and of the femoral neck ($p = 3.8 \times 10^{-5}$). Similarly, Stathopoulou et al. observed an association between the rs4988330 polymorphism with the corrected BMD value, and the presence of the A allele was connected with significantly lower BMD as compared to the GG genotype, although a higher calcium intake (>680 mg/day) diminished the unfavorable influence of that polymorphism on BMD.[19] In our study, all BMD values were higher only in the heterozygotes from the osteopenia group. Significant differences in the genotype distribution of the Val667Met (rs4988321) polymorphism were also reported for a population of Mexican women.[20] Analyses of the *LRP5* sequence polymorphism have visibly demonstrated ethnicity-related variations, as Sassi et al. found no correlation between the Val667Met genotype and the development of osteoporosis in Tunisian women.[1] Previously, SNP Val667Met had been suggested to determine BMD in men as well.[21] This might be explained by the fact that the polymorphic locus is located in the extracellular domain of the receptor, responsible for Dkk-1 binding, which – being the inhibitor of the pathway – might influence Wnt signaling activity.[1] The genetic factor continues to play an important role in BMD determination and in the variability of its values between individuals. Based on the International HapMap Project and GWAS, candidate genes which might modify BMD values have been selected. Regardless, despite numerous candidate gene association studies, identification of genetic predispositions for osteoporosis continues.[13] The literature offers countless examples that the Lrp5/Wnt/β-catenin pathway seems to be the main direction to establish effective therapies for diseases associated with lowered bone mass and increased risk for fractures. At present, although the influence of LRP5 and its homologues on BMD seems to be indisputable, the exact details of this association continue to be investigated.[22,23]

References

1. Sassi R, Sahli H, Souissi C, et al. Association of LRP5 genotypes with osteoporosis in Tunisian post-menopausal women. *BMC Musculoskelet Disord*. 2014;15:144.
2. Maupin KA, Droscha CJ, Williams BO. A comprehensive overview of skeletal phenotypes associated with alterations in Wnt/β-catenin signaling in humans and mice. *Bone Res*. 2013;1(1):27–71.
3. Lara-Castillo N, Johnson ML. LRP receptor family member associated bone disease. *Rev Endocr Metab Disord*. 2015;16(2):141–148.
4. Costantini A, Mäkitie O. Value of rare low bone mass diseases for osteoporosis genetic. *Bonekey Rep*. 2016;5:773.
5. Krishnan V, Bryant HU, Macdougald OA. Regulation of bone mass by Wnt signaling. *J Clin Invest*. 2006;116(5):1202–1209.
6. Johnson ML. LRP5 and bone mass regulation: Where are we now? *Bonekey Rep*. 2012;1:1. doi: 10.1038/bonekey.2012
7. Kato M, Patel MS, Levasseur R, et al. Cbfa1-independent decrease in osteoblast proliferation, osteopenia, and persistent embryonic eye vascularization in mice deficient in Lrp5, a Wnt coreceptor. *J Cell Biol*. 2002;157(2):303–314.
8. Babij P, Zhao W, Small C, et al. High bone mass in mice expressing a mutant LRP5 gene. *J Bone Miner Res*. 2003;18(6):960–974.
9. Akhter MP, Wells DJ, Short SJ, et al. Bone biomechanical properties in LRP5 mutant mice. *Bone*. 2004;35(1):162–169.
10. Liedert A, Röntgen V, Schinke T, et al. Osteoblast-specific Krm2 overexpression and Lrp5 deficiency have different effects on fracture healing in mice. *PloS One*. 2014;9(7):e103250.
11. Burgers TA, Williams BO. Regulation of Wnt/β-catenin signaling within and from osteocytes. *Bone*. 2013;54(2):244–249.
12. Wolski H, Drwęska-Matelska N, Seremak-Mrozikiewicz A, Lowicki Z, Czerny B. The role of Wnt/β-catenin pathway and LRP5 protein in metabolism of bone tissue and osteoporosis etiology [in Polish]. *Ginekol Pol*. 2015;86(4):311–314.
13. Zhang YP, Deng FY, Chen Y, et al. Replication study of candidate genes/loci associated with osteoporosis based on genome-wide screening. *Osteoporos Int*. 2010;21(5):785–795.
14. van Meurs JB, Trikalinos TA, Ralston SH, et al. GENOMOS Study. Large-scale analysis of association between LRP5 and LRP6 variants and osteoporosis. *JAMA*. 2008;299(11):1277–1290.
15. Van Hul E, Gram J, Bollerslev J, et al. Localization of gene causing autosomal dominant osteoporosis type I to chromosome 11q12-13. *J Bone Miner Res*. 2002;17(6):1111–1117.
16. Agueda L, Bustamante M, Jurado S. A haplotype-based analysis of the LRP5 gene in relation to osteoporosis phenotypes in Spanish postmenopausal women. *J Bone Miner Res*. 2008;23(12):1954–1963.
17. Agueda L, Velázquez-Cruz R, Urreizti R, et al. Functional relevance of the BMD-associated polymorphism rs312009: Novel involvement of RUNX2 in LRP5 transcriptional regulation. *J Bone Miner Res*. 2011;26(5):1133–1144.
18. Panach L, Mifsut D, Tarin JJ, Cano A, García-Pérez MÁ. Replication study of three functional polymorphisms associated with bone mineral density in a cohort of Spanish women. *J Bone Miner Metab*. 2014;32(6):691–698.
19. Stathopoulou MG, Dedoussis GV, Trovas G, et al. Low-density lipoprotein receptor-related protein 5 polymorphisms are associated with bone mineral density in Greek postmenopausal women: An interaction with calcium intake. *J Am Diet Assoc*. 2010;110(7):1078–1083.
20. Falcon-Ramirez E, Casas-Avila L, Cerda-Flores RM, et al. Association of LRP5 haplotypes with osteoporosis in Mexican women. *Mol Biol Rep*. 2013;40(3):2705–2710.
21. Grundberg E, Lau EM, Lorentzon M, et al. Large-scale association study between two coding LRP5 gene polymorphisms and bone phenotypes and fractures in men. *Osteoporos Int*. 2008;19(6):829–837.
22. Li WF, Hou SX, Yu B, Li MM, Férec C, Chen JM. Genetics of osteoporosis: Accelerating pace in gene identification and validation. *Hum Genet*. 2010;127(3):249–285.
23. Kumar J, Swanberg M, McGuigan F, Callreus M, Gerdhem P, Akesson K. LRP4 association to bone properties and fracture and interaction with genes in the Wnt- and BMP signaling pathways. *Bone*. 2011;49(3):343–348.

Cognitive impairment, event-related potentials and immunological status in patients with systemic lupus erythematosus

Magdalena Szmyrka[1,A–F], Anna Pokryszko-Dragan[2,A–F], Krzysztof Słotwiński[2,B,C,F], Ewa Gruszka[2,B,F], Lucyna Korman[1,B,F], Ryszard Podemski[2,E,F], Piotr Wiland[1,E,F]

[1] Department of Rheumatology and Internal Diseases, Faculty of Medicine, Wroclaw Medical University, Poland
[2] Department of Neurology, Faculty of Postgraduate Medical Training, Wroclaw Medical University, Poland

A – research concept and design; B – collection and/or assembly of data; C – data analysis and interpretation; D – writing the article; E – critical revision of the article; F – final approval of the article

Advances in Clinical and Experimental Medicine, ISSN 1899–5276 (print), ISSN 2451–2680 (online) *Adv Clin Exp Med*. 2019;28(2):185–192

Address for correspondence
Magdalena Szmyrka
E-mail: magdalena.szmyrka@umed.wroc.pl

Funding sources
Grant No. N N402 267336 obtained from the Committee for Research of the Polish Ministry of Science and Higher Education (KBN).

Conflict of interest
None declared

Received on June 6, 2017
Reviewed on June 27, 2017
Accepted on August 29, 2017

Published online on July 2, 2018

Abstract

Background. Cognitive impairment (CI) is a frequent problem in lupus patients, regardless of their overt neuropsychiatric (NP) involvement.

Objectives. The aim of our study was to test cognitive abilities in systemic lupus erythematosus (SLE) patients using neuropsychological testing and event-related potentials (ERPs), and to search for their cognitive abilities correlations with a wide range of auto-antibodies.

Material and methods. A total of 37 SLE patients were subjected to a battery of neuropsychological tests, recommended by the American College of Rheumatology (ACR), and to ERPs. They were also tested for a wide range of auto-antibodies (anti-cardiolipin (aCL), anti-β2-glycoprotein I (anti-β2-GPI), lupus anticoagulant, anti-dsDNA, anti-nucleosome, anti-ribosomal P (anti-Rib-P), anti-ganglioside, anti-Ro/SS-A, and anti-La/SS-B.

Results. Cognitive impairment was found in 35% of patients, mostly with NP SLE (NPSLE), and was associated with higher disease activity, measured by the SLE Disease Activity Index (SLEDAI), and with a longer duration of central nervous system (CNS) involvement. There were no differences in the immunological status between CI patients and those without cognitive decline, but some antibodies were correlated with worse results in certain neuropsychological tests (anti-dsDNA and worse results of Rey Complex Figure Test – RCFTc for copying and RCFTr for recall, and of verbal fluency test (VFT); aCL IgG and worse results in Digit Span (DS) and in RCFTc). Event-related potentials showed prolonged N200 and P300 latencies in SLE patients in comparison to controls, but no differences were found between SLE and NPSLE patients. Mean P300 latency was significantly longer in patients without anti-nucleosome antibodies.

Conclusions. Event-related potentials can be used as a complementary tool in assessing CI in SLE patients. The immunological status of patients with CI did not differ from that of patients without cognitive problems.

Key words: systemic lupus erythematosus, cognitive impairment, auto-antibodies, event-related potentials

Cite as
Szmyrka M, Pokryszko-Dragan A, Słotwiński K, et al. Cognitive impairment, event-related potentials and immunological status in patients with systemic lupus erythematosus. *Adv Clin Exp Med*. 2019;28(2):185–192. doi:10.17219/acem/76711

DOI
10.17219/acem/76711

Introduction

Systemic lupus erythematosus (SLE) is a chronic autoimmune disease with a heterogenous clinical picture. Nervous system involvement is frequently observed, affecting 14–75% of patients. In 1999, the American College of Rheumatology (ACR) proposed the nomenclature and definitions of 19 neuropsychiatric (NP) syndromes in SLE.[1] One of the most frequent neurological problems is cognitive impairment (CI).

Cognitive impairment may concern a various extent of particular domains, such as memory, executive function, visuospatial abilities, and others. It is characterized by a fluctuating course and may be affected by other factors (especially depression, fatigue and pain). Cognitive impairment has been observed both in patients with previous NP involvement in the course of neuropsychiatric SLE (NPSLE) and in patients without overt central nervous system (CNS) disease.

Over the past decade, there has been growing interest in cognitive dysfunction in SLE patients. Since 1999, ACR has recommended a battery of neuropsychological tests, validated by Kozora et al. in 2004 and dedicated to this particular group of patients, covering the cognitive domains most frequently affected in the course of SLE.[1,2] Apart from neuropsychological measures, event-related potentials (ERPs) are also considered a useful tool in an objective assessment of cognitive abilities. However, ERPs parameters as an electrophysiological index of cognitive function have rarely been investigated in SLE patients.[3–6]

The relationship between different auto-antibodies and NP syndromes in SLE remains a matter under investigation. Some auto-antibodies, such as antiphospholipid, are widely associated with nervous system involvement, while others (e.g., anti-Rib-P and anti-gangliosides) have been the subject of only a few studies and with equivocal results.

The purpose of our study was to use neuropsychological testing and ERPs in order to evaluate cognitive functions in SLE patients regarding their NPSLE status. We also aimed to analyze the relationships between cognitive performance and SLE clinical activity, as well as the immunological status of patients, including a wide range of auto-antibodies.

Material and methods

Patients

Thirty-seven patients (all Caucasian, 35 females, 2 males, aged 18–60 years, mean age: 38.3 years) were enrolled in the study (Table 1). All the patients fulfilled the 1997 updated ACR criteria for the diagnosis of SLE.[7,8] Patients were recruited from the Department of Rheumatology and Internal Diseases of Wroclaw Medical University, Poland. Subjects with a known history of comorbid neurological or psychiatric disorders not associated with SLE, with a history of substance abuse or with learning disability were excluded from the study. The control group consisted of 30 healthy volunteers, matched for age, gender and education level with the SLE patients.

Table 1. Demographic and clinical characteristics of patients with systemic lupus erythematosus (SLE)

Characteristic	Patients (n = 37)
Age [years]	18–60 (mean 38.3)
Gender	35 females, 2 males
Disease duration [years]	3–31 (mean 10)
NPSLE	24
Non-NPSLE	13
Mean NPSLE duration [years]	6
SLEDAI score	0–16 (mean 9.59)
Active NPSLE	14

NPSLE – neuropsychiatric systemic lupus erythematosus; SLEDAI – systemic lupus erythematosus Disease Activity Index.

The study was approved by the Bioethics Committee of Wroclaw Medical University (No. KB-117/2008) and carried out in accordance with the Helsinki protocol. Patients were enrolled after they had provided informed written consent.

Clinical assessment

Clinical assessment included the history based on medical records and physical examination. The following data was collected: disease duration, duration of CNS involvement and disease activity measured with the SLE Disease Activity Index (SLEDAI). In SLE patients, NP involvement was diagnosed in accordance with ACR nomenclature and case definitions.[1] Information on current and past medication was obtained.

Neuropsychological tests

To evaluate the patients' cognitive performance, the following neuropsychological tests were carried out: Auditory Verbal Learning Test (AVLT) – assessing short-term memory and the ability to learn new verbal material; Trail Making Test (TMT) – a measure of psychomotor speed, visuospatial operating memory and attention shifting; Rey Complex Figure Test (copying – RCFTc; recall – RCFTr) – evaluating visuospatial abilities, memory, attention, planning, working non-verbal memory, and executive functions; Digit Span (DS) from the Wechsler Adult Intelligence Scale (WAIS-R) – testing direct auditory memory and operating memory; Verbal Fluency Test (VFT; generating lists of words starting with K and belonging to the category "animals") – assessing categorization abilities and executive functions; and Stroop Test (ST) – as a measure of attention concentration and divisibility. From the battery recommended by ACR, we chose tests available in Polish

versions with adequate normative data. The Beck Depression Inventory (BDI) was applied to estimate the levels of depression. All the tests were explained to the subjects, administered and evaluated by a neuropsychologist, and the results were referred to normative age-adjusted values.

The tests were classified according to the assessed cognitive domains: AVLT, DS and RCFTr as a measure of memory; TMT, VFT, ST – as a measure of attention and executive functions; and RCFTc – as a measure of visuospatial skills. Those subjects who scored worse than the normative values in the tests representing at least 2 of these 3 cognitive domains were assigned as cognitively impaired. In addition, z-scores were calculated for the results of particular tests and they were averaged for the tests representing particular cognitive domains.

Event-related potentials

Auditory ERPs were elicited using the "oddball paradigm", with target stimuli randomly interspersed among non-target ones. Auditory stimuli were tones of 70 dB intensity and 200 ms duration. The target tones (high frequency: 2 kHz) accounted for 20% of the time of each trial and the non-target tones (low frequency: 1 kHz) for 80% of the time. The subjects lay awake in a semi-darkened room and were asked to count the target stimuli quietly in their heads. Event-related potentials were recorded in Fz, Cz and Pz (points on the skull surface according to the International 10–20 system of EEG/SEP recording) according to the 10–20 system, with reference to linked earlobes and with a forearm ground. Ag/AgCl surface electrodes were used and their impedance was maintained below 5 kΩ. The responses were analyzed with a Nicolet 1000 Viking (Natus Medical Inc., Pleasanton, USA), with a 0.30/s, 70 Hz bandpass filter, a sweep time of 1000 ms and a pre-stimulus baseline of 250 ms. At least 30 target trials were averaged in each run. Two runs were performed for every subject. P300 was identified as the positive component with a latency of 300–500 ms and N200 as the negative component with a latency of 180–300 ms after the start of the stimulus. The latencies and amplitudes ("peak to baseline") of P300 and N200 were determined.

The neuropsychological tests and ERPs in the patients were performed on the same day, in morning hours.

Antibodies

The auto-antibodies tested in patient sera included: antinuclear antibodies, anti-dsDNA antibodies, anti-nucleosome antibodies, anti-cardiolipin antibodies (aCL) IgG and IgM isotypes, anti-β2-glycoprotein I antibodies (anti-β2-GPI) IgM and IgG isotypes, anti-β2-GPI/oxLDL IgG and IgM antibodies, anti-ribosomal P antibodies (anti-Rib-P), anti-ganglioside antibodies, anti-Ro/SS-A, anti-La/SS-B, and lupus anticoagulant. We also evaluated the level of the following cytokines: interleukin (IL)-6, IL-10 (R&D Systems, Minneapolis, USA) and IL-17 (Diaclone SAS, Besançon, France). Anti-dsDNA, anti-nucleosome antibodies, aCL, anti-β2-GPI, and anti-Rib-P antibodies were tested with the enzyme-linked immunosorbent assay (ELISA) method (EUROIMMUN, Lübeck, Germany), anti-ganglioside with a dot blot test (EUROIMMUN), anti-Ro/SS-A and anti-La/SS-B with the ELISA method by Inova Health System (Falls Church, USA). All the tests were performed according to the manufacturers' recommendations. The lupus anticoagulant levels were measured with activated thromboplastin time, kaolin clotting time and diluted Russel viper venom time.

Statistical analysis

The subgroup of CI patients was compared with those without CI with regard to disease-related variables (duration of SLE, duration of CNS involvement, NPSLE criteria, SLEDAI score, dose of corticosteroids used) and all the studied immunological parameters. Potential relationships were also investigated between z-scores (for particular tests and cognitive domains), disease-related variables and immunological parameters.

The level of depression was referred to cognitive performance and immunological parameters.

The ERPs parameters in the SLE patients were analyzed in comparison to the controls. They were referred to disease-related variables and immunological parameters.

Parameters in groups were expressed as median and quartiles or as mean, median, quartiles, and standard deviation (SD). The statistical significance between means for different groups was calculated with the one-way analysis of variance (ANOVA), or alternatively by using the non-parametric Kruskal-Wallis test, when the variances in groups were not homogeneous (the homogeneity of variance was determined with Bartlett's test) or when the number of cases was too small. The statistical significance between frequencies was calculated with the χ^2 test with Yates's correction or, if the expected value was <5, with the Fisher's exact test.

Relationships between 2 parameters were assessed using a correlation analysis and Pearson's correlation coefficients were calculated.

A p-value <0.05 was required to reject the null hypothesis. Statistical analysis was performed using the EPIINFO v. 3.5.2 (December 17, 2010) software package (CDC, Atlanta, USA).

Results

In SLE patients, the disease duration was 3–31 years (mean: 10 years). The SLEDAI score ranged from 0 to 16 (mean: 9.59). There were 24 patients with NP involvement and 13 non-NPSLE patients. The mean duration of NP involvement was 6 years. Active NP symptoms were

diagnosed in 14 patients. The most common NP manifestations were mood disorders – mainly depression – in 18 patients; cerebrovascular disease (stroke or transient ischemic attack – TIA, or cerebral sinus thrombosis) was recognized in 7 patients, seizures in 4 patients, psychosis in 4 patients, polyneuropathy in 3 patients, cranial neuropathy in 2 patients, acute confusional state in 2 patients, and severe headache in 1 patient. More than 1 NP manifestation was diagnosed in 12 patients. All the patients were treated with corticosteroids; the mean dose used was 15 mg/day of prednisone.

Antibodies

Auto-antibodies and the cytokine status were evaluated in all the patients. Elevated levels of IL-6 were detected in 4 patients (10.8%), of IL-10 in 14 patients (37.8%) and of IL-17 in 10 patients (27%).

Anti-dsDNA antibodies were detected in 14 patients (38%), anti-Rib-P antibodies in 4 patients (11%) and anti-nucleosome antibodies in 18 patients (49%). Anti-phospholipid (APL) antibodies in medium and high titers were as follows: aCL IgG were detected in 15 patients (40.5%), aCL IgM in 10 (27%), anti-β2-GPI IgG in 4 (11%), and anti-β2-GPI IgM in 10 (27%). Lupus anticoagulant was detected in 9 patients (24%). Anti-ganglioside antibodies were detected in 12 patients (32%), anti-Ro/SSA antibodies in 16 patients (43%) and anti-La/SSB antibodies in 10 patients (27%).

Neuropsychological tests – cognitive impairment

In SLE patients, 21 subjects had abnormal scores in AVLT (25 in the delayed part of AVLT), 22 in TMT, 14 in DS, 7 in RCFTc, 13 in RCFTr, 25 in VFTl (VFT-letter), 14 in VFTs (VFT-sematic), and 4 in ST.

Fifteen patients showed impaired performance in at least 2 tests evaluating memory (AVLT, DS, RCFTr), 19 in the field of attention and executive functions (TMT, VF, ST) and 4 presented with impaired visuo-spatial skills (RCFTc). Overall, 13 subjects (35%) who showed deficits in at least 2 of these cognitive domains were assigned to the cognitively impaired (CI) subgroup. The CI subgroup, in comparison to the remaining patients, showed significantly higher SLEDAI scores (12.7 ±6.44 vs 7.8 ±4.4, respectively; p = 0.01). Among CI patients, 10 subjects fulfilled the criteria for NPSLE and 3 did not. Neuropsychiatric SLE patients with CI had a significantly longer duration of CNS involvement than those without CI (8 ±5 years vs 4 ±2 years, respectively; p = 0.01). There were no significant differences between patients with or without CI in terms of the duration of the disease, dose of corticosteroids, BDI score, or diagnosed depression.

Analyzing the relationships between z-scores for the neuropsychological tests and disease-related variables, we found a significant correlation between the z-score for the delayed part of AVLT and the SLEDAI results (R = 0.42, p = 0.006). No other significant relationships were found.

The subgroups with and without CI did not differ in the presence of particular auto-antibodies/cytokines. Several significant correlations were found between immunological markers and z-scores for particular neuropsychological tests. Patients with higher levels of IL-17 had higher z-scores (and worse results) for DS and RCFTc. Those with detectable anti-dsDNA antibodies had higher z-scores (and worse results) for RCFTc, RCFTr and VFT. The patients positive for anti-β2-GPI/oxLDL IgM antibodies showed lower z-scores (and worse results) for TMT. Those positive for ACL IgG antibodies had higher z-scores (and worse results) for DS and RCFTc (Table 2).

Table 2. Comparison of z-scores for neuropsychological tests between the subgroups of SLE patients with positive (+) or negative (–) immunological parameters

Parameters	DS z-score median (quartiles)	RCFTc z-score median (quartiles)	RCFTr z-score median (quartiles)	TMT z-score median (quartiles)	VFT z-score median (quartiles)
IL-17 (+)	1.132 (0.698–1.363)	0.522 (0.489–0.522)	1.261 (0.478–1.390)	0.485 (0.225–0.840)	0.748 (0.683–0.896)
IL-17 (–)	0.665 (0.300–0965)	0.185 (0.185–0.522)	0.603 (0.245–1.089)	0.799 (0.544–1.017)	0.534 (0.255–1.323)
p-value*	**0.044**	**0.026**	0.070	0.068	0.720
Anti-dsDNA (+)	0.965 (0.633–1.363)	0.522 (0.489–0.522)	1.321 (0.727–1.450)	0.691 (0.383–0.856)	0.896 (0.683–1.323)
Anti-dsDNA (–)	0.698 (0.300–1.030)	0.185 (0.185–0.522)	0.478 (0.245–1.020)	0.441 (0.256–0.835)	0.469 (0.255–0.896)
p-value*	0.260	**0.017**	**0.003**	0.230	**0.021**
oxLDL/β2 IgM (+)	0.965 (0.365–1.298)	0.185 (0.185–0.522)	0.486 (0.245–1.321)	0.370 (0.218–0.630)	0.427 (0.255–0.683)
oxLDL/β2 IgM (–)	0.698 (0.365–1.030)	0.522 (0.185–0.522)	0.603 (0.366–1.201)	0.609 (0.317–0.918)	0.896 (0.386–1.323)
p-value*	0.520	0.180	0.660	**0.049**	0.090
aCL IgG (+)	1.298 (0.633–1.363)	0.522 (0.185–0.522)	1.201 (0.478–1.390)	0.671 (0.256–0.856)	0.683 (0.469–1.323)
aCL IgG (–)	0.698 (0.300–0.965)	0.489 (0.185–0.522)	0.478 (0.306–1.080)	0.441 (0.297–0.835)	0.683 (0.255–1.026)
p-value*	**0.038**	0.250	**0.030**	0.720	0.310

SLE – systemic lupus erythematosus; IL-17 – interleukin-17; DS – Digit Span; RCFTc – Rey Complex Figure Test (copying); RCFTr – Rey Complex Figure Test (recall); TMT – Trail Making Test; VFT – Verbal Fluency Test; * Kruskal-Wallis test; p-values in bold are statistically significant.

Event-related potentials

The mean values for N200 and P300 latencies were significantly greater in SLE patients than in controls (Table 3). No significant differences were found for P300 amplitude, but there was a trend toward a higher N200 amplitude in SLE patients in comparison to controls. Abnormalities were found in 35% of SLE patients in terms of N200 (prolonged latency) and in 62.5% in terms of P300 (lack of the P300 component in 1 subject, prolonged latency and/or lowered amplitude in 24).

Within the NPSLE subgroup, abnormalities were found in 56% of N200 and in 68.7% of P300, while 18.7% had no ERPs abnormalities. Within the non-NPSLE subgroup, 28.6% presented with abnormal N200 and 62% with abnormal P300 parameters, while 33% had no ERPs abnormalities. The mean values of both N200 and P300 parameters did not differ significantly between the NPSLE and non-NPSLE subgroups, even after controlling for depression (Table 3).

There was a trend (but not significant, p = 0.06) toward longer N200 latency in the subgroup of patients with less active disease (SLEDAI <6), but no other relationships were found between the SLEDAI scores and ERPs parameters.

Mean P300 latency was significantly longer in the subgroup of patients with an absence of anti-nucleosome

Table 3. Comparison of the N200 and P300 parameters between patients with SLE and controls (A), NPSLE and non-NPSLE and patients with SLEDAI >6 and <6 (B)

A

Parameters	Controls mean median (quartiles) SD	SLE patients mean median (quartiles) SD	p-value
N200 Fz lat	209.6 205.0 (197.0–220.0) 22.1	224.8 223.0 (205.0–238.0) 30.1	0.0177*
N200 Fz ampl	4.25 3.60 (1.90–5.80) 2.97	5.86 5.20 (1.40–8.40) 4.41	0.203**
N200 Cz lat	208.0 204.0 (196.0–217.0) 21.5	223.1 221.0 (202.0–237.0) 31.0	0.0193*
N200 Cz ampl	3.38 2.10 (1.20–4.40) 2.98	5.17 3.90 (2.30–7.90) 3.66	0.0235**
N200 Pz lat	209.0 205.0 (19.0–219.0) 21.1	223.9 220.0 (204.0–235.0) 31.4	0.0216*
N200 Pz ampl	2.38 1.80 (1.00–3.00) 2.20	4.16 3.50 (1.60–6.10) 3.19	0.0073**
P300 Fz lat	320.6 323.0 (310.0–335.0) 22.5	347.8 349.5 (333.0–366.5) 31.1	0.00008*
P300 Fz ampl	7.30 6.40 (4.00–9.40) 4.49	5.69 5.75 (4.10–7.25) 2.82	0.190**
P300 Cz lat	321.6 326.0 (309.0–335.0) 23.1	348.4 352.5 (333.0–372.5) 32.3	0.00015*
P300 Cz ampl	8.30 8.30 (5.30–9.20) 4.26	7.26 7.45 (4.45–9.50) 3.64	0.271*
P300 Pz lat	324.1 324.0 (307.0–339.0) 24.1	350.5 353.0 (338.0–373.0) 30.6	0.00014*
P300 Pz ampl	8.60 7.60 (5.90–10.70) 4.18	8.52 8.25 (4.35–11.10) 4.71	0.944*

SLE – systemic lupus erythematosus; SD – standard deviation; NPSLE – neuropsychiatric systemic lupus erythematosus; SLEDAI – systemic lupus erythematosus Disease Activity Index; lat – latency; ampl – amplitude; Fz, Cz, Pz – points on the skull surface according to the International 10–20 system of EEG/SEP recording; * analysis of variance (ANOVA); ** Kruskal-Wallis test; p-values in bold are statistically significant.

B

Parameters	NPSLE subgroup (n = 16) median (quartiles)	Non-NPSLE subgroup (n = 21) median (quartiles)	p-value*	SLEDAI <6 (n = 11) median (quartiles)	SLEDAI >6 (n = 26) median (quartiles)	p-value*
N200 Fz lat	222.0 (203.5–247.0)	223.0 (210.0–226.0)	0.297	231.0 (223.0–253.0)	216.5 (203.0–233.0)	**0.0580**
N200 Fz ampl	4.80 (2.00–8.25)	5.20 (1.30–0.40)	0.854	5.20 (3.50–10.40)	4.70 (1.30–8.40)	0.506
N200 Cz lat	221.0 (198.5–244.5)	219.0 (210.0–226.0)	0.263	230.0 (215.0–251.0)	213.5 (198.0–233.0)	**0.0650**
N200 Cz ampl	3.85 (2.00–7.70)	4.20 (2.60–7.90)	0.759	5.20 (1.80–7.90)	3.85 (2.30–7.90)	0.842
N200 Pz lat	221.5 (200.5–253.0)	219.0 (210.0–228.0)	0.244	232.0 (215.0–270.0)	214.5 (200.0–233.0)	**0.0753**
N200 Pz ampl	2.70 (1.50–5.80)	4.00 (1.60–6.10)	0.783	2.90 (1.20–7.00)	3.60 (1.60–6.10)	0.947
P300 Fz lat	357.0 (334.0–374.0)	349.0 (332.0–358.0)	0.949	349.0 (319.0–378.0)	350.0 (334.0–363.0)	0.959
P300 Fz ampl	4.80 (3.40–7.20)	6.20 (4.90–7.30)	0.911	4.40 (4.40–7.30)	6.30 (4.40–7.20)	0.319
P300 Cz lat	356.0 (332.0–376.0)	350.0 (334.0–357.0)	0.974	352.0 (319.0–378.0)	353.0 (334.0–360.0)	0.945
P300 Cz ampl	5.40 (3.40–8.90)	8.90 (6.40–10.20)	0.531	4.30 (4.30–9.80)	8.40 (5.00–9.30)	0.303
P300 Pz lat	357.0 (339.0–376.0)	352.0 (337.0–356.0)	0.860	353.0 (321.0–376.0)	353.0 (339.0–364.0)	0.757
P300 Pz ampl	7.40 (3.60–10.20)	10.0 (7.6–12.6)	0.386	4.80 (4.80–10.20)	8.50 (6.70–11.60)	0.192

NPSLE – neuropsychiatric systemic lupus erythematosus; SLEDAI – systemic lupus erythematosus Disease Activity Index; lat – latency; ampl – amplitude; Fz, Cz, Pz – points on the skull surface according to the International 10–20 system of EEG/SEP recording; * Kruskal-Wallis test; p-values in bold are statistically significant.

antibodies (Fz: 360 ms, Cz: 362 ms and Pz: 364.3 ms vs 333.1 ms, 332.4 ms and 334.9 ms, respectively; p = 0.01). No other significant relationships were found between the ERPs parameters and immunological findings.

No correlations were found between the ERPs parameters and the duration of the disease, duration of CNS involvement in NPSLE patients or dose of corticosteroids.

Discussion

Neuropsychological assessment revealed CI (with at least 2 cognitive domains affected) in 35% of our SLE patients. A similar frequency of CI in the course of SLE was reported by some authors, while both higher and lower values were also described.[2,4,9–15] Our patients showed impaired performance mainly within the domains of memory (especially verbal), verbal fluency, attention, and executive functions, with visuospatial skills apparently being least affected. These findings are consistent with some studies on the subject, although other authors have found a predominant decline in the visuospatial domain or have shown that all cognitive domains have been similarly compromised.[11–20] Such a range of conclusions may be attributed to the different tests administered and the only recent application of specific nomenclature in this field in SLE.[16] Therefore, we chose the tests from the battery recommended by ACR, where adequate normative data is available.[1]

The majority of CI patients in our material fulfilled the criteria for NPSLE and they had a longer duration of CNS involvement than NPSLE subjects without CI. However, impaired cognitive performance (within at least 1 of the domains tested) was also found in non-NPSLE patients. Most authors agree that CI is more pronounced and more common in NPSLE, but may occur even in the absence of overt neurological and psychiatric symptoms.[4,19–22] It is a matter of debate whether CI can appear irrespective of clinically diagnosed CNS involvement or perhaps may precede other NPSLE features.[12,23]

Cognitive performance is claimed to be affected in its course by SLE activity and chronic CNS damage. We found higher SLEDAI scores in CI subjects, but without differences in the duration of the disease. Among particular neuropsychological tests, only the z-score for the delayed part of AVLT (a measure for long-term verbal memory) correlated significantly with the SLEDAI score. Systemic lupus erythematosus Disease Activity Index has been suggested as an independent predictor of CI and has been reported to correlate with the Global Cognitive Index as well as the tests measuring attention and executive domains.[16,24] Although in some studies, the relationships between SLEDAI and cognitive performance have been denied, this may be attributed to the heterogeneity of SLE patients.[13] The activity of the disease is associated with therapeutic strategies. All our patients were treated with corticosteroids, but no correlations were found between the medication dosage and cognitive performance, which is consistent with the majority of studies in this field.[4,13,15,17] Cognitive impairment has been described as a side effect of recent corticosteroid treatment, but its occurrence during regular corticosteroid use has been attributed rather to the severity of the disease itself than to any adverse effect of the medication.[25,26]

Auto-antibodies and cytokines are immunological markers of SLE. In our SLE patients, APL (especially aCL), anti-nucleosome and anti-dsDNA antibodies were most frequently detectable. In other studies on this subject, APL antibodies are predominantly associated with CNS involvement, followed by anti-NR2 and anti-Rib-P antibodies.[10,14,16] Antiphospholipids are supposed to modulate neuronal function by reacting directly with neurons and affecting them via cerebrovascular insufficiency due to thrombosis.[16,27] However, the relationships between the abovementioned autoantibodies and cognitive functioning remain a contested issue. Some authors have observed associations between the presence and level of APL and CI,[14,16,28,29] while others have not confirmed this.[14–16,28–30] Similar discrepancies have been found in the case of anti-NR2 antibodies.[10,13] We did not find any significant differences in terms of the immunological status between SLE patients with and without CI. However, we found some correlations between immunological findings and particular neuropsychological test results assessing nonverbal memory, attention, visuospatial skills, and executive functions. These findings seem especially interesting regarding aCl and anti-dsDNA antibodies, which were among the most frequently detected antibodies in the studied group. Similar associations between aCl and anti-dsDNA antibodies and the performance within visuospatial skills, attention and executive function domains were described by Conti et al. and Peretti et al.[16,17] The presence of these antibodies in SLE patients might be indicative of subtle and more selective cognitive deficit, and thus be helpful in identifying patients requiring a closer follow-up in this field.

As many as 48% of our patients had recognized depression and 18 had BDI scores indicating mild or moderate depressive symptoms. As depression is one of common psychiatric manifestations of SLE and can potentially be a confounding factor in the assessment of cognitive performance, we considered this fact in the analysis of the data.[13,31] We divided the patients into the NPSLE and non-NPSLE subgroups twice, including and not including depression in NPSLE criteria. For both versions, we obtained the same results regarding the correlations between cognitive performance, the ERPs results and the NPSLE status. We did not find significant relationships between the BDI results or the diagnosis of depression and neuropsychological or ERPs measures. Thus, the association between cognitive performance and depression in our SLE patients could be eliminated, as in the studies by Lapteva et al. and Cavaco et al.[13,32]

The ERPs analysis in our SLE patients showed mainly abnormalities of the P300 component. P300 is considered

an electrophysiological index of global cognitive functioning and – as it is not a source specific potential – its abnormalities correspond best with generalized or multifocal CNS damage. Prolonged P300 latency in our SLE patients suggests slowed information processing, while lowered amplitude (found in some patients, although without significant differences of mean values between SLE subjects and controls) may be associated with attention and motivation impairment. Similar abnormalities in the P300 parameters have already been reported in SLE patients, with their frequency ranging from 35% to over 70%.[3–6] Considering the mainly subcortical localization of CNS lesions in the course of SLE, one could expect more common abnormalities of the N200 component, which is attributed to early, subconscious stimulus processing. Prolonged latency of N200 was less commonly found in our patients than that of the P300 component. We also found, somewhat surprisingly, a trend for an increase in the N200 amplitude in patients in comparison to controls. It is possible that cognitive deficits in these patients made the ERPs task more effortful and caused increased attention concentration. Apart from the studies of Khedr et al., who found no N200 abnormalities in SLE patients, and Langosh et al., who reported decreased latency of the N100 component, using the mismatch negativity paradigm, early ERPs components have not been analyzed in SLE patients.[4,33]

Although the mean values of the ERPs parameters did not differ between our NPSLE and non-NPSLE patients, prolonged N200 latency occurred more frequently in the former subgroup. This finding may be associated with the mainly subcortical CNS involvement in SLE mentioned above. In the studies on ERP, P300 abnormalities have mainly been described as typical for NPSLE patients, and thus differentiating them from non-NPSLE ones.[3,4,6] We found a similar and rather high (over 60%) frequency of P300 abnormalities in both subgroups. Similar findings were reported by Mostafa et al., who also noticed that in 75% of patients with P300 abnormalities, but without clinical signs of CNS involvement, NPSLE developed during the 18 months of follow-up.[3] Moreover, we did not ascertain significant relationships between the ERPs parameters and SLE-related variables, including the duration of the disease, SLEDAI score and corticosteroid dosage, or immunological findings, apart from slightly prolonged P300 latency in patients with an absence of anti-nucleosome antibodies. Thus, ERPs abnormalities may already occur in early and less active phases of SLE, and indicate subclinical CNS involvement, which suggests their potential predictive value.

The strength of our study is associated with simultaneous neuropsychological and electrophysiological assessment of cognitive functions in SLE patients, as well as their reference to the clinical and immunological markers of SLE. To our knowledge, there has been so far no study analyzing such a wide range of auto-antibodies regarding cognitive performance in SLE. The limited number of patients and the fact that the assessment of cognition was performed only once may be considered the limitations of our study. Nevertheless, our findings, especially those concerning non-NPSLE patients, seem to encourage further investigation in this field, including follow-up of cognitive performance in SLE patients from the onset of the disease.

In conclusion, CI revealed by neuropsychological testing seems to be more closely related to the clinical and immunological features of SLE than ERPs abnormalities. However, ERPs are worth including as a complementary method in the assessment of cognitive performance in SLE patients. Cognitive impairment deserves attention as a specific aspect of CNS involvement in SLE, which should be evaluated from the early phase of the disease and monitored during its course.

References

1. The American College of Rheumatology nomenclature and case definitions for neuropsychiatric lupus syndrome. *Arthritis Rheum*. 1999; 42(4):599–608.
2. Kozora E, Ellison MC, West S. Reliability and validity of the proposed American College of Rheumatology neuropsychological battery for systemic lupus erythematosus. *Arthritis Rheum*. 2004;51(5):810–818.
3. Mostafa GA, Nazif HK, El-Shahawi HH, El-Aziz MMA, Hassan MA. Antineuronal antibodies and electroneurophysiological studies in pediatric patients with neuropsychiatric systemic lupus erythematosus. *Pediatr Allergy Immunol*. 2009;20(2):192–199.
4. Khedr EM, Khedr T, Farweez HM, Abdell G, El Beih EAS. Multimodal electroneurophysiological studies of systemic lupus erythematosus. *Neuropsychobiology*. 2001;43(3):204–212.
5. Ito J, Suwazono S, Kimura J, Shibasaki H. Auditory event-related potentials in patients with systemic lupus erythematosus. *Eur Neurol*. 1993;33(5):373–377.
6. Paiva T, da Silva JC, Pimentel T, et al. Neurophysiological tests in neurolupus. *Acta Med Port*. 1988;4/5/6:261–264.
7. Hochberg MC. Updating the American College of Rheumatology revised criteria for the classification of the systemic lupus erythematosus. *Arthritis Rheum*. 1997;40(9):1725.
8. Tan EM, Cohen AS, Fries JF, et al. The 1982 revised criteria for the classification of systemic lupus erythematosus. *Arthritis Rheum*. 1982;25(11): 1271–1277.
9. Hanly JG, Omisade A, Su L, Farewell V, Fisk JD. Assessment of cognitive function in systemic lupus erythematosus, rheumatoid arthritis and multiple sclerosis by computerized neuropsychological tests. *Arthritis Rheum*. 2010;62(5):1478–1486.
10. Harrison MJ, Ravdin LD, Lockshin MD. Relationship between serum NR2a antibodies and cognitive dysfunction in systemic lupus erythematosus. *Arthritis Rheum*. 2006;54(8):2515–2522.
11. Olazaran J, Lopez-Longo J, Cruz I, Bittini A, Carreno L. Cognitive dysfunction in systemic lupus erythematosus: Prevalence and correlates. *Eur Neurol*. 2009;62(1):49–55.
12. Tektonidou MG, Varsou N, Kotoulas G, Antoniou A, Moutsopoulos HM. Cognitive deficits in patients with antiphospholipid syndrome: Association with clinical, laboratory and brain magnetic resonance imaging findings. *Arch Intern Med*. 2006;166(20):2278–2284.
13. Lapteva L, Nowak M, Yarboro CH, et al. Anti-*N*-methyl-D-aspartate receptor antibodies, cognitive dysfunction and depression in systemic lupus erythematosus. *Arthritis Rheum*. 2006;54(8):2505–2514.
14. Denburg SD, Carbotte RM, Ginsberg JS, Denburg JA. The relationship of antiphospholipid antibodies to cognitive function in patients with systemic lupus erythematosus. *J Int Neuropsychol Soc*. 1997;3(4):377–386.
15. Emori A, Matsushima E, Amhara O, et al. Cognitive dysfunction in systemic lupus erythematosus. *Psychiatry Clin Neurosci*. 2005;59(5): 584–589.

16. Conti F, Alessandri C, Perricone C, et al. Neurocognitive dysfunction in systemic lupus erythematosus: Association with antiphospholipid antibodies, disease activity and chronic damage. *PLoS One*. 2012;7(3):e33824.
17. Peretti CS, Peretti CR, Kozora E, Papathanassiou D, Chouinard V-A, Chouinard G. Cognitive impairment in systemic lupus erythematosus women with elevated auto-antibodies and normal single photon emission computerized tomography. *Psychother Psychosom*. 2012;81(5): 276–285.
18. Sabbadini MG, Manfredi AA, Bozzolo E, et al. Central nervous system involvement in systemic lupus erythematosus patients without overt neuropsychiatric manifestations. *Lupus*. 1999;8(1):11–21.
19. Carbotte RM, Denburg SD, Denburg JA. Prevalence of cognitive impairment in systemic lupus erythematosus. *J Nerv Ment Dis*. 1986; 174(6):357–364.
20. Kozora E, Arciniegas DB, Filley CM, et al. Cognitive and neurologic status in patients with systemic lupus erythematosus without major neuropsychiatric syndromes. *Arthritis Rheum*. 2008;59(11):1639–1646.
21. Aharon-Peretz J, Brenne B, Amyel-Zvi E, Hemli JA. Neurocognitive dysfunction in the antiphospholipid antibody syndrome (APS). *Cogn Behav Neurol.* 1996;9(2):123–126.
22. Kozora E, Filley CM, Hang L, et al. Immune function and brain abnormalities in patients with systemic lupus erythematosus without overt neuropsychiatric manifestations. *Lupus*. 2012;21(4):402–411.
23. Loukkola J, Laine M, Ainiala H, et al. Cognitive impairment in systemic lupus erythematosus and neuropsychiatric systemic lupus erythematosus: A population-based neuropsychological study. *J Clin Exp Neuropsychol*. 2003;25(1):145–151.
24. Mikdashi J, Handwerger B. Predictors of neuropsychiatric damage in systemic lupus erythematosus: Data from the Maryland Lupus Cohort. *Rheumatology (Oxford)*. 2004;43(12):1555–1560.
25. Brown ES, Chandler PA. Mood and cognitive changes during systemic corticosteroid therapy. *Primary Care Companion J Clin Psychiatry*. 2001;3(1):17–21.
26. McLaurin EY, Holliday SL, Williams P, Brey RL. Predictors of cognitive dysfunction in patients with systemic lupus erythematosus. *Neurology*. 2005;64(2):297–303.
27. Tomietto P, Annese V, D'Agostini S, et al. General and specific factors associated with severity of cognitive impairment in systemic lupus erythematosus. *Arthritis Rheum*. 2007;57(8):1461–1472.
28. Afeltra A, Garzia P, Mitterhofer AP, et al. Neuropsychiatric lupus syndromes: Relationship with antiphospholipid antibodies. *Neurology*. 2003;61(1):108–110.
29. Schmidt R, Auer-Grumbach P, Fazekas F, Offenbacher H, Kapeller P. Anticardiolipin antibodies in normal subjects: Neuropsychological correlates and MRI findings. *Stroke*. 1995;26(5):749–754.
30. Monastero R, Bettini P, Del Zotto E, et al. Prevalence and pattern of cognitive impairment in systemic lupus erythematosus patients with and without overt neuropsychiatric manifestations. *J Neurol Sci.* 2001;184(1):33–39.
31. Petri M, Naqibuddin M, Carson KA, et al. Depression and cognitive impairment in newly diagnosed systemic lupus erythematosus. *J Rheumatol*. 2010;37(10):2032–2038.
32. Cavaco S, Martins da Silva A, Santos E, et al. Are cognitive and olfactory dysfunctions in neuropsychiatric lupus erythematosus dependent on anxiety or depression? *J Rheumatol.* 2012;39(4):770–776.
33. Langosch J, Rand S, Ghosh B, et al. A clinical electrophysiological study of emotional lability in patients with systemic lupus erythematosus. *J Neuropsychiatry Clin Neurosci.* 2008;20(2):201–209.

Clinical and nutritional correlations in Parkinson's disease: Preliminary report

Sławomir Budrewicz[1,A,E,F], Anna Zmarzły[2,B], Dominik Rączka[2,B], Aleksandra Szczepańska[1,C], Ewa Koziorowska-Gawron[1,B,D], Krzysztof Słotwiński[1,C,D], Magdalena Koszewicz[1,D–F]

[1] Department of Neurology, Wroclaw Medical University, Poland
[2] Clinical Nutrition Unit, J. Gromkowski Regional Specialist Hospital, Wrocław, Poland

A – research concept and design; B – collection and/or assembly of data; C – data analysis and interpretation; D – writing the article; E – critical revision of the article; F – final approval of the article

Advances in Clinical and Experimental Medicine, ISSN 1899–5276 (print), ISSN 2451–2680 (online) *Adv Clin Exp Med*. 2019;28(2):193–198

Address for correspondence
Magdalena Koszewicz
E-mail: magdalena.koszewicz@umed.wroc.pl

Funding sources
None declared

Conflict of interest
None declared

Received on July 19, 2017
Reviewed on July 24, 2017
Accepted on August 11, 2017

Published online on July 2, 2018

Abstract

Background. Parkinson's disease (PD) is one of the most common neurodegenerative disorders. Malnutrition is an essential problem in the late stage of PD. Lowering of body mass is seen in 30% of patients, and malnutrition or the risk of malnutrition in 24% and 60%, respectively.

Objectives. The aim of the study was an analysis of the relationships between the parameters of the nutritional stage and the advancement of clinical symptoms in PD patients.

Material and methods. A total of 40 patients (18 men, 22 women) with PD were analyzed, mean age: 70.7 years. In all patients, structured anamnesis, Nutrition Risk Screening (NRS 2002), body mass index (BMI), morphology, and basic biochemical tests were conducted. Skin fold thickness was also measured. The results were referred to the score of different scales.

Results. The study showed a lot of correlations between the severity of PD, mostly motor symptoms in the Unified Parkinson's Disease Rating Scale (UPDRS), and parameters characterizing the patient's nutritional status. We revealed a correlation between malnutrition and PD duration, and L-DOPA frequency intake. The global score of parts I, II and III of UPDRS were correlated with the nutritional status. The results confirmed the existence of more severe smell change and taste impairment in the late stage of PD, with more pronounced malnutrition.

Conclusions. The duration of PD, motor and non-motor PD symptoms, and the frequency of L-DOPA intake closely correlate with the nutritional status. Understanding of the multifactorial interdependence might be useful in the estimation of the algorithm for monitoring the nutritional status of PD patients and taking early nutritional intervention.

Key words: malnutrition, Parkinson's disease, Nutrition Risk Screening, Unified Parkinson's Disease Rating Scale, skin fold thickness

Cite as
Budrewicz S, Zmarzły A, Rączka D, et al. Clinical and nutritional correlations in Parkinson's disease: Preliminary report. *Adv Clin Exp Med*. 2019;28(2):193–198. doi:10.17219/acem/76375

DOI
10.17219/acem/76375

Introduction

Parkinson's disease (PD) has the 2nd highest incidence rate, after Alzheimer's disease, for neurodegenerative disorders in the population above 50 years of age. Parkinson's disease occurs in about 1% of the population above 65 years of age.[1] Malnutrition is an essential problem in the late stage of PD. Lowering of body mass is seen in 30% of patients, and malnutrition or the risk of malnutrition in 24% and 60%, respectively.[1] Malnutrition could be caused by lowering of food intake, motor dysfunctions, motor side effects of treatment (choreatic dyskinesia), dysphagia, or dysautonomia (gastroparesis, constipation).[2] Cognitive dysfunction, depression and/or a lack of family attention could exacerbate malnutrition in PD patients. Dietary protein manipulation, burning mouth syndrome, removable dentures in oral dyskinesia, and side effects of antiparkinsonian drugs (nausea, vomiting and xerostomia) could influence the nutritional status. Autonomic disturbance, e.g., dysfunction of the subthalamic region responsible for body mass control, is thought to be an important factor in the etiology of PD malnutrition. Other coexisting diseases must be considered in the analysis of malnutrition risk factors.[2–5]

The aim of the study was the analysis of the relationships between the parameters of the nutritional status and the advancement of clinical symptoms in PD patients.

Material and methods

All patients gave informed written consent to participate in the study. The study was approved by the local Bioethics Committee at Wroclaw Medical University (Poland).

Forty patients with a diagnosis of PD according to the Movement Disorder Society (MDS) clinical criteria from 2015 were analyzed.[6] There were 18 men and 22 women in the study group, mean age: 70.7 years. Five patients were professionally active, 35 were retired and all of them lived in a city having above 650,000 habitants. All of them were analyzed in an outpatient clinic. All examinations were conducted by clinical nutrition specialists and blinded neurologists specializing in extrapyramidal disorders. In all patients, structured anamnesis was performed: age, sex, disease duration, PD pharmacological therapy, disturbances of smell, taste and gastrointestinal tract, other disorders and their treatment, and addiction to stimulants. The risk of malnutrition was established based on the Nutrition Risk Screening (NRS 2002) and body mass index (BMI).[7] In NRS 2002, results ≥3 indicate the threat of malnutrition and the necessity for nutritional intervention. The thickness of 3 skin folds was measured: deltoid, abdominal, and subscapular. The neurological status was based on the Unified Parkinson's Disease Rating Scale (UPDRS, v. 1987; at the time of the study the new version, MDS-UPDRS, had not yet received official approval in Poland),[8] Schwab and England Activities of Daily Living Scale (SEADLS),[9] Hoehn-Yahr Standing Scale (H-YSS),[10] and Beck Depression Scale (BDS).[11]

Each of the points of UPDRS, the collective results of parts I, II and III of UPDRS, and the global result of UPDRS were compared with the parameters of the nutritional status. Blood samples with an estimation of morphology, urea, creatinine, electrolytes (sodium – Na, potassium – K, calcium – Ca), magnesium – Mg, and phosphorus – P), liver enzyme activity, as well as lipids, global protein and vitamin D levels were analyzed.

For pairs of parameters, we analyzed the correlation with an estimation of the Pearson's or Spearman's correlation coefficient. A p-value ≤0.05 was considered significant. We used the statistical software program EPIINFO 7.1.1.14 (CDC, Atlanta, USA).

Results

Nutrition Risk Screening 2002 correlations

In 10 (25%) PD patients, the result of NRS 2002 was ≥3 points. The results of NRS 2002 positively correlated with PD duration, while taste disturbances correlated negatively with BMI. A positive correlation was also seen between NRS 2002 result and the frequency of L-DOPA intake, while there was no such correlation between BMI and the frequency of L-DOPA intake (Tables 1, 2).

Table 1. Correlations between the nutritional parameters and the results of SEADLS and H-YSS

Parameter I	Parameter II	r	p-value
Abdominal fold*	SEADLS	0.43	0.017
Smell**	SEADLS	–0.34	0.0441
Abdominal fold**	H-YSS	–0.56	0.00122
Subscapular fold**	H-YSS	–0.40	0.0276
Frequency of L-DOPA intake*	NRS 2002	0.41	0.012

UPDRS – Unified Parkinson's Disease Rating Scale; H-YSS – Hoehn and Yahr Standing Scale; SEADLS – Schwab and England Activities of Daily Living Scale (Parkinson's Disease); NRS 2002 – Nutritional Risk Screening 2002; * Pearson's correlation; ** Spearman's correlation.

Table 2. Correlations between the nutritional parameters and the global results of UPDRS, and with parts I, II and III separately

Parameter I	Parameter II	r	p-value
Abdominal fold*	part I score of UPDRS	–0.36	0.040
Smell**	part I score of UPDRS	0.34	0.0442
Abdominal fold*	part II score of UPDRS	–0.46	0.010
Subscapular fold*	part II score of UPDRS	–0.42	0.019
BMI*	part III score of UPDRS	–0.39	0.020
Abdominal fold*	part III score of UPDRS	–0.37	0.044
Subscapular fold*	part III score of UPDRS	–0.37	0.041
NRS 2002**	part III score of UPDRS	0.35	0.0336
Abdominal fold*	global score of UPDRS	–0.49	0.006
Subscapular fold*	global score of UPDRS	–0.41	0.022

NRS 2002 – Nutritional Risk Screening 2002; UPDRS – Unified Parkinson's Disease Rating Scale; BMI – body mass index; * Pearson's correlation; ** Spearman's correlation.

Correlations of other parameters of the nutritional stage

We revealed a negative correlation between the thickness of the subscapular fold and PD duration, and between the thickness of the abdominal and subscapular folds and the results of H-YSS. The SEADLS scores positively correlated only with the thickness of the abdominal fold (Tables 1, 2).

Smell and taste correlations

We found a positive tendency, though not statistically significant, between disturbances in smell and taste, and H-YSS results. A negative correlation was observed between disturbances in smell and SEADLS score (Tables 2, 3, Fig. 1).

Unified Parkinson's Disease Rating Scale and the nutritional status correlations

In our study, negative correlations were seen between the collective result of part I of UPDRS and the thickness of the abdominal fold, as well as the collective results of parts I and III of UPDRS and the thickness of the abdominal and subscapular folds. The collective result of part III of UPDRS, the global UPDRS score and BMI negatively correlated with the thickness of the abdominal and subscapular folds. Point 3 (describing depression) and 4 (describing motivation and initiative) of UPDRS negatively correlated with BMI, and the thickness of the abdominal and subscapular folds. Paradoxically, the results from BDS did not correlate with NRS 2002 score, BMI or the thickness of the skin folds. Point 3 positively correlated with part III of UPDRS and with NRS 2002 score. The following points negatively correlated with the thickness of the skin folds: 9 (cutting food, handling utensils) with the abdominal fold, 14 (freezing when walking) with the abdominal and subscapular folds, 24 (bilateral hand movements) with the subscapular fold, and 29 (gait) and 30 (postural stability) with the abdominal fold. Positive correlations were noted for point 40 of UPDRS (anorexia, nausea, vomiting) and the thickness of the deltoid, abdominal and subscapular folds, and with BMI. We revealed positive correlations between NRS 2002 score and UPDRS points: 14 (freezing when walking), 28 (posture), 31 (body bradykinesia and hypokinesia), 32 (duration: in what proportion of the walking day are dyskinesias present?), and 33 (disability: how disabling are dyskinesias?).

Disturbances in smell positively correlated with points 9 (cutting food, handling utensils) and 20 (tremor at rest for the right upper limb), as well as the collective result of part I of UPDRS. Taste disturbances positively correlated with point 23 (finger taps for the right upper limb) of UPDRS. The level of vitamin D positively correlated with point 17 of UPDRS (sensory complaints related to parkinsonism). The correlations described above are shown in Tables 1–3.

Discussion

The study showed a lot of correlations between the severity of PD, mostly motor symptoms in UPDRS, and parameters characterizing the patient's nutritional status. In 25% of PD patients, we revealed the threat of malnutrition or undernutrition. Wang et al. presented similar results in PD patients in a Chinese population (22.9%) and Barichella et al. in an Italian patient group (20%).[12,13] In the Chinese group, malnutrition was seen in 2% of PD patients. In previous studies, detailed correlations between consequent clinical symptoms in UPDRS and nutritional status parameters were not analyzed. The authors focused only on a comparison between the nutritional parameters and

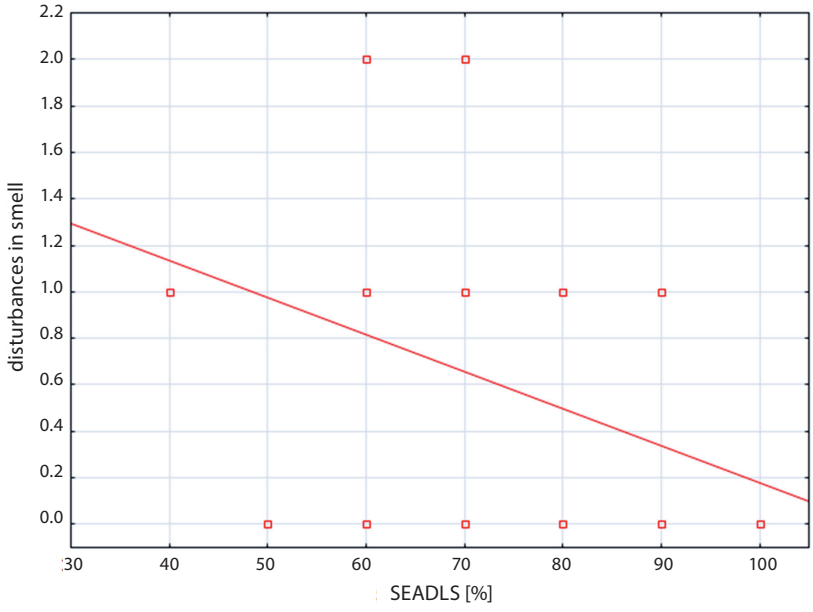

Fig. 1. A negative correlation observed between disturbances in smell and Schwab and England Activities of Daily Living Scale (SEADLS)

Table 3. Correlations between the nutritional parameters and the results of the respective points of UPDRS

Parameter I	Parameter II	r	p-value
Point 3 of UPDRS (depression)*	BMI	−0.37	0.0288
Point 3 of UPDRS (depression)*	abdominal fold	−0.36	0.0495
Point 3 of UPDRS (depression)*	subscapular fold	−0.46	0.00844
Point 4 of UPDRS (motivation/initiative)*	BMI	−0.35	0.0413
Point 4 of UPDRS (motivation/initiative)*	abdominal fold	−0.49	0.00623
Point 9 of UPDRS (cutting food and handling utensils)*	abdominal fold	−0.37	0.0414
Point 9 of UPDRS (cutting food and handling utensils)*	smell	0.37	0.0266
Point 14 of UPDRS (freezing when walking)*	deltoid fold	−0.41	0.0237
Point 14 of UPDRS (freezing when walking)*	abdominal fold	−0.46	0.00978
Point 17 of UPDRS (sensory complaints related to parkinsonism)**	vitamin D	−0.35	0.0406
Point 20 of UPDRS LLR (tremor at rest)**	vitamin D	0.35	0.0449
point 21 of UPDRS LLL (action or postural tremor of hands)*	deltoid fold	−0.36	0.0467
Point 23 of UPDRS L (finger taps)*	abdominal fold	−0.51	0.00375
Point 23 of UPDRS L (finger taps)*	subscapular fold	−0.45	0.0116
Point 24 of UPDRS R (hand movements)*	subscapular fold	−0.50	0.00435
Point 24 of UPDRS L (hand movements)*	subscapular fold	−0.37	0.0400
Point 26 of UPDRS L (leg agility)*	BMI	−0.37	0.0310
Point 26 of UPDRS L (leg agility)*	abdominal fold	−0.48	0.00788
Point 29 of UPDRS (gait)*	abdominal fold	−0.38	0.0380
Point 30 of UPDRS (postural stability)*	abdominal fold	−0.41	0.0241
Point 40 of UPDRS (anorexia, nausea or vomiting)*	BMI	−0.50	0.00199
Point 40 of UPDRS (anorexia, nausea or vomiting)*	deltoid fold	−0.43	0.0159
Point 40 of UPDRS (anorexia, nausea or vomiting)*	abdominal fold	−0.54	0.00197
Point 40 of UPDRS (anorexia, nausea or vomiting)*	subscapular fold	−0.55	0.00145

UPDRS – Unified Parkinson's Disease Rating Scale; ULR – upper limb right; LLL – lower limb left; LLR – lower limb right; L – left; R – right; BMI – body mass index; * Spearman's correlation.

the global score of parts I, II or III of UPDRS. Only the BMI results or unintended weight loss were considered the basic criteria of the nutritional status. There was no analysis of the skin fold thickness. Body mass index seems to be a rather limited parameter, because it relates only to body mass and not to the nutritional status, and it gives false results in some groups of patients (asthenic, very tall or very short), or in patients with posture changes resulting from the reductions in height.[14,15] Such a situation can cause BMI augmentation. In our study, a negative correlation

was seen between BMI and part III of UPDRS. Sheard et al. compared the Subjective Global Assessment (SGA) with the global score of UPDRS and showed a positive correlation between these parameters.[16] Fereshtehnejad et al. disputed these results, as they did not find any statistical differences in terms of malnutrition when comparing a large population of Iranian PD patients with healthy people.[17] Barichella et al. analyzed the clinical stage of PD patients with malnutrition in each part of UPDRS.[2] They revealed lower body mass and BMI in the patient group. The authors did not correlate the results of the executive parts of UPDRS with the nutritional status.

The most important correlation was seen between the risk of malnutrition in NRS 2002 and the duration of PD. These results were compatible with the findings of Jaafar et al.[18] Most of the previous studies indicated the loss of body mass with the rising severity of the disease.[4,12,19]

Our very interesting observation was the influence of the frequency of L-DOPA intake on the nutritional status. We revealed a greater risk of malnutrition in patients who took L-DOPA more frequently. We did not find any correlation between L-DOPA intake frequency and BMI. Sheard et al. and Fereshtehnejad et al. also did not show any relationship between the L-DOPA global dose and the nutritional status.[16,17] The dependence of the nutritional status and the risk of malnutrition in PD patients on the frequency of L-DOPA intake could be connected with the reduction of the amount of food intake, mainly proteinaceous. The reduction of food intake in order to improve L-DOPA absorption and high energy cost in the course of choreatic dyskinesia are important risk factors for malnutrition. Nausea, as a side effect of L-DOPA treatment, can also cause the reduction of food intake.

According to a theory presented by Braak et al., smell changes could be the 1st symptoms of PD.[20] In our patients, we revealed a negative correlation between these smell changes and SEADLS score. These results confirmed the existence of more severe smell changes in the late stage of PD, with more pronounced malnutrition. A positive correlation was seen between smell changes and the global score of part I of UPDRS, e.g., the intellectual status, mood and behavior. Taste impairment positively correlated with the results of NRS 2002. In the available literature, no one describes the influence of taste impairment on the risk of malnutrition.[3,12,13,15,19]

The estimation of skin fold thickness is a very important parameter in the analysis of malnutrition. According to our findings using UPDRS and H-YSS, skin fold thickness depends on PD duration and the grade of progression. Abdominal fold thickness seems to be the best parameter, which correlates with all used scales. The problems of self-feeding and alternative limb movements, and the occurrence of freezing (points 14, 23, 24, and 26 of UPDRS) negatively influence skin fold thickness. Parkinson's disease patients fed by their caregivers had smaller skin folds than PD patients with preserved self-feeding ability.

We also revealed the negative influence of depression, as well as motivation and initiative disturbances (point 3 and 4 of UPDRS) on BMI and skin fold thickness. Our results are compatible with those presented in the study by Fereshtehnejad et al.[21] Emotional disturbances influence the nutritional status, and the early recognition of these allows for preventative steps to be taken, as well as early treatment.

In the late stage of PD, the frequency of falls is greater. We observed a negative correlation between the thickness of the abdominal fold and postural stability. The enhancement of sensory complaints (point 17 of the UPDRS) and lowering of vitamin D level could be important factors for the risk of falling. The prevention of malnutrition with vitamin D supplementation could diminish the risk of falling and its complications, e.g., bone fractures.

Conclusions

The duration of PD, motor and non-motor PD symptoms, and the frequency L-DOPA intake closely correlate with the nutritional status. Understanding of the multifactorial interdependence might be useful in the estimation of an algorithm for monitoring the nutritional status of PD patients and early nutritional intervention.

References

1. World Health Organization. *Neurological Disorders. Public Health Challenges*. Geneva, Switzerland: WHO Press; 2007.
2. Barichella M, Cereda E, Cassani E, et al. Dietary habits and neurological features of Parkinson's disease patients: Implications for practice. *Clin Nutr*. 2016;36(4):1054–1061. doi: 10.1016/j.clnu.2016.06.020
3. Lindskov S, Sjöberg K, Hagell P, Westergren A. Weight stability in Parkinson's disease. *Nutr Neurosci*. 2016;19(1):11–20.
4. Bachmann CG, Trenkwalder C. Body weight in patients with Parkinson's disease. *Mov Disord*. 2006;21(11):1824–1830.
5. Lindskov S, Sjöberg K, Westergren A, Hagell P. Malnutrition risk in Parkinson's disease. *J Aging Res Clin Pract*. 2014;3:93–99.
6. Postuma RB, Berg D, Stern M, et al. MDS clinical diagnostic criteria for Parkinson's disease. *Mov Disord*. 2015;30(12):1591–1601.
7. Kondrup J, Rasmussen H, Hamberg O, Stanga Z; Ad Hoc ESPEN Working Group. Nutritional Risk Screening (NRS 2002): A new method based on an analysis of controlled clinical trials. *Clin Nutr*. 2003;22(3):321–336.
8. Fahn S, Elton R; Members of the UPDRS Development Committee. Unified Parkinson's Disease Rating Scale. In: Fahn S, Marsden CD, Calne DB, Goldstein M, eds. *Recent Developments in Parkinson's Disease, Vol 2*. Florham Park, NJ: Macmillan Health Care Information; 1987;153–163, 293–304.
9. Schwab RS, England AC. Projection technique for evaluating surgery in Parkinson's disease In: Gillingham FJ, Donaldson MC, eds. *Third Symposium on Parkinson's Disease*. Edinburgh, UK: E&S Livingston; 1969:152–157.
10. Hoehn M, Yahr M. Parkinsonism: Onset, progression and mortality. *Neurology*. 1967;17(5):427–442.
11. Beck AT. *Depression: Causes and Treatment*. Philadelphia, PA: University of Pennsylvania Press; 1972.
12. Wang G, Wan Y, Cheng Q, et al. Malnutrition and associated factors in Chinese patients with Parkinson's disease: Results from a pilot investigation. *Parkinsonism Relat Disord*.2010;16(2):119–123.
13. Barichella M, Villa MC, Massarotto A, et al. Nutritional assessment in patients with Parkinson's disease: Correlation between worsening of the malnutrition and increasing number of disease-years. *Nutr Neurosci*. 2008;11(3):128–134.

14. Cheshire WP Jr, Wszolek ZK. Body mass index is reduced early in Parkinson's disease. *Parkinsonism Relat Disord*. 2005;11(1):35–38.
15. van der Marck MA, Dicke HC, Uc EY, et al. Body mass index in Parkinson's disease: A meta-analysis. *Parkinsonism Relat Disord*. 2012;18(3): 263–267.
16. Sheard JM, Ash S, Mellick GD, Silburn PA, Kerr GK. Markers of disease severity are associated with malnutrition in Parkinson's disease. *PLoS One*. 2013;8(3):e57986.
17. Fereshtehnejad SM, Ghazi L, Sadeghi M, et al. Prevalence of malnutrition in patients with Parkinson's disease: A comparative study with healthy controls using Mini Nutritional Assessment (MNA) questionnaire. *J Parkinsons Dis*. 2014;4(3):473–481.
18. Jaafar AF, Gray WK, Porter B, Turnbull EJ, Walker RW. A cross-sectional study of the nutritional status of community-dwelling people with idiopathic Parkinson's disease. *BMC Neurol*. 2010;10:124. doi: 10.1186/1471-2377-10-124
19. Kashihara K. Weight loss in Parkinson's disease. *J Neurol*. 2006;253 (Suppl 7):38–41.
20. Braak H, Del Tredici K, Rüb U, de Vos RA, Jansen Steur EN, Braak E. Staging of brain pathology related to sporadic Parkinson's disease. *Neurobiol Aging*. 2003;24(2):197–211.
21. Fereshtehnejad SM, Ghazi L, Shafieesabet M, Shahidi GA, Delbari A, Lökk J. Psychiatric and fatigue features associated with nutritional status and its effects on quality of life in Parkinson's disease patients. *PLoS One*. 2014;9(3):e91153.

The role of *OPRM1* polymorphism in the etiology of alcoholism

Agnieszka Samochowiec[1,A–F], Jerzy Samochowiec[2,A–F], Justyna Pełka-Wysiecka[2,B], Jolanta Kucharska-Mazur[2,B], Elżbieta Grochans[3,C], Marcin Jabłoński[2,B], Przemysław Bieńkowski[4,C], Sławomir Murawiec[5,C], Iwona Małecka[2,B], Monika Mak[2,C], Łukasz Kołodziej[6,B,C], Janusz Heitzman[7,E], Anna Grzywacz[2,A–E]

[1] Department of Clinical Psychology, Institute of Psychology, University of Szczecin, Poland
[2] Department of Psychiatry, Faculty of Medicine, Pomeranian Medical University, Szczecin, Poland
[3] Department of Nursing, Faculty of Health Sciences, Pomeranian Medical University, Szczecin, Poland
[4] Department of Psychiatry, Faculty of Health Sciences, Medical University of Warsaw, Poland
[5] DIALOG Therapy Center, Warszawa, Poland
[6] Department of Orthopedics, Faculty of Medicine, Pomeranian Medical University, Szczecin, Poland
[7] Department of Forensic Psychiatry, Institute of Psychiatry and Neurology, Warszawa, Poland

A – research concept and design; B – collection and/or assembly of data; C – data analysis and interpretation; D – writing the article; E – critical revision of the article; F – final approval of the article

Advances in Clinical and Experimental Medicine, ISSN 1899–5276 (print), ISSN 2451–2680 (online) *Adv Clin Exp Med*. 2019;28(2):199–202

Address for correspondence
Jerzy Samochowiec
E-mail: samoj@pum.edu.pl

Funding sources
None declared

Conflict of interest
None declared

Received on February 5, 2017
Reviewed on March 7, 2017
Accepted on October 13, 2017

Published online on August 7, 2018

Abstract

Background. Numerous studies have investigated the association between the *OPRM1* A118G polymorphism (rs1799971) and alcohol dependence, but the results have been inconsistent. The endogenous opioid system has been implicated in the development of alcohol dependence for its prominent role in the central rewarding mechanism.

Objectives. The aim of this study was to evaluate the role of the A118G polymorphism of the *OPRM1* gene in the pathogenesis of alcohol dependence syndrome (ADS).

Material and methods. The *OPRM1* (rs1799971) polymorphism was investigated in an association study of a group of ADS patients (n = 177) and in subgroups (delirium tremens and/or seizures, age at onset <26 years, dissocial alcoholics, positive familial history of alcoholism, delirium tremens, and seizures). The control group consisted of healthy volunteers, with matched gender and age, and with psychiatric disorders excluded (n = 162).

Results. Our research shows that there are differences in the genotypes and alleles of the *OPRM1* polymorphism in the case-control study. Furthermore, we observed associations in our homogeneous subgroups – in the group of patients with ADS and accompanying delirium tremens and/or seizures at the genotype level, as well as in the subgroup of patients under 26 years of age with an early onset of dependence.

Conclusions. It is strongly possible that the G allele described in numerous studies can be associated with a response to treatment, but not typology, or the very predisposition toward alcoholism. It is necessary to carry out further research which would embrace a larger group of patients; it should be divided into other homogeneous subgroups, including, e.g., naltrexone pharmacotherapy.

Key words: alcohol dependence, *OPRM1* gene, opioid system

Cite as
Samochowiec A, Samochowiec J, Pełka-Wysiecka J, et al. The role of *OPRM1* polymorphism in the etiology of alcoholism. *Adv Clin Exp Med*. 2019;28(2):199–202. doi:10.17219/acem/78592

DOI
10.17219/acem/78592

Introduction

The history of research on the opioid system dates back to the period of interest in the physiological effects of morphine, which is one of the alkaloids found in poppy seeds, or more precisely, opium. Thanks to the experiments carried out 38 years ago, morphine-binding receptors have been discovered.[1,2] As part of the research, 3 basic types of opioid receptors – μ, δ, κ (mi, delta and kappa) – were singled out. Opioid receptors are mainly present in the central nervous system, in the cellular membrane of neurons. They can also be found in some types of smooth muscles, as well as the digestive tract, immune system cells, uterus, heart, and lungs.

The abovementioned receptors are essential for signal cascades, which are responsible for the feeling of pain, the regulation of motor and psychophysical functions, and mood control. Numerous studies have indicated the modulatory effects of opioid receptors on the frequency and intensity of drinking relapse.[3,4] In medical circles, these findings have aroused hopes for the development of effective therapies for addiction, tailored to the needs of individual patients.

Research results have also proven that endogenous opioid peptides play a role in alcohol-related mechanisms. A single dose of alcohol promotes the secretion of β-endorphins and enkephalins, which stimulate opioid receptors. A lower level of β-endorphins may be a direct consequence of chronic alcohol abuse.[5]

It has also been proven that alcohol stimulates opioid peptide secretion and activates the reward system in the brain, thereby developing alcohol dependence. Accordingly, drugs which affect the opioid system may influence many behaviors associated with getting and consuming natural rewards (water, food or sex) and chemical rewards (alcohol, opiates or nicotine).

The μ-opioid receptor (*OPRM1*) has been repeatedly investigated with special attention paid to its relationship with alcohol dependence syndrome (ADS), addiction to psychoactive substances, schizophrenia, obesity, Alzheimer's disease, palliative treatment, and sensitivity to pain. Many authors have indicated serious and numerous relationships between the effects of opioids and alcohol.[6–11]

In 2003, O'Brien's team conducted a study in which a response to naltrexone was associated with a specific genetic variant of the μ-opioid receptor.[12] The alcoholics with this genetic variant who were administered naltrexone were able to function without alcohol for a long time, had shorter periods of intensive drinking and could abstain from drinking (or drink very little), which made them less likely to relapse to addiction after their therapy. Individuals who respond to naltrexone show some similarities: a very strong craving for alcohol and a family history of alcoholism. They start drinking when they are young and have a so-called "strong head". On a biochemical level, their endorphin response is stronger than in those who do not respond to naltrexone.[13]

The aim of this study was to evaluate the role of the A118G polymorphism of the *OPRM1* gene in the pathogenesis of ADS.

Material and methods

The *OPRM1* (rs1799971) polymorphism (Fig. 1) was investigated in an association study of a group of ADS patients (n = 177) and its subgroups (delirium tremens and/or seizures, age at onset <26 years, dissocial alcoholics, positive familial history of alcoholism, delirium tremens, and seizures). The patients were screened for other psychiatric disorders. We used the Semi-Structured Assessment for the Genetics of Alcoholism (SSAGA) for patient phenotyping.

The control group consisted of healthy volunteers, with matched gender and age, and with psychiatric disorders excluded by using Primary Care Evaluation of Mental Disorders Patient Health Questionnaire (PRIME-MD) (n = 162) (Table 1).

Table 1. Statistical characteristics of age in patients with ADS and in controls

Group	n	Mean [years]	SD [years]	Range [years]
ADS (men)	177	33	8.8	20–61
Controls (men)	162	38	15.8	18–80

ADS – alcohol dependence syndrome; SD – standard deviation.

Genotyping using a real-time polymerase chain reaction apparatus

The genome DNA for the analysis was isolated from the leukocytes of circumferential blood using a salting method. Genotyping of the selected polymorphism in the *OPRM1* gene was performed with the real-time polymerase chain reaction (PCR) method based on the use of fluorescent oligonucleotide probes, which hybridize with unique DNA sequences. The analysis of the *OPRM1* gene polymorphisms was performed with a LightCycler 2.0 (Roche Diagnostics, Pleasanton, USA), using the melting curve analysis for specific alleles. Genotyping results after the completion of the reaction were analyzed using LightCycler software v. 4.1 (Roche Diagnostics).

Statistical analysis

Differences between the controls and the ADS subjects were tested with the χ^2 test and were considered significant when type 1 error was <5%, using Statistical Package for Social Sciences (SPSS) v. 9.0 for Windows (Microsoft Corp., Armonk, USA). The Hardy-Weinberg equilibrium was calculated using SAS v. 8.02 for Windows (SAS Institute, Cary, USA).

Results

We examined 162 alcohol-dependent patients vs 177 cases and found that there were differences in genotypes and alleles of the *OPRM1* polymorphism. What is more, we observed associations in our homogeneous subgroups – in the group of patients with ADS and accompanying delirium tremens and/or seizures (Table 2) at the genotype level, as well as in the subgroup of patients under 26 years of age with an early onset of dependence (Table 2).

Discussion

In 2007, Van den Wildenberg et al. stated that heavy-drinking individuals with a copy of the G allele are more prone to experiencing cue-induced craving after exposure to an alcoholic beverage.[14] Interestingly, carriers of at least 1 rs1799971(G) allele appear to have stronger cravings for alcohol than carriers of 2 rs1799971(A) alleles, and are thus hypothesized to be at a higher risk for alcoholism. On the basis of the abovementioned studies, we can conclude that these findings have several implications. Firstly, individuals with a copy of the G allele seem to be more sensitive to cue-induced subjective cravings for alcohol than individuals homozygous for the A allele.[14] Another interesting aspect of the literature in this respect is a study performed by Anton et al., in which among over 200 alcoholics treated with naltrexone, rs1799971(G) carriers receiving the drug had a higher percentage of abstinent days and a lower percentage of heavy drinking days (p = 0.04) compared to those receiving a placebo, whereas rs1799971(A;A) homozygotes showed no differences connected with medication. Upon treatment with naltrexone, 87% of rs1799971(G) carriers had a good clinical outcome, compared to only 55% of individuals with the (A;A) genotype.[15]

Although the association between a polymorphism of the *OPRM1* receptor gene and adolescent alcohol misuse was tested by Ray et al., our findings provide the first evidence that the A118G single-nucleotide polymorphism (SNP) of the *OPRM1* gene is associated with alcohol use disorder (AUD) diagnoses during adolescence, as well as with a greater number of alcohol-related problems among adolescent drinkers.[4] Those who carried the G allele turned

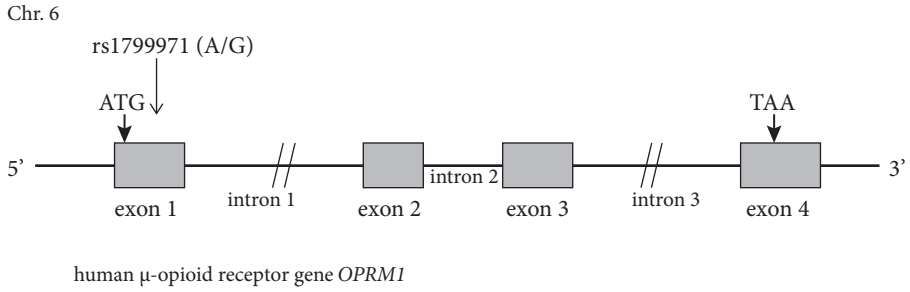

Fig. 1. The μ-opioid receptor gene (*OPRM1*) is located on chromosome 6, at [6q25.2]; it consists of 4 exons separated by introns

Table 2. Frequencies of genotypes and alleles of the investigated *OPRM1* (rs1799971) polymorphism in alcoholics (n = 177) and in the control group (n = 162)

Groups	n	Genotypes			p-value	Alleles		p-value
		A/A n (%)	A/G n (%)	G/G n (%)		A n (%)	G n (%)	
Controls	162	119 (0.73)	40 (0.25)	3 (0.02)	–	278 (0.86)	46 (0.14)	–
Cases	177	146 (0.82)	29 (0.16)	2 (0.02)	0.13	321 (0.91)	33 (0.09)	0.048*
Delirium tremens and/or seizures	51	45 (0.88)	4 (0.08)	2 (0.04)	0.02*	94 (0.92)	8 (0.08)	0.09
AOO <26	122	104 (0.85)	18 (0.15)	0 (0.0)	0.03*	226 (0.93)	18 (0.07)	0.01*
Dissocial alcoholics	63	52 (0.82)	10 (0.16)	1 (0.02)	0.35	114 (0.9)	12 (0.01)	0.18
Positive familial history of alcoholism	56	47 (0.84)	8 (0.16)	0 (0.0)	0.22	103 (0.92)	9 (0.08)	0.09
Delirium tremens	32	27 (0.84)	3 (0.1)	2 (0.06)	0.07	57 (0.89)	7 (0.11)	0.48
Seizures	31	27 (0.87)	3 (0.1)	1 (0.03)	0.17	57 (0.92)	5 (0.08)	0.19

AOO <26 – age of onset less than 26 years; p-values of the χ^2 test for genotypes; * statistical significance.

to drinking to enhance the positive affect more strongly than those who were homozygous for the A allele, and drinking to enhance the positive affect mediated the association between *OPRM1* and alcohol-related problems.[16]

The meta-analysis performed by Chen et al. in 2012 shows a list of 12 independent studies with 1,900 cases and 2,382 controls – 5 studies were conducted in Asians and 7 in Caucasians. Ethnicity-specific meta-analyses revealed that the A118G polymorphism significantly correlated with the risk for alcohol dependence in Asians, but not in Caucasians.[17] However, in central Sweden – according to Bart et al. – the functional variant 118G allele in exon 1 of *OPRM1* was associated with an increased attributable risk of alcohol dependence.[18]

Numerous researchers have associated the *OPRM1* gene and its polymorphic variant with a response to naltrexone. In the study performed by Bart et al., the results indicate that individuals with at least 1 copy of the G allele reported a lower alcohol craving and a stronger alcohol-induced "high" across rising breath alcohol concentrations.[18] Naltrexone was found to blunt the effects of alcohol on stimulation, positive mood, craving, and enjoyment. The effects of naltrexone on blunting the alcohol-induced "high" were stronger among individuals with the G allele.[4]

Rommelspacher et al. found little evidence in relation to these associations and concluded that there was no significant difference in the frequency of the Asp40 allele between the control subjects and the alcohol-dependent subjects with a family history of parental alcoholism, subjects with early-onset alcohol dependence or alcohol-dependent subjects with severe withdrawal symptoms. Their results provide only some evidence for an allelic association of the Asn40Asp SNP with alcohol dependence.[19]

Conclusions

In light of the abovedescribed findings we can say the results are unambiguous – we observed a frequent occurrence of the A allele in the control group and in selected homogeneous subgroups.

It is strongly possible that the G allele described in numerous studies can be associated with a response to treatment, but not with typology or the very predisposition toward alcoholism. It is necessary to carry out further research which would embrace a larger group of patients; it should be divided into other homogeneous subgroups, including, e.g., how the patients respond to naltrexone pharmacotherapy.[20]

References

1. Hughes J. Isolation of an endogenous compound from the brain with pharmacological properties similar to morphine. *Brain Res.* 1975; 88(2):295–308.
2. Terenius L, Wahlström A. Search for an endogenous ligand for the opiate receptor. *Acta Physiol Scand.* 1975;94(1):74–81.
3. Latt NC, Jurd S, Houseman J, Wutzke SE. Naltrexone in alcohol dependence: A randomised controlled trial of effectiveness in a standard clinical setting. *Med J Aust*. 2002;176(11):530–534.
4. Ray LA, Hutchison KE. Effects of naltrexone on alcohol sensitivity and genetic moderators of medication response. *Arch Gen Psychiatry.* 2007;64(9):1069–1077.
5. Kiefer F, Horntrich M, Jahn H, Wiedemann K. Is withdrawal-induced anxiety in alcoholism based on β-endorphin deficiency? *Psychopharmacology (Berl).* 2002;162(4):433–437.
6. Agabio R, Colombo G. GABAB receptor as therapeutic target for drug addiction: From baclofen to positive allosteric modulators [in Polish]. *Psychiatr Pol*. 2015;49(2):215–223.
7. Iwanicka KA, Olajossy M. The concept of alcohol craving [in Polish]. *Psychiatr Pol.* 2015;49(2):295–304.
8. Oswald LM, Wand GS. Opioids and alcoholism. *Physiol Behav.* 2004; 81(2):339–358.
9. Kiejna A, Piotrowski P, Adamowski T, et al. The prevalence of common mental disorders in the population of adult Poles by sex and age structure – an EZOP Poland study [in Polish]. *Psychiatr Pol.* 2015;49(1): 15–27.
10. Klimkiewicz A, Klimkiewicz J, Jakubczyk A, Kieres-Salomoński I, Wojnar M. Comorbidity of alcohol dependence with other psychiatric disorders. Part I. Epidemiology of dual diagnosis [in Polish]. *Psychiatr Pol.* 2015;49(2):265–275.
11. Klimkiewicz A, Klimkiewicz J, Jakubczyk A, Kieres-Salomoński I, Wojnar M. Comorbidity of alcohol dependence with other psychiatric disorders. Part II. Pathogenesis and treatment [in Polish]. *Psychiatr Pol*. 2015;49(2):277–294.
12. O'Brien CP. Research advances in the understanding and treatment of addiction. *Am J Addict*. 2003;12(Suppl 2):S36–47.
13. Anton RF, Oroszi G, O'Malley S, et al. An evaluation of mu-opioid receptor (*OPRM1*) as a predictor of naltrexone response in the treatment of alcohol dependence. *Arch Gen Psychiatry.* 2008;65(2): 135–144.
14. Van den Wildenberg E, Wiers RW, Dessers J, et al. A functional polymorphism of the mu-opioid receptor gene (*OPRM1*) influences cue-induced craving for alcohol in male heavy drinkers. *Alcohol Clin Exp Res.* 2007;1:1–10.
15. Anton R, Oroszi G, O'Malley S, Couper D, Swift R. An evaluation of μ-opioid receptor (*OPRM1*) as a predictor of naltrexone response in the treatment of alcohol dependence. *Arch Gen Psychiatry.* 2008;65(2): 135–144.
16. Miranda R, Ray L, Justus A, et al. Initial evidence of an association between *OPRM1* and adolescent alcohol misuse. *Alcohol Clin Exp Res.* 2010;34:112–122.
17. Chen D, Liu L, Xiao Y, Peng Y, Yang C, Wang Z. Ethnic-specific meta-analyses of association between the *OPRM1* A118G polymorphism and alcohol dependence among Asians and Caucasians. *Drug Alcohol Depend*. 2012;123(1–3):1–6.
18. Bart G, Kreek MJ, Ott J, et al. Increased attributable risk related to a functional mu-opioid receptor gene polymorphism in association with alcohol dependence in central Sweden. *Neuropsychopharmacology.* 2005;30(2):417–422.
19. Rommelspacher H, Smolka, M, Samochowiec J, Hoehe MR. Genetic analysis of the m-opioid receptor in alcohol-dependent individuals. *Alcohol*. 2001;24(2):129–135.
20. Bieńkowski P. Pharmacological features of naltrexone and its use in the treatment of alcohol dependence [in Polish]. *Psychiatr Pol*. 2013;47(1):117–126.

Technical aspects of nasal cavity surgery through the Le Fort I down-fracture approach: An otolaryngologist's point of view based on 90 patients' experience

Monika Morawska-Kochman[1,A–F], Kamil Nelke[2,3,B–D], Jan Nienartowicz[4,B,E,F], Wojciech Pawlak[4,A,C,F], Marek Bochnia[1,A,C,E]

[1] Department of Clinic Otolaryngology, Head and Neck Surgery, Faculty of Postgraduate Medical Training, Wroclaw Medical University, Poland
[2] Department of Maxillofacial Surgery, 4th Military Hospital, Wrocław, Poland
[3] Department of Maxillofacial Surgery, University Teaching Hospital, Wrocław, Poland
[4] Department of Maxillofacial Surgery, Faculty of Dentistry, Wroclaw Medical University, Poland

A – research concept and design; B – collection and/or assembly of data; C – data analysis and interpretation;
D – writing the article; E – critical revision of the article; F – final approval of the article

Advances in Clinical and Experimental Medicine, ISSN 1899–5276 (print), ISSN 2451–2680 (online) *Adv Clin Exp Med*. 2019;28(2):203–210

Address for correspondence
Kamil Nelke
E-mail: kamil.nelke@gmail.com

Funding sources
None declared

Conflict of interest
None declared

Received on May 14, 2017
Reviewed on June 20, 2017
Accepted on November 22, 2017

Published online on August 7, 2018

Abstract

Background. The downfracture access to septo- and turbinoplasty during maxillary osteotomy may be recommended in many cases. One or both of these laryngological interventions may be necessary when, after the patient's clinical evaluation, either an impaired function of nasal breathing or a deviated septum are present. The main postsurgical risk of the procedure is the destabilization of the cartilaginous septum position and its relation to adjacent anatomical structures, a change in the shape of the nose and the presence of a supratip break.

Objectives. In this paper, the authors present their own experience in intranasal procedures, the relevant surgical techniques and possible complications, based on their own clinical findings and on a literature review.

Material and methods. The general aim of the study was to describe the key points and differences between septo- and turbinoplasty performed classically and during Le Fort I osteotomy based on 90 orthognathic surgery patient cases. The procedures have been evaluated and compared regarding their advantages and disadvantages.

Results. Intraoperative downfracture of the maxilla facilitates the performance of various subsequent procedures in the regions of the nasal cavities and sinuses. Due to a very convenient access to the nasal cavities, it is possible to perform septo- or turbinoplasty in patients with nasal airway breathing problems, a deviated septum, and in others.

Conclusions. A combined effort of an otolaryngologist and a maxillofacial team improves the overall nasal breathing with a limited amount of complications. Endoscopy with low-dose computed tomography (CT) is a valuable diagnostic tool for measuring any breathing improvements in nasal capacity. Objective patient nasal breathing problems should be always investigated.

Key words: nasal septum, orthognathic surgery, maxillary osteotomy, intranasal procedure, septoplasty

Cite as
Morawska-Kochman M, Nelke K, Nienartowicz J, Pawlak W, Bochnia M. Technical aspects of nasal cavity surgery through the Le Fort I down-fracture approach: An otolaryngologist's point of view based on 90 patients' experience. *Adv Clin Exp Med*. 2019;28(2):203–210. doi:10.17219/acem/80746

DOI
10.17219/acem/80746

Introduction

The main aim of orthognathic surgery is not only focused on the improvement of facial esthetics, but also on the quality of breathing. Along with achieving proper jaw alignment, surgery may lead to an improvement in the patient's speech, swallowing, breathing, sleeping, and other functions. There are specific conditions, such as sleep apnea, that can be treated with advancement or segmental jaw movement. Additional procedures performed during jaw surgery can also include corrective chin surgery, rhino-, septo- or turbinoplasty, temporomandibular joint surgery, cheek implant insertion, tissue augmentation, and more. The intranasal approach after maxillary downfracture is a known method of access to both nasal cavities and sinuses that is well-described in the literature.[1,2] The indications and contraindications for this approach, and the usage of this technique are still under dispute worldwide.

Preoperative evaluation and measurement of the patient's quality of nasal airway breathing may include various diagnostic methods. They can be used along with the patient's medical history and a physical examination to evaluate the need for an additional surgery in the nasal cavities. To assess the patient's problems with nasal airway obstruction, some authors have used psychometric questionnaires, such as the Nasal Obstruction Symptom Evaluation (NOSE) scale. Studies seem to confirm the importance of the NOSE scale as an evaluation tool that may increase surgical indications for an additional nose surgery.[3,4] Nonetheless, the method is only a subjective evaluation of nasal obstruction. Nowadays, computed tomography (CT) is the gold standard for facial skeletal evaluation. Other methods lag behind CT.[5,6] Cephalometry performed as a non-routine examination, as well as other optional procedures – like video endoscopic photographic documentation of the nose and nasopharynx, rhinomanometry or acoustic rhinometry, nasal inspiratory peak flow, and visual analogue scales – are also used in the assessment of the efficiency of breathing through the nose.[7,8]

Le Fort I osteotomy is used for the correction of dentofacial deformities in the middle part of the facial skeleton. Indications for this osteotomy might include maxillary deficiency, hypoplasia or hyperplasia, gummy smile, or other types of dentofacial deformities.[9–12] Surgical repositioning of the maxilla, particularly its advancement, may result in an improvement in nasal breathing. This is due to the increase in the volume of the nasal cavity and the size of the nasolabial angle, which improves nasal ventilation.[8,12] Sometimes, to avoid functional problems in nasal breathing, an additional intervention is needed, particularly in patients with increased preoperative nasal airway resistance. In some of these patients, e.g., patients with a deviated nasal septum, their existing symptoms may be aggravated if such procedures are abandoned. Proper functioning of the upper airway has a considerable effect on the patient's quality of life. Improvement after orthognathic surgery combined with septo- or turbinoplasty applies not only to the nasal patency, but also to the sense of smell, sinus drainage, sleep comfort, effort, and daily fatigue tolerance.[13]

The majority of authors recommend providing the necessary concomitant septoplasty along with a reduction of the size of hypertrophic inferior nasal turbinates in the course of orthognathic surgery with Le Fort type osteotomy and the downfracture approach for exposure.[10,14] These procedures are most often executed by maxillofacial surgeons, and rarely by ear, nose and throat (ENT) specialists. In the presented paper, the authors collected a team of maxillofacial and ENT surgeons that evaluated and operated on orthognathic patients together.

In the course of our collaboration, we noticed some differences depending on the specialization of the surgeon performing the procedure. These differences involved the approach to the problem of the impaired nasal airflow and the surgical techniques selected to improve it. The general aim of this study was to describe the key points and differences between septo- and turbinoplasty performed classically and during Le Fort I osteotomy. Our own clinical experience on the simultaneous septo- and turbinoplasty technique with the downfracture access will be presented. Furthermore, an additional objective was to focus on improving nasal breathing in treated patients.

Ethics statement

This paper required approval from an institutional committee, since the study is related directly with human care and treatment. The presented paper is in full compliance with and corresponds to the Helsinki Declaration.

Material and methods

A total of 90 patients' charts were reviewed. In the study, 54% of patients were male (males (M): 49, 54.44%; females (F): 41, 45.55%). The average age of the patients was 26.6 years (range: 19–38 years). Qualification for nasal procedures was done after considering the medical history of anamneses, an endoscopic examination and evaluation of CT findings in particular. A total of 29 participants of the study group were diagnosed with bilateral decreased nasal patency, while 23 had permanent one-sided nasal obstruction. Another 23 patients had periodic nasal obstruction episodes and 15 had never reported any sensations of nasal patency. We carried out 46 septoplasties and 44 turbinoplasties (19 bilateral and 25 unilateral) in the presented group (Table 1). STATISTICA software v. 17 (StatSoft Polska, Kraków, Poland) was used for t-test evaluation. All surgical and clinical data was gathered and analyzed with Statistical Package for the Social Sciences (SPSS) v. 17 software (SPSS Polska, Kraków, Poland) with

Table 1. Detailed patient procedures

Procedure (n = 100)	Patient data n = 90 (M = 49; F = 41); p < 0.05			
Septoplasty n = 46; 100%; p > 0.05	M n = 27 58.7% p < 0.05		F n = 19 41.3% p > 0.05	
Turbinoplasty n = 44; 100%; p < 0.05	bilateral (n = 19)		unilateral (n = 25)	
	M n = 7 15.9% p > 0.05	F n = 12 27.28% p < 0.05	M n = 15 34.09% p < 0.05	F n = 10 22.73% p > 0.05

M – males; F – females.

Table 2. Access points to the nasal septal framework

Most common surgical approaches to the nasal septum	
Kilian incision (through the mucosa and perichondrium up to the septal cartilage)	transfixion incision (an incision made at the caudal end of the septal cartilage); a subperichondrial dissection can be provided on 1 or both sides of the septum
Partial-transfixion incision (a vertical incision of the skin of the nasal vestibule)	external approach; an incision performed in the open approach that combines the incision on the level of the columella with the horizontal marginal incision along the greater alar cartilages

the use of the χ^2 test and the analysis of variance (ANOVA). Most data was focused on improved nasal breathing estimation in the patients undergoing surgery.

The surgical technique that we suggested was used in each case presented in this paper. In order to understand changes in nasal breathing, it is essential to understand the key points of this team-approach surgical technique. Proper preparation of the nasal mucosa is a very important aspect in every procedure regarding the nasal septum. In the classic technique of septoplasty, the nasal mucosa is first sprayed with a combination of 2% lidocaine and 1:100,000 epinephrine. Next, 5 min later, 2 pledges soaked in the same solution are inserted into each nasal cavity for 5 min. After that, the mucosa of the septum is infiltrated on each side with 5 mL of 1% lidocaine and 1:100,000 epinephrine solution. The solution should be injected under the mucoperichondrium to elevate the mucosa. This should make the dissection much easier. In the case of exposure of the nasal septum by downfracture during orthognathic surgery, infiltration or local anesthesia are usually not applied. Two gauzes soaked with anticoagulant rinse (acidum tranexamicum) are placed into both nasal cavities while surgical burs are used and the frontal maxillary sinus walls are cut horizontally. The average time of gauze application is about 5 min.

Injection through the nasal passages is particularly difficult on the side of the naso-tracheal intubation. In our opinion, topical anesthesia at least should be applied at the beginning of the procedure – infiltration of both the side wall and the septum of the intubation-free side – since access to the nasal septum will be much more difficult after the exposure of the inferior part of the septum and downfracture. Even a unilateral injection applied under the mucoperichondrium decreases the risk of laceration and injury of the mucosa of the septum and the oral cavity floor. It also facilitates the following procedure. The most common access points to the nasal septum framework in the classic technique have been well-described (Table 2).[15]

Endonasal approaches to the nasal skeleton can be used for the primary treatment of traumatic injuries, and for secondary procedures, such as septorhinoplasty, but are useless in the Le Fort I downfracture procedures. The exposure of the septum after downfracture both facilitates and enforces a completely different surgical approach. We would like to distinguish our approach with a separate name: the downfracture approach.

During Le Fort I osteotomy from the sublabial approach, the anterior nasal spine is dissected, then a submucosal tunnel is made in the nasal floor; after that, the nasal crest is cut with a chisel. The nasal crest forms a groove for the reception of the septal framework. The inferior part of the quadrangular cartilage on the side of the nasal spine and the vomer in the posterior part are partially dissected. Usually, after chiseling above the bone groove (about 3 mm deep) and fracturing the vomer, the inferior part of the nasal septum is removed. Usually, its height is about 2–3 mm, which corresponds to the depth of the groove. The remaining part of the nasal crest is removed and the groove is dredged up to the proper depth depending on the extent of the impaction or advancement (and on other combinations of surgical moves, such as rotation or extrusion) of the maxilla during the procedure, mostly in the area of the pyriform aperture. After a controlled surgical break of the maxilla, an open access to the nasal septum is gained, from its bony base upward – a larger access in the anterior part and a smaller one in the posterior part, as well as access to the turbinates and the nasal cavity floor. The shortcoming is the limited visibility in the middle and superior posterior part of the septum, and in the posterior nares (Fig. 1,2).

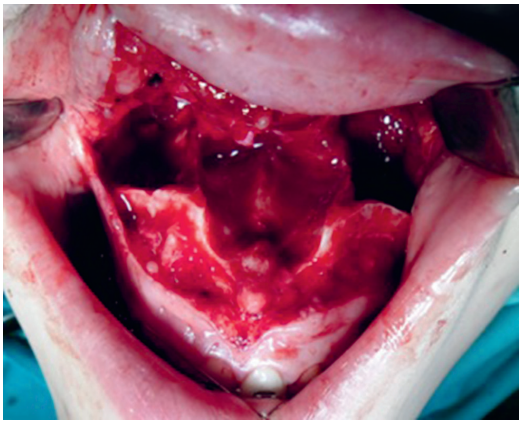

Fig. 1. Intranasal approach to the septum and conchae

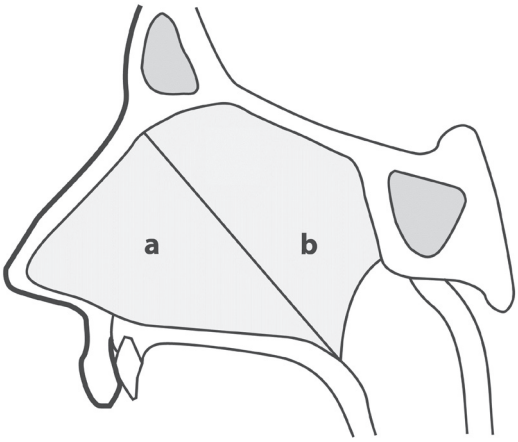

Fig. 2. Nasal septum projection with areas "a" and "b"

The next step of the procedure is the dissection of the mucoperichondrial and mucoperiosteal flaps, which facilitates the release and repositioning of deviated septal structures. Preparation of the mucoperiosteal flaps is usually easier in the posterior part of the septum. Using a Freer elevator in a sweeping motion, the surgeon is able to dissect the mucoperichondrium from the entire septal cartilage and septal bone (Fig. 3). This is typically performed on

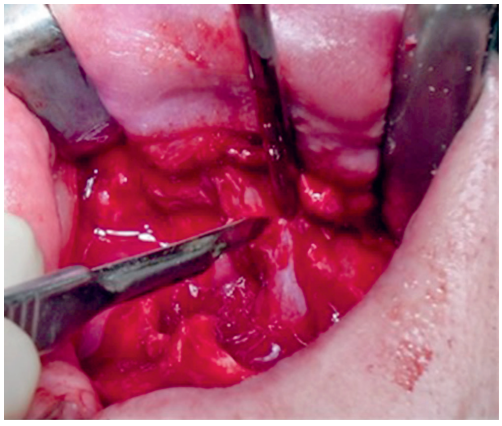

Fig. 3. Dissection of the mucoperichondrium from the entire septal cartilage and septal bone

1 side only in order to preserve blood supply to the septum. Sometimes, with a large area and complicated architecture of the deviation, unilateral dissection may be insufficient. In the discussed downfracture technique, the preparation is difficult, because the septum is mobile and unsupported, and the border between the mucoperichondrial layer, the mucoperiosteal layer, the cartilage, and the bone is poorly visible. A mass of connective tissue fibers, previously connecting the septal mucosa to the incisive bone, are cut while chiseling the bone groove, which complicates the situation even more. In order to protect the septal mucosa, it is often necessary to cut the superficial layer of fibers at the base of the septum with a scalpel. In our opinion, the initial dissection of the mucosa from the nasal cavity floor and the lower part of the septum, made under visual control before chiseling above the groove, may significantly facilitate further proceedings. This is because the inferior mucosal tunnel prepared at the beginning of the procedure is often injured and needs to be sutured at the end of the procedure. This kind of laceration also uncovers a subjacent part of the lower turbinate. If the surgeon is planning to perform a turbinoplasty and the whole mucosa is preserved, it should be cut parallel to the lower margin of the lower turbinate, as described by Posnick and Agnihotri (Fig. 1).[14] It is possible to modify the single incision into a T-shaped cut in order to gain better access to the surface of the turbinates and to limit the risk of uncontrolled laceration of the mucosa (Fig. 2).

This stage of the operation is preferable for turbinoplasty or turbinectomy procedures. We prefer submucosal thermal ablation, which can be performed with a cautery unit. This technique, as opposed to a partial or complete turbinate resection, ensures the preservation of the nasal mucosa. In some cases, cauterization can be completed with a partial resection of the overgrown posterior parts of the inferior turbinates with the loop.

In the next step, the chondro-osseal junction of the quadrangular cartilage, the perpendicular plate and the vomer are dissected. After that, the deviated part of the chondro-osseal septal framework is removed, with particular care to spare as much of the patient's tissue as possible. Fixing the anterior-inferior septal cartilaginous strut to the maxillary anterior nasal spine with a 4-0 polydioxanone (PDS) suture (Johnson & Johnson, Ethicon Inc., Bridgewater, USA) and the cartilage junction to the vertical part of the ethmoid bone is particularly important for the proper projection of the nose tip and for stable anchorage of the nasal septum. Failure in this element of the procedure may cause a rearward or bilateral shift of the nasal septum. We recommend controlling the position of the septum not only from the side of the maxilla, but also using a nasal speculum through the anterior nares on the side of the free nasal passage. This maneuver is particularly useful in the assessment of the necessary extent of the resection of the septal framework and of the patency of the inferior and middle nasal passage. At the end of the procedure, the

mucosa of the nasal cavity floor is stitched with a single 4-0 polydioxanone (PDS) suture. Silastic septal splints are then applied to each of the mucoperichondrial planes with a running 4-0 nylon suture to stabilize the mucosal flap and to prevent septal hematoma or scare formation.[2,16] It is more difficult to stitch the flaps and to place the splints in the nasal vestibule during orthognathic surgery than during the classic septoplasty. This is due to the intubation tube placed in one of the nose cavities. Limited visibility and placement of the naso-tracheal tube without adequate insight and careful septal splint suturing might lead to suturing or perforating the tube.

Our experience shows that the use of systemic steroids tends to be effective in the postoperative period to reduce mucosal edema. Patients receive intravenous steroids (dexamethasone, max 24 mg/day) on the day of surgery and 1 day postoperatively. First, 8 mg of dexamethasone is administered at the start of Le Fort I osteotomy and the 2nd dose is administered up to 4–6 h after surgery. The last dose (8 mg) is administered early in the morning on the 1st day after surgery.

The nasal packing and septal splints are removed in the 1st week after the operation. In order to minimize intranasal edema and crusting, patients are instructed to use an intranasal local vasoconstrictor agent (xylometazoline hydrochloride) 2–3 times per day in the 1st week and a saline mist 4–6 times per day for 2–3 weeks after the operation. Each patient is evaluated postoperatively by craniofacial surgeons and otolaryngologists at weekly intervals for a total of 3 consultations.

Results

Bilateral turbinoplasty with simultaneous septoplasty were performed in 36 cases (40%; $p < 0.05$) (Table 1). Improvement in nasal breathing after routine endoscopic and CT evaluation was found in 78 patients (86.7%; $p < 0.05$). In 2 cases, nasal breathing was greatly impaired, as shown in Fig. 2, because of subluxation of the nasal septum in area "a" and because of the presence of the nasal spine in the deviated area "b". No correlation between gender or age and nasal patency was noticed ($p > 0.05$).

Discussion

Various techniques are quite often performed in addition to standard procedures in orthognathic surgery.[17–20] Sarver and Rousso point out that rhinoplasty, submental liposuction, malar augmentation, lip lift and augmentation can easily be performed simultaneously with Le Fort I downfracture.[17] We would like to highlight that rhinoplasty is the most common technique here. It is also quite important to note that orthognathic surgery performed together with rhinoplasty can greatly influence the upper airway system. The authors of the studies on concurrent orthognathic and septo- and turbinoplasty procedures that were available for this review were mostly maxillofacial surgeons.[7,13,21,22] Most of them particularly recommend such proceedings in patients with pre-existing nasal patency disorders.[7,13,14] A study performed by Haarmann et al. in order to evaluate changes in nasal airways after Le Fort I osteotomy and functional rhinosurgery confirms a significant improvement in breathing in the entire study group.[7] The authors point out that during the impaction of the maxilla, additional rhinosurgery should always be performed. Waite et al. performed 22 septorhinoplasties simultaneously during orthognathic surgery.[18] No significant differences were noticed in either Le Fort I procedure or isolated sagittal split osteotomies of the mandible, and their influence on septorhinoplasties. Unlike the previously cited authors, Williams et al. examined the nasal airway function with a quality-of-life survey instrument in patients after Le Fort I osteotomy performed without any rhinosurgery.[23] As a result of maxillary advancement, patients scored >25 points on the NOSE scale and reported a lack of nasal obstructive symptoms. In our opinion, this may have resulted from the different rules of case selection, as well as from different preparation and procedure techniques that diverge from standard laryngological procedures. The main differences include limited visibility into the nasal passages (nasal intubation), an imposed operational approach, the need to adjust the septoplasty and the resection of the lower part of the septum and lower turbinates to the anatomical conditions altered in the orthognathic procedure, and a lack of anterior nose packing after the procedure. There are 3 essential problems that should be considered when qualifying patients for orthognathic procedures: determination of the indications for simultaneous septo- or turbinoplasty, the resection mode of the cartilaginous part of the septum framework and the scope of volume decrease of the lower nasal turbinates.

Preliminary psychological assessment seems to be necessary not only regarding the orthognathic procedure, but also the septoplasty procedure, which is due to the arduousness of the postoperative period. Such discomfort is mostly due to the necessary application of septal splints that fix the septum within the median line and prompt a temporary nasal blockage. The recent review of the literature made by Tang and Kacker suggests that many types of septal splints are used worldwide; however, the usage of improved thinner splints might lead to an improvement in the mucosal status with decreased postoperative pain and discomfort.[24] They can be used as an effective alternative to nasal packing after septoplasty.[25] We would like to stress that nasal packing after septoplasty in Le Fort I osteotomy is not only unnecessary, but it also can be life-threatening, as it blocks the nose, while the mandible and the maxilla are immobilized by the intermaxillary ligature steel wires used to fix the intraoral jaw.

Qualification for the surgery is usually based on a subjective and objective assessment of the patient. So far, there

have been no established criteria for patient qualification for the procedure, and Posnick et al. – among others – suggests that there is a need for such qualification.[10,13,14] Many subjective methods may be used in the assessment of nasal patency (visual analogue scales and psychometric questionnaires) as well as objective methods (pressure flowmeter, acoustic rhinomanometry and fiberoscopy).[7–10,26–28] In our opinion, problems with breathing through the nose which are revealed in the patient's medical history are the most important indication for any nasal procedure. If an additional examination does not lead to a conclusion of whether the surgeon should perform an additional nasal surgery, the NOSE scale evaluation with the patient's best interests should be taken into consideration. Also, additional questions about sleep position and the ability to breathe through the nose while sleeping on the back should be asked.

Fiberoscopy is an objective assessment that reveals anatomical changes in the nasal region both before and after the surgery. It is useful in diagnosing changes connected with a deviated septum, adhesions or perforations that may be overlooked during rhinoscopy. Moreover, it is a rather inexpensive and noninvasive examination performed under local anesthesia.[9] It should be performed preoperatively in every patient with a nasal patency disorder. Only an abnormal result in fiberoscopy may be a possible indication for extending the diagnostics with rhinomanometry.[8] Rhinomanometry is a useful, objective method of preoperative and postoperative assessment, though, next to the diagnostic imaging methods, it may only increase the costs of the preparation for the procedure.[7,8,27] It may reveal a possible nasal patency obstruction, but does not diagnose its anatomical cause. Otolaryngologists rarely make use of diagnostic imaging when preparing patients for septo- and turbinoplasty. Additionally, many clinicians use special computer planning before orthognathic surgeries. In most cases, it is used to evaluate and calculate bone and soft tissue changes, and it also helps to evaluate the upper respiratory tract patency and size.[29] We would like to point out that the examination which provides a precise assessment is CT with preliminary mucosal decongestion of the nasal turbinates. Nasal decongestants, in both topical and oral forms, are some of the most effective drugs available for reducing congestion of the turbinate mucosa, but only on the day of examination. Another way to reduce congestion is to use topical steroids a few days before the day of examination. During the initial clinical assessment of patients, in the process of qualification for surgery, we first performed the anterior rhinoscopy without topical decongestants. Then, a topical decongestant (oxymetazoline) was applied and rhinoscopy of the nasal airway was performed. We noted the nasal septum shape, the state of the mucosa and the size of the turbinates. Nasal endoscopy and CT not only facilitate imaging data collection and proper qualification for the procedure, but they also set the grounds for doctor–patient communication in order to explain the necessity of the procedure and the evaluation of its effects. At the qualification interview, the patient should always be informed about possible complications that may result from an extended orthognathic procedure, particularly with septoplasty.[8]

Another key technical problem is the extent of resection of the septal cartilage. This problem does not exist when the procedure is performed by a laryngologist in the classical manner. But when septoplasty is performed during orthognathic surgery, the extent of the resection of the inferior part of the septum should be taken into consideration in relation to dredging up the nasal cavity floor, widening the pyriform aperture and reducing the nasal spine, performed in order to reduce gummy smile. Those aspects of the procedure require the surgeon's close attention. In the case of orthognathic procedures, the proportions are altered and a mismatch may occur between the height of the septum that is mobilized at its entire length and the new dimensions of the advanced maxilla. It is important to try to resect the cartilage as sparingly as possible, as it can be reinserted after processing its shape and adjusting its dimensions to the new anatomical conditions. Laryngologists take care to preserve as much cartilaginous tissue as possible, particularly in the front part, in the nasal vestibule. Maxillofacial surgeons mostly pay attention to the shortening of the cartilaginous part of the septum, so after closing the edges of the bones, it rests "comfortably" in the groove made in the median line. When the remaining fragment is too high, the cartilage may dislocate sideways, narrowing the light of the nasal passages. In some cases, it might also increase the nasal supratip break (Fig. 4). A resection of the inferior part which is too large may induce – without correction of the deviation

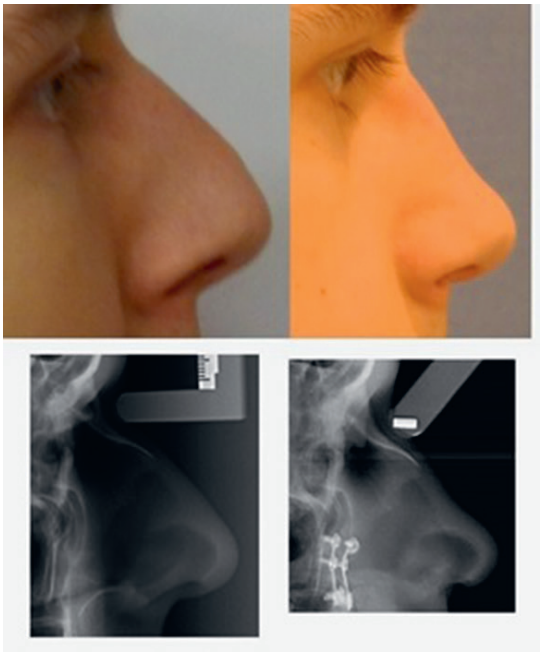

Fig. 4. Nasal tip and supra tip-notch projection before and after septoplasty and additional Le Fort I osteotomy

– a transverse dislocation of the free fragment of the cartilage, which may block the nasal airways and decrease its patency after the procedure. This problem only concerns the flexible part of the septum – the cartilage. The rigid, bony part of the septum imposes the proper height by itself. Depending on the extent of the resection, a significant change in the shape of the nose may occur (into a saddle shape with an uplifted or dropped nose tip, a nasal hump, and a change in the shape of the nostrils).[22] In our opinion, it is useful to jointly adjust the extent of the resection during the procedure, based on several fittings after the impaction of the maxilla.

Another problem is the approach to the surgery of the inferior nasal turbinates. The pathology of the turbinates is inseparably connected with their hypertrophy. The turbinate on the side of the deviation is usually small and atrophic, while the one on the other side is hypertrophic. Only the obstructive hypertrophy may be an indication for turbinoplasty, not the edema of the mucosa of the turbinate. The excessive tissue should be assessed after decongestion of the mucosa, by both endoscopy and a radiological examination. On the other hand, mucosal edema occurs during orthognathic procedures despite the application of decongestants at the beginning of the procedure. It seems that this problem is not usually taken into consideration, and the procedure may be performed too radically or not radically enough.

The techniques of volume reduction of the lower turbinate include turbinate outfracture, resection (submucosal resection, partial resection, trimming of the turbinates and inferior turbinoplasty, reduction by a microdebrider, and laser vaporization), electrocautery, cryosurgery, or coablation.[30] In the most commonly used resection technique, it is recommended to reduce the inferior turbinate by 2/3 of the volume.[14,21] However, turbinectomy performed along the lower edge of the turbinate may result in massive hemorrhage, the development of granulation tissue or necrosis of the exposed bone. Radical removal of the inferior turbinate tissue may also provoke symptoms of so-called "empty nose syndrome." As a result of extensive scar formation after the turbinate resection, the patient may not feel hot and cold stimuli properly, having the impression of obstruction, with a substantial width of the nasal cavity. Extensive scars also impair the physiological functions of the nasal mucosa (warming, humidification and air filtration) predisposing the patient to the formation of crusts and recurrent pharyngitis.[15,30,31] Physical injury to the mucosa may also be caused by cryosurgery, thermal ablation or radiofrequency ablation. The submucosal resection of the inferior turbinate is worth recommending, because it preserves most of the mucosa and preserves mucosal functions. Moreover, this technique is less likely to cause atrophic rhinitis. A new technique using a microdebrider blade through a small incision shows great results in reducing the size of the inferior turbinates.[31,32] We recommend submucosal ablation, which can be performed by submucosal cautery – it reduces the turbinate tissue with minimal damage to the surface. Submucosal ablation can also be provided by a radiofrequency device.[33] Our experience indicates that there was no significant hemorrhage after the procedure using this technique. Also, after the extended procedure, with the loop resection of the hypertrophic posterior part of the turbinate, no massive hemorrhage was observed.[34]

Other complications of septoplasty, besides hemorrhages, include perforation of the septum, which, according to Erbe et al., occurs in 15% of patients being simultaneously operated on.[8] A hematoma or septal abscess, adhesions between the septal mucosa and turbinates, deterioration in the sense of smell, or leakage of cerebrospinal fluid are rarely observed. Patients with those complications are usually referred to otolaryngological departments. A full discussion about the treatment undertaken exceeds the scope of this study. The number of centers undertaking surgical treatment of craniofacial deformations is steadily growing. At the same time, the popularization of simultaneously performed orthognathic surgery and septoplasty with possible turbinoplasty can be observed. We also recommend that those 2 procedures should be performed jointly by maxillofacial surgeons and laryngologists (a postulate of Posnick and Agnihotri, among others).[13] Exploiting the laryngologists' knowledge of the anatomy and physiology of the upper part of the respiratory tract is meant to translate into better postoperative results and a higher degree of patient satisfaction. However, even an experienced laryngologist may be surprised during the procedure, as there is a different surgical approach – the downfracture access – a different manner and size of the septal framework resection, the need to fix the cartilage after the procedure and the impossibility of applying a bilateral nasal package. A proper volume reduction of the lower turbinates in the altered anatomical conditions of the orthognathic procedure may also constitute a problem. Therefore, the experience exchange between the 2 teams seems to be essential for achieving the best results.

References

1. Posnick JC. *Orthognathic Surgery: Principles and Practice of Orthognathic Surgery*. St. Louis, MO: Elsevier Saunders; 2013:517.
2. Farrior RT, Farrior EH. Chapter 48: Special rhinoplasty techniques. In: Richardson M, Flint P, Haughey B, et al. *Cummings Otolaryngology – Head and Neck Surgery*. 5th ed. Philadelphia, PA: Mosby Elsevier; 2010:545–566.
3. Stewart MG, Smith TL, Weaver EM, et al. Outcomes after nasal septoplasty: Results from the Nasal Obstruction Septoplasty Effectiveness (NOSE) study. *Otolaryngol Head Neck Surg*. 2004;130(3):283–290.
4. Stewart MG, Witsell DL, Smith TL, Weaver EM, Yueh B, Hannley MT. Development and validation of the Nasal Obstruction Symptom Evaluation (NOSE) scale. *Otolaryngol Head Neck Surg*. 2004;130(2):157–163.
5. Seth V, Kamath P, Venkatesh MJ, Prasad R, Vishwanath F. Cone beam computed tomography: Third eye in diagnosis and treatment planning. *Virtual Journal of Orthodontics*. 2011;3:1–11.
6. Wheeler SM, Corey JP. Evaluation of upper airway obstruction – an ENT perspective. *Pulm Pharmacol Ther*. 2008;21(3):433–441.

7. Haarmann S, Budihardja AS, Wolff KD, Wangerin K. Changes in acoustic airway profiles and nasal airway resistance after Le Fort I osteotomy and functional rhinosurgery: A prospective study. *Int J Oral Maxillofac Surg*. 2009;38(4):321–325.
8. Erbe M, Lehotay M, Göde U, Wigand ME, Neukam FW. Nasal airway changes after Le Fort I – impaction and advancement: Anatomical and functional findings. *Int J Oral Maxillofac Surg*. 2001;30(2):123–129.
9. Pingarrón ML, Arias Gallo LJ, López-Arcas JM, Chamorro Pons M, Cebrián Carretero JL, Burgueño García M. Fibroscopic findings in patients following maxillary osteotomies in orthognathic surgery. *J Craniomaxillofac Surg*. 2011;39(8):588–592.
10. Posnick JC, Fantuzzo J, Troost T. Simultaneous intranasal surgery at the time of Le Fort I downfracture. *J Oral Maxillofac Surg*. 2007;65(11): 2273–2281.
11. Epker BN, Turvey T, Fish LC. Indications for simultaneous mobilization of the maxilla and mandible for the correction of dentofacial deformities. *Oral Surg Oral Med Oral Pathol*. 1982;54(4):369–381.
12. Götzfried HF, Masing H. On the improvement of nasal breathing following mid-face osteotomies, and possible reasons for the phenomenon. *J Maxillofac Surg*. 1984;12(1):29–32.
13. Posnick JC, Agnihotri N. Consequences and management of nasal airway obstruction in the dentofacial deformity patient. *Curr Opin Otolaryngol Head Neck Surg*. 2010;18(4):323–331.
14. Posnick JC, Agnihotri N. Managing chronic nasal airway obstruction at the time of orthognathic surgery: A twofer. *J Oral Maxillofac Surg*. 2011;69(3):695–701.
15. Theissing J, Rettinger G, Werner JA. *ENT – Head and Neck Surgery: Essential Procedures*. Stuttgart–New York: Georg Thieme Verlag; 2010: 45–109.
16. Persichetti P, Toto V, Signoretti M, et al. The correction of nasal septal deviations in rhinoplasty. *Annals of Oral & Maxillofacial Surgery* 2013;1:13.
17. Sarver DM, Rousso DR. Plastic surgery combined with orthodontic and orthognathic procedures. *Am J Orthod Dentofacial Orthop*. 2004;126(3):305–307.
18. Waite PM, Matukas VJ, Sarver DM. Simultaneous rhinoplasty and orthognathic surgery. *Int J Oral Maxillofac Surg*. 1988;17(5):298–302.
19. Nocini PF, Chiarini L, Bertossi D. Cosmetic procedures in orthognathic surgery. *J Oral Maxillofac Surg*. 2011;69(3):716–723.
20. Elsalanty ME, Genecov DG, Genecov JS. Functional and aesthetic endpoints in orthognathic surgery. *J Craniofac Surg*. 2007;18(4):725–733.
21. Movahed R, Morales-Ryan C, Allen WR, Warren S, Wolford LM. Outcome assessment of 603 cases of concomitant inferior turbinectomy and Le Fort I osteotomy. *Proc (Bayl Univ Med Cent)*. 2013;26(4):376–381.
22. Mommaerts MY, Lippens F, Abeloos JVS, Neyt LF. Nasal profile changes after maxillary impaction and advancement surgery. *J Oral Maxillofac Surg*. 2000;58(5):470–475.
23. Williams BJD, Isom A, Filho JRL, O'Ryan FS. Nasal airway function after maxillary surgery: A prospective cohort study using the Nasal Obstruction Symptom Evaluation scale. *J Oral Maxillofac Surg*. 2013; 71(2):343–350.
24. Tang S, Kacker A. Should intranasal splints be used after nasal septal surgery? *Laryngoscope*. 2012;122(8):1647–1648.
25. Wadhera R, Zafar N, Gulati SP, Kalra V, Ghai A. Comparative study of intranasal septal splints and nasal packs in patients undergoing nasal septal surgery. *Ear Nose Throat J*. 2014;93(9):396–408.
26. Warren DW, Hershey HG, Turvey TA, Hinton VA, Hairfield WM. The nasal airway following maxillary expansion. *Am J Orthod Dentofacial Orthop*. 1987;91(2):111–116.
27. Kunkel M, Hochban W. The influence of maxillary osteotomy on nasal airway patency and geometry. *Mund Kiefer Gesichtschir.* 1997;1(4): 194–198.
28. Pourdanesh F, Sharifi R, Mohebbi A, Jamilian A. Effects of maxillary advancement and impaction on nasal airway function. *Int J Oral Maxillofac Surg*. 2012;41(11):1350–1352.
29. Iorio ML, Masden D, Blake CA, Baker SB. Presurgical planning and time efficiency in orthognathic surgery: The use of computer-assisted surgical simulation. *Plast Reconstr Surg*. 2011;128(3):179.
30. Rice DH, Kern EB, Marple BF, Mabry RL, Friedman WH. The turbinates in nasal and sinus surgery: A consensus statement. *Ear Nose Throat J*. 2003;82(2):82–84.
31. Nurse LA, Duncavage JA. Surgery of the inferior and middle turbinates. *Otolaryngol Clin North Am*. 2009;42(2):295–309.
32. Liu CM, Tan CD, Lee FP, Lin KN, Huang HM. Microdebrider-assisted versus radiofrequency-assisted inferior turbinoplasty. *Laryngoscope*. 2009;119(2):414–418.
33. Garzaro M, Pezzoli M, Landolfo V, Defilippi S, Giordano C, Pecorari G. Radiofrequency inferior turbinate reduction: Long-term olfactory and functional outcomes. *Otolaryngol Head Neck Surg*. 2012;146(1): 146–150.
34. Hwang SH, Kang JM, Cho JH, Kim BK. What is the relationship between the localization of maxillary fungal balls and intranasal anatomic variations? *Clin Exp Otorhinolaryngol.* 2012;5(4):213–217.

Optical coherence tomography as a non-invasive method of enamel thickness diagnosis after orthodontic treatment by 3 different types of brackets

Monika E. Machoy[1,A–F], Robert Koprowski[2,B,C,E,F], Liliana Szyszka-Sommerfeld[3,B,F], Krzysztof Safranow[4,C,F], Tomasz Gedrange[5,E,F], Krzysztof Woźniak[3,A,E,F]

[1] Division of Orthodontics, Pomeranian Medical University in Szczecin, Poland
[2] Department of Biomedical Computer Systems, Faculty of Computer Science and Materials Science, Institute of Computer Science, University of Silesia, Sosnowiec, Poland
[3] Division of Orthodontics, Pomeranian Medical University in Szczecin, Poland
[4] Department of Biochemistry and Medical Chemistry, Pomeranian Medical University in Szczecin, Poland
[5] Division of Orthodontics, Technical University Dresden, Germany

A – research concept and design; B – collection and/or assembly of data; C – data analysis and interpretation; D – writing the article; E – critical revision of the article; F – final approval of the article

Advances in Clinical and Experimental Medicine, ISSN 1899–5276 (print), ISSN 2451–2680 (online) *Adv Clin Exp Med*. 2019;28(2):211–218

Address for correspondence
Monika E. Machoy
E-mail: m.machoy@gmail.com

Funding sources
None declared

Conflict of interest
None declared

Received on August 23, 2017
Reviewed on September 13, 2017
Accepted on November 8, 2017

Published online on July 26, 2018

Cite as
Machoy ME, Koprowski R, Szyszka-Sommerfeld L, Safranow K, Gedrange T, Woźniak K. Optical coherence tomography as a non-invasive method of enamel thickness diagnosis after orthodontic treatment by 3 different types of brackets. *Adv Clin Exp Med*. 2019;28(2):211–218. doi:10.17219/acem/79974

DOI
10.17219/acem/79974

Abstract

Background. Medical digital imaging is the basis of effective medical diagnosis and is now in the mainstream of a dynamically developing branch of science. Optical coherence tomography (OCT) enables real-time in situ imaging of tissues without the need for biopsy, histological procedures or X-rays.

Objectives. The aim of the study was to evaluate the application of OCT in orthodontic diagnostics and clinical practice by assessing the thickness of the enamel before and after orthodontic treatment.

Material and methods. A hundred and eighty teeth in this in vitro study were divided into 3 groups of 60 teeth each. In each group (Group 1 – metal brackets, Group 2 – ceramic brackets and Group 3 – composite brackets), the orthodontic brackets were attached to the enamel using the 5th-generation adhesive system. The image of the enamel tissue was captured with a 3D–OCT camera before installing orthodontic brackets and after debonding and mechanical processing. The obtained OCT scans were subjected to expert IT analysis. For the statistical analysis, the Shapiro-Wilk test, the median test, the Mann-Whitney U test, Friedman two-way analysis of variance (ANOVA), Wilcoxon matched pairs signed ranks test, the χ^2 test of independence with Yates's correction, and Fisher's exact test were used. Maxwell's general principle was followed when using this type of test. The level of significance was set at $p = 0.05$.

Results. The thickness of the enamel varied least when metal brackets were used. The changes in enamel thickness in the composite and ceramic bracket groups were not statistically significant.

Conclusions. Optical coherence tomography is an effective diagnostic tool to evaluate the thickness of the enamel tissue before and after orthodontic treatment. Changes in the enamel layer thickness after orthodontic treatment are determined by the type of material which the orthodontic bracket is made of.

Key words: tomography, optical coherence, orthodontics, optical coherence tomography, enamel

Background

The concept of tomography refers to a method that provides images showing sections of the tested structure. The 1st CT scanner, constructed in 1967, initiated the rapid development of medical imaging. A common feature among the different types of CT devices is the non-invasive imaging of tissue structures and internal organs. The desire to minimize invasive methods, such as biopsy or exploratory surgery, which are painful and may cause deterioration in the patient's condition, was the impetus for the improvement of CT equipment. As a result, completely new technologies were developed, such as magnetic resonance imaging (MRI), ultrasonography (USG), positron emission tomography (PET), single photon emission computed tomography (SPECT), and the latest and more widely used optical coherence tomography (OCT).

The method of OCT using interferometry with partially coherent light was first presented in 1991 at the Massachusetts Institute of Technology (MIT), Cambridge, USA.[1] The 1st in vivo measurements of the section of the human retina were made 2 years later in Vienna, Austria.[2] The 1st commercial optical tomography device was produced in 1996 by Zeiss-Humphrey.[3]

Optical coherence tomography provides images of the sections of tissues in a non-contact and non-invasive manner. The device measures the time delay and intensity of the light scattered or reflected from biological tissues, which results in tomographic imaging of their internal structure. This is achieved by scanning tissues at a resolution ranging from 1 to 15 μm. Optical coherence tomography enables real-time in situ imaging of tissues without the need for biopsy, histological procedures or X-rays, so it can be used in many fields of medicine. Its properties are particularly used in ophthalmology – in the diagnosis of all layers of the retina – but also increasingly in cardiology, gastroenterology, pulmonology, oncology, and dermatology.

The latest studies focus primarily on the early diagnosis of caries, the assessment of dental fillings, and the evaluation of periodontal and mucosal tissues and tooth structure.[4–13]

Objectives

In this article, we illustrated the application of OCT in orthodontic diagnostics and clinical practice by assessing the thickness of the enamel before and after orthodontic treatment. This method has a great impact on the proper treatment and choice of material and is already used by us. The possibility of appraising the enamel state and thickness enables the correct selection of the adhesive materials and type of bracket. Therefore, it should be introduced widely for clinical practitioners.

Material and methods

The study was carried out in an in vitro environment. The material comprised 180 teeth, divided into 3 groups of 60 teeth each. In each group, the orthodontic brackets were attached to the tooth surface using the 5th-generation adhesive system that uses the classic method of enamel etching with orthophosphoric acid. In the 1st group, steel orthodontic brackets were used. The 2nd group had ceramic brackets attached, while the 3rd group was given composite brackets.

The experiment was carried out on premolars, extracted for orthodontic and periodontal reasons. The exclusion criteria were defined by the following conditions: the presence of developmental defects of enamel, i.e., hypoplasia, turbidity or discoloration (which is a symptom of caries), and fillings on the vestibular surface.

The teeth which qualified for research were stored for 30 days in demineralized water with a crystal of thymol (0.1%) at room temperature. Before fastening orthodontic brackets, the tooth surface was cleaned using a polisher (TopDental, Bielsko-Biała, Poland) with fluoride-free toothpaste, Pressage (Shofu Inc., Kyoto, Japan), designed to prepare the enamel before fastening orthodontic brackets. Then, the teeth were washed with distilled water and dried with compressed air for 15 s. For fastening orthodontic brackets, an orthodontic composite material, Transbond™ XT Light Cure Adhesive (3M Unitek, Diegem, Belgium), was used.

In the 1st group, the vestibular surface of the tooth was etched for 30 s with a 37% solution of phosphoric acid – Blue-Etch (Cerkamed, Stalowa Wola, Poland) – rinsed with distilled water for 15 s, and dried using compressed air. The adhesive system OptiBond Plus Solo (Kerr, Orange, USA) was rubbed with an applicator into the etched enamel surface for 15 s, then the surface was dried under a gentle stream of air for 3 s and cured with a halogen lamp with a light intensity of 750 mW/cm^2 for 20 s. The orthodontic composite material Transbond™ XT Light Cure Adhesive was applied to the bracket surface. The bracket was pressed against the enamel surface with common tweezers. The orthodontic bracket was placed in the middle of the mesial-distal axis of the tooth, moving its center 3.5 mm away from the edge of the occlusal surface. The distance was measured using an orthodontic positioner. After the proper placement of the bracket, the material was subjected to polymerization with a halogen lamp for 40 s.

In the 2nd group, the self-etching adhesive system G-Bond (GC, Tokyo, Japan) was used. The self-etching primer was left for 10 s after being applied to the tooth surface using an applicator, and then the excess was removed via an air stream for 5 s. After this time, the system was polymerized with a halogen lamp with a light intensity of 750 mW/cm^2 for 20 s. The orthodontic composite material Transbond™ XT Light Cure Adhesive was applied to the surface of the hook. The orthodontic hook was placed onto the tooth

surface using the method described above. The teeth with the fixed orthodontic brackets were stored in demineralized water at room temperature for 24 h. After this time, the hooks were removed mechanically with ix827 pliers (DB Orthodontics Ltd, Silsden, UK), designed for removing all types of brackets. Residues of the adhesive material were removed from the enamel surface using a cemented carbide milling cutter – H390.204 AGK (Komet URPOL, Kędzierzyn-Koźle, Poland) – which has 8 notches, a length of 3.6 mm, and a diameter of 0.1 mm. The enamel was processed with the use of a micromotor commonly mounted to a dental unit at a speed of 40,000 rpm with water cooling and a pressure force of 1.0 N. The force was measured on a test stand consisting of scales, on which the processed tooth was placed. The procedure of cleaning the enamel was considered to be finished based on a naked-eye examination and by touching with a 23-cm stylet under the dental unit light. The assessment criteria were the smoothness of the tooth surface and the absence of the composite material residues. Tooth scans were performed using 3D-OCT tomography. The area of the test teeth was imaged with a 3D-OCT camera (Topcon, Las Vegas, USA) (Fig. 2) in 2 modes T0, imaging of the tooth surface before installing orthodontic brackets, and T1, imaging of the tooth surface after debonding and mechanical processing. Each time, 2-dimensional scans were performed, allowing for a clear illustration of the enamel damage in a vertical plane. The procedure showed the entire surface of the tissue and allowed for the subsequent comparative analysis of changes in its structure. The 3D-OCT device, in addition to CT, has a coupled digital camera with a resolution of 16.2 Mpix, which provides highly accurate images of the test area with 20-fold zoom without a loss in image quality. The technology of Fourier Domain OCT (S-OCT), which uses spectral analysis, provides very quick scanning (27,000 A-scans/s), a high axial resolution of 5 μm and a horizontal resolution of 20 μm. The use of a pulsed light source, which is a superelectroluminescent diode (SLED) in the OCT, allows for better detection of low-contrast centers. The wavelength is 840 nm and the half-width is 50 nm. The 3D OCT-2000 has a scanning range of 6 × 6 mm horizontally and 2.3 mm into the tissue. It is a device designed for ophthalmic diagnostics, whose system enables the virtual segmentation of the retina into layers, allowing for the assessment of the photoreceptors and pigment epithelium. The wavelength of 840 nm and the depth of penetration into the tissue also allow for imaging of the tooth enamel tissue through its entire thickness. It was possible to obtain accurate scans of the surface and enamel structure of the teeth with appropriate repeatability during 3 examinations owing to a special matrix made for each tooth. The matrix allowed for repeatable tooth positioning in the frontal, sagittal and horizontal plane relative to the optical axis of the OCT. The matrix was made of c-silicone Zetalabor hard 85 Shore A (Zhermack, Badia Polesine, Italy), on the basis of the tooth impression in the long axis, so that the vestibular surface of the crown remained above the silicone. The support for the silicone was a mold with an attachment fixed with respect to the optical axis of the OCT.

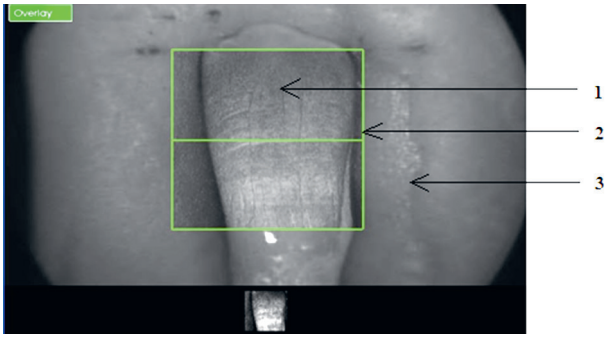

Fig. 1. 1 – extracted central lower incisor, captured using a digital camera with the resolution of 16.2 Mpix; coupled with tomography; 2 – window of the scanning area; 3 – the silicone matrix made for repeatable tooth positioning in the frontal, sagittal and horizontal plane relative to the optical axis of the optical coherence tomography (OCT)

Fourier Domain OCT technology (S-OCT) allows for high-resolution spectral analysis, greater than 5 μm axially and 20 μm horizontally, and a quick scan of 27,000 A-scans/s. A 2-dimensional tomographic scan of the tooth is composed of 3 types of scans: A, B and C. Scan A measures the axial penetration depth of light in comparison to the reflectance curve. Scan B gives sagittal scans of the object and scan C provides lateral scanning images at

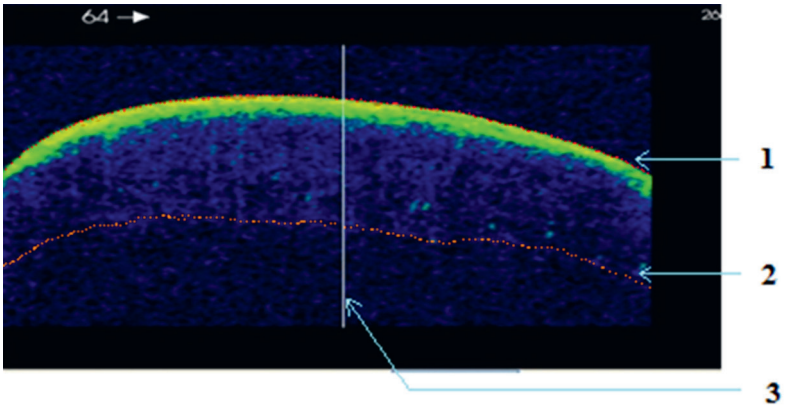

Fig. 2A. The axial aspect of the scan presented in Fig. 1, the A scan

1 – the outer layer of the enamel; 2 – the inner layer of the enamel; 3 – the axial plane in relation to which the scan was made.

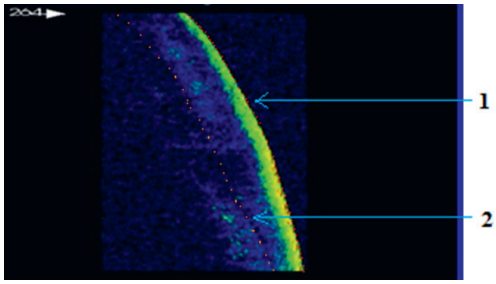

Fig. 2B. The sagittal aspect of the scan presented in Fig. 1, the B scan

1 – the outer layer of the enamel; 2 – the inner layer of the enamel.

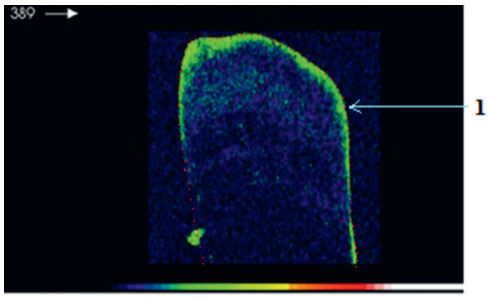

Fig. 2C. Coronal lateral scanning at a constant depth of the tooth presented in Fig. 1, the C scan

1 – the contour of a tooth at the 389 layer of the enamel tomographic scan.

a constant depth. Figures 1, 2A, 2B, and 2C show examples of the individual scans of the tooth.

The resulting OCT scans were subjected to an expert IT analysis. Image pre-processing involved automatic reading of the order of OCT images from the source file with the *.fds file extension, allowing for the development of matrices of individual images.

The IT analysis, which was performed owing to a specially developed algorithm, was accurately described and published previously.[14] The algorithm allowed for an automatic measurement of every tooth's enamel thickness before and after treatment. The determination of enamel thickness was possible because the algorithm automatically determined the position of both the outer and inner enamel layers directly in the image. In this manner, 20,000 scans were measured.

The results obtained in the study were statistically analyzed. The Shapiro-Wilk test was used to verify the hypothesis of normality of the variable distribution. To verify the hypothesis of the existence and non-existence of differences between the mean values for the independent variables, the median test and the Mann-Whitney U test were used. To verify the hypothesis of the existence or non-existence of differences between the mean values for the dependent variables, the Friedman two-way analysis of variance (ANOVA) and Wilcoxon matched pairs signed ranks tests were used. In order to assess the correlation between saccadic and qualitative variables, the χ^2 test of independence, the χ^2 test of independence with Yates's correction and the Fisher's exact test were used. Maxwell's general principle was followed when using this type of tests. The diversity of many variables in the categories determined by qualitative factors was analyzed using the analysis of variance/analysis of covariance (ANOVA/ANCOVA) models of univariate analysis of variance. When verifying all hypotheses, the level of significance was set at $p = 0.05$.

Results

The 1st step in the analysis was to measure the enamel thickness before the orthodontic treatment in all of the test samples. The calculation of the average, minimum, and maximum enamel thickness before the orthodontic treatment and the average, minimum and maximum enamel

Table 1. The characteristics of the variables obtained

Variables	n	M	Me	Min	Max	Q1	Q3	R	SD	p-value
I_Avg	180	564.53	539.85	257.50	1,093.05	476.53	643.75	167.22	137.30	0.0003
I_Min	180	183.14	185.00	0.00	400.00	140.00	245.00	105.00	83.23	0.0042
I_Max	180	1,515.91	1,297.50	600.00	4,255.00	1,015.00	1,900.00	885.00	700.86	2.1865
I_Stdev	180	201.22	163.84	57.95	740.54	118.66	226.71	108.05	126.67	1.3077
V_Avg	180	470.85	447.85	172.14	844.79	369.96	564.13	194.16	130.87	2.2849
V_Min	180	130.27	135.00	0.00	360.00	80.00	185.00	105.00	76.77	0.0023
V_Max	180	1,098.84	1,037.50	450.00	2,755.00	825.00	1,280.00	455.00	424.24	1.3652
V_StDev	180	149.46	130.94	35.11	618.01	92.91	185.42	92.51	87.49	2.2893
Dif_Avg	180	93.67	67.72	–142.77	563.03	29.20	150.83	121.62	100.24	1.0034
Dif_Min	180	52.87	50.00	–185.00	220.00	15.00	85.00	70.00	53.02	0.0001
Dif_Max	180	417.06	197.50	–1,415.00	3,215.00	25.00	685.00	660.00	636.66	1.3414

n – number of samples; M – arithmetic mean; Me – median; Min–Max – range of variation; Q1 – 1st quartile; Q3 – 3rd quartile; R – interquartile range; SD – standard deviation; I_Avg – average enamel thickness before the orthodontic treatment; I_Min – minimum enamel thickness before the orthodontic treatment; I_Max – maximum enamel thickness before the orthodontic treatment; V_Avg – average enamel thickness prior to orthodontic treatment; V_Min – minimum enamel thickness prior to orthodontic treatment; V_Max – maximum enamel thickness prior to orthodontic treatment; Dif_Avg – difference in average enamel thickness prior to orthodontic treatment and after its completion; Dif_Min – difference in minimum enamel thickness prior to orthodontic treatment and after its completion; Dif_Max – difference in maximum enamel thickness prior to orthodontic treatment and after its completion.

thickness, after the orthodontic treatment was conducted. All of the outcomes are presented in Table 1.

By using the metal brackets, the average thickness of the enamel after the end of treatment (V_Avg) was 487.05 μm, the minimum (V_Min) was 125.41 μm and the maximum (V_Max) was 1046.50 μm. To find the differences between the thickness of the initial and final values (before and after treatment), the 2 equitable values were subtracted. By those means, the variables Dif_Avg (difference in average enamel thickness prior to orthodontic treatment and after its completion), Dif_Min (difference in minimum enamel thickness prior to orthodontic treatment and after its completion) and Dif_Max (difference in maximum enamel thickness prior to to orthodontic treatment and after its completion) were achieved. All of the described variables are presented in Table 2. The average difference (Dif_Avg) between the thickness of the enamel before and after orthodontic treatment using the metal brackets was 63.15 μm and was statistically lower in comparison with ceramic ($p < 0.018$) and composite brackets ($p < 0.006$). Statistical analysis confirmed that the thickness of the enamel varies least using metal brackets.

The average thickness of the enamel after treatment with ceramic brackets (V_Avg) was 461.00 μm, the minimum

Table 2. Thickness of the vestibular enamel [μm] after the orthodontic treatment in the metal bracket group

Variables	n	M	Me	Min	Max	Q1	Q3	R	SD
V_Avg	60	487.05	460.82	259.16	844.79	379.82	565.94	186.12	137.13
V_Min	60	125.41	132.50	0.00	360.00	75.00	177.50	102.50	84.14
V_Max	60	1,046.50	1,010.00	540.00	2,075.00	8,300.00	1,210.00	380.00	303.21
Dif_Avg	60	63.15	39.11	–142.77	286.02	22.88	113.18	90.30	73.09
Dif_Min	60	51.25	45.00	–80.00	220.00	10.00	72.50	62.50	54.52
Dif_Max	60	485.83	185.00	–915.00	3,215.00	47.50	740.00	692.50	752.51

n – number of samples; M – arithmetic mean; Me – median; Min–Max – range of variation; Q1 – 1st quartile; Q3 – 3rd quartile; R – interquartile range; SD – standard deviation; V_Avg – average enamel thickness prior to orthodontic treatment; V_Min – minimum enamel thickness prior to orthodontic treatment; V_Max – maximum enamel thickness prior to orthodontic treatment; Dif_Avg – difference in average enamel thickness prior to orthodontic treatment and after its completion; Dif_Min – difference in minimum enamel thickness prior to orthodontic treatment and after its completion; Dif_Max – difference in maximum enamel thickness prior to orthodontic treatment and after its completion.

Table 3. Thickness of the vestibular enamel [μm] after the orthodontic treatment in the ceramic bracket group

Variables	n	M	Me	Min	Max	Q1	Q3	R	SD
V_Avg	60	461.44	454.39	269.35	744.30	375.32	542.99	202.88	143.29
V_Min	60	150.90	150.00	0.00	310.00	100.00	200.00	105.00	75.57
V_Max	60	1,077.45	1,005.00	450.00	2,640.00	810.00	1,220.00	525.00	437.81
Dif_Avg	60	111.14	81.53	–53.98	563.03	30.68	153.72	119.33	96.04
Dif_Min	60	44.01	35.00	–185.00	200.00	5.00	80.00	80.00	58.68
Dif_Max	60	486.55	270.00	–595.00	2,200.00	60.00	935.00	650.00	610.66

n – number of samples; M – arithmetic mean; Me – median; Min–Max – range of variation; Q1 – 1st quartile; Q3 – 3rd quartile; R – interquartile range; SD – standard deviation; V_Avg – average enamel thickness prior to orthodontic treatment; V_Min – minimum enamel thickness prior to orthodontic treatment; V_Max – maximum enamel thickness prior to orthodontic treatment; Dif_Avg – difference in average enamel thickness prior to orthodontic treatment and after its completion; Dif_Min – difference in minimum enamel thickness prior to orthodontic treatment and after its completion; Dif_Max – difference in maximum enamel thickness prior to orthodontic treatment and after its completion.

Table 4. Thickness of the vestibular enamel [μm] after the orthodontic treatment in the composite bracket group

Variables	n	M	Me	Min	Max	Q1	Q3	R	SD
V_Avg	60	464.73	418.98	172.14	774.27	354.87	589.92	167.67	116.14
V_Min	60	115.38	115.00	0.00	250.00	70.00	170.00	100.00	74.75
V_Max	60	1,167.23	1,075.00	465.00	2,755.00	850.00	1,310.00	410.00	438.62
Dif_Avg	60	105.45	95.45	–138.47	461.71	37.12	165.78	123.03	113.02
Dif_Min	60	62.69	60.00	–50.00	180.00	30.00	95.00	75.00	55.63
Dif_Max	60	288.38	125.00	–1,415.00	1,505.00	10.00	515.00	875.00	632.78

n – number of samples; M – arithmetic mean; Me – median; Min–Max – range of variation; Q1 – 1st quartile; Q3 – 3rd quartile; R – interquartile range; SD – standard deviation; V_Avg – average enamel thickness prior to orthodontic treatment; V_Min – minimum enamel thickness prior to orthodontic treatment; V_Max – maximum enamel thickness prior to orthodontic treatment; Dif_Avg – difference in average enamel thickness prior to orthodontic treatment and after its completion; Dif_Min – difference in minimum enamel thickness prior to orthodontic treatment and after its completion; Dif_Max – difference in maximum enamel thickness prior to orthodontic treatment and after its completion.

(V_Min) was 150.90 μm and the maximum (V_Max) was 1077.45 μm. The average difference (Dif_Avg) between the thickness of the enamel at the beginning and at the end of treatment amounted to 111.14 μm. The differences between the initial and final values were found in the same manner as in the metal bracket group. All of the variables are presented in Table 3.

In the groups treated with composite brackets, the thickness of the enamel after the treatment was 464.73 μm (V_Avg), 115.38 μm (V_min) and 1,167.23 μm (V_max). The average loss of enamel was 105.45 μm. The differences between the initial and final values were found in the same manner as in the metal and ceramic bracket groups. All of the variables are presented in Table 4. Enamel thickness changes in the composite and ceramic bracket groups were not statistically significant ($p < 0.005$).

Discussion

The presented results show that the enamel thickness after completed treatment and its possible damage is dependent on the type of orthodontic bracket. So far, evaluation of the full tissue thickness has been difficult to carry out, so there are not many publications to refer to when discussing the results. To date, only 2 recent publications have revealed significant agreement in the potential of OCT as a clinical tool to effectively measure the whole enamel layer thickness.[15,16] Some publications have acknowledged the risk of using ceramic brackets and Suliman et al. widened the available knowledge on the topic by evaluating 2 types of these brackets, in which polycrystalline brackets were found to be more dangerous to the enamel structure.[17–19]

A number of studies evaluating the loss of enamel thickness and surface damage following the removal of brackets have been published, in which the measuring tools were a planer surfometer and profilometer.[20–23] These methods allow for a small number of single tooth surface measurements, while the studies carried out with a profilometer and surface analyzer do not show the examined structure. The newest methods of tooth enamel analysis include assessment by means of an atomic force microscope (AFM). This method shows promising results in depicting the enamel surface, but still it does not allow to analyze the whole tissue.[24–27] These methods, however, do not enable automatic, quantitative measurement of the enamel thickness in automatic comparison of image groups. This is the case, where comparisons between specific areas of the tooth enamel were made manually in OCT images.[28] Automatic measurement was presented in the article.[29] However, the article concerns polarization-sensitive optical coherence tomography (PS-OCT) and is not related to the problem of overlapping individual images in the subsequent processing stages of the tooth, as shown in this paper.

It can be assumed that residues which are invisible after polishing the local resin may stay unrecognized and may be confused with enamel damage. Such phenomena can have a major impact on the results of the examination. The actual size of the resulting enamel damage can be diametrically different than previously supposed. In addition, tooth surfaces which are not fully flat make it difficult to carry out meaningful analysis. Only optical sensors and scanning lasers can allow accurate volume and vertical measurements of the enamel.[30] Recently, the use of scanning electron microscope (SEM) after bracket debonding has shown accuracy in conceptualizing the proper protocol in removing the bonding remnants and in evaluating the eventual damage after the finished treatment.[31–33] The distinction between the loss of enamel and residual resins is only credible in the 3-dimensional evaluations that have so far only been possible with laser scanning techniques.[34]

A new application of the abovementioned device was employed to evaluate the diversity of the image depending on the size and depth of the generated pores of the enamel, which affect the propagation of light waves in the tissue and the appropriate image registration. Automatic analysis of tooth enamel thickness as a tool for digital intraoral imaging provides a number of possibilities. These include area analysis of the enamel thickness (for each individual tooth area separately) and enamel texture analysis. Imaging and quantitative measurement of the enamel structure before the installation of braces and after their removal enables the exposure of the extent of the tooth tissue damage depending on the brackets used and on the method of attachment. Such method makes it possible to deduce which bracket material and which installation technique are the safest for tooth enamel.

The OCT capabilities commonly applied in many fields of medicine (such as ophthalmology) are not yet fully used in dentistry, mainly due to the low availability of customized intraoral equipment and the insufficient range of OCT rays, which penetrate into the tissue to a depth of only a few millimeters, depending on the apparatus type. Lesions within the tooth tissue usually reach deeper, and are often measured in centimeters, which makes it necessary to perform hundreds or even thousands of scans to illustrate the entire lesion. To maximize the efficiency of the dental diagnostic OCT, the wavelengths of light responsible for generating the image should be subjected to testing. In the near-infrared light range, the central wavelength determines the maximum depth of penetration into the tissue due to scattering and absorption properties.[35] A wavelength below 1000 nm provides the greatest imaging efficiency because the light scattering properties are similar to the size of the tissue particles. Hydrated tissues dissipate much more energy than hard tissues containing a small percentage of water. For this reason, universal dental OCT should offer the possibility to control the wavelength depending on the type of tissue tested. A different wavelength must be used to image the periodontal and tooth tissue per se.

Another problem arising in dental diagnosis is the quality of individual teeth. The enamel can vary in its structure

in a single subject. Likewise, dental fillings or prosthetic materials having a different composition reflect or absorb light to varying degrees, which has a decisive effect on the image quality and the correct interpretation of it. Materials whose reflectance index is similar to that of the background will give a similar image. In addition to image quality, the ability to perform objective measurements of the obtained scans is very important. To date, publications have been mainly focused on the ability to obtain images of individual structures and on their acquisition rate, which is especially important in in vivo studies. We attempted to develop an algorithm for rapid and accurate measurements of tooth tissues. The presented algorithm is only one way to complete the described task. Other authors are already interested in the topic of OCT imaging in the field of orthodontics, proving our hypothesis that OCT should be incorporated into clinical diagnostics.[19,36–40]

Conclusions

Optical coherence tomography is an effective diagnostic tool to evaluate the thickness of the enamel tissue before and after orthodontic treatment. It provides tissue sections in a non-contact and non-invasive manner and allows for real-time tissue imaging in situ, without the need for histological procedures or, especially, the use of X-rays. Therefore, it is suitable for dental and orthodontic diagnostics in patients of any age. It is first and foremost important in pediatric patients, where the safe X-ray dose has not been precisely determined. Also, in this group of patients, orthodontic treatment is often performed. Considering the structure of young teeth susceptible to damage caused by plaque, caries and acids, it is very important in clinical practice to examine the structure of the enamel before starting treatment, especially because changes in the enamel layer thickness after orthodontic treatment have proved to be determined by the type of material which the orthodontic bracket is made of. This analysis informs orthodontists as to which braces should be used in specific cases. The method has great applications in clinical practice, which will be shown in an upcoming publication.

References

1. Huang D, Swanson EA, Lin CP, et al. Optical coherence tomography. *Science*. 1991;254(5035):1178–1181.
2. Fercher AF, Hitzenberger CK, Drexler W, Kamp G, Sattmann H. In vivo optical coherence tomography. *Am J Ophtalmol*. 1993;116(1):113–114.
3. Fercher AF, Hitzenberger CK, Kamp G, El-Zaiat SY. Measurement of intraocular distances by backscattering spectral interferometry. *Opt Commun*. 1995;117(1-2):30–43.
4. Simon JC, Kang H, Staninec M, et al. Near-IR and CP-OCT imaging of suspected occlusal caries lesions. *Lasers Surg Med*. 2017;49(3):215–224.
5. Maia AM, de Freitas AZ, de L Campello S, Gomes AS, Karlsson L. Evaluation of dental enamel caries assessment using quantitative light induced fluorescence and optical coherence tomography. *J Biophotonics*. 2016;9(6):596–602.
6. Horie K, Shimada Y, Matin K, et al. Monitoring of cariogenic demineralization at the enamel–composite interface using swept-source optical coherence tomography. *Dent Mater*. 2016;32(9):1103–1112.
7. Damodaran V, Ranga RS, Vasa NJ. Optical coherence tomography based imaging of dental demineralisation and cavity restoration in 840 nm and 1310 nm wavelength regions. *Opt Lasers Eng*. 2016;59:14.
8. Adegun OK, Tomlins PH, Hagi-Pavli E, Bader DL, Fortune F. Quantitative optical coherence tomography of fluid-filled oral mucosal lesions. *Lasers Med Sci*. 2013;28(5):1249–55.
9. Sanda M, Shiota M, Imakita C, Sakuyama A, Kasugai S, Sumi Y. The effectiveness of optical coherence tomography for evaluating peri-implant tissue: A pilot study. *Imaging Sci Dent*. 2016;46(3):173–178.
10. Adegun OK, Tomlins PH, Hagi-Pavli E, et al. Quantitative analysis of optical coherence tomography and histopathology images of normal and dysplastic oral mucosal tissues. *Lasers Med Sci*. 2012;27(4):795–804.
11. Kim SH, Kang SR, Park HJ, Kim JM, Yi WJ, Kim TI. Improved accuracy in periodontal pocket depth measurement using optical coherence tomography. *J Periodontal Implant Sci*. 2017;47(1):13–19.
12. Fernandes LO, Mota CC, de Melo LS, da Costa Soares MUS, da Silva Feitosa D, Gomes ASL. In vivo assessment of periodontal structures and measurement of gingival sulcus with optical coherence tomography: A pilot study. *J Biophotonics*. 10(6-7):862–869.
13. Kim JM, Kang SR, Yi WJ. Automatic detection of tooth cracks in optical coherence tomography images. *J Periodontal Implant Sci*. 2017;47(1):41–50.
14. Koprowski R, Machoy M, Woźniak K, Wróbel Z. Automatic method of analysis of OCT images in the assessment of the tooth enamel surface after orthodontic treatment with fixed braces. *Biomed Eng Online*. 2014;13:48.
15. Algarni A, Kang H, Fried D, Eckert GJ, Hara AT. Enamel thickness determination by optical coherence tomography: In vitro validation. *Caries Res*. 2016;50(4):400–406.
16. Seeliger J, Machoy M, Koprowski R, et al. Enamel thickness before and after orthodontic treatment analysed in optical coherence tomography. *Biomed Res Int*. 2017;2017:8390575.
17. Suliman SN, Trojan TM, Tantbirojn D, Versluis A. Enamel loss following ceramic bracket debonding: A quantitative analysis in vitro. *Angle Orthod*. 2015;85(4):651–656.
18. Bernard-Granger C, Gebeile-Chauty S. Enamel cracks: Influence of orthodontic process [in French]. *Orthod Fr*. 2014;85(3):245–251.
19. Leão Filho JC, Braz AK, de Araujo RE, Tanaka OM, Pithon MM. Enamel quality after debonding: Evaluation by optical coherence tomography. *Braz Dent J*. 2015;26(4):384–389.
20. Davis VA, Staley RN, Bigelow HF, Jakobsen JR. Remnant amount and cleanup for 3 adhesives after debracketing. *Am J Orthod Dentofacial Orthop*. 2002;121(3):291–296.
21. Hosein I, Sherriff M, Ireland AJ. Enamel loss during bonding, debonding, and cleanup with use of a self-etching primer. *Am J Orthod Dentofacial Orthop*. 2004;126(6):717–724.
22. Eliades T, Gioka C, Eliades G, Makou M. Enamel surface roughness following debonding using two resin grinding methods. *Eur J Orthod*. 2004;26(3):333–338.
23. Kim SS, Park WK, Son WS, Ahn HS, Ro JH, Kim YD. Enamel surface evaluation after removal of orthodontic composite remnants by intraoral sandblasting: A 3-dimensional surface profilometry study. *Am J Orthod Dentofacial Orthop*. 2007;132(1):71–76.
24. Finke M, Parker DM, Jandt KD. Influence of soft drinks on the thickness and morphology of in situ acquired pellicle layer on enamel. *J Colloid Interface Sci*. 2002;251(2):263–270.
25. Watari F. In situ quantitative analysis of etching process of human teeth by atomic force microscopy. *J Electron Microsc (Tokyo)*. 2005;54(3):299–308.
26. Mohebi S, Shafiee HA, Ameli N. Evaluation of enamel surface roughness after orthodontic bracket debonding with atomic force microscopy. *Am J Orthod Dentofacial Orthop*. 2017;151(3):521–527.
27. Lorenzo MC, Portillo M, Moreno P, et al. Ultrashort pulsed laser conditioning of human enamel: In vitro study of the influence of geometrical processing parameters on shear bond strength of orthodontic brackets. *Lasers Med Sci*. 2015;30(2):891–900.

28. Wilder-Smith CH, Wilder-Smith P, Kawakami-Wong H, Voronets J, Osann K, Lussi A. Quantification of dental erosions in patients with GERD using optical coherence tomography before and after double-blind, randomized treatment with esomeprazole or placebo. *Am J Gastroenterol*. 2009;104(11):27–88.
29. Le MH, Darling CL, Fried D. Automated analysis of lesion depth and integrated reflectivity in PS-OCT scans of tooth demineralization. *Lasers Surg Med*. 2010;42(1):42–62.
30. Oliver RG, Griffiths J. Different techniques of residual composite removal following debonding: Time taken and surface enamel appearance. *Br J Orthod*. 1992;19(2):131–137.
31. Vidor MM, Felix RP, Marchioro EM, Hahn L. Enamel surface evaluation after bracket debonding and different resin removal methods. *Dental Press J Orthod*. 2015;20(2):61–67.
32. Faria-Júnior ÉM, Guiraldo RD, Berger SB, et al. In-vivo evaluation of the surface roughness and morphology of enamel after bracket removal and polishing by different techniques. *Am J Orthod Dentofacial Orthop*. 2015;147(3):324–329.
33. Fan XC, Chen L, Huang XF. Effects of various debonding and adhesive clearance methods on enamel surface: An in vitro study. *BMC Oral Health*. 2017;17(1):58.
34. Al Shamsi AH, Cunningham JL, Lamey PJ, Lynch E. Three-dimensional measurement of residual adhesive and enamel loss on teeth after debonding of orthodontic brackets: An in vitro study. *Am J Orthod Dentofacial Orthop*. 2007;131(3):301e9–e15.
35. Wang LV, Wu HI. *Biomedical Optics*. Hoboken, NJ: John Wiley & Sons; 2007.
36. Baek JH, Na J, Lee BH, Choi E, Son WS. Optical approach to the periodontal ligament under orthodontic tooth movement: A preliminary study with optical coherence tomography. *Am J Orthod Dentofacial Orthop*. 2009;135(2):252–259.
37. Garcez AS, Suzuki SS, Ribeiro MS, Mada EY, Freitas AZ, Suzuki H. Biofilm retention by 3 methods of ligation on orthodontic brackets: A microbiologic and optical coherence tomography analysis. *Am J Orthod Dentofacial Orthop*. 2011;140(4):e193–198.
38. Pithon MM, Santos Mariana de J, de Souza CA, et al. Effectiveness of fluoride sealant in the prevention of carious lesions around orthodontic brackets: An OCT evaluation. *Dental Press J Orthod*. 2015;20 (6):37–42.
39. Nee A, Chan K, Kang H, Staninec M, Darling CL, Fried D. Longitudinal monitoring of demineralization peripheral to orthodontic brackets using cross polarization optical coherence tomography. *J Dent*. 2014;42(5):547–555.
40. Leão Filho JC, Braz AK, de Souza TR, de Araujo RE, Pithon MM, Tanaka OM. Optical coherence tomography for debonding evaluation: An in-vitro qualitative study. *Am J Orthod Dentofacial Orthop*. 2013; 143(1):61–68.

Fibrinogen concentrate replacement in ischemic stroke patients after recombinant tissue plasminogen activator treatment

Laura Vandelli[1,A–E], Marco Marietta[2,A,E], Tommaso Trenti[3,B,E], Manuela Varani[3,B,E], Guido Bigliardi[1,B,E], Francesca Rosafio[1,B,E], Maria Luisa Dell'Acqua[1,B,E], Livio Picchetto[1,B,E], Paolo Nichelli[1,B,E], Andrea Zini[1,A,C–F]

[1] Stroke Unit, Neurology Clinic, Department of Neuroscience, Nuovo Ospedale Civile S. Agostino-Estense, University of Modena and Reggio Emilia, Modena, Italy
[2] Department of Oncology and Hematology, Polyclinic of Modena, University of Modena and Reggio Emilia, Modena, Italy
[3] Clinical Pathology – Toxicology Department, Nuovo Ospedale Civile S. Agostino-Estense, Azienda Unita' Sanitaria Locale di Modena, Italy

A – research concept and design; B – collection and/or assembly of data; C – data analysis and interpretation;
D – writing the article; E – critical revision of the article; F – final approval of the article

Advances in Clinical and Experimental Medicine, ISSN 1899-5276 (print), ISSN 2451-2680 (online) *Adv Clin Exp Med*. 2019;28(2):219–222

Address for correspondence
Andrea Zini
E-mail: andrea.zini@me.com

Funding sources
None declared

Conflict of interest
None declared

Received on November 15, 2016
Reviewed on January 10, 2017
Accepted on January 31, 2018

Published online on December 3, 2018

Abstract

Background. Post-thrombotic intracerebral hemorrhage (ICH) is experienced by 6–8% of stroke patients and is associated with multiple factors, including acquired coagulopathy induced by the thrombolytic drug.

Objectives. The objective of this study was to assess the outcome of the intravenous (IV) administration of fibrinogen concentrate in a series of acute stroke patients who developed iatrogenic fibrinogen critical depletion after IV thrombolysis.

Material and methods. Of the 39 ischemic stroke patients treated with IV thrombolysis with a severe hypofibrinogenemia requiring infusion with IV fibrinogen concentrate, 30 patients were treated with 2 g of IV recombinant tissue plasminogen activator (rt-PA), followed by further doses until the fibrinogen level reached 200 mg/dL in hemorrhagic patients or 100 mg/dL in non-hemorrhagic patients, and 9 were treated with IV rt-PA followed by endovascular thrombectomy.

Results. Pre- and post-thrombolysis National Institutes of Health Stroke Scale (NIHSS) scores were statistically different for the Cochran-Mantel-Haenszel test overall ($p = 0.0002$), at 24-hour evaluation ($p = 0.0455$) and at 7-day assessment ($p = 0.0006$). Within the first 7 days post-thrombolysis, the brain computed tomography (CT) scans showed that 20/39 (51.28%) patients had ICH. Of the whole sample, 25.6% of the ICH patients had symptomatic intracerebral hemorrhage (SICH), according to National Institute of Neurological Disorders and Stroke (NINDS) classification. After rt-PA treatment, the median pre-thrombolysis fibrinogenemia of 332 mg/dL significantly dropped to 133 mg/dL ($p < 0.0001$). After the fibrinogen concentrate infusion, the median level of fibrinogenemia rose to 160 mg/dL, which was significantly higher than the median post-thrombolysis levels ($p < 0.0001$). Recanalization was observed in 25/28 patients (89.29%): complete in 18 and partial in 7 patients. After fibrinogen IV infusion, no thrombotic complications were seen in 37 out of 39 patients (94.77%); 2/39 (0.05%) patients experienced a pulmonary embolism, 1 of them a segmental one.

Conclusions. This study showed the clinical safety of administering IV fibrinogen concentrate in order to increase plasma fibrinogen levels in a series of acute stroke patients with iatrogenic fibrinogen depletion after IV thrombolysis.

Key words: ischemic stroke, fibrinogen concentrate replacement, recombinant tissue plasminogen activator

Cite as
Vandelli L, Marietta M, Trenti T, et al. Fibrinogen concentrate replacement in ischemic stroke patients after recombinant tissue plasminogen activator treatment. *Adv Clin Exp Med*. 2019;28(2):219–222. doi:10.17219/acem/84936

DOI
10.17219/acem/84936

Background

Intravenously (IV) recombinant tissue plasminogen activator (rt-PA) is the recommended treatment for eligible acute stroke patients[1] associated with an increased risk of intracerebral hemorrhage (ICH) that mainly occurs within 24–36 h after thrombolysis. About 6–8% of stroke patients undergoing IV thrombolysis experienced symptomatic intracerebral hemorrhage (sICH, as defined by National Institute of Neurological Disorders and Stroke – NINDS), and an additional 1.6–3.6% of them had major systemic bleeding events.[2,3]

Numerous studies have identified different hemorrhagic risk factors for post-thrombolytic ICH, but none was recognized as a determinant, given the possible association of multiple factors. Another important hemorrhagic risk factor seems to be an acquired coagulopathy induced by the thrombolytic drug itself, due to incomplete fibrin-specificity causing a fibrinogen consumption and formation of fibrinogen degradation products, which may lead to a pro-hemorrhagic state supporting bleeding complications.[4–6]

This observational study assessed the clinical outcome of the IV administration of fibrinogen concentrate in a series of acute stroke patients who developed iatrogenic fibrinogen critical depletion after IV thrombolysis.

Material and methods

In the Stroke Unit in Modena University Hospital (Italy), from among 700 ischemic stroke patients treated with IV thrombolysis, data of 39 patients who had experienced severe hypofibrinogenemia and required infusion with IV fibrinogen concentrate (Haemocomplettan P) was collected: 30 patients were treated with IV rt-PA (76.9% of cases) and 9 were treated with IV rt-PA followed by endovascular thrombectomy (23.1% of cases). Fibrinogen values pre-rt-PA infusion and 2 h after the end of the treatment were measured.

In collaboration with the Modena Hospital hematology consultant, to manage the iatrogenic fibrinogen critical depletion after IV thrombolysis, we created hospital standard operating procedures (SOPs) for fibrinogen supplementation considering, as a threshold level for severe hypofibrinogenemia post-thrombolysis, an absolute value <100 mg/dL of fibrinogen level for patients without ICH, and a threshold <200 mg/dL in case of ICH or, in both cases, a relative decrease of fibrinogen levels pre- and post-thrombolysis) >30%.[4]

Patients fulfilling the inclusion criteria (fibrinogen supplementation considering, as a threshold level for severe hypofibrinogenemia post-thrombolysis, an absolute value <100 mg/dL of fibrinogen level for patients without ICH, and a threshold <200 mg/dL in case of ICH or, in both cases, a relative decrease of fibrinogen levels pre- and post-thrombolysis) >30%) were treated with 2 g of IV fibrinogen, followed by further doses until the fibrinogen level reached 200 mg/dL in hemorrhagic patients or 100 mg/dL in non-hemorrhagic patients (Haemocomplettan P mean dose 2 g; 5 patients with 4 g and 2 patients with 6 g).

Statistical analysis

Patients' characteristics will be summarized by means of cross-tabulations for categorical variables or by means of quintiles for continuous variables. Distribution differences of continuous variables over time were assessed using the Mann–Whitney U test. All tests were two-sided, accepting $p < 0.05$ as indicating a statistically significant difference. Analyses were performed by SAS v. 9.1.3 statistical software (SAS Institute, Cary, USA).

Results

Among the 39 patients enrolled, there were 15 females (38.5%) and 24 males (61.5%), with a median age of 78 years (range: 30–96 years) and with a baseline median National Institutes of Health Stroke Scale (NIHSS) clinical stroke severity grade of 14 (range: 2–24). Table 1 provides a short description of patient characteristics.

The overall difference between the NIHSS scores pre- and post-thrombolysis was statistically significant ($p = 0.0002$), as well as the difference between the NIHSS scores pre- and post-thrombolysis at 24-hour evaluation ($p = 0.0455$), and between the NIHSS scores

Table 1. Patient characteristics

Age mean (range) [years]		78.4 (30.9–96.7)
Sex, n, [%]	M	24 (61.5)
	F	15 (38.5)
Type of thrombolysis, n, [%]	IV	31 (79.5)
	IV plus endovascular treatment	8 (20.5)
Fibrinogen pre-thrombolysis, median (range) [mg/dL]		332.0 (170.0–815.0)
Fibrinogen pre-infusion, median (range) [mg/dL]		133.0 (18.0–231.0)
Fibrinogen post-infusion, median (range) [mg/dL]		160.5 (56.0–337.0)
Reduction pre-thrombolysis–pre-infusion, median (range) [%]		66.3 (0.0–97.8)
NIHSS pre-thrombolysis, median (range)		14.0 (2.0–24.0)
NIHSS after 24 h, median (range)		9.0 (0.0–31.0)
NIHSS after 7 days, median (range)		5.0 (0.0–37.0)

IV – intravenous; M – male; F – female; NIHSS – National Institutes of Health Stroke Scale.

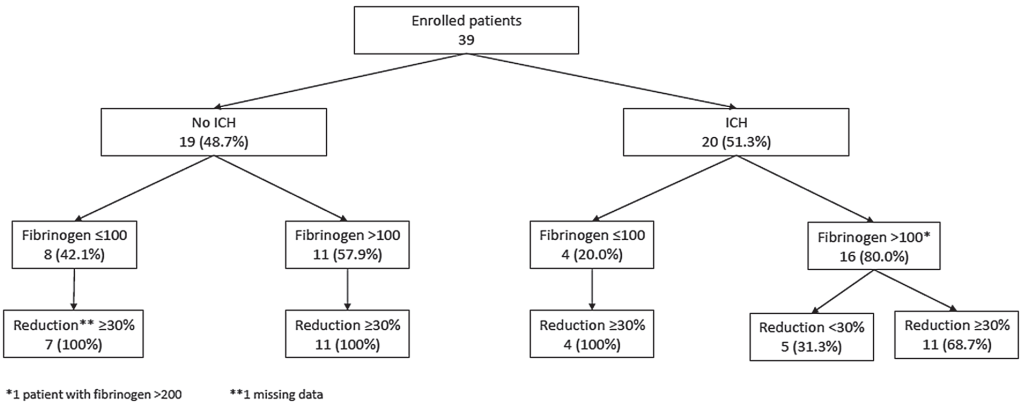

Fig. 1. Patients enrolled and divided according to intracerebral hemorrhage (ICH)/no ICH, fibrinogen levels <100 mg/dL and reduction rate more or less than 30%

pre- and post-thrombolysis at 7-day assessment ($p = 0.0006$).

After 24 h post-thrombolysis, the median NIHSS score was 9 (min 0, max 31) and after 7 days it was 5 (min 0, max 37). The brain computed tomography (CT) scans performed within the first 7 days post-thrombolysis showed that 20 out of 39 patients (51.28%) had ICH (1 with hemorrhagic infarction type 1 (H1) and 6 with parenchymal hemorrhage type 1 (PH1); 4 with hemorrhagic infarction type 2 (H2), and 9 with parenchymal hemorrhage type 2 (PH2) (Fig. 1).

The patients had symptomatic and asymptomatic hemorrhages. Symptomatic hemorrhage, defined according to the NINDS classification, was present in half of the ICH patients (25.6% of the whole sample). The median pre-thrombolysis fibrinogenemia was 332 mg/dL (range: 170–815 mg/dL), which significantly dropped to 133 mg/dL (range: 18–231 mg/dL ($p < 0.0001$) after rt-PA, with a median drop rate of 60%.

After the infusion of fibrinogen concentrate, the median level of fibrinogenemia rose to 160 mg/dL (min 56 mg/dL, max 337 mg/dL), was significantly higher than the post-thrombolysis median levels ($p < 0.0001$), and with a median decrease of –64.61 mg/dL (min –97.8 mg/dL, max 42.2 mg/dL) compared with the pre-thrombolysis levels.

Subsequent controls showed a recanalization in 25 out of 28 patients (89.29%): complete in 18/28 patients (46.15%) and partial in 7/28 patients (17.95%). Hence, a complete or partial recanalization was observed in more than 60% of the patients. Data from 11 out of 28 patients (28.19%) was not available due to missing neurological or radiological assessments.

Regarding the safety of fibrinogen supplementation with Haemocomplettan P, in this case a series of 37 out of 39 patients (94.77%) had no thrombotic complications after fibrinogen IV infusion, while 2/39 (0.05%) patients experienced a pulmonary embolism, 1 of them a segmental one. For 1 of these 2 cases, further investigations gave a subsequent diagnosis of a metastatic pancreatic tumor, which likely had a relevant role in this case, given the well-known paraneoplastic pro-thrombotic condition of pancreatic cancer.

Discussion

In this study, we selected a treatment based on the supplementation of fibrinogen concentrate, taking into account the pathogenesis and mechanism of early rt-PA coagulopathy and the allergic infections and hypervolemic concerns likely associated with fresh frozen plasma and cryoprecipitate.

Most of the patients were supplemented with a limited amount of fibrinogen concentrate (2 g), which significantly increased their final fibrinogen levels, mainly to counteract the fibrinogen consumption due to the previous thrombolytic procedure. The final median fibrinogen level of 64.61 mg/dL was lower than pre-rt-PA levels. The clinical conditions of the patients globally improved, with a significant decrease of the median NIHSS score from 14 at baseline to 9 after 24 h post-thrombolysis, and to 5 after 7 days.

Relevant worsening after fibrinolytic treatment was limited to 6 patients; 5 of them experienced a severe sICH associated with fibrinogen depletion and infusion of IV fibrinogen concentrate after detection of post-thrombolysis ICH. This data could suggest the possible role of hypofibrinogenemia in increasing the risk of bleeding (in particular for sICH) and subsequent poor clinical outcome.

Several studies have highlighted that a critical drop in fibrinogen levels after IV thrombolysis, due to so-called "early rt-PA coagulopathy", is associated with an increased risk of bleeding.[5,6] Apart from a pro-hemorrhagic effect, fibrin and fibrinogen concentrates may have a direct role in the coagulation cascade, as reported by several studies, whereby the fibrinogen supplementation is applied with anti-hemorrhagic purposes in patients with severe hemorrhages and related fibrinogen deficiency following trauma, surgery, etc.[7–10]

In a previous study of Vandelli et al., performed on 104 ischemic stroke patients undergoing rt-PA therapy, the subsequent bleeding rate in the low fibrinogen group was significantly higher (43.9%) than in the normal fibrinogen group (9.5%; odds ratio (OR) = 7.43, $p = 0.001$). The fibrinogen depletion emerged as a highly significant predictor for bleeding risk, underlying a close temporal

relationship with the manifestation of hemorrhage, and accounted for approx. 40% of bleeding events.[4]

Currently, in the absence of evidence-based guidelines for managing thrombolysis-associated sICH, current clinical management is empiric and based on expert opinions, and includes the infusion of fresh frozen plasma, cryoprecipitate or fibrinogen concentrate.[11] In a previous study conducted on patients with occlusions of the intracranial internal carotid artery or the first segment of the middle cerebral artery (or both), IV rt-PA treatment resulted in early reperfusion in 13–50% of the subjects.[12] The high reperfusion rate in our sample shows that the infusion of fibrinogen does not reduce the rate of recanalization; hence, it does not affect negatively the chances of the vessel reopening.

Medical literature regarding the rate of thrombotic complication after fibrinogen concentrate use in stroke patients is relatively lacking. However, experiences in cardiac surgery showed that administration of fibrinogen concentrate was not associated with an increased risk of mortality and thromboembolic events,[13] and a recent Cochrane review (www.cochranelibrary.com) on fibrinogen concentrate in bleeding patients did not show any adverse events such as thrombotic episodes following the use of fibrinogen concentrate.[14] Moreover, thromboembolic complications reported by a large observational study occurred as pulmonary embolism in 0.51%, deep vein thrombosis (DVT) in 0.74% and venous thromboembolism (VTE) in 1.71% of 14,109,000 hospitalized patients with stroke not treated with fibrinogen concentrate.[15]

Conclusions

This observational study showed the clinical safety of administering IV fibrinogen concentrate in order to increase plasma fibrinogen levels in a series of acute stroke patients developing iatrogenic fibrinogen critical depletion after IV thrombolysis. Further and broader studies are needed to evaluate the clinical efficacy as the rationale for administering IV fibrinogen concentrate in order to reduce the risk of intracranial hemorrhage when administered before hemorrhagic complication or to prevent hematoma expansion when administered after bleeding.

References

1. Powers WJ, Derdeyn CP, Biller J, et al; American Heart Association Stroke Council. 2015 American Heart Association / American Stroke Association focused update of the 2013 guidelines for the early management of patients with acute ischemic stroke regarding endovascular treatment: A guideline for healthcare professionals from the American Heart Association / American Stroke Association. *Stroke*. 2015;46(10):3024–3039.
2. Graham GD. Tissue plasminogen activator for acute ischemic stroke in clinical practice: A meta-analysis of safety data. *Stroke*. 2003;34(12):2847–2850.
3. Wahlgren N, Ahmed N, Davalos A, et al; SITS-MOST Investigators. Thrombolysis with alteplase for acute ischemic stroke in the Safe Implementation of Thrombolysis in Stroke-Monitoring Study (SITS-MOST): An observational study. *Lancet*. 2007;369(9558):275–282.
4. Vandelli L, Marietta M, Gambini ME, et al. Fibrinogen decrease after intravenous thrombolysis in ischemic stroke patients is a risk factor for intracerebral hemorrhage. *J Stroke Cerebrovasc Dis*. 2015;24(2):394–400.
5. Trouillas P, Derex L, Philippeau F, et al. Early fibrinogen degradation coagulopathy is predictive of parenchymal hematomas in cerebral rt-PA thrombolysis: A study of 157 cases. *Stroke*. 2004;35(6):1323–1328.
6. Matosevic B, Knoflach M, Werner P, et al. Fibrinogen degradation coagulopathy and bleeding complications after stroke thrombolysis. *Neurology*. 2013;80(13):1216–1224.
7. Danés AF, Cuenca LG, Bueno SR, Mendarte Barrenechea L, Ronsano JB. Efficacy and tolerability of human fibrinogen concentrate administration to patients with acquired fibrinogen deficiency and active or in high-risk severe bleeding. *Vox Sang*. 2008;94(3):221–226.
8. Gollop ND, Chilcott J, Benton A, Rayment R, Jones J, Collins PW. National audit of the use of fibrinogen concentrate to correct hypofibrinogenemia. *Transfus Med*. 2012;22(5):350–355.
9. Weiss G, Lison S, Glaser M, et al. Observational study of fibrinogen concentrate in massive hemorrhage: Evaluation of a multicenter register. *Blood Coagul Fibrinolysis*. 2011;22(8):727–734.
10. Fenger-Eriksen C, Lindberg-Larsen M, Christensen AQ, Ingerslev J, Sørensen B. Fibrinogen concentrate substitution therapy in patients with massive hemorrhage and low plasma fibrinogen concentrations. *Br J Anaesth*. 2008;101(6):769–773.
11. Hemphill JC, Greenberg SM, Anderson CS, et al; American Heart Association Stroke Council; Council on Cardiovascular and Stroke Nursing; Council on Clinical Cardiology. Guidelines for the management of spontaneous intracerebral hemorrhage: A guideline for healthcare professionals from the American Heart Association / American Stroke Association. *Stroke*. 2015;46(7):2032–2060.
12. De Silva DA, Brekenfeld C, Ebinger M, et al; Echoplanar Imaging Thrombolytic Evaluation trial (EPITHET) Investigators. The benefits of intravenous thrombolysis relate to the site of baseline arterial occlusion in the Echoplanar Imaging Thrombolytic Evaluation Trial (EPITHET). *Stroke*. 2010;41(2):295–299.
13. Fassl J, Lurati Buse G, Filipovic M, et al. Perioperative administration of fibrinogen does not increase adverse cardiac and thromboembolic events after cardiac surgery. *Br J Anaesth*. 2015;114(2):225–234.
14. Wikkelsø A, Lunde J, Johansen M, et al. Fibrinogen concentrate in bleeding patients. *Cochrane Database Syst Rev*. 2013;8:CD008864.
15. Skaf E, Stein PD, Beemath A, Sanchez J, Bustamante MA, Olson RE. Venous thromboembolism in patients with ischemic and hemorrhagic stroke. *Am J Cardiol*. 2005;96(12):1731–1733.

Calophyllum inophyllum in vaginitis treatment: Stimulated by electroporation with an in vitro approach

Jerzy Zalewski[1,C,E,F], Justyna Mączyńska[2,B,C], Katarzyna Bieżuńska-Kusiak[2,B,F], Julita Kulbacka[2,A,D,F], Anna Choromańska[2,C,E], Monika Przestrzelska[1,E], Maciej Zalewski[1,C,E], Zbigniew Saczko[3,C], Łucja Cwynar-Zając[4,B,E], Agnieszka Rusak[4,B,E], Jolanta Saczko[2,A,D,F]

[1] Department of Gynecology and Obstetrics, Faculty of Health Sciences, Wroclaw Medical University, Poland
[2] Department of Molecular and Cellular Biology, Faculty of Pharmacy with Division of Laboratory Diagnostics, Wroclaw Medical University, Poland
[3] Antoni Falkiewicz Specialized Hospital, Wrocław, Poland
[4] Department of Histology and Embryology, Faculty of Medicine, Wroclaw Medical University, Poland

A – research concept and design; B – collection and/or assembly of data; C – data analysis and interpretation;
D – writing the article; E – critical revision of the article; F – final approval of the article

Advances in Clinical and Experimental Medicine, ISSN 1899-5276 (print), ISSN 2451-2680 (online) *Adv Clin Exp Med*. 2019;28(2):223–228

Address for correspondence
Julita Kulbacka
E-mail: julita.kulbacka@umed.wroc.pl

Funding sources
This work was supported with the Wroclaw Medical University Statutory Funds ST.E130.16.060 (Prof. J. Zalewski).

Conflict of interest
None declared

Acknowledgements
We owe special thanks to Thomas A. Burley for critical review of the manuscript. Authors would like to express their gratitude to Professor Małgorzata Kotulska from the Wrocław University of Science and Technology for the possibility of performing electroporation tests on ECM 830 Square Wave Electroporation System (BTX, Syngen Biotech, Poland).

Received on August 9, 2017
Reviewed on October 25, 2017
Accepted on March 19, 2018

Published online on November 22, 2018

Cite as
Zalewski J, Mączyńska J, Bieżuńska-Kusiak K, et al. *Calophyllum inophyllum* in vaginitis treatment: Stimulated by electroporation with an in vitro approach. *Adv Clin Exp Med*. 2019;28(2):223–228. doi:10.17219/acem/87045

DOI
10.17219/acem/87045

Abstract

Background. Vaginitis is one of the most common problems in clinical medicine and is cited most often during visits to obstetricians and gynecologists. Most of the inflammation cases are caused by candidiasis trichomoniasis and bacterial vaginosis. Therefore, treatment of vaginal infections must use antibiotic or antifungal drugs, which often provide quick relief to the patient. The real cause of the problem – disrupting the ecosystem of the vagina – remains unchanged. Thus, new therapeutic compounds are being explored.

Objectives. The aim of our study was to evaluate the effect of a natural substance: tamanu oil, an extract from the plant *Calophyllum inophyllum*, applied to the human fibroblast cell line (normal human dermal fibroblasts – NHDFs) and to the isolated human fibroblasts from the vagina (human vaginal fibroblasts – HVFs) in vitro.

Material and methods. We evaluated the viability of cells with 3-(4,5-dimethylthiazol-2-yl)-2,5 diphenyl tetrazolium bromide (MTT) assay after incubation only with tamanu oil and with electroporation (EP). We also examined the immunocytochemical reaction of collagen type III and mitochondrial superoxide dismutase (MnSOD) under established conditions.

Results. Tamanu oil increased the proliferation of cells and the amount of collagen III. It has been shown that the *C. inophyllum* extract stimulates the proliferation of commercial fibroblasts. For direct application in patients, one should use *C. inophyllum* extract in the range of 1:10–1:100 (saline dilution).

Conclusions. The use of this extract (at concentrations indicated by the studies presented here) stimulates the healing processes (increased expression of collagen type III), and has anti-inflammatory, analgesic and antiseptic qualities.

Key words: electroporation, vaginitis inflammation, primary fibroblasts culture, tamanu oil

Introduction

Currently, obstetricians and gynecologists often struggle to treat vaginitis, which is one of the most common problems in clinical medicine. This problem affects women of various ages during their reproductive stage and menopause. Commonly, it is defined as a change in the normal vaginal bacterial flora, in which the normal *Lactobacilli* production is disturbed and, consequently, leads to the overgrowth of a predominant anaerobic bacteria species, such as *Gardnerella vaginali*, *Protea* spp., *Bacteroides* spp., *Mobiluncus* spp., Gram-positive bacteria, and *Mycoplasma*, which can lead to serious complications.[1] Untreated vaginal infection can result in chronic infection of the vagina, and when the infection reaches the fallopian tubes and cervix, infertility can occur. Maintaining a healthy vaginal ecosystem remains an issue underestimated by both patients and the doctors treating them. Most of the cases of vaginitis are caused by candidiasis, trichomoniasis and bacterial vaginosis.[2,3] The pathomechanisms responsible for the bacterial and fungal infections remain unknown. The most significant role in the elimination of vaginal inflammation (VI) is played by non-specific immunity: macrophages, natural killer (NK) cells and neutrophils. Eosinophils indifference and other humoral factors (lysozyme, low pH) constitute a barrier and play an important role in long-term humoral immune protection. However, specific immunity based on the production of antibodies does not serve an important function in VI. Bacterial vaginosis is caused by an imbalance in bacteria colonizing the vagina. A characteristic feature of bacterial vaginosis is the lack of leukocyte infiltration. It is thought that succinic acid and acetic acid are secreted by the bacteria in order to suppress the local immune response. However, in recurrent infections of the vagina and cervix, immune disorders are diagnosed by increased levels of heat shock proteins. This indicates that the normal immune status of women may be imperative in preventing the development of vaginal infections. However, this problem is more complicated, particularly when the immunological system is impaired through disease, immunosuppressants or cancer.[4] Some authors have highlighted the role of cytokines (e.g., recombinant proinflammatory cytokines) in the immune response to fungal pathogens and bacterial infections, and their potential use for prevention or treatment of fungal infections.[5]

The most common cause of vaginal infection is due to a chronic disorder of the vaginal ecosystem. Normal microflora of the vagina, which consists of naturally occurring bacteria in the reproductive tract – primarily of the *Lactobacillus* genus – is essential for the protection of these areas. These bacteria maintain an acidic environment (pH 3.8–4.5) in the vagina and produce substances that prevent the growth of pathogenic bacteria and fungi. Disturbance of the vaginal ecosystem and the reduction in the number of these bacteria contributes to the development of vaginal infections.[1,3] Therefore, treatment of vaginal infections with antibiotic or antifungal drugs is often successful only for a limited time, as the root cause of the problem, the disrupted ecosystem of the vagina, remains unaddressed. For this reason, it is important to discover and develop new therapeutic compounds to improve the treatment of vaginal infections. In recent years, interest in the use of plant or animal extracts for the production of pharmacological compounds has increased. Additionally, numerous studies have shown that natural components can prevent different diseases.[6–9] The introduction of new natural substances with medicinal properties can increase the effectiveness and quality of treatment. Therefore, we decided to evaluate another natural substance for vaginitis treatment: an extract from the plant *Calophyllum inophyllum,* tamanu oil. It contains a lot of unsaturated acids, which are necessary, i.a., to keep the skin healthy and properly hydrated. We hypothesize that this examined extract can be used as a potential therapeutic factor for healing wounds in gynecological diseases as well as protecting mucous membrane integrity. Additionally, we used the electroporation (EP) process to improve therapeutic effects of the tested compound. Electroporation has been widely utilized in recent years as a safe and effective technique to successfully deliver drugs into target cells for both experimental and therapeutic approaches.[10]

Material and methods

Cell culture

The established fibroblast cell line (Normal Human Dermal Fibroblasts – NHDF; PromoCell, Biomedica Poland, Piaseczno, Poland) and normal human primary fibroblast isolated from the vaginal mucus fragment (human vaginal fibroblasts – HVFs) of a healthy patient were used. The primary human fibroblasts were used as a comparison to the established human fibroblast line. The cell lines were grown in Dulbecco's Modified Eagle Medium (DMEM) (Sigma-Aldrich, St. Louis, USA) containing 2mM glutamine, 50 μg/mL streptomycin and 10% fetal bovine serum. Cells were incubated at 37°C in 5% CO_2. The culture medium was replaced twice a week. Before every experiment, cells were detached by 0.25% trypsin with 0.02% ethylenedinitrilotetraacetic acid (EDTA) (Sigma-Aldrich). The appropriate dilutions (1:2–1:100) of tamanu oil, the pure extract from the plant *C. inophyllum*, were prepared in cell culture medium and examined.

Electroporation

Cells were grown as monolayers in 75 cm^2 flasks; then they were trypsinized and centrifuged (5 min, 1000 rpm). Next, cells were counted to obtain the volume of 3×10^6/mL and resuspended in 200 μL of EP buffer

with a low electrical conductivity of 0.14 S/m (10mM KH_2PO_4/K_2HPO_4, 1mM $MgCl_2$, and 250mM sucrose; pH 7.4). The cell suspension was pulsed in a cuvette with 2 aluminum plate electrodes (4 mm space between electrodes) with electrical field strength up to 3,000 V/cm using 8 pulses of 100 µs duration. Rectangular electrical pulses were delivered by an electroporator ECM 830 (BTX Harvard Apparatus; Syngen Biotech, Wrocław, Poland). In the case of the cells being treated with tamanu oil and undergoing EP, electrical fields with the intensity of 800 and 1,000 V/cm were used. Following pulsation, the cells were left for 10 min at 37°C, centrifuged, resuspended in fresh cell culture medium, and reseeded for a viability assay and immunocytochemistry (ABC method).

Cellular viability

Cellular viability was studied by the 3-(4,5-dimethylthiazol-2-yl)-2,5-diphenyltetrazolium bromide (MTT) assay (In Vitro Toxicology Assay; Sigma-Aldrich), which assesses the mitochondrial redox activity as an indicator of the cellular proliferation potential. The MTT assay was performed 24 h and 72 h post-treatment, according to the manufacturer's protocol. The absorbance was measured at 570 nm using a multiwell plate reader (EnSpire Multimode Reader; Perkin Elmer Polska, Kraków, Poland). The assay was performed independenly 3 times using 3 repetition samples, and the mean values and standard deviation (SD) of combined results were calculated.

Immunocytochemical ABC staining of collagen III and mitochondrial superoxide dismutase

The expression of selected proteins was examined by the immunocytochemical Avidin-Biotin Complex (ABC) method. After fixation in 4% paraformaldehyde, the samples were permeabilized and blocked by incubation with 0.1% Triton X-100 (Sigma-Aldrich) in phosphate-buffered saline (PBS). The protein expression was visualized with a polyclonal antibody COL-III (1:100, anti-collagen III) and anti-SOD2 (Santa Cruz Biotechnology, Dallas, USA). Immunocytochemical staining was performed with ImmPRESS Universal Reagent (Vector Laboratories, Burlingame, USA).

Results

Cellular viability

The influence of tamanu oil, electric field intensity and the combination of both on cellular viability was assessed using MTT assay. The investigation indicated that using the tamanu oil increased viability in human fibroblast cell line, stimulating the proliferation of NHDF cells at every dilution, in contrast to HVF cells, in which higher viability

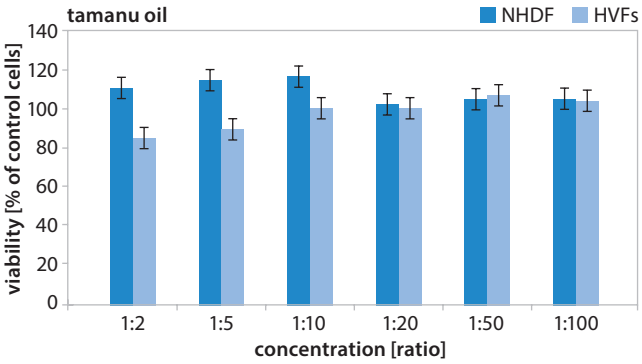

Fig. 1. The effect of *Calophyllum inophyllum* extract on the viability of normal human dermal fibroblast (NHDF) cells and cells from primary cell cultures (human vaginal fibroblasts – HVFs)

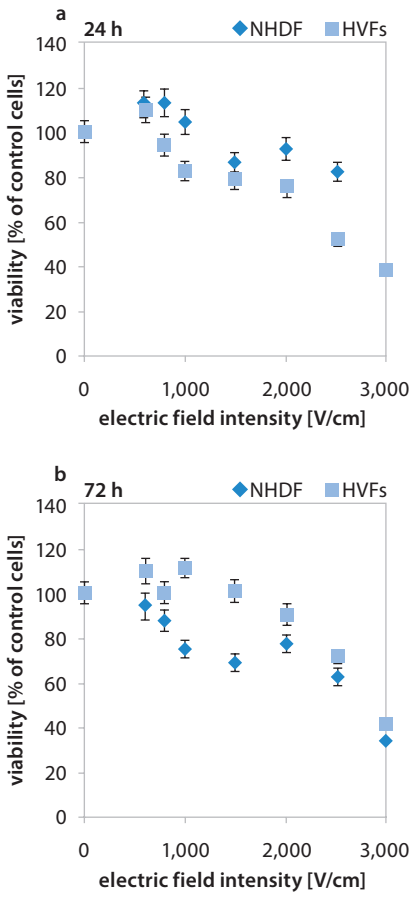

Fig. 2. The impact of pulsed electric field on human fibroblast (normal human dermal fibroblasts (NHDFs) and human vaginal fibroblasts (HVFs)) viability a) 24 h and b) 72 h after exposition

was observed only for further dilutions (1:20; 1:50; 1:100) (Fig. 1). From the experiment in which different currents were used, we selected the electric field of 800 V/cm intensity as the most beneficial for further experiments with the application of the oil extract from *C. inophyllum* on both cell lines (Fig. 2). Surprisingly, combining EP with tamanu oil resulted in a much greater increase in cell proliferation of HVF cells compared to NHDF cells. The highest proliferation was observed at 800 V/cm electrical field intensity and 1:10 dilution of tamanu oil (Fig. 3).

Immunocytochemical ABC reaction: collagen III and MnSOD

The results of immunostaining with anti-collagen III and anti-mitochondrial superoxide dismutase 2 (anti-MnSOD2) are presented in Tables 1–4 and in Fig. 4 and 5. An increase in collagen III expression was noted only 24 h post-incubation with tamanu oil (Table 1, Fig. 4). The most intense immune reaction was observed after incubation with tamanu oil at a dilution of 1:10 with application of an electric field of 800 V/cm intensity (c.a. 70% for NHDF and 30% for HVF) after 24 h of incubation. After 72-hour incubation with tamanu oil in combination with EP, the level of COL-III insignificantly decreased in NHDF cells and increased in primary HVF cells (Table 1, Fig. 4). Contrary to collagen III, the MnSOD expression indicated more intense staining reaction. The intensity of anti-MnSOD reaction increased proportionally with the increasing electric field intensity (Tables 1,2, Fig. 5) in NHDF cells. The highest expression was noted after a 24-hour incubation for cells treated only with tamanu oil and for cells treated with oil-EP combination (90% and 100%, respectively) (Table 1, Fig. 5). The expression of this antioxidant enzyme was lower after 72 h than 24 h post-treatment for cells treated only with tamanu oil and for the combined treatment (Table 2, Fig. 5). In HVF cells, the expression of MnSOD also increased at the higher EP parameters after 72 h in 100% of cells (Tables 3,4).

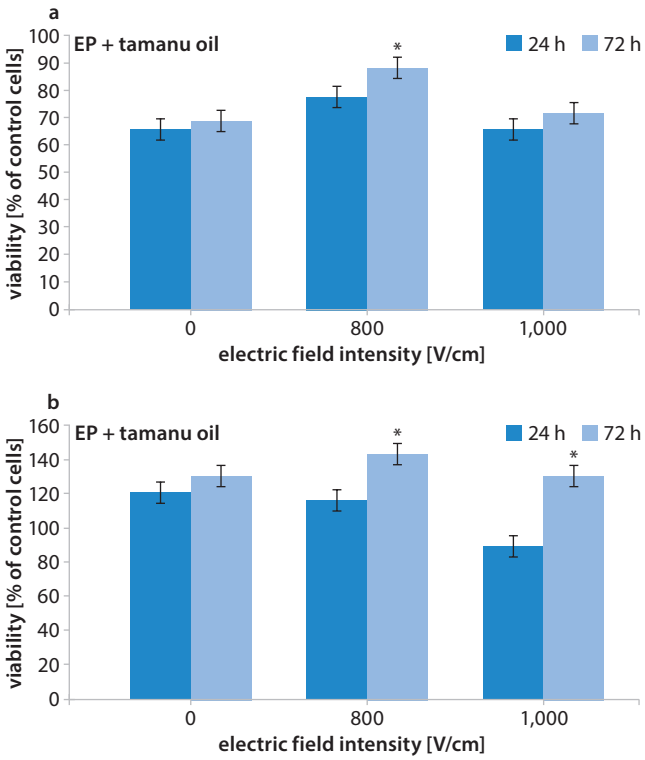

Fig. 3. The influence of *Calophyllum inophyllum* extract combined with electroporation (EP) on human fibroblasts viability 24 h and 72 h post-treatment in: a) normal human dermal fibroblasts (NHDFs) and b) human vaginal fibroblasts (HVFs)

Discussion

Prognosis of vaginitis in many cases is promising, but most of the infections are not completely cured and, therefore, reoccur. The recurring vaginal infection might lead to chronic infections and scarring,[10] but in most cases when suitably treated do not cause permanent problems. Conversely, untreated vaginal infections can spread to other pelvic structures and result in chronic diseases.[11] In such cases, another course of treatment is necessary. Natural compounds are commonly applied in many diseases of the human body, against both the precancerous state and cancer. However, it is commonly known that some of these compounds can be used in other non-cancer diseases. As an example can serve tropical tamanu oil, an extract from *C. inophyllum*. The properties of this oil have been known for a long time, especially for healing wounds. Women frequently use tamanu oil to achieve healthy, clear skin, as it helps to clear acne and scars. These compounds

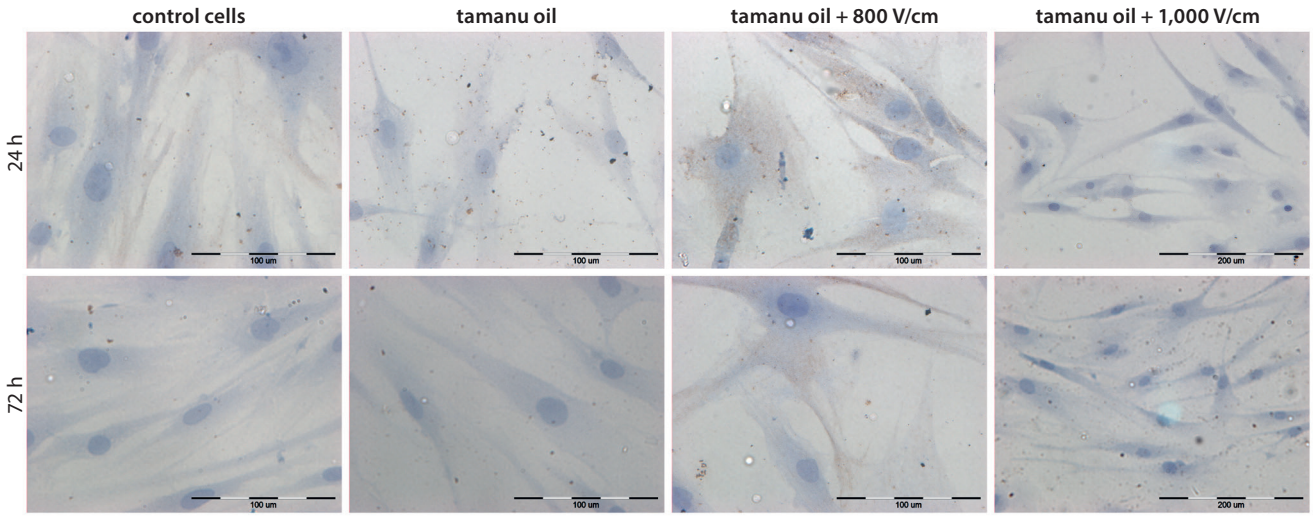

Fig. 4. The immunocytochemical staining reaction of collagen III in normal human dermal fibroblasts (NHDFs) 24 h and 72 h post-treatment

also have anti-inflammatory properties reducing swelling of rashes, insect bites and sunburns. Tamanu oil additionally possesses significant antimicrobial, antibacterial and antifungal qualities.[11] In this investigation, we examined the effect of tamanu oil on the proliferation of human established cell line fibroblast line (NHDF) and human primary fibroblast isolated from vagina (HVF). Additionally, we used EP in order to improve the transport of the examined compound. However, we observed an increase in proliferation in both human fibroblast cell lines

Table 1. The immunocytochemical evaluation of collagen III and mitochondrial superoxide dismutase (MnSOD) proteins in established normal human dermal fibroblast (NHDF) cells 24 h after incubation with tamanu oil and after electroporation (EP) combined with examined compound for 800 V/cm and 1,000 V/cm electric field intensity

Sample group	Tamanu oil concentration	EP (V/cm)	Intensity of immunoreaction	
			collagen III	MnSOD
Control group	no tamanu oil used	no EP applied	<5% +	55% +/++
Group I	1:10	0	50% +	90% ++
Group II	1:10	800	75% ++	100% ++
Group III	1:10	1,000	<5% +	100% ++

Table 2. The immunocytochemical evaluation of collagen III and mitochondrial superoxide dismutase (MnSOD) proteins in established normal human dermal fibroblast (NHDF) cells 72 h after incubation with tamanu oil and after electroporation (EP) combined with examined compound for 800 V/cm and 1,000 V/cm electric field intensity

Sample group	Tamanu oil concentration	EP (V/cm)	Intensity of immunoreaction	
			collagen III	MnSOD
Control group	no tamanu oil used	no EP applied	<5% +	70% +/++
Group I	1:10	0	<5% –/+	80% ++
Group II	1:10	800	35% +/++	85% ++
Group III	1:10	1,000	10% +	95% +++

Table 3. The immunocytochemical evaluation of collagen III and mitochondrial superoxide dismutase (MnSOD) proteins in primary human vaginal fibroblast (HVF) cells 24 h after incubation with tamanu oil and after electroporation (EP) combined with examined compound for 800 V/cm and 1,000 V/cm electric field intensity

Sample group	Tamanu oil concentration	EP (V/cm)	Intensity of immunoreaction	
			collagen III	MnSOD
Control group	no tamanu oil used	no EP applied	–	45% ++
Group I	1:10	0	10% ++	100% ++
Group II	1:10	800	30% ++	90% ++
Group III	1:10	1,000	35% ++	100% +++

Table 4. The immunocytochemical evaluation of collagen III and mitochondrial superoxide dismutase (MnSOD) proteins in primary human vaginal fibroblast (HVF) cells 72 h after incubation with tamanu oil and after electroporation (EP) combined with examined compound for 800 V/cm and 1,000 V/cm electric field intensity

Sample group	Tamanu oil concentration	EP (V/cm)	Intensity of immunoreaction	
			collagen III	MnSOD
Control group	no tamanu oil used	no EP applied	–	100% +++
Group I	1:10	0	15% ++	100% ++/+++
Group II	1:10	800	40% ++	100% +++
Group III	1:10	1,000	75% ++	100% +++

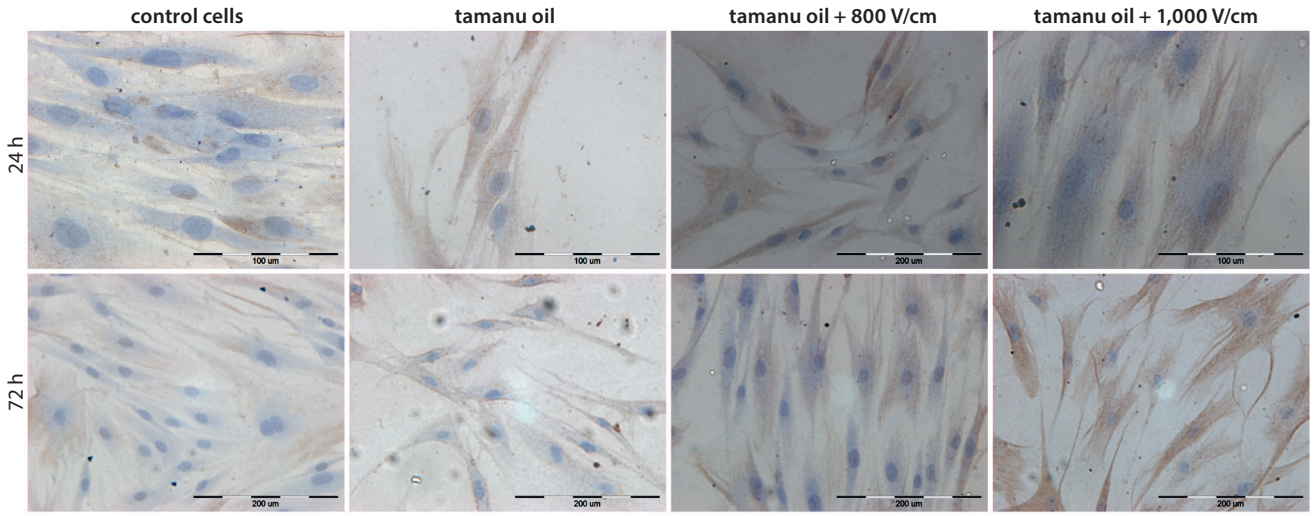

Fig. 5. The immunocytochemical staining reaction of superoxide dismutase (anti-MnSOD) in normal human dermal fibroblasts (NHDFs) 24 h and 72 h post-treatment

only for the electric field strength of 800 V/cm. A higher electric field intensity caused a similar effect in the control non-treated cells. Our results indicated that it stimulated cell proliferation, which suggests that tamanu oil could become a promising agent for human fibroblast re-growth. Therefore, it could help in developing a new, more effective method in vaginitis treatment. During the healing phase (so-called "proliferation") collagen and elastin fibers are formed to build up a strong and flexible skeleton, which is then filled by proteoglycan molecules and glycoproteins that combine matrix and healing cells in the wound.[12,13] In order to verify the healing properties of the chosen natural oil, the expression of selected extracellular matrix protein (collagen III) was examined. An increase of collagen III expression was noted 24 h and 72 h after incubation with the extract from *C. inophyllum* seeds. The highest expression was observed after incubation with tamanu oil at a dilution of 1:10, with a pulsed electric field (800 V/cm). Higher (1,000 V/cm) EP parameters induced decrease of immunoassayed reaction with anti-collagen III, suggesting that the higher EP parameters in combination with tamanu oil do not support collagen expression in NHDF and HVF cells. Initial wound healing involves the synthesis of type III collagen, which is characteristic for immature connective tissue. As wound healing progresses, type III collagen, which is the main component of the granulation tissue, is replaced by type I collagen. Type I collagen is the main and most common type present in dermal tissue and is responsible for the tensile strength of the tissue.[14] Our results suggest that tamanu oil can aid in early stages of the healing process by increasing the expression of type III collagen by human fibroblasts. In wound healing and inflammatory processes, the development of scar remodeling is important in order to obtain a sufficiently strong substitute tissue that is resistant to mechanical stimuli.[15,16] The synthesis of collagen proteins is a very complex process, which is dependent on the level of the natural antioxidant, vitamin C.[17,18] Thus, the expression of main antioxidant enzyme MnSOD was evaluated. The MnSOD protein content was found to increase with increasing pulsed electric field intensity combined with tamanu oil use, in comparison to control non-treated cells.

Conclusions

It has been shown that the *C. inophyllum* extract stimulates the proliferation of established and primary fibroblasts to a different degree. The use of tamanu oil at the concentrations indicated by this study suggests that the stimulated proliferation process could be utilized as an anti-inflammatory, analgesic and antiseptic agent in the healing process (increased expression of collagen type III) of vaginal infections. Moreover, tamanu oil is known for its strong antimicrobial properties. The obtained results might be the basis for the future development of protocols involving the application of the EP method combined with the oil extract from *C. inophyllum* in preclinical and clinical treatment.

References

1. Abbaspoor Z, Rabee Z, Najjar S. Efficacy and safety of oral tinidazole and metronidazole in treatment of bacterial vaginosis: A randomized control trial. *Int J Clin Pharmacol Res.* 2014;4(2):2277–3312.
2. Edwards L. The diagnosis and treatment of infections vaginitis. *Dermatol Ther.* 2004;17(1):102–110.
3. Mitchell H. ABC of sexually transmitted infections. Vaginal discharge: Causes, diagnosis and treatment. *BMJ.* 2004;29(7451):1306–1308.
4. Edwards L. Dermatologic causes of vaginitis: A clinical review. *Dermatol Clin.* 2010;28(4):727–735.
5. Antachopoulos C, Roilides E. Cytokines and fungal infections. *Br J Haematol.* 2005;129(5):583–596.
6. Choromańska A, Kulbacka J, Rembiałkowska N, et al. Anticancer properties of low molecular weight oat beta glucan: An in vitro study. *Int J Biol Macromol.* 2015;80:23–28.
7. Rahar S, Swami G, Nagpal N, Nagpal MA. Preparation, characterization and biological properties of b-glucans. *J Adv Pharm Technol Res.* 2011;2(2):94–103.
8. Drag-Zalesińska M, Wysocka T, Borska S, et al. The new esters derivatives of betulin and betulinic acid in epidermoid squamous carcinoma treatment: In vitro studies. *Biomed Pharmacother.* 2015;72:91–97.
9. Bautista CT, Wurapa E, Sateren WB, Morris S, Hollingsworth B, Sanchez JL. Bacterial vaginosis: A synthesis of the literature on etiology, prevalence, risk factors, and relationship with chlamydia and gonorrhea infections. *Mil Med Res.* 2016;3:4.
10. Saczko J, Kamińska I, Kotulska M, et al. Combination of therapy with 5-fluorouracil and cisplatin with electroporation in human ovarian carcinoma model in vitro. *Biomed Pharmacother.* 2014;68(5):573–580.
11. Hasan AM. Review on: Vaginitis. A problem to be solved! *J Pharm Chem Biol Sci.* 2016;4(1):104–110.
12. Léguillier T, Lecsö-Bornet M, Lémus C, et al. The wound healing and antibacterial activity of five ethnomedical *Calophyllum inophyllum* oils: An alternative therapeutic strategy to treat infected wounds. *PLoS One.* 2015;10(9):e0138602.
13. Smith JD, Garber GE. Trichomonas vaginalis infection induces vaginal CD4 cell infiltration in a mouse model: A vaccine strategy to reduce vaginal infection and HIV transmission. *J Infect Dis.* 2015; 212(2):285–293.
14. Darby IA, Laverdet B, Bonté F, Desmoulière A. Fibroblast and myofibroblast in wound healing. *Clin Cosmet Investig Dermatol.* 2014;7:301–311.
15. Osiak K. Przerostowe blizny, bliznowce i przykurcze bliznowate. *Post Nauk Med.* 2005;18:17–23.
16. Xue M, Jackson CJ. Extracellular matrix reorganization during wound healing and its impact on abnormal scarring. *Adv Wound Care (New Rochelle).* 2016;4(3):130–136.
17. Grosso G, Bei R, Mistretta A, et al. Effects of vitamin C on health: A review of evidence. *Front Biosci (Landmark Ed).* 2013;18:1017–1029.
18. van Kessel K, Assefi N, Marrazzo J, Eckert L. Common complementary and alternative therapies for yeast vaginitis and bacterial vaginosis: A systematic review. *Obst Gynecol Surv.* 2003;58(5):351–358.

Thermal imaging and planimetry evaluation of the results of chronic wounds treatment with hyperbaric oxygen therapy

Justyna Glik[1,2,A,B,D], Armand Cholewka[3,B–D], Agata Stanek[4,C–E], Beata Englisz[3,B], Karolina Sieroń[5,C], Karolina Mikuś-Zagórska[1,A–C], Grzegorz Knefel[1,B,C], Mariusz Nowak[1,C,F], Marek Kawecki[1,6,A,E,F]

[1] Dr Stanisław Sakiel Centre for Burns Treatment, Siemianowice Śląskie, Poland
[2] Department of Chronic Wounds Management Organization, School of Health Sciences in Katowice, Medical University of Silesia, Poland
[3] August Chełkowski Institute of Physics, University of Silesia, Katowice, Poland
[4] School of Medicine with the Division of Dentistry in Zabrze, Department and Clinic of Internal Diseases, Angiology and Physical Medicine in Bytom, Medical University of Silesia, Poland
[5] Chair of Physiotherapy, Department of Physical Medicine, School of Health Sciences in Katowice, Medical University of Silesia, Poland
[6] Department of Health Sciences, Technical-Humanistic Academy, Bielsko-Biała, Poland

A – research concept and design; B – collection and/or assembly of data; C – data analysis and interpretation;
D – writing the article; E – critical revision of the article; F – final approval of the article

Advances in Clinical and Experimental Medicine, ISSN 1899-5276 (print), ISSN 2451-2680 (online) *Adv Clin Exp Med*. 2019;28(2):229–236

Address for correspondence
Armand Cholewka
E-mail: armand.cholewka@gmail.com

Funding sources
None declared

Conflict of interest
None declared

Received on July 11, 2017
Reviewed on May 9, 2018
Accepted on June 15, 2018

Published online on September 21, 2018

Abstract

Background. One of the methods to treat chronic wounds is the use of hyperbaric oxygen (HBO). Objective measurement of the wound surface is an important element in the process of monitoring and predicting the progress of treatment.

Objectives. The aim of the study was to evaluate the effect of hyperbaric oxygen therapy (HBOT) on ulcer wound healing in patients with chronic venous insufficiency ulcers and diabetic foot syndrome using thermal imaging and computerized planimetry.

Material and methods. During a 3-year period, 284 digital computer planimetry measurements were gathered from 142 patients treated for leg ulcers caused by chronic venous insufficiency and ulcers from diabetic foot syndrome at HBOT Unit of the Dr Stanisław Sakiel Centre for Burns Treatment in Siemianowice Śląskie (Poland). Each patient took 30 HBOT sessions using a Haux multiplace HBO chamber at a pressure of 2.5 atmospheres absolute (ATA). The results of the treatment were monitored using thermovision and computer-assisted planimetry measurements performed before and after HBOT.

Results. Both groups of patients exhibited a reduction in the surface and perimeter of the wound after HBOT. The treatment effects were also confirmed with thermal imaging. The areas calculated from thermal imaging and planimetry are different but correlated.

Conclusions. It seems that a combination of thermal imaging and planimetry may enhance the diagnosis as well as provide the physician with more information about therapy effects.

Key words: chronic wounds, thermal imaging, planimetry, hyperbaric oxygen therapy

Cite as
Glik J, Cholewka A, Stanek A, et al. Thermal imaging and planimetry evaluation of the results of chronic wounds treatment with hyperbaric oxygen therapy. *Adv Clin Exp Med*. 2019;28(2):229–236. doi:10.17219/acem/92304

DOI
10.17219/acem/92304

Introduction

Numerous studies have focused on the treatment of chronic wounds and, in particular, their objective assessment, as well as simple, effective and objective monitoring of the healing process, with emphasis on the possibility of storing data for subsequent comparison. Hyperbaric oxygen therapy (HBOT) is a non-invasive method that includes breathing pure oxygen under increased pressure conditions, which facilitates the healing of chronic wounds.[1] Sometimes it is the only therapeutic method which allows for avoiding limb amputation after all other available treatment methods have failed.[2] There are numerous factors indicating wound healing, such as reduction of wound exudate and bacterial load, speed of granulation tissue formation, rapidity of epithelialization, etc.[3] However, the assessment of wound healing is based in most of the cases only on clinical signs, manual measurements or photographic documentation, which are more or less objective and can cause errors in the assessment of healing process dynamics. Making a distinction between a healing and a non-healing wound allows the physician to decide whether to continue the selected therapy or to use alternative methods of treatment. Measurements using a ruler or a transparent film placed over the wound to trace its contours can be used to assess the ulceration surface. Despite being suitable for small area wounds with regular shapes, these methods have many disadvantages.[4–6] Digital computer planimetry allows for measuring of wounds on digital images by tracing their contours using specialized computer software.[7,8] The wound measurement is performed automatically. The digital system provides recording, processing and analyses of the images obtained. The reference scale used in the photograph guarantees the accuracy of the measurements.[8]

Methods like planimetry and oximetry are used in the qualification of a patient for HBOT and in the evaluation of the therapy effects. However, a non-invasive, easy to perform and quick method of evaluating the treatment effects as well as of the diagnosis of the patient's condition is still needed. Such method might be thermovision, which is used more and more widely in medicine.[9] That is why the aim of presented work is to determine and compare the diagnostic value of computer planimetry and thermal imaging of patients treated with HBOT.

Material and methods

Inclusion criteria to the study population were as follows:
- presenting with 2 selected types of chronic wounds: leg ulcers due to chronic venous insufficiency in the phase C6 active venous ulcers according of Clinical-Etiology-Anatomy-Pathophysiology classification (CEAP) (Group A) and the diabetic foot stage 1 and 2 ulcers according to Wagner Classification (Group B);
- signed informed consent for participation in the objective (planimetric) assessment of wound surface and perimeter before and after HBOT;
- participation in 30 HBOT sessions.

According to the general HBOT contraindications, only patients without any respiratory obstruction or other conditions such as pneumothorax, active neoplastic process, claustrophobia, or psychiatric disease in medical history were included in HBOT group.

All patients from both groups were referred for HBOT after ineffective conservative treatment: compression therapy, targeted antibiotic treatment, local use of antiseptics, phlebotropic drugs, diabetes medications, and special dressings. Before the beginning of treatment in the hyperbaric chamber, all patients were prepared and qualified for HBOT by their physicians-in-charge or were referred to the Hyperbaric Oxygen Therapy Unit at the Dr Stanisław Sakiel Centre for Burns Treatment in Siemianowice Śląskie (Poland) after hospitalization at internal medicine, surgery or dermatology departments, or after outpatient treatment. The patient's qualification for HBOT was finally approved by a multidisciplinary medical council. Apart from the medical history, physical examination and photographic documentation, planimetric measurements and partial oxygen concentration measurements in the skin around the wound were performed using transcutaneous oximetry. Each patient qualified for HBOT was provided with local and general treatment at the Outpatient Unit of the Centre for Burns Treatment. If pain symptoms occurred, all patients took nonsteroidal anti-inflammatory drugs. A coexisting disease stabilization standard was applied in all patients. In patients with diabetes, glucose levels were stabilized before start of HBOT and maintained during the entire treatment period. Each patient qualified for HBOT received standard local treatment in accordance with the guidelines of Polish Wound Treatment Society.[10,11] Before the start of the therapy, each patient was informed about the principles of safety, as well as about the objects and substances which could not be used during treatment in the hyperbaric chamber. All data was encoded to prevent identification of patients.

The study was approved by the local research ethics committee and was carried out in accordance with the principles set forth in the Declaration of Helsinki.

The study material is based on 142 patients treated in the Hyperbaric Oxygenation Ward of the Centre for Burns Treatment in Siemianowice Śląskie between 2009 and 2012. The study population characteristics are shown in Table 1.

No complications were observed during HBOT in any patients. From the total number of 432 patients, 290 were

Table 1. Characteristics of studied patient population

Group	Number of patients	Males	Females	Age
A – with venous ulcers due to chronic venous insufficiency	98 (69%)	39 (40%)	59 (60%)	19–85 (60.38 ±13.87)
B – with diabetic foot ulcer	44 (31%)	22 (50%)	22 (50%)	34–79 (58.06 ±10.40)

excluded from the research. Among them, 227 (52.5%) patients were excluded due to incompatibility with diagnosis inclusion criteria; 25 patients (5.8%) were excluded as they withdrew from the treatment before completing the obligatory 30 HBOT sessions, and 38 patients (8.8%) were excluded due to the absence of objective examination process (patients with circular wounds).

Hyperbaric oxygen application

All patients underwent 30 sessions of HBOT in a multiplace hyperbaric oxygen (HBO) chamber (Haux-Life Support GmbH, Karlsbad-Ittersbach, Germany). Sessions were performed every 24 h, 5 times per week. During 90-minute sessions in a HBO chamber, patients were breathing pure oxygen for 60 min (under pressure of 2.5 atmospheres absolute – ATA) with 2 5-minute air breaks.

Wound evaluation

Each ulcer was marked initially by tracing its borders before and after HBOT, and was documented by digital pictures. The pictures were then analyzed by computerized wound planimetry.

Planimetric system IRIS® (Medicom, Wrocław, Poland), used for planimetric examination, enabled the measurement of the wound size (surface and perimeter) by specialized computer software (images with regions of interest and parameters can be seen in Fig. 1A and B. Additionally, once a week photographic documentation of all wounds was performed and clinical wound evaluation data was recorded. Both planimetric measurements and clinical evaluation records were used for the analysis of results.

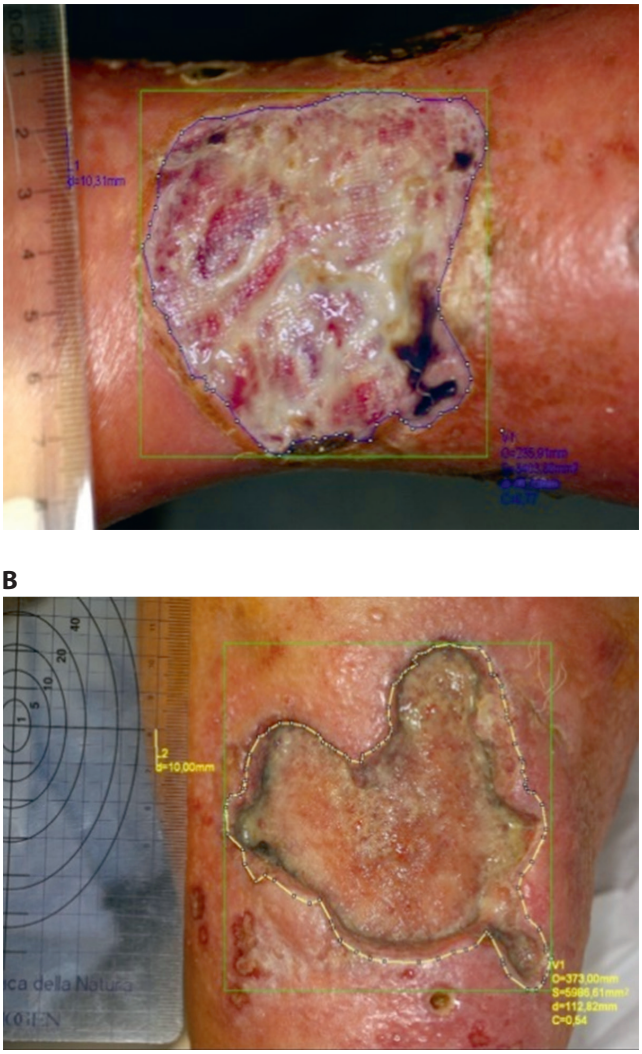

Fig. 1. Digital computerized wound planimetry

Thermal imaging

The distribution of the skin surface temperature was monitored with the use of a Thermovision Camera E60 (Flir Systems, Täby, Sweden) calibrated by black body. The thermograms of the chosen regions of interest were performed before and immediately after HBOT in a special room outside the chamber. There were 30 cases studied by thermal imaging. Thermal imaging was performed according to Glamorgan Protocol and took into account the standardization of infrared thermal imaging.[12,13]

Statistical analysis was done using STATISTICA v. 10.1 (StatSoft Inc., Tulsa, USA) and the data was analyzed based on the calculation of median values and the range for collected data, including demography/age of treatment group. In order to study the impact of one variable on another, Spearman's rank correlation coefficient was determined. Moreover, paired-sample t-test for normal values distribution and Mann-Whitney U test or Wilcoxon test were used when data was characterized by abnormal distribution. The normality of distribution was checked by Levene's test. When more than 2 groups were compared, the analysis of variance (ANOVA) test was used. Differences with a p-value <0.05 were considered significant.

Results

Analysis of clinical results of treatment in both groups after hyperbaric oxygen therapy

In 16 patients (16.32%) from Group A, complete wound healing was achieved. In 82 patients (83.67%), wound reduction was observed and they were qualified for further treatment with split-thickness skin grafts.

In 9 patients (20.45%) from Group B, complete wound healing was achieved. In 35 patients (79.55%), wound reduction was observed and they were qualified for further treatment with split-thickness skin grafts.

Planimetry measurements results

In Group A, the average wound perimeter after HBOT was 128.80 ±122.81 mm, which was significantly lower than the average wound perimeter 171.70 ±123.76 mm ($p = 0.001$) before HBOT (Fig. 2).

The average wound surface area after HBOT was 954.90 ±1349.97 mm^2, which was found again to be significantly lower than the average wound surface area of 1636.60 ±2101.22 mm^2 ($p = 0.0005$) before HBOT (Fig. 3).

In Group B, we observed that the average wound perimeter was 75.20 ±51.23 mm after HBOT and it was significantly lower than the average wound perimeter of 99.00 ±66.06 mm ($p = 0.0101$) before HBOT (Fig. 4).

The average wound surface area after HBOT was 303.40 ±288.04 mm^2 and it was significantly lower than the average wound surface of 663.80 ±745.38 mm^2 before HBOT ($p = 0.011$) (Fig. 5).

Thermal imaging results

The thermal images for representative patients (the images were chosen for the best illustration of the studied problem) suffering from venous crural ulceration were performed before (a) and after (b) HBOT session, with the collected temperature parameters derived from chosen areas, are presented in Fig. 6.[14]

The region of interest (part of the lower extremities) was divided into 3 parts (area 1 (AR01) – ulceration, area 2 (AR02) – closer area above the wound, area 3 (AR03) – further areas below the wound). It is clearly visible that the skin temperature changes due to HBOT. However, to see the problem more clearly, some statistical analysis had to be performed. The mean temperature changes due to HBOT are presented in Fig. 7. Despite no statistical significance between the mean temperature of the whole studied region of interest before as well as after hyperbaric oxygenation ($p > 0.05$), it can be seen that the temperature range of these areas was less differentiated after HBOT than before HBOT. However, the situation changed when the temperature difference

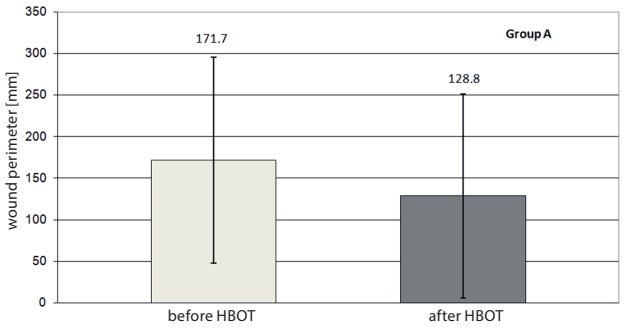

Fig. 2. Comparison of average wound perimeter before and after hyperbaric oxygen therapy (HBOT) in Group A

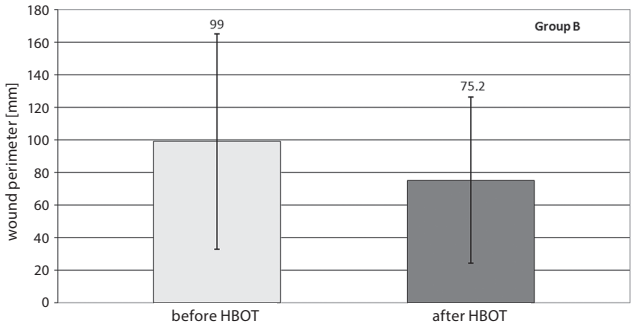

Fig. 3. Comparison of average wound perimeter before and after hyperbaric oxygen therapy (HBOT) in Group B

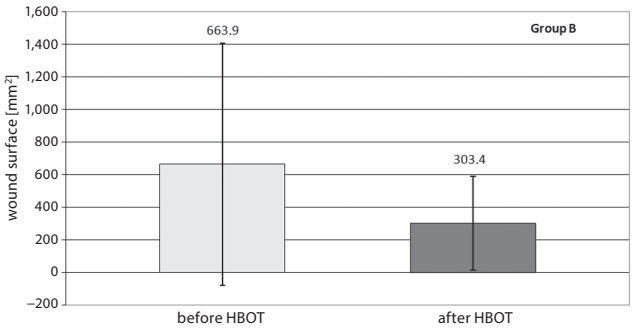

Fig. 4. Comparison of average wound surface before and after hyperbaric oxygen therapy (HBOT) in Group B

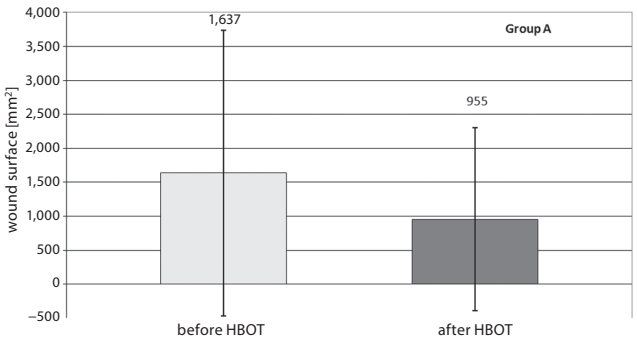

Fig. 5. Comparison of average wound surface before and after hyperbaric oxygen therapy (HBOT) in Group A

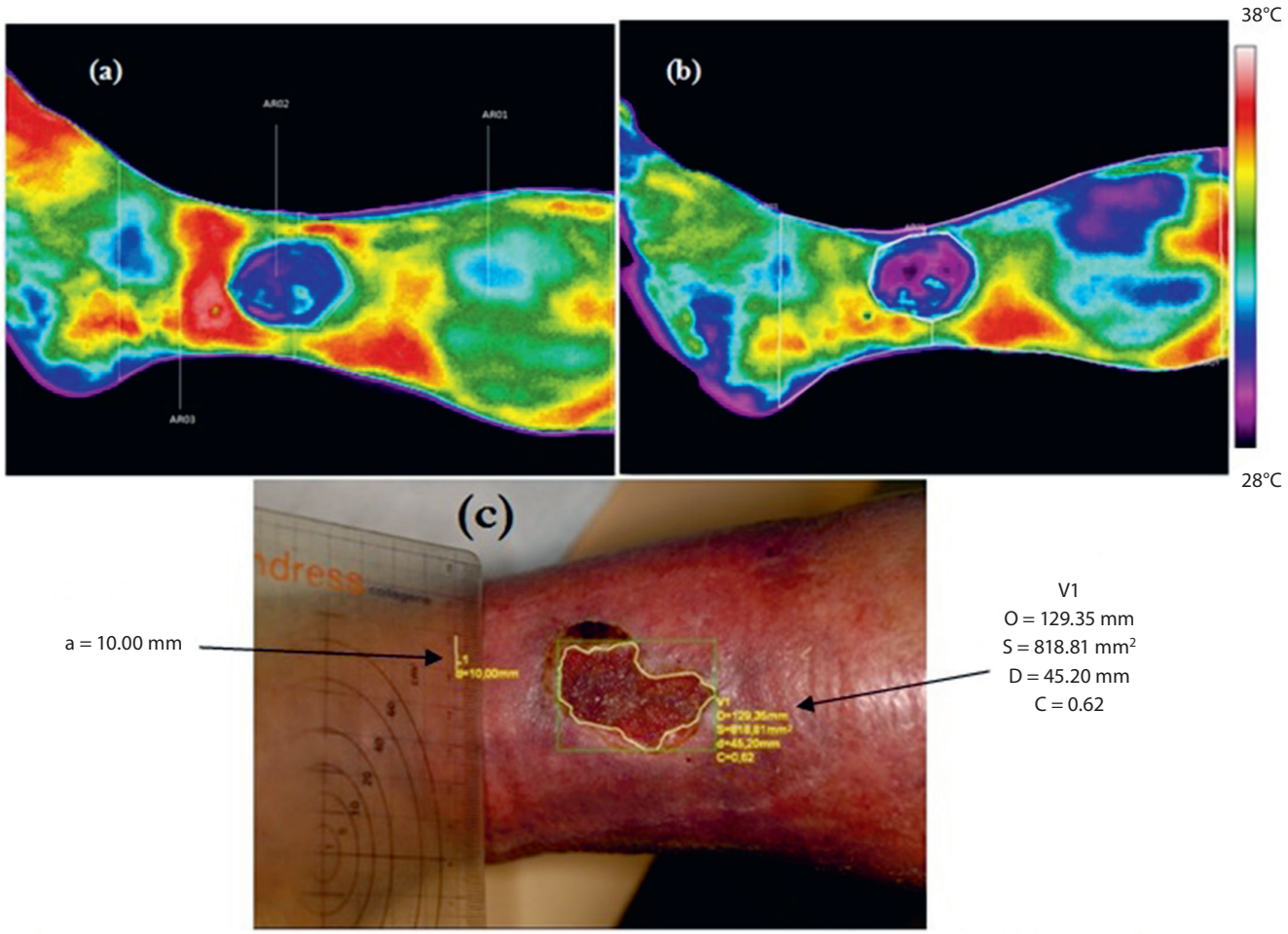

Area	T_{mean} before HBOT [°C]	T_{mean} after HBOT [°C]	Area [mm^2]	Number of pixels counted from thermal imaging
AR01	33.0	31.6	–	–
AR02	31.3	30.5	818.8	2,330.0
AR03	33.2	31.8	–	–

Fig. 6. The thermal image of representative patients suffering from venous chronic ulceration, performed before (a) and after (b) the hyperbaric oxygen therapy (HBOT) session, planimetry image (c) and results of temperature and planimetry parameters obtained from chosen areas[14]

between AR01 and AR02 before and after HBOT was considered. A deeper analysis showed that the decrease of the mean temperature difference between AR01 and AR02 (marked in Fig. 7 with an arrow) was nearly 3 times smaller: $\Delta T = 0.9$ observed before hyperbaric oxygenation in comparison to $\Delta T = 0.3$ observed after hyperbaric oxygenation.[14] The difference was statistically significant ($p = 0.031$).

Similar tendencies can also be observed in other thermal imaging results (Fig. 8). The differences between the areas derived from planimetry and from thermal images as a number of pixels (Fig. 6) are determined by 2 different ways of analysis – structural in the case of planimetry and metabolical in thermovision. Connecting these 2 imaging techniques may provide additional information in diagnosis, as well as in the evaluation of therapy effects.

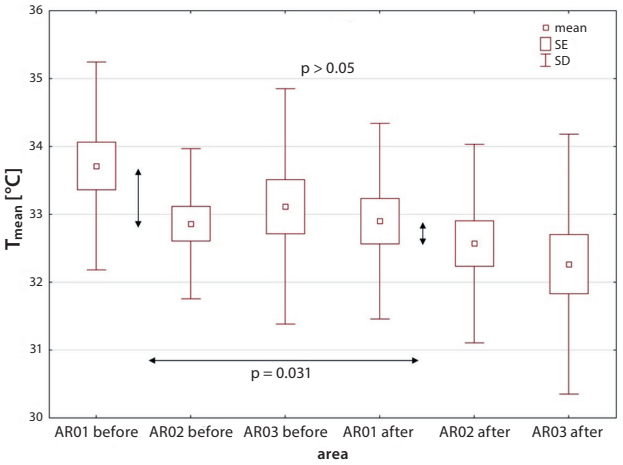

Fig. 7. Changes of T_{mean} obtained from chosen areas for studied group of patients performed before and after hyperbaric oxygen therapy (HBOT)[14]

SE – standard error; SD – standard deviation.

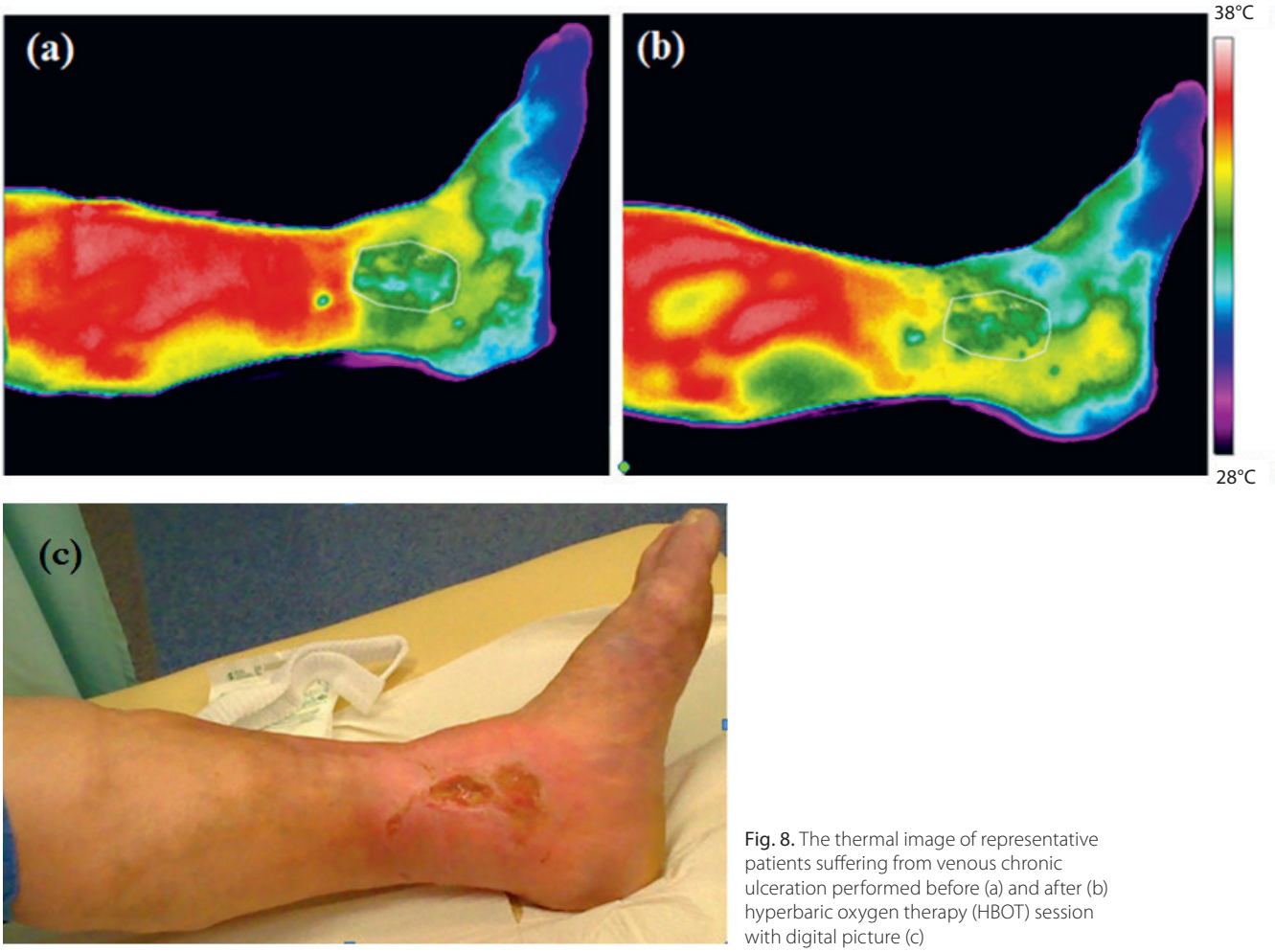

Fig. 8. The thermal image of representative patients suffering from venous chronic ulceration performed before (a) and after (b) hyperbaric oxygen therapy (HBOT) session with digital picture (c)

Discussion

Considering the fact that ulcers resulting from the diabetic foot syndrome and lower limb venous ulcers are a significant health problem in contemporary society, attempts were made to perform an objective assessment of the efficacy of the HBOT in chronic wounds treatment.[10] The positive influence of HBOT observed in our study included a reduced wound perimeter as well as greater healing progress, allowing for earlier wound closure by intermediate thickness skin grafts. To obtain objective data on the wound healing process, digital planimetry (computer measurement) and thermal imaging were used. The monitoring of wound healing progress by planimetry influenced the patient's attitude towards the treatment process and increased the patient's involvement in the therapy. On the other hand, thermal imaging provides important information about inflammatory state changes and increased or decreased metabolism processes occurring in the ulcer area. This is connected with problems in blood microcirculation, which are a significant problem in pharmacotherapy.

The measurement of wounds using computerized digital planimetry allowed the physicians to objectively assess the effectiveness of the treatment, had a direct influence on the decisions pertaining to the selection of optimal wound treatment methods and reduced the costs of therapy. The clinical effects of the treatment could be assessed on the basis of objective results of planimetric measurements as well as a thermal analysis, which was reported in literature.[6,7,14–18] In our study, the planimetric measurements showed that the surface area and the perimeter of the wound had decreased after the completion of HBOT in both groups of patients. Rogers et al. compared the accuracy of the wound measurement according to its shape and the method used (manual measurement using a rope and a measurement using digital planimetry). The results of their study also described the risk of error in the assessment of the surface area of the wound.[19] Sieroń et al. described a method for objective ulcer healing assessment using digital computer planimetry, in which the results of measurements allowed for a more accurate assessment of the wound healing process.[20] The authors of the study described the frequent measurement errors using other techniques, i.e., a ruler or transparent film placed over the wound, which result from a curved surface of the skin (e.g., on the limb), or problems with proper identification of the wound edges . Moreover, the authors emphasize low accuracy of measurements and doubt

the repeatability of results. Errors in the wound surface area assessments varied in range from 0.72 cm^2 to even 10 cm^2, and they could reach as much as 33% if a ruler was used.[20] Goldman et al. described that the repeatability index for assessing the surface area and perimeter of the wound using computer planimetry was nearly 93%, which allowed for using this method effectively in a clinical assessment of wound healing. In the same study, they emphasized that linear measurements based on the 2 longest dimensions of the wounds, depending on their shape, resulted in overestimation of their surface areas by as much as 25%.[21] In the presented study, all measurements (the patient's position and the setting of the distance between the lens and the wound surface) were performed using repeatable conditions. Samad et al. stated that these conditions play the key role in determining margins of the wound and in their digital assessment.[22] Wounds with a large surface area, which affect the lower leg circumferentially, continue to be a problem, as photographs of wounds can be taken only perpendicularly. Hence, patients with circumferential ulcers were excluded from the research, as it was not possible to perform accurate measurements. Both domestic and foreign research on the impact of HBOT on chronic wound treatment indicates its beneficial influence.[23,24] A systematic overview of research revealed a statistically significant difference in the reduction of the risk of large amputations and increased chances of wound healing.[24–26] In the presented study, a reduced perimeter and surface area of the wounds was observed; therefore, it can be said that the therapy was successful. As HBOT is known to be an effective tool, it would be reasonable to focus on this form of therapy. If it is combined with other well-established wound management methods, such as new dressing types, negative pressure wound therapy, etc., the rate of successfully cured patients would likely increase and a reduced number of amputations could be expected.

Moreover, taking into consideration thermal imaging as a non-invasive technique that allows to see metabolic tissue activity, it was reported in literature that the skin temperature changes due to the HBOT, which can be clearly seen in Fig. 6.[15–17] According to thermal imaging performed before HBOT, the increased temperature is observed around the ulceration. It can be recognized as an inflammatory state and increased metabolism processes occurring in this area. It may also be associated with the wrong functioning of microcirculation due to capillary circulation malfunction. The thermal map seems to be changed after HBOT and the temperature generally decreases in the regions of interest. This might be the result of improved thermoregulation resulting from improved microcirculation due to the start of angiogenesis. The temperature drop is observed mainly in the area above the wound. Such observation may be useful in evaluation of treatment effects as a symptom of healing process. It might be the result of a decrease in swelling observed above the wound and of improvement in blood microcirculation, which can play a main role in improving thermoregulation. It may have therapeutic meaning, because it leads to better oxygen transport to further parts of the tibia and increase oxygen concentration in the tissues, which was disturbed when the swelling occurred. These processes may improve the blood supply, start neoangiogenesis and, therefore, neovascularization, which is an indication of wound healing.

It seems that the temperature changes corresponding with planimetry measurements can be connected with patient's state of health (structurally in the case of planimetry and metabolically in the case of thermal imaging), which seems to be very useful in prognosis and qualification for further therapies.

Conclusions

The performed thermal imaging and planimetry studies showed a decrease in the wound area due to HBOT in patients with ulcers, chronic venous insufficiency and diabetic foot syndrome; HBOT has been proven to have a beneficial influence on the healing process. It seems that joint use of thermal imaging and planimetry may provide additional information about the wound structure and metabolism activity in the wound vicinity, and lead to increased accuracy of diagnosis as well as better therapy effects.

On the other hand, digital computer planimetry, as an objective assessment method of the healing process of selected chronic wounds before and after HBOT, allows for the monitoring of the healing process and makes it possible to plan further therapeutic actions.

References

1. Fife CE, Hopf H. Hyperbaric oxygen: Its mechanisms and efficacy. *Plast Reconstr Surg*. 2011;127(Suppl 1):131–141.
2. Brown ML, Tang W, Patel A, Baumhauer JF. Partial foot amputation in patients with diabetic foot ulcers. *Foot Ankle Int*. 2012;33(9):707–716.
3. Jones V, Grey JE, Harding KG. ABC of wound healing. *BMJ*. 2006; 332(7544):777–780.
4. Oien RF, Håkansson MD, Hansen BU, Bjellerup MD. Measuring the size of ulcers by planimetry: A useful method in the clinical setting. *J Wound Care*. 2002;11(5):165–168.
5. Woodbury MG, Houghton PE, Campbell KE, Keast DH. Pressure ulcer assessment instruments: A critical appraisal. *Ostomy Wound Manage*. 1999;45(5):42–55.
6. Shah A, Wollak C, Shah JB. Wound measurement techniques: Comparing the use of ruler method, 2D imaging and 3D scanner. *J Am Coll Clin Wound Spec*. 2015;5(3):52–57.
7. Kawecki M, Knefel G, Wróblewski P. Przydatność planimetrii komputerowej w ocenie wyników leczenia ran przewlekłych. *Pol Przegl Chir*. 2011;83(1);1.
8. Foltynski P, Ladzynski P, Ciechanowska A, Migalska-Musial K, Judzewicz G, Sabalinska S. Wound area measurement with digital planimetry: Improved accuracy and precision with calibration based on 2 rulers. *PLoS One*. 2015;7;10(8):e0134622.
9. Bauer J, Hurnik P, Zdziarski J, et al. Thermovison and its application in medicine. *Acta Bio-Optica et Informatica Medica Inżynieria Biomedyczna*. 1997;3(2–4):121–131.
10. Jawień A, Szewczyk MT, Kaszuba A, et al. Guidelines for the management of chronic venous leg ulceration. Recommendations of a multidisciplinary expert group [in Polish]. *Leczenie Ran*. 2011;8(3):59–80.

11. Szewczyk MT, Mościcka P, Cierzniakowska K, Jawień A. Opieka nad raną przewlekłą. *Zakażenia*. 2010;10(5):70–76.
12. Ring EFJ, Ammer K. The technique of infrared imaging in medicine. *Thermology International*. 2000;10(1):7–14.
13. Bauer J, Dereń E. Standardization of infrared thermal imaging in medicine and physiotherapy. *Acta Bio-Optica et Informatica Medica Inżynieria Biomedyczna*. 2014;20(1):11–20.
14. Liszka G, Englisz B, Knefel G, et al. Evaluation of hyperbaric oxygen therapy effects in ulceration of cruras studied by thermal imaging and planimetry: Preliminary results. *Thermology International*. Vol 26 (2016), Supplement: 16–18.
15. Cholewka A, Knefel G, Stanek A, et al. Thermal imaging and TC oximetry measurements of hyperbaric oxygen therapy (HBO) effects on trophic ulceration of the crura. *J Therm Anal Calorim*. 2012;108(1):25–31.
16. Cholewka A, Stanek A, Sieroń A, Drzazga Z. Thermovision in physical medicine. In: Podbielski, H, Skrzek A, eds. *Biomedical Application of Thermovision*. Wrocław, Poland: OWPW; 2014:37–48.
17. Cholewka A, Drzazga Z, Sieron A, Stanek A, Knefel G, Kawecki M, Nowak M. Some Applications of Thermal Imaging in Medicine. In Drzazga Z, Slosarek K. eds, Some Aspects Of Medical Physics – In Vivo And In Vitro Studies (Monographs of Polish Journal of Environmental Studies) 1: 51–58, 2010.
18. Jørgensen LB, Sørensen JA, Jemec GB, Yderstraede KB. Methods to assess area and volume of wounds: A systematic review. *Int Wound J*. 2015;13(4):540–553.
19. Rogers LC, Bevilacqua NJ, Armstrong DA, Andros G. Digital planimetry results in more accurate wound measurements: A comparison to standard ruler measurements. *J Diabetes Sci Technol*. 2010;(4)4: 799–802.
20. Sieroń A, Nowak M, Knefel G, Szymańska B, Kawecki M. Obiektywizacja gojenia ran przewlekłych aparatem IRIS S firmy Medicom. *Leczenie Ran*. 2007;4(4):141–144.
21. Goldman RJ, Salcido R. More than one way to measure a wound: An overview of tools and techniques. *Adv Skin Wound Care*. 2002; 15(5):236–245.
22. Samad A, Hayes S, French L, Dodds S. Digital imaging versus conventional contact tracing for the objective measurement of venous leg ulcers. *J Wound Care*. 2002;11(4):137–140.
23. Kranke P, Bennett MH, Martyn-St James M, Schnabel A, Debus SE, Weibel S. Hyperbaric oxygen therapy for chronic wounds. *Cochrane Database Syst Rev*. 2015;6:CD004123.
24. Huang ET, Mansouri J, Murad MH, et al; UHMS CPG Oversight Committee. A clinical practice guideline for the use of hyperbaric oxygen therapy in the treatment of diabetic foot ulcers. *Undersea Hyperb Med*. 2015;42(3):205–247.
25. Löndahl M. Hyperbaric oxygen therapy as treatment of diabetic foot ulcers. *Diabetes Metab Res Rev*. 2012;28(Suppl 1):78–84.
26. Schreml S, Szeimies RM, Prantl L, Landthaler M, Babilas P. Wound healing in the 21st century. *J Am Acad Dermatol*. 2010;63(5):866–881.

Postnatal condition of the second twin in respect to mode of delivery, chorionicity and type of fetal growth

Jerzy S. Florjański[1,A–F], Wojciech Homola[1,A–D,F], Tomasz Fuchs[1,B,E,F], Agata Pawłosek[2,B,E,F], Mariusz Kasperski[2,B,E,F]

[1] II Department of Gynecology and Obstetrics, Faculty of Medicine, Wroclaw Medical University, Poland
[2] Clinic of Gynecology and Obstetrics, Jan Mikulicz-Radecki University Teaching Hospital, Wrocław, Poland

A – research concept and design; B – collection and/or assembly of data; C – data analysis and interpretation;
D – writing the article; E – critical revision of the article; F – final approval of the article

Advances in Clinical and Experimental Medicine, ISSN 1899-5276 (print), ISSN 2451-2680 (online) *Adv Clin Exp Med*. 2019;28(2):237–242

Address for correspondence
Jerzy Florjański
E-mail: jerzyflorjanski@wp.pl

Funding sources
None declared

Conflict of interest
None declared

Received on December 21, 2017
Reviewed on April 17, 2018
Accepted on May 5, 2018

Published online on November 22, 2018

Abstract

Background. The increased use of assisted reproductive techniques (ART) contributes to the increased rate of twin pregnancies, which are burdened with a higher risk of complications. Factors that affect the condition of the second twin are understudied.

Objectives. The objective of this study was to assess the impact of the delivery mode, chorionicity, amnionicity, and the type of fetal growth on the postnatal condition of the second twin.

Material and methods. The study included data from 475 pregnant women with twin pregnancies. Maternal age, parity, chorionicity, amnionicity, type of fetal growth, mode of delivery, gestational weeks at delivery, Apgar score, and umbilical arterial blood pH were retrospectively analyzed. Data normality was checked with the Kolmogorov-Smirnov test. The paired Wilcoxon signed-rank test and χ^2 test were used for comparisons between groups. To check predictive value of the analyzed variables multiple linear regression was used.

Results. The mean maternal age was 29.22 (standard deviation (SD) ±5.19) years. The maternal age and gestational age at delivery did not differ significantly between women who delivered by cesarean section (CS) and vaginal delivery (VD). In the second twin, the Apgar score and values of arterial umbilical blood pH were lower in infants delivered by VD than in those delivered by CS (6.30 ±2.83 and 7.30 ±0.12; $p = 0.0209$ and 7.26 ±0.12 and 7.30 ±0.11; $p = 0.0236$, respectively). In monochorionic diamniotic twins with asymmetric growth, the second twin achieved significantly lower outcome than the first twin. Vaginal delivery was a predictive factor for a lower Apgar score and lower values of umbilical arterial blood pH in second twins, while not in first twins. Symmetrical fetal growth of twins was a predictive factor for better postnatal condition for both twins.

Conclusions. In twin pregnancies, VD, but not CS, is associated with increased risk of worse postnatal condition of the second twin. In monochorionic diamniotic pregnancies complicated by growth discordance, CS seems to be a reasonable mode of delivery.

Key words: twin pregnancy, mode of delivery, chorionicity, type of twin growth, postnatal condition of the second twin

Cite as
Florjański JS, Homola W, Fuchs T, Pawłosek A, Kasperski M. Postnatal condition of the second twin in respect to mode of delivery, chorionicity and type of fetal growth. *Adv Clin Exp Med*. 2019;28(2):237–242. doi:10.17219/acem/90765

DOI
10.17219/acem/90765

Introduction

Difficulties in obtaining offspring and delayed child bearing are associated with the increased use of assisted reproductive techniques (ART). This trend translates into the occurrence of multiple births. Historically, multiple birth rates began to decline in the 1950s, with the minimum rates in the 1970s, and then, after the introduction and popularization of ART and pharmacological ovulation stimulation, they began to rise since 1998. As the ART become more advanced and tailored, the incidence of triplets and higher order pregnancies decreases, which contributes to a further increase in twin rate.[1,2] Multiple gestations are considered a potential complication of ART.[3]

Births in twin pregnancies pose an increased risk of complications to the second fetus. During vaginal delivery (VD) after birth of the first twin, the uterus contracts rapidly, and the uterine contractile function weakens or disappears, which may significantly prolong the 2nd stage of the labor of the second twin. Also, a rapid change in hemodynamic conditions occurs and may negatively affect the condition of the second twin. Therefore, 10–20% of the second twins may require a cesarean section (CS).[4,5]

The incidence of twin deliveries remains on a similar level in developed countries across the world. In the USA, the rate of twin deliveries was 33.5 per 1,000 total births in 2015.[2] Multifetal pregnancies are associated with a higher risk of perinatal complications compared to singleton pregnancies, both conceived naturally and after ART.[6,7] Some authors reported that factors such as chorionicity, mode of delivery, type of fetal growth (discordant or symmetric), and birth mass worsen perinatal outcomes and increase the rate of neonatal complications in the second twin compared to the first one.[8–10] On the other hand, broad trials have been conducted which did not show the superiority of CS vs VD in terms of complications in neonates, especially in the absence of risk factors and when the first twin is in the cephalic presentation.[11–13] The authors of the meta-analysis from 2011, which included nearly 40,000 twin pairs, concluded that, in the absence of risk factors, VD is safer than CS for the first twin but for the second twin, the mode of delivery had no effect on perinatal outcome.[14] In light of controversies and inconsistent reports on the impact of selected parameters on the condition of the second twin in the literature, we decided to perform an analysis of the postnatal condition of the fetuses from twin pregnancies among the population of Wrocław, Poland.

The aim of the study was to assess the influence of the delivery mode, chorionicity, and type of fetal growth on the postnatal condition of twins, as measured with an Apgar score and umbilical arterial blood pH in neonates.

Material and methods

The study included data from 475 pregnant women with twin pregnancies, who delivered in the II Department of Gynecology and Obstetrics, Wroclaw Medical University, Poland. The data for retrospective analysis included maternal age, parity, chorionicity, type of fetal growth, mode of delivery, gestational weeks at delivery, Apgar score, and umbilical arterial blood pH. Discordance was defined as 18% intertwin birthweight difference, as reports from the literature suggest that perinatal mortality increases with birthweight discordance exceeding 18% in twins without twin-twin transfusion syndrome (TTTS).[15] Subjects with pregnancies complicated by genetic and developmental defects in twins or TTTS, and those with a history of intrauterine death of one of the twins were excluded from the study. The study was approved by the Bioethics Committee at the Wroclaw Medical University.

Data was collected in the Excel spreadsheet (MS Office 2010; Microsoft Corp., Redmond, USA) and statistically analyzed with the R Project for Statistical Computing v. 3.4.1 (www.r-project.org). Summary values were given as a mean (± standard deviation – SD) or median (interquartile rage – IQR). The normality of the data was checked with the Kolmogorov-Smirnov test. The paired Wilcoxon signed-rank test was used for comparisons between fetuses and the unpaired test was used for other comparisons. To compare categorical variables, the χ^2 test was used. To check the predictive value of the analyzed variables, a multiple linear regression was used. The p-value <0.05 was considered statistically significant.

Results

Data from 475 pregnant women with twin pregnancies was analyzed. Out of these 475 women, 313 (65%) were dichorionic diamniotic (DCDA), the remaining ones were monochorionic diamniotic (MCDA) and 1 was monochorionic monoamniotic (MCMA). Due to the fact that there was only 1 case of the MCMA pregnancy, this case was excluded from the analysis. The mean maternal age was 29.22 (SD ±5.19) years (range: 18–47 years). Differences in the maternal age and gestational weeks at delivery between pregnancies ended by CS and VD were insignificant. Primigravidae constituted the majority of the study group – 270 (57%), and additionally, they significantly more frequently delivered by CS. The second twins delivered vaginally achieved a significantly lower Apgar score and had a significantly lower umbilical arterial blood pH than those delivered by CS. The comparison of clinical characteristics regarding delivery mode is presented in Table 1.

A paired comparison of the postnatal condition as measured with Apgar score and values of umbilical arterial blood pH by chorionicity and fetal growth type is presented in Table 2. It can be seen that a twin born second achieved

Table 1. Clinical characteristics of the study group

Variable	Total (n = 474)	Vaginal delivery (n = 105)	Cesarean section (n = 369)	p-value
Maternal age [years], mean ±SD	29.21 ±5.19	29.07 ±5.71	29.25 ±5.04	0.7468
Gestational age [weeks], mean ±SD	35.41 ±3.44	35.22 ±4.77	35.46 ±2.95	0.0779
Parity, n (%) primiparae multiparae	 270 (56.96) 204 (43.04)	 41 (15.18) 64 (31.37)	 229 (84.82) 140 (68.63)	**<0.001**
Growth type, n (%) symmetrical twins discordant twins	 308 (64.98) 166 (35.02)	 62 (20.07) 43 (25.90)	 246 (79.87) 123 (74.10)	0.149
Chorionicity/amnionicity, n (%) DCDA MCDA	 311 (65.61) 163 (34.39)	 74 (23.79) 31 (19.02)	 237 (76.21) 132 (80.98)	0.234
Apgar score – first twin, median (IQR)	8 (6–9)	7 (6–9)	8 (6–9)	0.3703
Apgar score – second twin, median (IQR)	7 (6–9)	7 (6–9)	8 (6–9)	**0.0206**
pH – first twin, mean ±SD	7.29 ±0.12	7.28 ±0.12	7.30 ±0.12	0.3108
pH – second twin, mean ±SD	7.29 ±0.11	7.26 ±0.12	7.30 ±0.11	**0.0237**

DCDA – dichorionic diamniotic; IQR – interquartile range; MCDA – monochorionic diamniotic; SD – standard deviation; p-values in bold denote statistical significance.

significantly worse outcome in comparison to the one born first, but only in the case of monochorionic diamniotic pregnancies with asymmetric growth delivered vaginally. In the case of CS, those differences were insignificant. Differences between twins with other types of growth and chorionicity/amnionicity were insignificant.

Vaginal delivery was a significant predictive factor for a lower Apgar score and a lower value of umbilical arterial blood pH after adjustment for gestational age, maternal age, parity, type of growth, and chorionicity/amnionicity only for the second twin. For the first twin, the delivery mode did not play a significant predictive role. Symmetric growth was a positive predictive factor for better perinatal condition for both twins. Also, gestational age was a significant predictive factor for a higher Apgar score and a higher umbilical arterial blood pH value. With every additional gestational week, the pH increased by 0.0180 for the first twin and by 0.0177 for the second twin. With every additional gestational week, the Apgar score increased by 0.3875 for the first twin and by 0.3480 for the second twin. Regression coefficients are presented in Table 3.

Discussion

Our study identifies VD as a risk factor for a worse perinatal status in the second twins, when factors such as twin discordance, preterm delivery and monochorionicity coexist. In the present study, the Apgar score and values of umbilical arterial blood pH were lower in the second twins delivered by VD than in those delivered by CS. In monochorionic diamniotic twins with discordant growth, the second twin achieved significantly lower outcome than the first twin. Additionally, VD was a negative predictive factor for worse perinatal outcome in the group of the second twins, while not in the group of the first ones.

Twin pregnancy is burdened with a higher risk of adverse perinatal outcomes and of maternal complications than a singleton pregnancy.[16,17] Thus, obstetricians search

Table 2. Comparison of Apgar score and umbilical arterial blood pH between the first and the second twin regarding type of growth and mode of delivery

Variable	Delivery mode	n (%)	Apgar score; median (IQR)		p-value	pH; mean (SD)		p-value
			first twin	second twin		first twin	second twin	
DCDA concordant	VD	49 (21)	8 (6–9)	7 (6–9)	0.3564	7.28 (0.12)	7.28 (0.10)	0.5934
	CS	184 (79)	8 (7–9)	8 (7–9)	0.5381	7.31 (0.11)	7.32 (0.10)	0.8218
DCDA discordant	VD	25 (32)	7 (5–8)	8 (5–9)	0.7195	7.28 (0.11)	7.29 (0.11)	0.1806
	CS	53 (68)	7 (6–8)	7 (5–8)	0.7923	7.27 (0.10)	7.27 (0.10)	0.9183
MCDA concordant	VD	13 (17)	7 (7–8)	7 (4–9)	0.3586	7.28 (0.11)	7.26 (0.13)	0.5291
	CS	62 (83)	8 (7–9)	8 (6–9)	0.1287	7.33 (0.12)	7.32 (0.10)	0.5587
MCDA discordant	VD	18 (20)	7 (3.4–8.0)	5.5 (1.25–7.00)	**0.0334**	7.28 (0.13)	7.18 (0.17)	**0.0274**
	CS	70 (80)	7 (4.25–8.00)	6 (4–8)	0.5109	7.25 (0.13)	7.23 (0.13)	0.3583
Total VD		105	7 (6–9)	7 (5–8)	0.1034	7.28 (0.12)	7.26 (0.13)	0.3438
Total CS		369	8 (6–9)	8 (6–9)	0.5591	7.30 (0.12)	7.30 (0.11)	0.5593
Total concordant		308	8 (7–9)	8 (7–9)	0.4217	7.31 (0.11)	7.31 (0.10)	0.6276
Total discordant		166	7 (5–8)	7 (4.25–8.00)	0.2442	7.26 (0.12)	7.25 (0.13)	0.2959
Total		474	8 (6–9)	7 (6–9)	0.1904	7.29 (0.12)	7.29 (0.11)	0.3156

CS – cesarean section; IQR – interquartile range; DCDA – dichorionic diamniotic; MCDA – monochorionic diamniotic; VD – vaginal delivery; p-values in bold denote statistical significance.

Table 3. Multiple linear regression model

Intercept/variable	Estimate	p-value	Estimate	p-value
	first twin		second twin	
Intercept – pH	6.6305	<0.0001	6.6385	<0.0001
Gestational weeks	0.0180	<0.0001	0.0177	<0.0001
Concordant growth	0.0344	0.0004	0.0445	<0.0001
Vaginal delivery	–	–	–0.0320	0.0027
Intercept – Apgar	–7.3666	<0.0001	–6.0940	<0.0001
Gestational weeks	0.3875	<0.0001	0.3480	<0.0001
Concordant growth	1.0271	<0.0001	1.2131	<0.0001
Vaginal delivery	–	–	–0.5876	0.0104

pH – arterial umbilical blood pH.

for optimal planning and timing of the delivery to increase the safety of both the fetuses and the mother. Some reports from the literature suggest that outcomes achieved after CS and VD are comparable in normal pregnancies without risk factors. A randomized trial conducted by Barrett et al. compared the 2 modes of planned delivery. The study group included twins with cephalic presentation and an estimated fetal weight between 1,500 g and 4,000 g. Monoamniotic twins and pregnancies with any complications that could negatively affect the course of labor were excluded. As a result, the difference in fetal/neonatal death or serious neonatal morbidity between the study groups was insignificant.[11] A 2-year observation of children conducted within the framework of the Twin Birth Study, which aimed to evaluate the incidence of death or neurodevelopmental delay, revealed no benefit of planned CS when compared to VD in uncomplicated twin pregnancies between 32 and 38 weeks of gestation.[18] Nevertheless, there are also reports on large populations of normal twins at or after 36 weeks of gestation, which show that planned CS reduces the risk of perinatal death of the second twin in comparison with attempting a VD.[19] On the other hand, a recent study showed that in women with dichorionic diamniotic twins, attempted VD was followed by a spontaneous VD of both twins in only 46% of cases. The later required instrumental VD and an emergency CS.[4] Additionally, a VD in twin pregnancies increases maternal morbidity, especially in terms of increased rate of postpartum hemorrhage.[13,20]

Some authors assessed selected risk factors that may potentially affect the postnatal condition of twins or increase the risk of neonatal morbidity for both twins. Zipori et al. reported a higher percentage of respiratory distress syndrome (RDS) and transient tachypnea of the newborn (TTN) in twins delivered by VD in comparison to those delivered by CS.[21] Shinwell et al. evaluated a group of twins with a birthweight lower than 1,500 g. They found that the risk for RDS and death was higher for the second twin than for the first twin, but was independent of the mode of the delivery.[10] Hartley and Hitti showed that the highest rate of combined poor short-term perinatal outcomes occurred in fetuses delivered by operative VD.[22] These reports are in line with the results of the present study which revealed that in the group of twin with risk factors, VD contributed to the worsening of the second fetus condition. Regression analysis from our study highlights that prematurity may worsen the condition of both fetuses, while asymmetric growth affects especially the condition of the second fetus.

Newborn babies are routinely assessed with an Apgar score. A low score at 1 min and 5 min indicates that a newborn requires medical attention. It is also a predictor for neonatal survival. A score of 8 and above was considered normal in our study. In the present study, the mean value of the Apgar score was 6.30 ±2.83 with a median of 7 in the group of second twins delivered by VD and was significantly lower than the value obtained in babies delivered by CS – 7.06 ±2.37 with the median of 8. Multiple regression analysis showed that VD was a negative predictive factor for a lower Apgar score in the group of second twins. Similar outcomes were reported by other researchers. Hartley and Hitti reported that the relative risk for low 5-minute Apgar score was 1.4 (95% confidence interval (CI) = 1.1–1.8) for VD or CS during labor in comparison with CS without labor.[22] Jhaveri and Nadkarni found that odds ratio (OR) for an Apgar score of 7 or lower was 3.385 (95% CI = 1.2099–9.4684, p = 0.02) in the vaginal group compared to the CS group.[23] And recently, Ylilehto et al. showed that VD affected the condition of the second twin without differences in the rate of serious neonatal morbidity and as a result, the second VD twins more often had 5-minute Apgar scores <7 (p = 0.002) than second twins delivered by CS.[24]

Umbilical arterial blood pH is measured in infants at high risk for neonatal asphyxia after delivery. This parameter is strongly associated with neonatal mortality and morbidity; thus, obstetricians try to undertake possible actions early enough to prevent a drop in umbilical arterial blood pH.[25] In the present study, the mean umbilical arterial blood pH value was 7.26 ±0.12 in the group of second twins delivered vaginally in comparison to 7.30 ±0.11 in second twins delivered by CS. This difference was statistically significant. Vaginal delivery was a significant predictive factor for low pH value only in the group of second twins. Our findings are consistent with reports from the literature. Sato et al. reported that umbilical arterial blood pH was significantly lower in the case of VD in comparison to CS (7.26 ±0.009 vs 7.30 ±0.006; p = 0.0003) in second twins, but not in the first twins. Additionally, in the second twins the percentage of umbilical arterial blood pH below 7.20 was significantly higher in VD than this in CS group (20% vs 4%; p = 0.0001).[8] Ylilehto et al. showed that umbilical arterial blood pH < 7.05 appeared more often in VD second twins than in second CS twins (p = 0.003).[24] The team headed by Leung draws attention to the effect of delivery interval between twins and the duration of the 2nd stage of labor. According to their outcomes, prolonged delivery interval

deteriorates blood parameters. Changes in the umbilical cord blood gas status become significant when the interval between births exceeds 30 min.[26] Also, as the duration of the 2nd stage of labor is prolonged, the umbilical cord blood gas status deteriorated in both twins, but to a greater degree in the second twin than in the first twin.[27]

Growth discordance between twins is considered an important predictor of worse perinatal outcomes, but its definition may vary. In the present study, growth discordance was defined as 18% difference in birthweight between twins without TTTS.[15] Our analysis confirmed that discordant growth is a significant predictive factor for a lower Apgar score and a lower umbilical arterial blood pH for both twins. In addition, second twins from discordant monochorionic diamniotic pregnancies ended by a VD achieved significantly worse perinatal outcomes that those of the first twin. Data from the literature indicates that the greater difference in estimated twin mass is, the greater neonatal morbidity and mortality.[28,29] Thus, in the case of a big difference in estimated twin mass (over 30%) detected in ultrasound examination, we preferred CS as a delivery mode. This led to difficulties in assessing the impact of the delivery mode on perinatal outcomes.

In the literature, a comparison of the status between smaller and larger fetuses is more common than between the first and second twin. There are some reports documenting decreased well-being of the second twins. However, there are also several reports regarding the postnatal status of the second twins.

Kontopoulos et al. showed that in pregnancies complicated by discordance greater than 40%, the mode of delivery had no effect on perinatal outcomes, but in the case of discordance between 20% and 40%, delivery by CS was associated with a lower rate of neonatal mortality.[30] Canpolat et al. found that the second twin had an increased risk of RDS (OR = 1.3; 95% CI = 0.6–2.4) after adjustment for birthweight.[31] Usta et al. found that in pregnancies in which the second twin is more than 250 g larger than the first twin, no differences in the incidence of intraventricular hemorrhage, seizures, sepsis, and neonatal death between twins were noted, except for the a lower median Apgar score in the second twin.[32] It is worth noting that growth discordance often coexists with head-to-abdominal circumference asymmetry or intrauterine growth restriction (IUGR) in one of the twins, or with being small for gestational age (SGA), which can further deteriorate perinatal outcomes.[33]

Conclusions

In twin pregnancies, VD is associated with an increased risk of a worse postnatal condition of the second twin in comparison with delivery by CS. In monochorionic diamniotic pregnancies complicated by growth discordance, CS seems to be a reasonable mode of delivery.

References

1. Collins J. Global epidemiology of multiple birth. *Reprod Biomed Online.* 2007;15(Suppl 3):45–52.
2. Martin JA, Hamilton BE, Osterman MJ, Driscoll AK, Mathews TJ. Births: Final data for 2015. *Natl Vital Stat Rep.* 2017;66(1):1.
3. Huang JY, Rosenwaks Z. Assisted reproductive techniques. *Methods Mol Biol.* 2014;1154:171–231.
4. Rzyska E, Ajay B, Chandraharan E. Safety of vaginal delivery among dichorionic diamniotic twins over 10 years in a UK teaching hospital. *Int J Gynaecol Obstet.* 2017;136(1):98–101.
5. Kong CW, To WWK. The predicting factors and outcomes of caesarean section of the second twin. *J Obstet Gynaecol.* 2017;37(6):709–713.
6. Qin JB, Wang H, Sheng X, Xie Q, Gao S. Assisted reproductive technology and risk of adverse obstetric outcomes in dichorionic twin pregnancies: A systematic review and meta-analysis. *Fertil Steril.* 2016;105(5):1180–1192.
7. Rao A, Sairam S, Shehata H. Obstetric complications of twin pregnancies. *Best Pract Res Clin Obstet Gynaecol.* 2004;18(6):557–576.
8. Sato Y, Emoto I, Maruyama S, Taga A, Fujii T. Twin vaginal delivery is associated with lower umbilical arterial blood pH of the second twin and less intrapartum blood loss. *J Matern Fetal Neonatal Med.* 2016;29(19):3067–3071.
9. Kosińska-Kaczyńska K, Szymusik I, Bomba-Opoń D, et al. Perinatal outcome according to chorionicity in twins: A Polish multicenter study. *Ginekol Pol.* 2016;87(5):384–389.
10. Shinwell ES, Blickstein I, Lusky A, Reichman B. Effect of birth order on neonatal morbidity and mortality among very low birthweight twins: A population based study. *Arch Dis Child Fetal Neonatal Ed.* 2004;89(2):F145–F148.
11. Barrett JF, Hannah ME, Hutton EK, et al; Twin Birth Study Collaborative Group. A randomized trial of planned cesarean or vaginal delivery for twin pregnancy. *N Engl J Med.* 2013;369(14):1295–1305.
12. Schmitz T, Prunet C, Azria E, et al; JUmeaux MODe d'Accouchement (JUMODA) Study Group and the Groupe de Recherche en Obstétrique et Gynécologie (GROG). Association between planned cesarean delivery and neonatal mortality and morbidity in twin pregnancies. *Obstet Gynecol.* 2017;129(6):986–995.
13. Sadeh-Mestechkin D, Daykan Y, Bustan M, Markovitch O, Shechter-Maor G, Biron-Shental T. Trial of vaginal delivery for twins: Is it safe? A single center experience. *J Matern Fetal Neonatal Med.* 2018;31(15):1967–1971.
14. Rossi AC, Mullin PM, Chmait RH. Neonatal outcomes of twins according to birth order, presentation and mode of delivery: A systematic review and meta-analysis. *BJOG.* 2011;118(5):523–532.
15. Breathnach FM, McAuliffe FM, Geary M, et al; Perinatal Ireland Research Consortium. Definition of intertwin birth weight discordance. *Obstet Gynecol.* 2011;118(1):94–103.
16. Kiely JL. The epidemiology of perinatal mortality in multiple births. *Bull N Y Acad Med.* 1990;66(6):618–637.
17. Barrett JF. Twin delivery: Method, timing and conduct. *Best Pract Res Clin Obstet Gynaecol.* 2014;28(2):327–338.
18. Asztalos EV, Hannah ME, Hutton EK, et al. Twin Birth Study: 2-year neurodevelopmental follow-up of the randomized trial of planned cesarean or planned vaginal delivery for twin pregnancy. *Am J Obstet Gynecol.* 2016;214:371.
19. Smith GC, Shah I, White IR, Pell JP, Dobbie R. Mode of delivery and the risk of delivery-related perinatal death among twins at term: A retrospective cohort study of 8073 births. *BJOG.* 2005;112(8):1139–1144.
20. Easter SR, Robinson JN, Lieberman E, Carusi D. Association of intended route of delivery and maternal morbidity in twin pregnancy. *Obstet Gynecol.* 2017;129(2):305–310.
21. Zipori Y, Smolkin T, Makhoul IR, Weissman A, Blazer S, Drugan A. Optimizing outcome of twins by routine cesarean section beyond 37 weeks. *Am J Perinatol.* 2011;28(1):51–56.
22. Hartley RS, Hitti J. Please exit safely: Maternal and twin pair neonatal outcomes according to delivery mode when twin A is vertex. *J Matern Fetal Neonatal Med.* 2017;30(1):54–59.
23. Jhaveri RR, Nadkarni TK. Perinatal outcome of second twin with respect to mode of delivery: An observational study. *J Clin Diagn Res.* 2016;10(12):QC26–QC28.
24. Ylilehto E, Palomäki O, Huhtala H, Uotila J. Term twin birth: Impact of mode of delivery on outcome. *Acta Obstet Gynecol Scand.* 2017;96(5):589–596.

25. Malin GL, Morris RK, Khan KS. Strength of association between umbilical cord pH and perinatal and long term outcomes: Systematic review and meta-analysis. *BMJ*. 2010;340:c1471.
26. Leung TY, Tam WH, Leung TN, Lok IH, Lau TK. Effect of twin-to-twin delivery interval on umbilical cord blood gas in the second twins. *BJOG*. 2002;109(1):63–67.
27. Leung TY, Lok IH, Tam WH, Leung TN, Lau TK. Deterioration in cord blood gas status during the second stage of labour is more rapid in the second twin than in the first twin. *BJOG*. 2004;111(6):546–549.
28. Hollier LM, McIntire DD, Leveno KJ. Outcome of twin pregnancies according to intrapair birth weight differences. *Obstet Gynecol*. 1999; 94(6):1006–1010.
29. Demissie K, Ananth CV, Martin J, Hanley ML, MacDorman MF, Rhoads GG. Fetal and neonatal mortality among twin gestations in the United States: The role of intrapair birth weight discordance. *Obstet Gynecol*. 2002;100(3):474–480.
30. Kontopoulos EV, Ananth CV, Smulian JC, Vintzileos AM. The influence of mode of delivery on twin neonatal mortality in the US: Variance by birth weight discordance. *Am J Obstet Gynecol*. 2005;192(1): 252–256.
31. Canpolat FE, Yurdakök M, Korkmaz A, Yigit S, Tekinalp G. Birthweight discordance in twins and the risk of being heavier for respiratory distress syndrome. *Twin Res Hum Genet*. 2006;9(5):659–663.
32. Usta IM, Nassar AH, Abu Musa AA, Awwad JT, Yunis KA, Seoud MA. Perinatal outcome of vaginally delivered twin gestations with a larger twin B. *J Perinatol*. 2003;23(5):409–413.
33. Dashe JS, McIntire DD, Santos-Ramos R, Leveno KJ. Impact of head-to-abdominal circumference asymmetry on outcomes in growth-discordant twins. *Am J Obstet Gynecol*. 2000;183(5):1082–1087.

A comparative assessment of the antibacterial activity of root canal sealers on 2 *Actinomyces* species: An in vitro study

Małgorzata Pawińska[1,A–F], Elżbieta Łuczaj-Cepowicz[2,A–D], Grzegorz Szczurko[1,A–D], Anna Kierklo[3,A–C], Grażyna Marczuk-Kolada[3,C–E], Katarzyna Leszczyńska[4,B,C,F]

[1] Department of Integrated Dentistry, Faculty of Medicine with the Division of Dentistry and Division of Medical Education in English, Medical University of Bialystok, Poland
[2] Department of Pediatric Dentistry, Faculty of Medicine with the Division of Dentistry and Division of Medical Education in English, Medical University of Bialystok, Poland
[3] Department of Dentistry Propedeutics, Faculty of Medicine with the Division of Dentistry and Division of Medical Education in English, Medical University of Bialystok, Poland
[4] Department of Microbiology, Faculty of Medicine with the Division of Dentistry and Division of Medical Education in English, Medical University of Bialystok, Poland

A – research concept and design; B – collection and/or assembly of data; C – data analysis and interpretation;
D – writing the article; E – critical revision of the article; F – final approval of the article

Advances in Clinical and Experimental Medicine, ISSN 1899–5276 (print), ISSN 2451–2680 (online) *Adv Clin Exp Med*. 2019;28(2):243–248

Address for correspondence
Grzegorz Szczurko
E-mail: grzesiekszczurko@gmail.com

Funding sources
This research was supported with a grant from the Medical University of Bialystok (project No. 133-09752L).

Conflict of interest
None declared

Received on February 28, 2017
Reviewed on April 30, 2017
Accepted on September 26, 2017

Published online on August 7, 2018

Abstract

Background. *Actinomyces* species have a low virulence and pathogenicity, but under specific circumstances they may be involved in root canal and periapical tissue infections.

Objectives. The aim of the study was to investigate the antibacterial activity of various root canal sealers on standardized strains of *Actinomyces*.

Material and methods. The materials tested in this study included AH Plus™ Jet (AH), Apexit® Plus (AP), Endomethasone N (EN), GuttaFlow® (GF), Hybrid Root SEAL (HB), MTA Fillapex (FL), Real® Seal (RCS), Roeko Seal Automix (RSA), Sealapex™ (SP), and Tubli-Seal™ (TS). The antibacterial effect of the freshly mixed sealers on standardized strains of *Actinomyces israelii* NCTC 8047 and *Actinomyces viscosus* ATCC 15987 was evaluated with the use of the agar diffusion test (ADT). The results were obtained with measuring the diameter of the growth inhibition zone at 96 h and 1, 2, 3, and 4 weeks, and were analyzed in time using repeated measures analysis of variance (ANOVA). Statistically significant differences among the materials were determined using one-way ANOVA and Tukey's post hoc testing. A paired Student's t-test was applied to compare the susceptibility of particular strains to each sealer. The critical level of significance for all tests was $p < 0.05$.

Results. Most sealers demonstrated growth inhibition zones against both tested bacteria, except for RSA and GF. *Actinomyces viscosus* was significantly more susceptible than *A. israelii* to AP, RCS ($p < 0.001$) and TS ($p = 0.012$). *Actinomyces israelii* was significantly more susceptible than *A. viscosus* to EN, HB and SP ($p < 0.001$).

Conclusions. The antimicrobial effect of the examined materials varied considerably depending on the type of material and bacterial species tested. Most of the tested root canal sealers exhibited antibacterial activity on standardized strains of *Actinomyces*, with FL showing the highest antibacterial effect on both bacterial strains. Importantly, both standardized strains of *Actinomyces* were characterized by varied sensitivity to root canal sealers.

Key words: *Actinomyces*, antibacterial agents, root canal sealers

Cite as
Pawińska M, Łuczaj-Cepowicz E, Szczurko G, Kierklo A, Marczuk-Kolada G, Leszczyńska K. A comparative assessment of the antibacterial activity of root canal sealers on 2 *Actinomyces* species: An in vitro study. *Adv Clin Exp Med*. 2019;28(2):243–248. doi:10.17219/acem/78022

DOI
10.17219/acem/78022

Introduction

The genus *Actinomyces* contains Gram-positive, pleomorphic or filamentous, non-spore forming, non-motile, obligately and facultatively anaerobic bacteria. They are normal inhabitants of the oral microbiota and the primary colonizers of dental hard tissues. Although *Actinomyces* species have a low virulence and pathogenicity, under specific circumstances they may be involved in serious oral diseases, including root canal and periapical tissue infections. Most *Actinomyces* species have fimbriae – structures that enable bacterial cells to adhere to root canal walls and dentinal shavings forced out through the apical foramen during endodontic treatment.[1] Moreover, fimbriae are involved in colonizing the extraradicular area by attaching to the cementum around the root apex and bacterial coaggregation.[2] A recent study by Yamane et al. showed that *Actinomyces* species have a capacity to produce exopolysaccharides (EPSs), and thus contribute to biofilm formation, which can be essential to their pathogenic potential and the development of persistent infections in the periapical tissues.[3]

Bacterial cells embedded in an extracellular matrix can more easily survive in a nutritionally deprived environment and can evade neutrophilic phagocytosis and other host defense mechanisms.[4] Actinomycotic colonies are known to have low pathogenicity, they also induce a minimal host response in the form of chronic endodontic infections, accompanied by the sinus tract, which discharges bright yellow granules referred to as sulfur granules. These granules consist of bacterial aggregates held together by an extracellular matrix. They are more likely formed in response to host defenses and can provide some resistance to phagocytosis or other immunological mechanisms.[1] Several authors have reported that *Actinomyces* have been frequently cultured from the root canals of teeth with primary and post-treatment apical periodontitis.[2,4–6] It is commonly believed that these bacteria are associated with persistent extraradicular infections, a lack of periradicular healing and cases of failed endodontic therapy.[7–9] *Actinomyces* species are able either to survive intracanal procedures as resistant microorganisms or, as secondary invaders, to penetrate the root canal during or after endodontic therapy.[2,10] In light of this evidence, the final stage of endodontic treatment – filling the root canal – becomes of significant importance. After chemomechanical preparation, the root canal should be obturated 3-dimensionally to entomb residual bacteria that could be untouched by irrigants or medications, and to prevent subsequent apical or coronal reinfection.

Most of the currently employed techniques used to obturate the root canal do not provide a long-term and fluid-tight seal within the entire root canal system.[11,12] Therefore, the use of root-filling materials with antimicrobial properties may contribute to improving the outcome of endodontic treatment.[13,14] This may be an interesting approach to intensify root canal disinfection.

Therefore, the aim of our study was to investigate and compare the antibacterial activity of various root canal sealers on standardized strains of *Actinomyces*.

Material and methods

Table 1 presents the materials used for the experiment and their composition.

Strains and media

The standardized *Actinomyces israelii* NCTC 8047 and *Actinomyces viscosus* ATCC 15987 strains were obtained from the Health Protection Agency (London, UK) and Microbiologics Inc. (St. Cloud, USA), respectively. The strains were cultured on Schaedler agar (Emapol sp. z o.o., Gdańsk, Poland), supplemented with 5% of sheep's blood for 48–72 h at 35–37°C under anaerobic conditions. The antibacterial activity of root canal sealers against the standardized strains of anaerobic bacteria was determined using the agar diffusion method on Brucella Blood Agar (Oxoid Limited, Basingstoke, UK), enriched with 5% of sheep's blood, vitamin K_1 and 1% of hemin. After 48–72 h, suspensions of the bacterial strains in the Brucella broth of 1.0 on the McFarland turbidity scale were prepared.

Agar diffusion test

The bacterial suspension was distributed with a sterile cotton swab on the surface of Brucella Blood Agar with wells 7 mm in diameter and 5 mm in depth. In order to seal up the wells, the bottom was covered with 10 µL of liquid Triptic Soya Agar (TSA) (Oxoid Limited), and the wells were filled with freshly mixed sealers prepared in aseptic conditions according to the manufacturer's instructions. The plates were left at room temperature for 30 min, and then incubated for 96 h in anaerobic conditions at 37°C. To control the growth of the standardized strain on the agar used for the experiment, positive control plates were streaked with bacteria, but no root canal sealers were used. Three samples were prepared for each material.

Reading the size of the inhibition zone

The plates were examined and evaluated for growth inhibition zones at 96 h and 1, 2, 3, and 4 weeks. An absence of bacterial growth around each well indicated antibacterial activity. The most uniform segment at the largest point of the growth inhibition zone was measured with a ruler, and the results were recorded in millimeters. A cut-off value of 7 mm (the diameter of the well) was subtracted from the measurement.[15] Wider zones of inhibition were interpreted to indicate greater antimicrobial activity of the involved materials.

Table 1. Compositions of materials tested for antibacterial activity

Name	Source	Active ingredients
AH Plus™ Jet	Dentsply DeTrey GmbH, Konstanz, Germany	bisphenol-A epoxy resin, bisphenol-F epoxy resin, calcium tungstate, zirconium oxide, silica, iron oxide pigments, dibenzyldiamine, aminoadamantane, tricyclodecane-diamine, silicone oil
Apexit® Plus	Ivoclar Vivadent AG, Schaan, Liechtenstein	calcium salts (hydroxide, oxide, phosphate), hydrogenized colophony, disalicylate, bismuth salts (oxide, carbonate), highly dispersed silicon dioxide, alkyl ester of phosphoric acid
Endomethasone N Eugenol	Septodont Saint-Maur-des-Fossés, Cedex, France Chema-Elektromet, Rzeszów, Poland	zinc oxide, hydrocortisone acetate, thymol iodide, barium sulfate, magnesium stearate eugenol
GuttaFlow®	Coltene/Whaledent GmbH + Co. KG, Langenau, Germany	gutta-percha powder, polydimethylsiloxane, silicone oil, platinum catalyst, zirconium dioxide, nanosilver, coloring
Hybrid Root SEAL	Sun Medical, Tokyo, Japan; Parkell Inc., Farmingdale, USA	liquid: 4-methacryloxyethyl trimellitate anhydride (4-META), 2-hydroxyethyl methacrylate (HEMA), difunctional methacrylate monomers powder: zirconium oxide, silica, hydrophilic initiator
MTA Fillapex	Angelus Ind. de Prod. Odontológicos S/A, Londrina, Brazil	paste A: salicylate resin, bismuth trioxide, fumed silica paste B: fumed silica, titanium dioxide, mineral trioxide aggregate, base resin
Real®Seal	SybronEndo Co., Orange, USA	organic part: 1,6-bis(methacryloxy-2-ethoxycarbonylamino)-2,4,4-trimethylhexane (UDMA), pyromellitic glycerol dimethacrylate (PEGDMA), ethoxylated bisphenol A dimethacrylate (EBPADMA), ethylene glycol dimethacrylate (EDMA), bisphenol A-glycidyl methacrylate (BisGMA) inorganic part: barium borosilicate, barium sulfate, bismuth oxychloride, calcium hydroxide, photoinitiators
Roeko Seal Automix	Coltene/Whaledent GmbH + Co. KG, Langenau, Germany	polydimethylsiloxane, silicone oil, paraffin-base oil, platinum catalyst, zirconium dioxide
Sealapex™	Kerr Italia S.p.A., Salerno, Italy	calcium oxide, bismuth trioxide, zinc oxide, sub-micron silica, 2% titanium dioxide, zinc stearate, tricalcium phosphate, blend
Tubli-Seal™	Kerr Italia S.p.A., Salerno, Italy	zinc oxide, barium sulfate, oleo resin, oils/modifiers, thymol iodide, eugenol

Statistical analysis

The differences between the diameters of the bacterial growth inhibition zones over time were evaluated statistically by applying repeated measures analysis of variance (ANOVA). Statistically significant differences among the materials were determined by using one-way ANOVA and Tukey's post hoc testing. A paired Student's t-test was applied to compare the susceptibility of particular strains to each sealer. Statistical significance was set at $p < 0.05$. All statistical analyses were performed using SPSS v. 21.0 (IMB Corp., Armonk, USA).

Results

All data is presented in Tables 2–4 as means and standard deviations (SD) of the bacterial growth inhibition zones for each sealer. Zones of bacterial inhibition equal to 0 indicated that the sealer did not act during the whole experiment. Most sealers demonstrated growth inhibition zones against both tested bacteria, except for Roeko Seal Automix (RSA) and GuttaFlow® (GF). Positive control plates exhibited bacterial growth in all cases. Analysis of variance revealed that the size of the bacterial growth inhibition zone was significantly influenced by the kind of material tested ($p < 0.001$).

The highest antibacterial effect against *A. viscosus* was exhibited by MTA Fillapex (FL), followed by Real® Seal (RCS), Sealapex™ (SP), Endomethasone N (EN), Apexit® Plus (AP), Tubli-Seal™ (TS), Hybrid Root SEAL (HB), and AH Plus™ Jet (AH). The highest dimension of growth inhibition zones against *A. israelii* was revealed in FL, EN, SP HB, RCS, TS, AH, and AP, in a descending order. A comparison of the materials revealed significant differences between almost all the sealers in the varying sizes of growth inhibition zones within particular strains. Details of the statistical analysis results are presented in Table 2.

To compare the susceptibility of particular strains to each sealer, the mean values of the growth inhibition zones obtained with all measurements for each material (excluding materials with a zone of growth inhibition of 0) were calculated and analyzed. Statistical analysis showed that *A. viscosus* was significantly more susceptible than *A. israelii* to AP, RCS ($p < 0.001$) and TS ($p = 0.012$). On the other hand, *A. israelii* was significantly more susceptible than *A. viscosus* to EN, HB and SP ($p < 0.001$) (Table 3).

The antibacterial effect of all the tested root canal sealers on individual strains varied considerably during the entire experiment. For *A. israelii*, the antibacterial activity of the materials (AH, EN, FL, and SP) increased significantly throughout the experiment (AH, FL, SP $p < 0.001$; EN $p = 0.037$). The diameter of growth inhibition zones with AP and TS remained stable, and RCS showed a significant decrease in antibacterial action over time ($p = 0.045$) (Table 4). For *A. viscosus*, the antibacterial effect of SP and RCS rose, whereas with FL and EN it decreased gradually.

Table 2. Zones of bacterial growth inhibition (mean ±SD) provided by root canal sealers (in millimeters)

Material	Time															
	96 h				1 week				2 weeks				3 weeks			
	Actinomyces viscosus		*Actinomyces israelii*		*Actinomyces viscosus*		*Actinomyces israelii*		*Actinomyces viscosus*		*Actinomyces israelii*		*Actinomyces viscosus*		*Actinomyces israelii*	
	mean	SD	mean	SD	mean	SD	mean	SD	mean	SD	mean	SD	mean	SD	mean	SD
AH	15.00	1.00	12.67^{a}	0.58	14.67	0.58	13.67^{a}	0.58	15.00	0.00	15.00	0.00	15.00	0.00	16.00	0.00
AP	$18.67^{a,b,c}$	0.58	13.33^{a}	0.58	$18.33^{c,d}$	0.58	13.33^{a}	0.58	18.00^{a}	0.00	13.67	0.58	18.00^{a}	0.00	14.00	0.00
EN	$20.67^{a,d,e}$	0.58	26.67^{c}	0.58	20.00^{b}	0.00	27.33^{c}	0.58	20.00	0.00	27.00	0.00	19.67	0.58	27.67^{b}	0.58
GF	0.00^{g}	0.00	0.00^{d}	0.00	0.00^{e}	0.00	0.00^{d}	0.00	0.00^{b}	0.00	0.00^{b}	0.00	0.00^{b}	0.00	0.00^{c}	0.00
FL	32.33	0.58	29.67	0.58	30.67	0.58	28.33^{c}	0.58	28.00	0.00	29.00	0.00	28.00	0.00	30.67	0.58
HB	$18.67^{b,e,f}$	0.58	20.67^{b}	0.58	$18.00^{a,d}$	0.00	21.67	0.58	18.00^{a}	0.00	21.67	0.58	18.00^{a}	0.00	22.00	0.00
RCS	26.67	0.58	19.33^{b}	0.58	26.67	0.58	18.67^{b}	0.58	27.33	0.58	18.00^{a}	0.00	27.00	0.00	18.00^{a}	0.00
RSA	0.00^{g}	0.00	0.00^{d}	0.00	0.00^{e}	0.00	0.00^{d}	0.00	0.00^{b}	0.00	0.00^{b}	0.00	0.00^{b}	0.00	0.00^{c}	0.00
SP	21.00^{d}	0.00	25.3^{c}	0.58	22.00	0.00	24.33	0.58	22.00	0.00	25.00	0.00	22.33	0.58	27.33^{b}	0.58
TS	$18.33^{c,f}$	0.58	17.67	0.58	$18.67^{a,b,c}$	0.58	18.00^{b}	0.00	18.00^{a}	0.00	18.00^{a}	0.00	18.00^{a}	0.00	18.00^{a}	0.00

Material	4 weeks			
	Actinomyces viscosus		*Actinomyces israelii*	
	mean	SD	mean	SD
AH	15.00	0.00	16.33	0.58
AP	$18.33^{a,b,d}$	0.58	13.67	0.58
EN	$19.33^{d,e}$	0.58	28.33^{b}	0.58
GF	0.00^{g}	0.00	0.00^{c}	0.00
FL	28.33[c]	0.58	31.67	0.58
HB	$18.00^{b,f}$	0.00	21.67	0.58
RCS	27.33[c]	0.58	18.33^{a}	0.58
RSA	0.00^{g}	0.00	0.00^{c}	0.00
SP	22.67	0.58	28.00^{b}	0.00
TS	$18.33^{a,e,f}$	0.58	17.67^{a}	0.58

There are no significant differences at a level of $p < 0.05$ between values tagged with identical letters (a, b, c, d, e, f, g) in the same columns. AH – AH Plus™ Jet; A – Apexit® Plus; EN – Endomethasone N; GF – GuttaFlow®; HB – Hybrid Root SEAL; FL – MTA Fillapex; RCS – Real® Seal; RSA – Roeko Seal Automix; SP – Sealapex™; TS – Tubli-Seal™; SD – standard deviation.

Table 3. Mean growth inhibition zones [mm] from all periods of observation for *Actinomyces israelii* and *Actinomyces viscosus* for each material (excluding materials showing no bacterial growth inhibition zone)

Material	Strains	N	Mean	SD	p-value
AH	*A. israelii*	15	14.73	1.49	ns
	A. viscosus	15	14.93	0.46	
AP	*A. israelii*	15	13.60	0.51	<0.001
	A. viscosus	15	18.27	0.46	
EN	*A. israelii*	15	27.40	0.74	<0.001
	A. viscosus	15	19.93	0.59	
FL	*A. israelii*	15	29.87	1.30	ns
	A. viscosus	15	29.47	1.92	
HB	*A. israelii*	15	21.53	0.64	<0.001
	A. viscosus	15	18.13	0.35	
RCS	*A. israelii*	15	18.47	0.64	<0.001
	A. viscosus	15	27.00	0.53	
SP	*A. israelii*	15	26.00	1.51	<0.001
	A. viscosus	15	22.00	0.93	
TS	*A. israelii*	15	17.87	0.35	0.012
	A. viscosus	15	18.27	0.46	

ns – not significant. AH – AH Plus™ Jet; A – Apexit® Plus; EN – Endomethasone N; GF – GuttaFlow®; HB – Hybrid Root SEAL; FL – MTA Fillapex; RCS – Real® Seal; RSA – Roeko Seal Automix; SP – Sealapex™; TS – Tubli-Seal™; SD – standard deviation.

Table 4. Statistical analysis of the differences between the mean of bacterial growth inhibition zones over time exhibited by the sealers (excluding materials showing no bacterial growth inhibition zone)

Material	*Actinomyces israelii*	*Actinomyces viscosus*
AH	$p < 0.001$*	$p = 0.925$
AP	$p = 0.545$	$p = 0.461$
EN	$p = 0.037$*	$p = 0.045$*
FL	$p < 0.001$*	$p < 0.001$*
HB	$p = 0.134$	$p = 0.045$*
RCS	$p = 0.045$*	$p = 0.390$
SP	$p < 0.001$*	$p = 0.284$
TS	$p = 0.633$	$p = 0.232$

* level of significance $p < 0.05$. AH – AH Plus™ Jet; A – Apexit® Plus; EN – Endomethasone N; GF – GuttaFlow®; HB – Hybrid Root SEAL; FL – MTA Fillapex; RCS – Real® Seal; RSA – Roeko Seal Automix; SP – Sealapex™; TS – Tubli-Seal™.

The diameter of growth inhibition zones with AH, AP, HB, and TS remained stable over the experimental period. Differences between the bacterial growth inhibition zones over time were not significant for almost all the tested materials ($p > 0.05$), with the exception of FL ($p < 0.001$) and EN ($p = 0.045$) (Table 4).

Discussion

The presence of bacteria in the root canal at the time of filling is the main causative factor of the initiation and perpetuation of apical periodontitis. Therefore, the eradication of bacteria from the root canal system should be the

main goal of endodontic therapy.[3,5,7] Although the cleaning and shaping of the root canals with various instrumentation techniques significantly reduces the intracanal bacterial load, complete eradication is still unattainable in many cases. Studies have demonstrated that after chemomechanical preparation, untouched biofilm remained in lateral canals, ramifications, isthmuses, and dentinal tubules.[10] Persistent bacteria are able to induce or sustain apical periodontitis.[5,9,10] Therefore, the use of root canal sealer with antimicrobial activity is widely recommended.[2,14–18]

Obturation of the root canal involves the use of guttapercha in combination with a sealer to provide an adequate seal. The use of a sealer is necessary to fill voids and gaps between the main material and root canal walls. Currently, numerous root canal sealers are available, based on various formulas, such as zinc oxide–eugenol paste, calcium hydroxide epoxy and methacrylate-based components, as well as mineral trioxide aggregate (MTA)- and silicone-containing materials.[19] After being placed into the root canal system, sealers may penetrate into root canal irregularities. Supposing they have antimicrobial activity, sealers might help eliminate residual microorganisms unaffected by both chemomechanical preparation and intracanal medication.[2,20,21]

The agar diffusion test (ADT) is a well-established and simple method used to assess the antibacterial activity of dental materials.[14,15,22,23] It is suitable for evaluating freshly mixed materials, allowing a direct comparison of sealers and indicating which sealers probably have antimicrobial action within the root canal system. However, the results of the ADT depend on the solubility of the material and its diffusibility in the culture medium used.[23]

It is extremely difficult to accurately compare bacterial inhibition data between different authors – even for identical materials – with the ADT due to difficulties in controlling the large number of variables. This means that there are no standardized in vitro protocols for testing the antimicrobial activity of materials.[22]

In this study, the vast majority of sealers showed an antimicrobial effect on both bacterial strains of *Actinomyces*. There were substantial differences in the antibacterial action of root canal sealers, which depended on the material tested and the bacterial strains used.

MTA Fillapex, EN, SP, and RCS produced the largest bacterial growth inhibition zones against both microorganisms at all times of the experiment. MTA Fillapex is a new material containing MTA – it simultaneously has the chemo-physical properties of a root canal sealer. Its antibacterial activity could be attributed precisely to MTA, which consists of calcium oxide and silicon dioxide, and produces calcium hydroxide on hydration, thus causing an increase in pH.[24] It has been shown that FL has pH values between 9.86 and 10.06.[20] According to Estrela et al., at pH > 9, bacterial enzymes can be irreversibly inactivated, resulting in loss of their biological activity.[25]

A similar mechanism of antibacterial action concerns calcium hydroxide root canal sealars (SP and AP), which in our study also inhibited the bacterial growth of both strains of *Actinomyces*. Faria-Junior et al. evaluated the antibiofilm activity on *Enterococcus faecalis* of various sealers in bovine dentine.[20] Among the 7 materials studied, only FL and SP showed antibiofilm activity. The authors believe that this strong antibacterial effect of both sealers is not only related to the pH increase, but also to their high solubility. Morgental et al. claim that the antimicrobial potential of FL is comparable to zinc oxide–eugenol sealers, which have been used as a positive control in antimicrobial activity assays.[23]

Our results confirmed previous findings that both zinc oxide–eugenol containing sealers were effective in inhibiting the bacterial growth of *Actinomyces*.[14,21] Eugenol, continuously eluted from these materials in relatively high concentrations, may contribute to their antibacterial activity by inhibiting cell growth or even inducing cell death.[22,26]

In the present study, AH, an epoxy-based sealer, demonstrated less antimicrobial effect than zinc oxide–eugenol ones. Our findings are in agreement with other authors who studied identical materials against *Actinomyces*.[14,21] Furthermore, Gjorgievska et al. noted that AH reduced bacterial growth much more when freshly mixed than after 21 days.[14] The adverse effect of epoxy-resin-based sealers might be related either to bisphenol-A diglicidyl ether or the release of formaldehyde during the polymerization process.[15] Both methacrylate--based sealers (RCS and HB) had a varied effect on the tested *Actinomyces* strains. Real® Seal inhibited *A. viscosus* much more strongly than HB, whilst HB, inhibited *A. israelii* much more than RCS. It has been hypothesized that the mechanism of antibacterial action of these materials may be explained by the toxicity of methacrylate resins and residual monomers leached from poorly polymerized materials.[27] Some reports indicate that complete setting of methacrylate-based sealers can vary from 30 min to 7 days depending on the environment.[28] Real® Seal SE and HB have been developed as alternatives to conventional endodontic sealers and gutta-percha. They offer the ability to bond to both root canal walls and the core material, and to create a so-called monoblock obturation to provide a durable hermetic seal, and therefore to ensure a favorable prognosis after endodontic therapy. However, there are also bad reviews. Nevertheless, a recently published in vivo study has not confirmed this assumption.[29] Nawal et al. compared the antimicrobial efficacy of Epiphany® (identical to RCS) AH and GF on *E. faecalis*, using the ADT and the direct contact test (DCT).[30] For both the ADT and DCT, Epiphany® produced a significant reduction in bacterial counts compared to the other 2 materials. Zhang et al. studied a new version of the sealer, Epiphany® SE (a self-adhesive sealer containing acidic monomers that are originally found in primers), with the DCT and reported that the freshly mixed material reduced the number

of *E. faecalis* significantly within 60 min of contact with the bacterial suspension, but after setting it showed only slight antibacterial activity.[18] On the other hand, other authors in their studies with the ADT and DCT demonstrated poor action of Epiphany® SE against *E. faecalis*, or they even observed an enhanced bacterial growth in contact with the material.[13,20]

In the present study, silicone-based root canal sealers (RSA and GF) were completely ineffective in inhibiting the bacterial growth of both *Actinomyces* strains. Our results are in accordance with findings of other authors who used the ADT.[15,22,30] Cobankara et al. claimed that the absence of antibacterial activity might be caused by insolubility and a lack of diffusion of silicone materials in the agar medium.[22]

According to Gomes et al., in order to work effectively in terms of antimicrobial action, the materials used in endodontics should act both in the root canal space and at some distance into the dentinal tubules, and even reach the outer root surface.[31]

Conclusions

We have shown that the antimicrobial effect of the examined materials varied considerably depending on the type of material and bacterial species tested. We have established that most of the tested root canal sealers exhibited antibacterial activity on standardized strains of *Actinomyces*, with FL showing the highest antibacterial effect on both bacterial strains. Importantly, both standardized strains of *Actinomyces* were characterized by varied sensitivity to the root canal sealers.

References

1. Siqueira JF Jr. Periapical actinomycosis and infection with *Propionibacterium propionicus*. *Endod Topics*. 2003;6:78–95.
2. Wang J, Jiang Y, Chen W, Zhu C, Liang J. Bacterial flora and extraradicular biofilm associated with the apical segment of teeth with posttreatment apical periodontitis. *J Endod*. 2012;38(7):954–959.
3. Yamane K, Yamanaka TN, Ishihara K, et al. Pathogenicity of exopolysaccharide-producing *Actinomycesoris* isolated from an apical abscess lesion. *Int Endod J*. 2013;46(2):145–154.
4. Nair PNR, Brundin M, Sundqvist G, Sjögren U. Building biofilms in vital host tissues: A survival strategy of *Actinomyces radicidentis*. *Oral Surg Oral Med Oral Pathol Oral Radiol Endod*. 2008;106(4):595–603.
5. Subramanian K, Mickel AK. Molecular analysis of persistent periradicular lesions and root ends reveals a diverse microbial profile. *J Endod*. 2009;35(7):950–957.
6. Al-Ahmadi A, Ameen H, Pelz K, et al. Antibiotic resistance and capacity for biofilm formation of different bacteria isolated from endodontic infections associated with root-filled teeth. *J Endod*. 2014;40(2):223–230.
7. Tennert C, Fuhrmann N, Wittmer A, et al. New bacterial composition in primary and persistent/secondary endodontic infections with respect to clinical and radiographic findings. *J Endod*. 2014;40(2):670–677.
8. Signoretti FG, Endo MS, Brenda PF, et al. Persistent extraradicular infection in root-filled asymptomatic human tooth: Scanning electron microscopic analysis and microbial investigation after apical microsurgery. *J Endod*. 2011;37(12):1696–1700.
9. Signoretti FG, Gomes PF, Montagner F, Jacinto RC. Investigation of cultivable bacteria isolated from longstanding retreatment-resistant lesions of teeth with apical periodontitis. *J Endod*. 2013;39(10):1240–1244.
10. Rocas IN, Lima KC, Siqueira JF Jr. Reduction in bacterial counts in infected root canals after rotary or hand nickel–titanium instrumentation: A clinical study. *Int Endod J*. 2013;46(7):681–687.
11. Hammad M, Qualtrough A, Silikas N. Evaluation of root canal obturation: A three-dimensional in vitro study. *J Endod*. 2009;35(4):541–544.
12. Li G, Niu L, Zhang W, et al. Ability of new obturation materials to improve the seal of the root canal system: A review. *Acta Biomater*. 2014;10(3):1050–1063.
13. Slutzky-Goldberg I, Slutzky H, Solomonov M, Moshonov J, Weiss EI, Matalon S. Antibacterial properties of four endodontic sealers. *J Endod*. 2008;34(6):735–738.
14. Gjorgievska E, Apostolska S, Dimkov A, Nicholson JW, Kaftandzieva A. Incorporation of antimicrobial agents can be used to enhance the antibacterial effect of endodontic sealers. *Dent Mater*. 2013;29(3):29–34.
15. Eldeniz AU, Erdemir A, Hadimli HH, Belli S, Erganis O. Assessment of antibacterial activity of EndoREZ. *Oral Surg Oral Med Oral Pathol Oral Radiol Endod*. 2006;102(1):119–126.
16. Bailon-Sanchez ME, Baca P, Ruiz-Linares M, Ferrer-Luque CM. Antibacterial and anti-biofilm activity of AH Plus with chlorhexidine and cetrimide. *J Endod*. 2014;40(2):977–981.
17. Barros J, Silva MG, Rocas IN, et al. Antibiofilm effects of endodontic sealers containing quaternary ammonium polyethylenimine nanoparticles. *J Endod*. 2014;40(2):1167–1171.
18. Zhang H, Shen Y, Ruse ND, Haapasalo M. Antibacterial activity of endodontic sealers by modified direct contact test against *Enteroccocus faecalis*. *J Endod*. 2009;35(4):1051–1055.
19. Reszka P, Nowicka A, Lipski M, Dura W, Droździk A, Woźniak K. A comparative chemical study of calcium silicate-containing and epoxy resin-based root canal sealers. *Biomed Res Int*. 2016; 2016:9808432. doi: 10.1155/2016/9808432
20. Faria-Junior NB, Tanomaru-Filho M, Berbert FL, Guerreiro-Tanomaru JM. Antibiofilm activity, pH and solubility of endodontic sealers. *Int Endod J*. 2013;46(8):755–762.
21. Barbero-Navarro I, Galera-Ruiz H, Pereira M, Guerreiro D, Machuca-Portillo MC, López del Valle L. In vitro antimicrobial effects of 3 root canal sealers on *Actinomyces radicidentis*. *P R Health Sci J*. 2014;33(2):71–73.
22. Cobankara FK, Altinoz HC, Erganis O, Kav K, Belli S. In vitro antibacterial activities of root canal sealers by using two different methods. *J Endod*. 2004;30(1):57–60.
23. Morgental RD, Vier-Pelisser FV, Oliveira SD, Antunes FC, Cogo DM, Kopper PM. Antibacterial activity of two MTA-based root canal sealers. *Int Endod J*. 2011;44(12):1128–1133.
24. Mohammadi Z, Shalavi S, Giardino L, Palazzi F, Mashouf RY, Soltanian A. Antimicrobial effect of three new and two established root canal irrigation solutions. *Gen Dent*. 2012;60(6):534–537.
25. Estrela C, Sydney GB, Bammann LL, Felippe O Jr. Mechanism of action of calcium and hydroxyl ions of calcium hydroxide on tissue and bacteria. *Braz Dent J*. 1995;6(2):85–90.
26. Sipert CR, Hussne RP, Nishiyama CK, Torres SA. In vitro antimicrobial activity of Fill Canal, Sealapex, Mineral Trioxide Aggregate, Portland cement and EndoRez. *Int Endod J*. 2005;38(8):539–543.
27. Bouillaguet S, Wataha JC, Tay FR, Brackett MG, Lockwood PE. Initial in vitro biological response to contemporary endodontic sealers. *J Endod*. 2006;32(10):989–992.
28. Nielsen BA, Beeler WJ, Vy C, Baumgartner JC. Setting times of resilon and other sealers in aerobic and anaerobic environments. *J Endod*. 2006;32(10):130–132.
29. Barborka BJ, Woodmansey KF, Glickman GN, Schneiderman E, He J. Long-term clinical outcome of teeth obturated with Resilon. *J Endod*. 2017;43(4):556–560.
30. Nawal RR, Parande M, Sehgal R, Naik A, Rao NR. A comparative evaluation of antimicrobial efficacy and flow properties for Epiphany, Guttaflow and AH-Plus sealer. *Int Endod J*. 2011;44(4):307–313.
31. Gomes PF, Montagner F, Bellocchio Berber V, et al. Antimicrobial action of intracanal medicaments on the external root surface. *J Dent*. 2009;37(1):76–81.

Emergence of Enterobacteriaceae co-producing CTX-M-15, ArmA and PMQR in Poland

Katarzyna Piekarska[A,D,F], Katarzyna Zacharczuk[C], Tomasz Wołkowicz[C], Natalia Wolaniuk[B], Magdalena Rzeczkowska[B], Rafał Gierczyński[E,F]

Department of Bacteriology, National Institute of Public Health–National Institute of Hygiene, Warszawa, Poland

A – research concept and design; B – collection and/or assembly of data; C – data analysis and interpretation; D – writing the article; E – critical revision of the article; F – final approval of the article

Advances in Clinical and Experimental Medicine, ISSN 1899-5276 (print), ISSN 2451-2680 (online) *Adv Clin Exp Med*. 2019;28(2):249–254

Address for correspondence
Katarzyna Piekarska
E-mail: kpiekarska@pzh.gov.pl

Funding sources
This research was partially supported with a grant No. NN 404 0850 40 from the National Science Centre (NCN) and with an internal grant from National Institute of Public Health–National Institute of Hygiene (NIZP–PZH) No. 4/EM/2017.

Conflict of interest
None declared

Received on April 26, 2017
Reviewed on July 9, 2017
Accepted on August 9, 2018

Published online on November 30, 2018

Abstract

Background. Plasmid-mediated extended-spectrum β-lactamases (ESBLs), 16S rRNA methylases and quinolone resistance mechanisms (PMQRs) are well-known agents conferring resistance to more than 1 antimicrobial in its group. The accumulation of these agents poses, therefore, a serious risk to public health.

Objectives. The objective of this study was to investigate the presence of common ß-lactamases and 16S rRNA methylases in Qnr-producing Enterobacteriaceae and their genetic relatedness.

Material and methods. We examined 18 Qnr-producing isolates (*Klebsiella pneumoniae* n = 8, *Enterobacter cloacae* n = 6 and *Escherichia coli* n = 4) selected from a collection of 215 ciprofloxacin-resistant strains obtained from patients in a 1030-bed tertiary hospital from 1 March to 31 August 2010. The antibiotics minimum inhibitory concentration (MIC) was determined using E-test. The detection of common ß-lactamases, 16S rRNA methyltransferases and PMQR genes was performed using polymerase chain reaction (PCR) and sequencing. Genetic relatedness was assessed with pulsed-field gel electrophoresis (PFGE) and multilocus sequence typing (MLST).

Results. All the isolates tested were susceptible to carbapenems and colistin, while 16 were multidrug-resistant. Thirteen, 2 and 2 isolates carried *qnr*B1, *qnr*A1 and *qnr*S1, respectively. Ten of 13 *qnr*B1-positive Enterobacteriaceae also carried genes encoding for *aac(6')-Ib-cr* and at least 1 ESBL. The *blaCTX-M-15* gene was the most common ESBL. The most prevalent combination of genes was *qnr*B1+*aac(6')-Ib-cr*+$bla_{\text{TEM-1}}$+$bla_{\text{CTX-M-15}}$. Two isolates of *K. pneumoniae* and *E. cloacae* were found to bear multiple extended range resistance traits: ArmA, CTX-M-15, QnrB1, and AAC (6')-Ib-cr. The PFGE showed that most of the isolates exhibited individual DNA patterns, whilst MLST assigned *K. pneumoniae* (n = 8) to 5 sequence types (STs) (ST15, ST323, ST336, ST147, and ST525), *E. coli* (n = 4) to 2 (ST131 and ST1431) and *E. cloacae* (n = 5) to 4 (ST90, ST89, ST133, and the novel ST407).

Conclusions. Our findings reveal the accumulation of resistance traits and their important role in spreading of multiresistant bacteria among hospitalized patients.

Key words: PMQR, ESBLs, MDR, Enterobacteriaceae, Poland

Cite as
Piekarska K, Zacharczuk K, Wołkowicz T, et al. Emergence of Enterobacteriaceae co-producing CTX-M-15, ArmA and PMQR in Poland. *Adv Clin Exp Med*. 2019;28(2):249–254. doi:10.17219/acem/94165

DOI
10.17219/acem/94165

Introduction

Currently, the global spread of multidrug resistant (MDR) bacteria is considered a major public health concern. In the last decade, we have witnessed a dramatic increase in the number of MDR Enterobacteriaceae. Data from the European Antimicrobial Resistance Surveillance Network (EARS-Net)[1] indicates that a majority of the *Escherichia coli* and *Klebsiella pneumoniae* had combined resistance to third generation cephalosporins, aminoglycosides and fluoroquinolones. Furthermore, the combined resistance has increased significantly also in Poland since 2010, especially for *K. pneumoniae,* with levels ranging from 23% to 52.5% in 2013.[1] However, data on molecular characteristics of MDR Enterobacteriaceae simultaneously resistant to the aforementioned antimicrobial agents is still insufficient in Poland.

Because of their broad-spectrum antimicrobial activity, fluoroquinolones are commonly used agents in clinical and veterinary medicine to treat a wide variety of microbiological infections. The stepwise mutations in gyrase and topoisomerase IV subunits are recognized as the most common mechanism of quinolone resistance in Enterobacteriaceae. Moreover, plasmid-mediated quinolone resistance (PMQR) determinants were also reported in MDR strains as contributing to the increase of fluoroquinolones resistance.[2] We previously[3] described the coexistence of PMQR determinants (*qnr*A, *qnr*B, *qnr*S and *aac(6')-Ib*-cr) and mutations in *gyrA* and *parC* among fluoroquinolone-resistant clinical Enterobacteriaceae.[3]

It is worth noting that previous studies have shown the association of PMQR-encoding genes with other antibiotic resistance genes, such as extended-spectrum β-lactamases (ESBL), including CTX-M-15 or plasmid-mediated AmpC genes.[2,4–6] In addition, PMQRs may also be co-transferred with plasmid-mediated 16S rRNA methylase-encoding genes.[7] However, data on coexistence of PMQRs with the other resistance traits in Enterobacteriaceae collected in Poland is lacking.

In the present study, we investigated the presence of ESBLs, pAmpC and 16S rRNA methylases in Qnr-producing Enterobacteriaceae from clinical sites in Poland, and determined their genetic relatedness. We described the Qnr-producing Enterobacteriaceae strain with the accumulation of plasmid-mediated, broad range resistance traits: ArmA, CTX-M-15, QnrB1, and AAC (6')-Ib-cr that, to the best of our knowledge, has not been yet reported from Poland.

Material and methods

Study population

A retrospective study was conducted of 18 Qnr-producing Enterobacteriaceae (*K. pneumoniae* n = 8, *Enterobacter cloacae* n = 6 and *E. coli* n = 4) found among the previously described 215 fluoroquinolone-resistant clinical isolates collected from 2017 inpatients in a 1030-bed tertiary hospital in a period from 1 March to 31 August 2010.[3]

Phenotypic and genotypic investigation of resistance

Minimum inhibitory concentrations (MICs) to 11 antibiotics were determined using E-test Strips (bioMerieux, Marcy-l'Etoile, France) and interpreted according to the European Committee on Antimicrobial Susceptibility Testing (EUCAST) recommendations (http://eucast.org). For the Qnr-producing isolates, amplification of genes encoding ß-lactamases of the most common families was performed with primers for bla_{TEM}, bla_{SHV} and bla_{CTX-M}.[8] The multiplex polymerase chain reaction (PCR) with family-specific primers which detected the plasmid-mediated AmpC genes bla_{MOX}, bla_{FOX}, bla_{EBC}, bla_{ACC}, bla_{DHA}, and bla_{CIT} was performed as described previously.[9] The characterization of 16S rRNA methyltransferase genes (*armA*, *rmtA*, *rmtB*, and *rmtC*) was done in isolates with resistance to amikacin with PCR using primers as described previously.[10] Furthermore, the DNA sequencing of genes encoding for PMQRs, the selected ß-lactamases and 16S rRNA methyltransferase ArmA was performed. The nucleotide sequences of the PCR products were determined using conventional Sanger method. All the DNA sequences were compared with sequences in the GenBank database using the BLAST algorithm (http://www.blast.ncbi.nlm.nih.gov).

Molecular typing

The genetic relatedness of tested isolates was studied by pulsed-field gel electrophoresis (PFGE) and multilocus sequence typing (MLST). The PFGE was conducted using *Xba*I endonuclease. The PFGE patterns were analyzed using BioNumerics software v. 6.6 (Applied Maths, Sint-Martens-Latem, Belgium). Sequence types (STs) were determined using 7 highly conserved housekeeping genes according to appropriate MLST schemes.[11–13] The MLST Databases available at http://mlst.warwick.ac.uk/mlst/dbs/Ecolia; http://pubmlst.org/ecloacae/ and http://bigsdb.web.pasteur.fr were used for assigning each sequence type.

Plasmid isolation and electrophoresis

The plasmid DNAs from Qnr-producing isolates was extracted using the NucleoBond PC20 kit (Macherey-Nagel, Düren, Germany) according to the manufacturer's instruction. Plasmid size was determined with extraction and electrophoresis using a 0.8% agarose gel (Prona Plus, Burgos, Spain) in Tris-borate-EDTA (TBE) buffer. *Klebsiella pneumoniae* DM0269 containing 50 kb, 90 kb and 180 kb, respectively, were used as molecular weight plasmid calculation.[14]

Results

Multidrug resistance and genotyping of PMQR-producing isolates

The majority of tested isolates were MDR, with resistance to antimicrobial agents showed in Table 1. Additional resistance was found to the following: amoxicillin and clavulanic acid (94%; R >8 mg/L), cefotaxime (72%; R >2 mg/L), ceftazidime (72%; R >4 mg/L), gentamicin (67%; R >4 mg/L), ciprofloxacin (100%; R >1 mg/L), trimethoprim/sulfamethoxazole (78%; R >4 mg/L), and chloramphenicol (72%; R >8 mg/L). All isolates were susceptible to carbapenems and colistin.

Sequencing analysis showed that *qnrB*1, *qnrA*1 and *qnrS1* were found in 13, 2 and 2 isolates, respectively. Ten of 13 *qnrB*1-positive Enterobacteriaceae also carried genes encoding for *aac(6')-Ib-cr* and at least 1 ESBL (Fig. 1). Among them, the most prevalent combination was *qnrB*1+*aac(6')-Ib-cr*+$bla_{\text{TEM-1}}$+$bla_{\text{CTX-M-15}}$, which was detected in 6 isolates, and the $bla_{\text{CTX-M-15}}$ gene was the most common in all the QnrB1-producing isolates (61%). Furthermore, 2 QnrB1- and CTX-M-15-producing isolates (No. 088 and No. 216) possessed additionally the *armA* gene coding for 16S rRNA methyltransferase ArmA. In contrast, pAmpC genes were not detected in any of isolates tested.

All the tested isolates were distinguished by the PFGE with similarity ranging from 50% to 92% (Fig. 1). Four clonal groups were distinguished, each encompassing strains with the PFGE profiles similarity ≥80%. Two clonal groups (A and B) were found in *K. pneumoniae* and single clonal groups (C and D) occurred in *E. coli* and *E. cloacae*, respectively. By the multilocus sequence typing (MLST), 5 STs were identified for *K. pneumoniae*: ST15, ST323, ST336, ST147, and ST525, 2 for *E. coli*: ST131 and ST1431, and 4 for *E. cloacae*: ST90, ST89, ST133, and the novel ST407. Isolates belonging to the same PFGE clonal group belonged also to the same ST. With the single exception (clonal group C), isolates belonging to the same clonal group shared the same resistance traits. In the clonal group C, 2 *E. coli* isolates (No. 155 and No. 169) of ST131 with 83% of PFGE patterns similarity revealed different resistance traits (Fig. 1). These 2 isolates revealed multiple plasmids (5 and 6), including both large and small plasmids (Fig. 2).

Discussion

A significant increase in MDR Enterobacteriaceae has been reported worldwide.[1] The occurrence of MDR is usually concomitant with the acquisition of fluoroquinolone resistance.[2] According to EARS-Net data, in Poland from 2010 to 2013 fluoroquinolone resistance rates for *E. coli* remained almost constant (>25%) but significantly increased from 33% to 70.1% for *K. pneumoniae*.[1] What is noteworthy is that the horizontally transferable PMQRs, which are considered to support the development of the high-level

Table 1. Antimicrobial minimum inhibitory concentrations for the 18 Qnr-producing Enterobacteriaceae

No.	Species	Specimen	Minimum inhibitory concentration [mg/L]										
			AMC	CTX	CAZ	IPM	MEM	GEN	CIP	TGC	CST	SXT	CML
088	Kpn	blood	64	32	4	0.190	0.016	>1024	16	1	0.750	>32	12
036	Kpn	urine	32	0.190	0.750	0.125	0.016	1	128	3	0.750	2	64
060	Kpn	urine	64	32	12	0.125	0.023	64	1,024	1.500	0.500	>32	>256
158	Kpn	urine	16	48	>256	0.125	0.047	256	128	2	0.380	>32	16
159	Kpn	urine	24	>256	128	0.190	0.047	0.500	16	0.500	0.380	>32	6
215	Kpn	urine	32	>32	256	0.032	0.125	64	128	0.500	0.500	>32	16
091	Kpn	intubation tube swab	24	>256	64	0.250	0.064	32	64	1.500	0.380	>32	6
209	Kpn	tracheotomy tube swab	16	0.500	12	0.032	0.003	0.750	64	0.750	0.380	0.250	12
003	Ecl	urine	>256	>256	64	0.190	0.016	128	2	1	0.190	>32	>256
092	Ecl	urine	32	>256	16	0.250	0.047	32	16	1.500	0.380	>32	>256
110	Ecl	urine	>256	12	64	0.250	0.032	8	4	0.250	0.380	>32	>256
118	Ecl	urine	>256	>256	>256	0.250	0.032	48	64	3	0.380	>32	>256
214	Ecl	urine	32	>256	24	0.190	0.023	32	1.500	1	0.380	>32	6
216	Ecl	urine	>256	>256	>256	0.500	0.380	256	64	2	0.500	>32	16
169	Ec	blood	16	0.125	0.380	NT	0.016	12	64	0.250	0.500	0.064	16
014	Ec	urine	16	0.047	0.125	0.190	0.012	0.750	64	0.190	0.380	>32	4
064	Ec	urine	1.50	0.016	0.064	0.190	0.016	0.380	64	0.190	0.250	0.047	2
155	Ec	urine	24	32	8	0.125	0.016	0.500	256	1	0.500	>32	>256

Kpn – *Klebsiella pneumoniae*; Ecl – *Enterobacter cloacae*; Ec – *Escherichia coli*; AMC – amoxicillin-clavulanic acid; CTX – cefotaxime; CAZ – ceftazidime; IPM – imipenem; MEM – meropenem; GEN – gentamicin; CIP – ciprofloxacin; TGC – tigecycline; CST – colistin; SXT – trimethoprim/sulphamethoxazole; CML – chloramphenicol; NT – not tested.

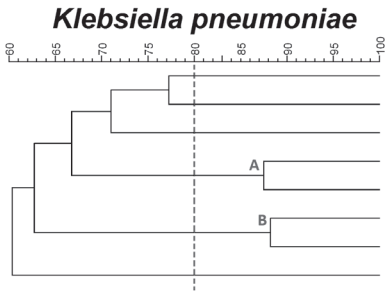

Strain number	ST	Date of isolation	PMQR genes profile	β-lactamases profile	16S rRNA methylase genes
060	15	17.05.10	*qnrB*1, *aac(6')-Ib-cr*	TEM-1, SHV-28, CTX-M-15	-
088	323	05.06.10	*qnrB*1, *aac(6')-Ib-cr*	TEM-1, CTX-M-15	*armA*
159	336	09.08.10	*qnrB*1, *aac(6')-Ib-cr*	TEM-1, SHV-11, CTX-M-15	-
091	323	05.06.10	*qnrB*1, *aac(6')-Ib-cr*	TEM-1, SHV-1, CTX-M-15	-
215	323	15.09.10	*qnrB*1, *aac(6')-Ib-cr*	TEM-1, SHV-1, CTX-M-15	-
158	147	09.08.10	*qnrB*1	SHV-12	-
209	147	23.08.10	*qnrB*1	SHV-12	-
036	525	06.05.10	*qnrA*1	SHV-11	-

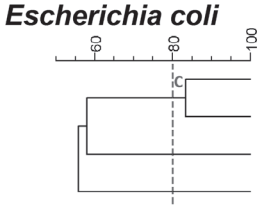

155	131	03.08.10	*qnrB*1, *aac(6')-Ib-cr*	TEM-1, CTX-M-15	-
169	131	28.07.10	*qnrS*1	TEM-1	-
014	1431	05.03.11	*qnrS*1, *aac(6')-Ib-cr*	TEM-1	-
064	-	25.05.11	*qnrS*1, *qnrA-like*	TEM-1	-

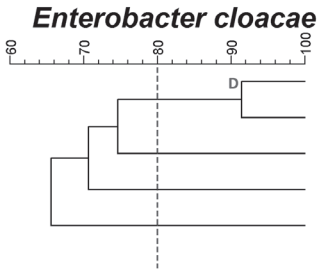

003	90	04.03.10	*qnrB*1, *aac(6')-Ib-cr*	TEM-1, CTX-M-15	-
092	90	02.06.10	*qnrB*1, *aac(6')-Ib-cr*	TEM-1, CTX-M-15	-
214	90	15.09.10	*qnrB*1, *aac(6')-Ib-cr*	TEM-1, CTX-M-15	-
216	89	14.09.10	*qnrB*1	CTX-M-15	*armA*
118	407	23.06.10	*qnrB*1, *aac(6')-Ib-cr*	TEM-1, CTX-M-15	-
110	133	17.06.10	*qnrA*1	SHV-12	-

Fig. 1. Characterization of 18 Qnr-producing Enterobacteriaceae isolates. The dendrogram based on pulsed-field gel electrophoresis (PFGE)
ST – sequence type; PMQR – plasmid-mediated quinolone resistance.

fluoroquinolone resistance, are frequently reported to spread together with ESBLs on the same plasmid.[4–6,15] In this study, we screened clinical Qnr-producing Enterobacteriaceae for the presence of multiple antimicrobial resistance genes. The majority of tested isolates possessed the PMQR determinants – QnrB1 and AAC (6')-Ib-cr – and were identified mainly in combination with CTX-M-15 as the most common ESBL. However, we found no co-existence of Qnr genes and plasmid-mediated AmpC ß-lactamases determinants.

It is well-known that CTX-M-15-producing isolates are commonly multiresistant to various antibiotic agents, among them fluoroquinolones or aminoglycosides.[4] Furthermore, the coexistence of QnrB1 and CTX-M-15 was also frequently observed in other European countries.[4,5] Notably, our data shows that in Poland, the aforementioned combination of resistance traits was extended by the 16S rRNA methyltransferase ArmA that confers the high-level resistance to almost all clinically relevant aminoglycosides. Moreover, the herein reported resistance triangle (QnrB1, CTX-M-15 and ArmA) was found in 2 Enterobacteriaceae species. Notably, one of them contained an additional PMQR gene: *aac(6')-Ib-cr*. Taking into account the relatively low number of isolates tested in this study, the incidence of 2 isolates with the aforementioned resistance triangle may reveal only "the tip of iceberg". Thus, our findings may argue for the need of further specific monitoring of resistance. Interestingly, the coexistence of QnrB, CTX-M-15 and ArmA in *K. pneumoniae* has been reported in China.[7] In Europe, the coexistence of QnrA, CTX-M-15 and ArmA was reported in *K. pneumoniae* in Switzerland, which also co-produced CMY-16 together with carbapenemases OXA-48 and NDM-1.[16] In Poland, we have also reported *K. pneumoniae* co-producing *Klebsiella pneumoniae* carbapenemase (KPC) with ArmA and CTX-M-3 ESBL.[14] To the best of our knowledge, the presented study is the first report on clinical Enterobacteriaceae isolates co-producing PMQR, CTX-M-15 and ArmA in Poland.

In this study, we identified FQ-resistant isolates belonging to different STs possessing CTX-M-15. We found *K. pneumoniae* isolate (No. 088) and *E. cloacae* isolate (No. 216) to bear QnrB1, CTX-M-15 and ArmA, and belong to ST323 and ST89, respectively. Although there is not enough data to consider these 2 STs epidemic, in our study we also found *K. pneumoniae* of ST15, ST336, ST147, and *E. coli* of ST131. These STs have been reported in many countries and, therefore, are considered international clones.[17,18] In addition, *K. pneumoniae* ST15 and ST336 have not been reported in Poland yet. Interestingly, in this study we found *K. pneumoniae* ST15 and ST336 isolates with 2 PMQRs (QnrB1 and AAC (6')-Ib-cr) and 2 ESBLs (CTX-M-15 and SHV-11 or SHV-28) accompanied with TEM-1 β-lactamase. We also observed *E. coli* ST131 isolate No. 155 co-producing PMQR (QnrB1 and AAC (6')-Ib-cr), TEM-1 and CTX-M-15. Interestingly, this isolate revealed

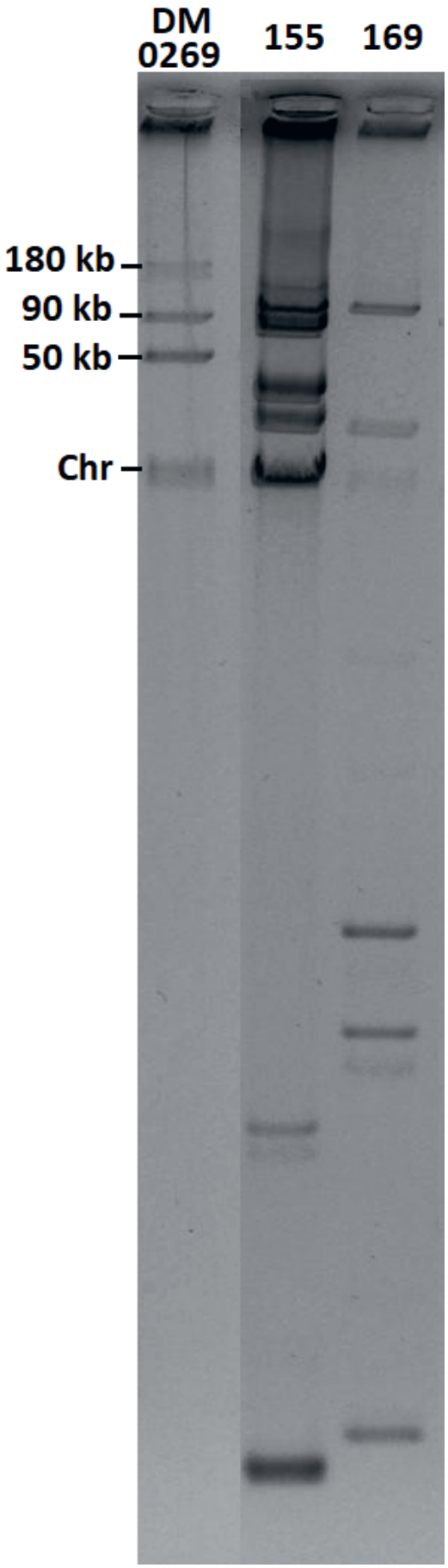

Fig. 2. Plasmids profiles

83% PFGE-profile similarity with other ST131 isolate No. 169 that shared only QnrS1 and TEM-1. Notably, both these isolates differed by plasmid content that may reflect the dynamics of plasmid-mediated resistance traits exchange in clinical settings. Moreover, we found the novel *E. cloacae* ST 407 co-producing QnrB1 and AAC (6')-Ib-cr together with CTX-M-15. What is worthy of note is that all the aforementioned PMQR-producing isolates have been previously found to have mutations in quinolone resistance-determining regions (QRDR) *gyrA* and *parC*.[3]

In conclusion, the presented study provides baseline information on the "successful clones" possessing plasmid-mediated resistance genes providing resistance to most of clinically relevant group of antimicrobial agents including ß-lactams, aminoglycosides and fluoroquinolones. It is also worth noting that fluoroquinolones (mainly ciprofloxacin) are able to induce bacterial SOS response to DNA damage and potentially enhance the transmission of resistance traits by promoting horizontal dissemination of various antibiotic resistance determinants, and increase the frequency of mutants.[19] The herein reported coincidence of PMQRs with other resistance traits, often multiple and broad-range plasmid-mediated mechanisms, may suggest a significant contribution of fluoroquinolone therapy in increasing the MDR phenotype in clinical Enterobacteriaceae strains.

References

1. European Centre for Disease Prevention and Control. Antimicrobial resistance surveillance in Europe 2013. Annual Report of the European Antimicrobial Resistance Surveillance Network (EARS-Net). Stockholm: ECDC , Sweden; 2014. http://ecdc.europa.eu/en/publications/Publications/antimicrobial-resistance-europe-2013.pdf.
2. Hooper DC, Jacoby GA. Mechanisms of drug resistance: Quinolone resistance. *Ann N Y Acad Sci*. 2015;1354:13–31.
3. Piekarska K, Wołkowicz T, Zacharczuk K, et al. Co-existence of plasmid-mediated quinolone resistance determinants and mutations in gyrA and parC among fluoroquinolone-resistant clinical Enterobacteriaceae isolated in tertiary hospital in Warsaw, Poland. *Int J Antimicrob Agents*. 2015;45(3):238–243.
4. Dolejska M, Villa L, Dobiasova H, Fortini D, Feudi C, Carattoli A. Plasmid content of a clinically relevant *Klebsiella pneumoniae* clone from the Czech Republic producing CTX-M-15 and QnrB1. *Antimicrob Agents Chemother*. 2013;57(2):1073–1076.
5. Filippa N, Carricajo A, Grattard F, et al. Outbreak of multidrug-resistant *Klebsiella pneumoniae* carrying qnrB1 and $bla_{CTX-M-15}$ in a French intensive care unit. *Ann Intensive Care*. 2013;3:18.
6. Tóth Á, Kocsis B, Damjanova I, et al. Fitness cost associated with resistance to fluoroquinolones is diverse across clones of *Klebsiella pneumoniae* and may select for CTX-M-15 type extended-spectrum ß-lactamase. *Eur J Clin Microbiol Infect Dis*. 2014;33(5):837–843.
7. Luo Y, Yang J, Zhang Y, Ye L, Wang L, Guo L. Prevalence of β-lactamases and 16S rRNA methylase genes amongst clinical *Klebsiella pneumoniae* isolates carrying plasmid-mediated quinolone resistance determinants. *Int J Antimicrob Agents*. 2011;37(4):352–355.
8. Zacharczuk K, Piekarska K, Szych J, et al. Plazmid-borne 16S rRNA methylase ArmA in aminoglicoside-resistant *Klebsiella pneumoniae* in Poland. *J Med Microbiol*. 2011;60(Pt 9):1306–1311.
9. Pérez-Pérez FJ, Hanson ND. Detection of plasmid-mediated AmpC beta-lactamase genes in clinical isolates by using multiplex PCR. *J Clin Microbiol*. 2002;40(6):2153–2162.
10. Piekarska K, Zacharczuk K, Wołkowicz T, et al. Distribution of 16S rRNA methylases among different species of aminoglycoside-resistant Enterobacteriaceae in tertiary care hospital in Poland. *Adv Clin Exp Med*. 2016;25(3):539–544.

11. Miyoshi-Akiyama T, Hayakawa K, Ohmagari N, Shimojima M, Kirikae T. Multilocus Sequence Typing (MLST) for characterization of *Enterobacter cloacae*. *PLoS One*. 2013;8(6):e66358.
12. Mellmann A, Bielaszewska M, Kock R, et al. Analysis of collection of hemolytic uremic syndrome-associated enterohemorrhagic *Escherichia coli*. *Emerg Infect Dis*. 2008;14(8):1287–1290.
13. Diancourt L, Passet V, Verhoef J, Grimont PAD, Brisse S. Multilocus sequence typing of *Klebsiella pneumoniae* nosocomial isolates. *J Clin Microbiol*. 2005;43(8):4178–4182.
14. Zacharczuk K, Piekarska K, Szych J, et al. Emergence of *Klebsiella pneumoniae* coproducing KPC-2 and 16S rRNA methylase ArmA in Poland. *Antimicrob Agents Chemother.* 2011;55(1):443–446.
15. Briales A, Rodríguez-Martínez JM, Velasco C, et al. Prevalence of plasmid mediated quinolone resistance determinants *qnr* and *aac(6')-Ib-cr* in *Escherichia coli* and *Klebsiella pneumoniae* producing extended-spectrum ß-lactamases in Spain. *Int J Antimicrob Agents*. 2012;39(5): 431–434.
16. Seiffert SN, Marschall J, Perreten V, Carattoli A, Furrer H, Endimiani A. Emergence of *Klebsiella pneumoniae* co-producing NDM-1, OXA-48, CTX-M-15, CMY-16, QnrA and ArmA in Switzerland. *Int J Antimicrob Agents*. 2014;44(3):260–262.
17. Paltansing S, Kraakman MEM, Ras JMC, Wessels E, Bernards AT. Characterization of fluoroquinolone and cephalosporin resistance mechanisms in Enterobacteriaceae isolated in a Dutch teaching hospital reveals the presence of an *Escherichia coli* ST131 clone with a specific mutation in parE. *J Antimicrob Chemother.* 2013;68(1):40–45.
18. Rodrigues C, Machado E, Ramos H, Peixe L, Novais Â. Expansion of ESBL-producing *Klebsiella pneumoniae* in hospitalized patients: A successful story of international clones (ST15, ST147, ST336) and epidemic plasmids (IncR, $IncFII_K$). *Int J Med Microbiol*. 2014;304(8):1100–1108.
19. Beaber JW, Hochhut B, Waldor MK. SOS response promotes horizontal dissemination of antibiotic resistance genes. *Nature*. 2004; 427(6969):72–74.

A meta-analysis of the relationship between vitamin D receptor gene *ApaI* polymorphisms and polycystic ovary syndrome

Fang Liang[1,A,B,D,E], Na Ren[2,A,D,E], Hongxia Zhang[1,C], Jian Zhang[1,E], Qingguo Wu[1,D], Rui Song[1,B], Zhenfeng Shi[1,E], Zhanxiu Zhang[3,B], Kuixiang Wang[3,B,E,F]

[1] Departments of Endocrinology, Xingtai People's Hospital, Hebei Medical University, China
[2] Departments of Endocrinology, 3rd Xiangya Hospital of Central South University, Changsha, China
[3] Departments of Joint Orthopedics, Xingtai People's Hospital, Hebei Medical University, China

A – research concept and design; B – collection and/or assembly of data; C – data analysis and interpretation; D – writing the article; E – critical revision of the article; F – final approval of the article

Advances in Clinical and Experimental Medicine, ISSN 1899-5276 (print), ISSN 2451-2680 (online) *Adv Clin Exp Med*. 2019;28(2):255–262

Address for correspondence
Kuixiang Wang
E-mail: kxe721@163.com

Funding sources
None declared

Conflict of interest
None declared

Received on August 10, 2017
Reviewed on October 27, 2017
Accepted on February 28, 2018

Published online on December 20, 2018

Abstract

Background. Emerging evidence from pre-clinical and clinical studies has shown that vitamin D (VD) plays an important role in the pathogenesis of polycystic ovary syndrome (PCOS). Potentially functional *ApaI* polymorphism of vitamin D receptor (*VDR*) gene has been implicated in PCOS risk, but individually published studies have yielded inconclusive results.

Objectives. Studies on the associations of *VDR* gene polymorphisms with PCOS susceptibility reported conflicting results. The objective of this study was to perform a systematic meta-analysis to clarify this issue.

Material and methods. We searched for all publications regarding the associations mentioned above in PubMed, Web of Science, Embase, and China National Knowledge Infrastructure (CNKI) databases updated up to April 2017. A meta-analysis of the overall odds ratios (ORs) with 95% confidence interval (CI) was calculated with the fixed or random effect model.

Results. A total of 7 studies fulfilling the inclusion criteria were included in this meta-analysis (1,350 cases and 960 controls). Pooled ORs showed a significant association between *ApaI* polymorphism and PCOS risk in all 4 genetic models. Subgroup analysis by ethnicity showed that *ApaI* polymorphism was associated with the risk of PCOS in Asians (aa vs AA: OR = 1.54, 95% CI = 1.04–2.28, p = 0.03). However, *ApaI* polymorphism (a vs A: OR = 1.34, 95% CI = 1.00–1.79, p = 0.02; aa+Aa vs AA: OR = 1.36, 95% CI = 1.04–1.79, p = 0.03) was associated with the risk of PCOS in Caucasians.

Conclusions. Our meta-analysis demonstrated that PCOS risk was significantly associated with *VDR* gene *ApaI* polymorphism. However, due to the relatively small sample size in this meta-analysis, further studies with a larger sample size should be conducted to confirm the findings.

Key words: meta-analysis, polycystic ovary syndrome, vitamin D receptor, genetic polymorphisms, *ApaI*

Cite as
Liang F, Ren N, Zhang H, et al. A meta-analysis of the relationship between vitamin D receptor gene *ApaI* polymorphisms and polycystic ovary syndrome. *Adv Clin Exp Med*. 2019;28(2):255–262. doi:10.17219/acem/85882

DOI
10.17219/acem/85882

Introduction

Polycystic ovary syndrome (PCOS) is a common multifaceted metabolic disease with a strong genetic component in women of fertile age.[1] The PCOS incidence increased and ranges from 5% to 10%, with the age of affected females ranging from 12 years to 45 years.[2–4] Being a complex multigenic and heteroplasmy disease, PCOS results in several disorders, such as infertility,[5] myocardial infarction,[6] dysfunctional uterine bleeding,[7] cardiovascular risk,[8] endometrial carcinoma,[9] insulin resistance (IR),[10] diabetes mellitus,[10] hyperandrogenism (hirsutism, acne, male pattern hair loss),[11] oligoanovulation and polycystic ovaries, dyslipidemia, amenorrhea, and hypertension, as well is associated with obesity and high levels of cholesterol.[12]

As a secosteroid hormone, vitamin D (VD) is acquired and synthesized from the diet and ultraviolet radiation.[13] Besides its calciotropic function, VD has potent non-classical properties, including immunomodulatory, anti-inflammatory, antioxidant, antiangiogenic, and antiproliferative properties.[14] It is well-known that the interaction of VD with target tissues is mediated by the VD receptor, a member of the steroid/thyroid hormone receptor family with the function of a transcriptional activator of many genes. There is accumulating evidence suggesting that the VD endocrine system is involved in a wide variety of biological processes, including IR and type 2 diabetes mellitus.[10] Insulin resistance, which is commonly present in women with PCOS, may play an important role in the long-term complications of PCOS.[15] Accumulating evidence suggests that VD deficiency might be a causal factor in the pathogenesis of IR and the metabolic syndrome in PCOS.[16] The *VDR* gene is located on chromosome 12q13.1, consists of 11 exons and has an extensive promoter region capable of generating multiple tissue-specific transcripts. There are 4 single-nucleotide polymorphisms (SNPs) in the *VDR* gene, *FokI* (rs10735810), *BsmI* (rs1544410), *ApaI* (rs7975232), and *TaqI* (rs731236), which have been studied most frequently.[17] Moreover, previous studies have revealed significant associations between *VDR* gene polymorphisms and PCOS.[18–20]

Considering the past establishment of the important functions of *VDR* gene *ApaI* polymorphism, many studies have explored the association between *VDR* gene *ApaI* polymorphism and PCOS risk.[20–26] However, individual studies yielded inconsistent and even conflicting results. This may be attributed to limited sample sizes and inadequate statistical power, which might affect their reliability. A meta-analysis is a statistical procedure of pooling the data from individual studies, increasing effective sample size, enhancing statistical power of the analysis, and producing a single estimate of an effect. Therefore, we performed a comprehensive meta-analysis to further evaluate the association of *VDR* gene *ApaI* (rs7975232) polymorphism and PCOS.

Material and methods

Literature search

Eligible studies were systematically searched in PubMed, Web of Science, Embase, and China National Knowledge Infrastructure (CNKI) databases up to April 2017, with keywords including: [PCOS OR Polycystic Ovary Syndrome] and [*VDR ApaI* OR VD receptor *ApaI*] and [polymorphism OR mutation OR variation OR SNP]. All studies that showed potential relevance of genetic association were assessed by examining their titles and abstracts. All published studies matching the abovementioned eligibility criteria were obtained and tested for their eligibility for incorporation in the present meta-analysis (Fig. 1).

Inclusion and exclusion criteria

Studies were chosen if they met the following criteria: 1) published studies; 2) evaluated association between *VDR* gene *ApaI* polymorphism and PCOS risk; 3) a case-control or cohort study based on unrelated individuals; 4) sufficient data for examining odds ratios (ORs) with 95% confidence interval (CI); and 5) genotype distributions of polymorphism of the control population consistent with Hardy-Weinberg equilibrium (HWE). The most recent article was used to extract data if the authors published more than 1 article with the same study data. Case reports, editorials, reviews, abstracts from conferences, republished or duplicate studies, and studies with insufficient information on data extraction were excluded.

Data extraction and quality assessment

The following information was extracted independently by 2 authors from each study: 1) name of the 1st author; 2) year of publication; 3) country of origin; 4) ethnicity of the study population; 5) genotype distribution or allele frequencies; and 6) sample sizes of cases and controls, and the SNPs included (Table 1). The 2 authors independently assessed the articles for compliance with the inclusion/exclusion criteria, resolved disagreements and reached a consistent decision.

Statistical analysis

Review Manager v. 5.3 software (Cochrane Collaboration, Oxford, UK) was used for all statistical analyses. Genotype frequency was assessed by the χ^2 test in the control group for HWE. The strength of the association between *VDR* gene *ApaI* polymorphism and PCOS susceptibility was assessed by calculating the pooled ORs and 95% CI of the Z-test. *ApaI* genetic models were used for analyses: allelic model, common model, risk model, and additive model; the p-values were corrected for multiple testing using the false discovery rate. I^2 statistic were used to test

Table 1. Characteristics of experimental methods in the 7 studies included in the meta-analysis

Author (publication year)	Case selection	Control selection	Genotyping method	NOS score
Mahmoudi et al. (2009)[24]	NIH criteria	normal healthy women	PCR-RFLP	6
El-Shal et al. (2013)[23]	Rotterdam criteria	normal healthy women	PCR-RFLP	7
Dasgupta et al. (2015)[22]	Rotterdam criteria	normal healthy women	PCR-RFLP	5
Wehr et al. (2011)[19]	Rotterdam criteria	normal healthy women	genotyping assay	8
Huabin et al. (2016)[26]	Rotterdam criteria	a contemporaneous hospitalized woman with benign ovarian tumors	PCR-RFLP	5
Mahmoudi et al. (2015)[21]	NIH criteria	normal healthy women	PCR-RFLP	5
Jędrzejuk et al. (2015)[20]	Rotterdam criteria	normal healthy women	PCR-RFLP	7

NIH – National Institutes of Health; NOS – Newcastle-Ottawa Scale; PCR-RFLP – polymerase chain reaction – restriction fragments length polymorphism.

the heterogeneity among studies, and studies with $I^2 < 50\%$ were considered to be of low heterogeneity. Publication bias was assessed by funnel plot. A p-value <0.05 was considered significant for all tests.

Table 2. Characteristics of experimental groups in the 7 studies included in the meta-analysis

Author (publication year)	Region	Latitude	Ethnicity	Age (case/control)
Mahmoudi et al. (2009)[24]	Tehran, Iran	36°N	Asian	19–42/18–54
El-Shal et al. (2013)[23]	Zagazig, Egypt	30°N	Caucasian	29.8 ±5.6/29.3 ±6.2
Dasgupta et al. (2015)[22]	Hyderabad, India	18°N	Asian	no mention
Wehr et al. (2011)[19]	Graz, Austria	47°N	Caucasian	23–31/26–36
Huabin et al. (2016)[26]	Jiangxi, China	28°N	Asian	22.56 ±4.56/23.14 ±3.21
Mahmoudi et al. (2015)[21]	Tehran, Iran	36°N	Asian	19–42/19–44
Jędrzejuk et al. (2015)[20]	Lower Silesia, Poland	50°N	Caucasian	20–35

Table 3. Genotype frequencies of *VDR ApaI* polymorphisms in 7 studies included

Author (publication year)	Genotype frequency (AA/Aa/aa/total)		Allele-wise frequency (A/a)		HWE (p-value)
	case	control	case	control	
Mahmoudi et al. (2009)[24]	58/68/36/16	49/90/23/162	184/140	188/136	NS
El-Shal et al. (2013)[23]	63/65/22/150	68/64/18/150	191/109	200/100	0.800
Dasgupta et al. (2015)[22]	12/120/118/250	12/117/121/250	144/356	141/359	0.014
Wehr et al. (2011)[19]	142/274/127/543	48/60/37/145	558/528	156/134	0.155
Huabin et al. (2016)[26]	22/58/40/120	39/55/26/120	102/138	133/107	0.021
Mahmoudi et al. (2015)[21]	8/21/6/35	15/11/9/35	37/33	41/29	0.054
Jędrzejuk et al. (2015)[20]	19/52/19/90	32/49/17/98	90/90	113/83	0.204

NS – not significant; HWE – Hardy-Weinberg equilibrium.

Results

Characteristics of the studies

A comprehensive flowchart of the selection process of the studies is shown in Fig. 1. Our initial search of the literature yielded 161 publications. After reading the titles and abstracts, 21 potential studies were included for full-text view. After reading full texts, 4 studies were excluded for not reporting usable data. Finally, a total of 7 case-control studies in 7 articles were identified and met our inclusion criteria, encompassing 1,350 PCOS patients and 960 controls in total. The main characteristics of these selected studies were summarized in Table 1, Table 2 and Table 3, including 1st author, publication year, country of origin, ethnicity of the study group, genotype distribution, and HWE. Generally, most of the studies (>80%) scored 5 stars or more in the Newcastle-Ottawa scale (NOS), and indicated modest to decent quality (Table 1).

Meta-analysis of VDR *ApaI* polymorphism and PCOS susceptibility

The heterogeneity of the 7 selected studies were employed to assess the overall association between the *VDR* gene *ApaI* polymorphism and the risk of PCOS. When $I^2 > 50\%$, we selected random-effects, and for $I^2 < 50\%$ we selected the fixed model. Variant allele genetic model (a compared with A: p = 0.01; OR = 1.2, 95% CI = 1.04–1.37), additive/homozygous genetic model (aa compared with AA: p = 0.01; OR = 1.41, 95% CI = 1.08–1.84) and risk genetic model (aa+Aa compared with AA: p = 0.01; OR = 1.29, 95% CI = 1.05–1.59) showed the risk of the occurrence of PCOS in response to the *VDR* gene *ApaI* polymorphism, whereas the common model (aa compared with AA+Aa: p = 0.29; OR = 1.11, 95% CI = 0.91–1.36) did not show any risk of PCOS associated with *VDR* gene *ApaI* polymorphism (Fig. 2A–D, Table 4).

Subgroup analysis

Subgroup analysis based on the ethnicity of the study group was performed to detect any relationship between *VDR* gene *ApaI* polymorphism and PCOS risk. Then, we conducted a subgroup analysis stratified by population

(Caucasian vs Asian). In the Asian population,[21,22,24,26] we found statistically significant increased risk of PCOS in additive or homozygous genetic model (aa compared with AA: p = 0.03; OR = 1.54, 95% CI = 1.04–2.28) (Fig. 2B). However, other genetic models, i.e., allele model (a compared with A: p = 0.21; OR = 1.18, 95% CI = 0.91–1.54), common model (aa compared with AA+Aa: p = 0.24; OR = 1.17, 95% CI = 0.90–1.50) and risk model (aa+Aa compared with AA: p = 0.33; OR = 1.35, 95% CI = 0.74–2.47) did not show any risk of PCOS associated with *VDR* gene *ApaI* polymorphism (Fig. 2A, 2C, 2D). In the Caucasian population,[20,23,25] we found statistically significant increased risk of PCOS in allele genetic model (a compared with A: p = 0.02; OR = 1.34, 95% CI = 1.00–1.79) and risk genetic model (aa+Aa compared with AA: p = 0.03; OR = 1.36, 95% CI = 1.04–1.79) (Fig. 2A, 2D). However, in other genetic models, i.e., additive/homozygous model (aa compared with AA: p = 0.15; OR = 1.31, 95% CI = 0.91–1.89) and common model (aa compared with AA+Aa: p = 0.83; OR = 1.04, 95% CI = 0.75–1.43) did not show any risk of PCOS associated with *VDR* gene *ApaI* polymorphism (Fig. 2B, 2C).

Publication bias

Funnel plot was carried out to estimate the publication bias among the studies included in this meta-analysis (Fig. 3–6). The emergence of the shape of the funnel plots has not revealed any evidence of publication bias for all the comparison models (a compared with A, aa compared with AA, aa+Aa compared with AA, and aa compared with Aa+AA).

Discussion

Lately, genetic susceptibility to PCOS has led to increasing interest in the study of polymorphisms of genes. This has resulted in the investigation of a number of candidate genes as a way to analyze the possible connection between modulations of PCOS risk across various populations.[20–27] To date, various reports have been published that have evaluated the possible association of *VDR* gene *ApaI* polymorphism and PCOS development, but the findings from different studies were inconsistent and contradictory. Hence, pooled analysis with sufficient power was needed to summarize individual studies. In the present meta-analysis, we aimed to obtain summary estimates for the strength

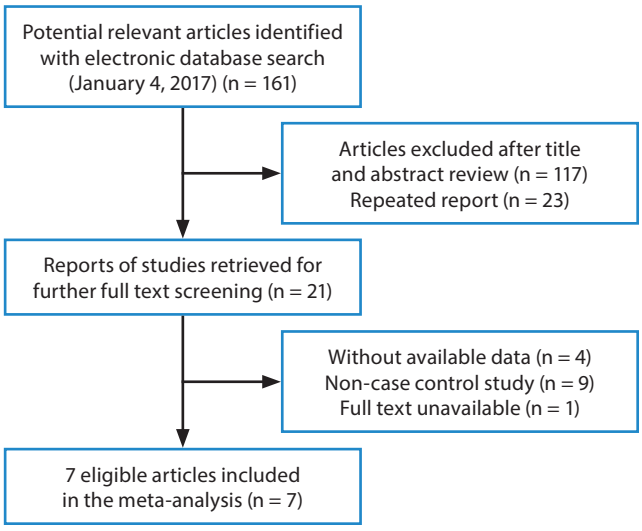

Fig. 1. Results of the literature search strategy

of the association of the *VDR* gene *ApaI* polymorphism and PCOS risk from 7 case-control studies,[20–26] as pooling of the data from individual studies has the advantage of reducing random errors. Also, most of the included studies scored 5 or more stars in NOS quality assessment score criteria and suggested good to moderate quality by clearly stating the sample size, genotype, inclusion criteria of patients, and characteristics of healthy controls.

Our novel findings concerning gene models analysis are the following: the frequency of haplotype *ApaI* "a" was significantly increased in PCOS women compared to that in the controls, while the additive "aa" and risk "aa+Aa" genotype appeared to confer an increased risk for PCOS. The pathophysiological mechanism of these associations is still unclear. Previously, Mahmoudi et al. also reported a relationship between *ApaI* polymorphisms and PCOS risk.[21] A previous report by Dasgupta et al. reported that *VDR* gene polymorphisms have not shown

Table 4. Meta-analysis of *VDR* gene *ApaI* polymorphism and polycystic ovary syndrome (PCOS) susceptibility

Genetic model	Subgroups	Number of studies	Heterogeneity		Effect model	Meta-analysis		
			I^2 [%]	p-value		OR (95% CI)	Z-test	p-value
a/A	total	7	14	0.24	fixed	1.20 (1.04~1.37)	2.57	0.01
	Asians	4	51	0.08	random	1.18 (0.91~1.54)	1.23	0.21
	Caucasians	3	0	0.74	fixed	1.25 (1.04~1.50)	2.36	0.02
aa/AA	total	7	0	0.53	fixed	1.41 (1.08~1.84)	2.51	0.01
	Asians	4	23	0.28	fixed	1.54 (1.04~2.28)	2.13	0.03
	Caucasians	3	0	0.64	fixed	1.31 (0.91~1.89)	1.44	0.15
aa/AA+Aa	total	7	14	0.32	fixed	1.11 (0.91~1.36)	1.05	0.29
	Asians	4	46	0.14	fixed	1.17 (0.90~1.50)	1.17	0.24
	Caucasians	3	0	0.57	fixed	1.04 (0.75~1.43)	0.22	0.83
aa+Aa/AA	total	7	44	0.10	fixed	1.34 (1.00~1.79)	1.95	0.05
	Asians	4	67	0.03	random	1.35 (0.74~2.47)	0.98	0.33
	Caucasians	3	0	0.52	fixed	1.36 (1.04~1.79)	2.22	0.03

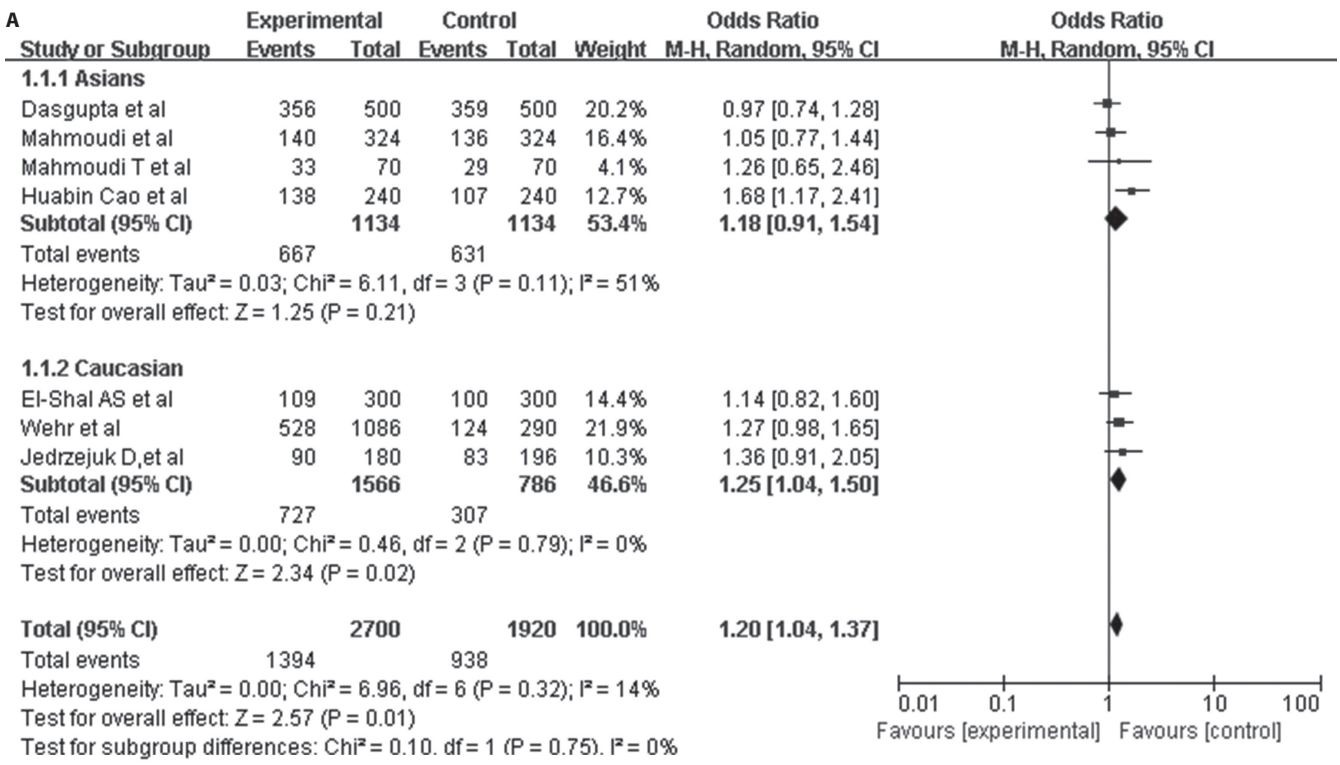

Fig. 2. A – allelic model, B – additive model

a significant association with PCOS, which is inconsistent with several previous independent studies.[22] Also, they found some contradictory results of increased PCOS risk and suggested that this may have been a result of different experimental designs or methods, and that the issue warranted further investigation. In comparison with previously published reports, the present study has major improvements, as it included only specific PCOS cases of relevant published studies. When we studied the Asian and Caucasian population separately, we found strong evidence that variant additive "aa" confers susceptibility to PCOS in Asians, while haplotype *ApaI* "a" and risk "aa+Aa" genotype appeared to confer an increased risk for PCOS in Caucasians. This finding may help to explain

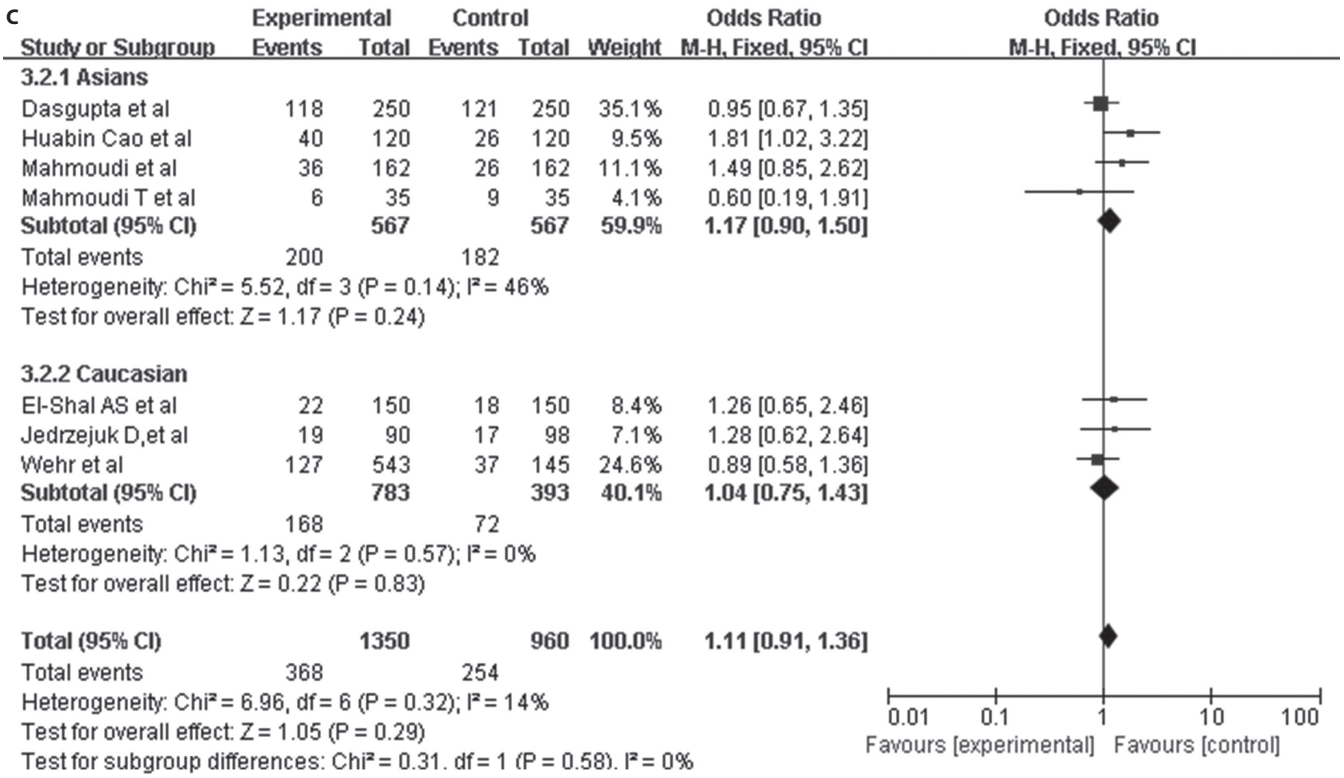

Fig. 2. A. Allelic model. B. Additive model (cont.)

the individual differences in the susceptibility to PCOS. A study by El-Shal et al. reported that *ApaI* was associated with a higher PCOS risk more than control genes in Egyptian women.[23] However, more experimental studies with a larger sample size or alternative methods must be applied for further investigation to verify such findings, as only the mutant genes showed a significant outcome.

As it has been established that PCOS is a complex, multifactorial disease influenced by both environmental and genetic factors,[28] a single genetic variant is normally insufficient to prevent susceptibility toward this disease. The important feature of this gene polymorphism is that its occurrence can vary sufficiently among different races or ethnic populations.

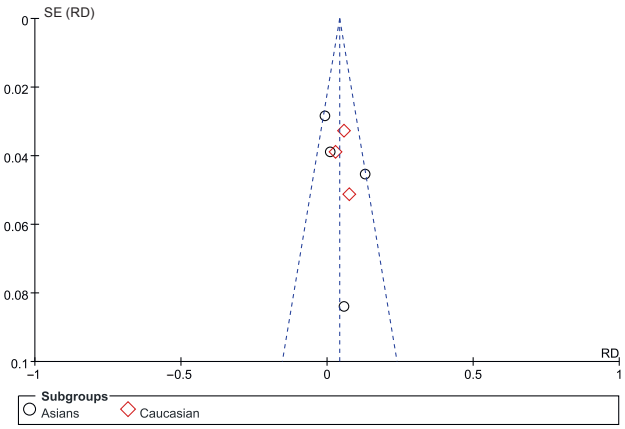

Fig. 3. Publication bias of allelic model

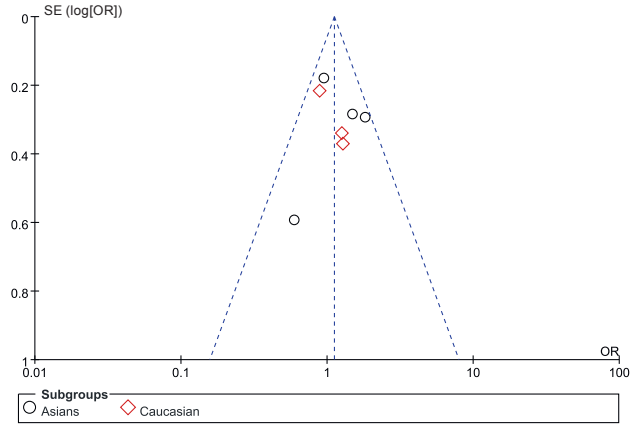

Fig. 4. Publication bias of recessive model

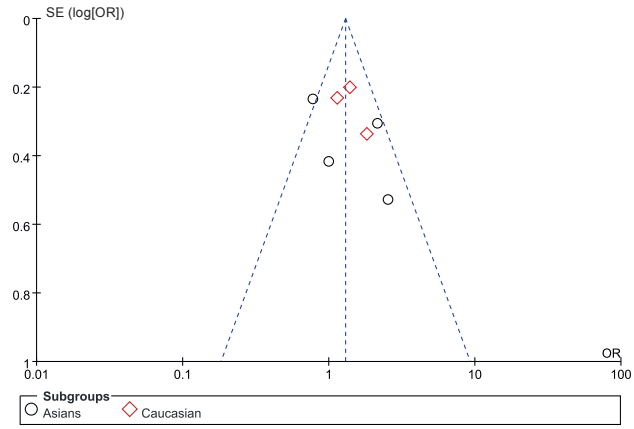

Fig. 5. Publication bias of dominant model

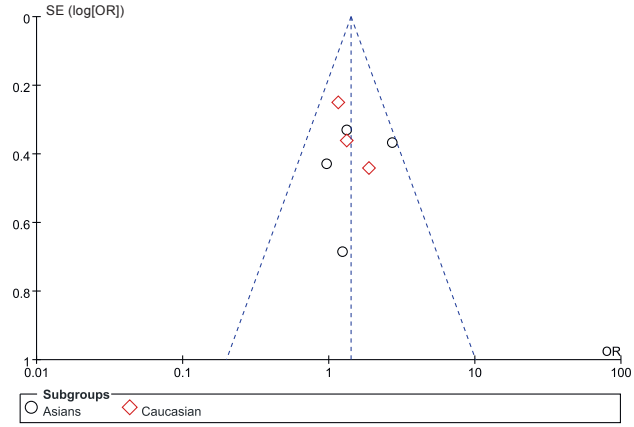

Fig. 6. Publication bias of addictive model

Prior to reaching a final conclusion, limitations of this meta-analysis should also be acknowledged.[29–31] Firstly, we found significant heterogeneity in the overall analysis. Many factors might have contributed to this heterogeneity, e.g., variation in patients' characteristics might have been an important source of heterogeneity. Some studies used matched controls (e.g., age- and sex-matched), while other studies did not perform matching. Secondly, only reports published in English were considered in the present study. The 3rd and the most important limitation is that the studies searched for in this pooled data analysis were indexed by the selected electronic web-databases (i.e., PubMed, Web of Science, Embase). There is, therefore, a possibility there that some pertinent articles published in other languages and/or indexed in other databases (which are not known to us) may have been missed. The 4th limitation is that since the relevant complete data is not available for most of the time, we failed to adjust the confounding factors, such as age, sex and PCOS severity in this meta-analysis. The 5th constraint was that we were unsuccessful in computing the gene and environmental interactions because of lack of sufficient information in the primary studies.

Despite the abovementioned drawbacks, there are some strong points of our meta-analysis that support the reliability of the present results. Firstly, this meta-analysis involved a large set of harmonized individual level data from 7 independent studies, which provided enough statistical power to confirm our results. Secondly, funnel plot indicated no publication bias. Also, all the included studies were of good to modest quality, fulfilling the preset needful criteria as tested by NOS quality assessment scale. Thirdly, although plenty of meta-analyses considering various case-control studies have been performed in the past, we further analyzed the relationship from the point of ethnicity subgroup.[32,33]

In summary, this data suggests that the *VDR* gene *ApaI* polymorphism is associated with PCOS. Therefore, *VDR* gene *ApaI* polymorphism is considered to be one of the possible factors of PCOS predisposition. Furthermore, it is possible that the *VDR* gene, at least in part, through its effects on insulin resistance and serum levels of insulin, is involved in the pathology of PCOS. However, further studies are needed to confirm the findings and clarify the biological mechanisms by which the polymorphism influences the PCOS risk.

Conclusions

Our meta-analysis demonstrated that PCOS was significantly associated with *VDR* gene *ApaI* polymorphism. However, due to the relatively small sample size in this meta-analysis, further studies with a larger sample size should be conducted to confirm the findings.

References

1. Ranjzad F, Mahban A, Shemirani AI, et al. Influence of gene variants related to calcium homeostasis on biochemical parameters of women with polycystic ovary syndrome. *J Assist Reprod Genet*. 2011;28(3):225–232.
2. Dunaif A. Insulin resistance and the polycystic ovary syndrome: Mechanism and implications for pathogenesis. *Endocr Rev*. 1997;18(6):774–800.
3. Diamanti KE, Kouli CR, Bergiele AT, et al. A survey of the polycystic ovary syndrome in the Greek island of Lesbos: Hormonal and metabolic profile. *J Clin Endocrinol Metab*. 1999;84(11):4006–4011.
4. Asunción M, Calvo RM, San Millán JL, Sancho J, Avila S, Escobar-Morreale HF. A prospective study of the prevalence of the polycystic ovary syndrome in unselected Caucasian women from Spain. *J Clin Endocrinol Metab*. 2000;85(7):2434–2438.
5. Voulgaris N, Papanastasiou L, Piaditis G, et al. Vitamin D and aspects of female fertility. *Hormones (Athens)*. 2017;16(1):5–21.
6. Okoroh EM, Boulet SL, George MG, Craig Hooper W. Assessing the intersection of cardiovascular disease, venous thromboembolism, and polycystic ovary syndrome. *Thromb Res*. 2015;136(6):1165–1168.
7. Deligeoroglou E, Karountzos V. Dysfunctional uterine bleeding as an early sign of polycystic ovary syndrome during adolescence: An update. *Minerva Ginecol*. 2017;69(1):68–74.
8. Gunning MN, Fauser BCJM. Are women with polycystic ovary syndrome at increased cardiovascular disease risk later in life? *Climacteric*. 2017;20(3):222–227.
9. Shafiee MN, Seedhouse C, Mongan N, et al. Up-regulation of genes involved in the insulin signaling pathway (*IGF1*, *PTEN* and *IGFBP1*) in the endometrium may link polycystic ovarian syndrome and endometrial cancer. *Mol Cell Endocrinol*. 2016;424:94–101.
10. Condorelli RA, Calogero AE, Di Mauro M, La Vignera S. PCOS and diabetes mellitus: From insulin resistance to altered beta pancreatic function, a link in evolution. *Gynecol Endocrinol*. 2017;33(9):665–667.
11. Al Nofal A, Viers LD, Javed A. Can the source of hyperandrogenism in adolescents with polycystic ovary syndrome predict metabolic phenotype? *Gynecol Endocrinol*. 2017;33(11):882–887.
12. Lazúrová I, Figurová J, Lazúrová Z. Diagnostics of polycystic ovary syndrome [in Czech]. *Vnitr Lek*. 2015;61(Suppl 5):40–44.
13. Gruber BM. The phenomenon of vitamin D [in Polish]. *Postepy Hig Med Dosw (Online)*. 2015;69:127–139.
14. Trochoutsou AI, Kloukina V, Samitas K, Xanthou G. Vitamin-D in the immune system: Genomic and non-genomic actions. *Mini Rev Med Chem*. 2015;15(11):953–963.
15. Macut D, Bjekić-Macut J, Rahelić D, Doknić M. Insulin and the polycystic ovary syndrome. *Diabetes Res Clin Pract*. 2017;130:163–170.
16. He C, Lin Z, Robb SW, Ezeamama AE. Serum vitamin D levels and polycystic ovary syndrome: A systematic review and meta-analysis. *Nutrients*. 2015;7(6):4555–4577.
17. Liu Z, Liu L, Chen X, He W, Yu X. Associations study of vitamin D receptor gene polymorphisms with diabetic microvascular complications: A meta-analysis. *Gene*. 2014;546(1):6–10.
18. Zadeh-Vakili A, Ramezani Tehrani F, Daneshpour MS, Zarkesh M, Saadat N, Azizi F. Genetic polymorphism of vitamin D receptor gene affects the phenotype of PCOS. *Gene*. 2013;515(1):193–196.
19. Wehr E, Trummer O, Giuliani A, Gruber HJ, Pieber TR, Obermayer-Pietsch B. Vitamin D-associated polymorphisms are related to insulin resistance and vitamin D deficiency in polycystic ovary syndrome. *Eur J Endocrinol*. 2011;164(5):741–749.
20. Jędrzejuk D, Łaczmański Ł, Milewicz A, et al. Classic PCOS phenotype is not associated with deficiency of endogenous vitamin D and *VDR* gene polymorphisms rs731236 (*TaqI*), rs7975232 (*ApaI*), rs1544410 (*BsmI*), rs10735810 (*FokI*): A case-control study of lower Silesian women. *Gynecol Endocrinol*. 2015;31(12):976–979.
21. Mahmoudi T, Majidzadeh-A K, Farahani H, et al. Association of vitamin D receptor gene variants with polycystic ovary syndrome: A case control study. *Int J Reprod Biomed (Yazd)*. 2015;13(12):793–800.
22. Dasgupta S, Dutta J, Annamaneni S, Kudugunti N, Battini MR. Association of vitamin D receptor gene polymorphisms with polycystic ovary syndrome among Indian women. *Indian J Med Res*. 2015;142(3):276–285.
23. El-Shal AS, Shalaby SM, Aly NM, Abdelaziz AM. Genetic variation in the vitamin D receptor gene and vitamin D serum levels in Egyptian women with polycystic ovary syndrome. *Mol Biol Rep*. 2013;40(11):6063–6073.
24. Mahmoudi T. Genetic variation in the vitamin D receptor and polycystic ovary syndrome risk. *Fertil Steril*. 2009;92(4):1381–1383.
25. Wehr E, Trummer O, Giuliani A, Gruber HJ, Pieber TR, Obermayer-Pietsch B. Vitamin D-associated polymorphisms are related to insulin resistance and vitamin D deficiency in polycystic ovary syndrome. *Eur J Endocrinol*. 2011;164(5):741–749.
26. Huabin CAO, Ling TU. Association between vitamin D receptor gene polymorphism and polycystic ovary syndrome. *Pract Clin Med*. 2017;17:40–53.
27. Santos BR, Mascarenhas LP, Satler F, Boguszewski MCS, Spritzer PM. Vitamin D receptor gene polymorphisms and sex steroid secretion in girls with precocious pubarche in southern Brazil: A pilot study. *J Endocrinol Invest*. 2012;35(8):725–729.
28. Fenichel P, Rougier C, Hieronimus S, Chevalier N. Which origin for polycystic ovaries syndrome: Genetic, environmental or both? *Ann Endocrinol (Paris)*. 2017;78(3):176–185.
29. Sahin OA, Goksen D, Ozpinar A, Serdar M, Onay H. Association of vitamin D receptor polymorphisms and type 1 diabetes susceptibility in children: A meta-analysis. *Endocr Connect*. 2017;6(3):159–171.
30. Wang Q, Xi B, Reilly KH, Liu M, Fu M. Quantitative assessment of the associations between four polymorphisms (*FokI*, *ApaI*, *BsmI*, *TaqI*) of vitamin D receptor gene and risk of diabetes mellitus. *Mol Biol Rep*. 2012;39(10):9405–9414.
31. Areeshi MY, Mandal RK, Dar SA, et al. A reappraised meta-analysis of the genetic association between vitamin D receptor BsmI(rs1544410) polymorphism and pulmonary tuberculosis risk. *Biosci Rep*. 2017;37(3):BSR20170247.
32. Yu M, Chen GQ, Yu F. Lack of association between vitamin D receptor polymorphisms ApaI (rs7975232) and BsmI (rs1544410) and osteoporosis among the Han Chinese population: A meta-analysis. *Kaohsiung J Med Sci*. 2016;32(12):599–606.
33. Liang F, Wang K, Zhang H, et al. Serum 25-hydroxyvitamin D levels and diabetic retinopathy: A systematic meta-analysis. *Int J Clin Exp Pathol*. 2016;9(12):12843–12848.

Infections of cardiac implantable electronic devices: Epidemiology, classification, treatment, and prognosis

Grzegorz Sławiński[A–F], Ewa Lewicka[A–F], Maciej Kempa[A–F], Szymon Budrejko[A–F], Grzegorz Raczak[A–F]

Department of Cardiology and Electrotherapy, Medical University of Gdańsk, Poland

A – research concept and design; B – collection and/or assembly of data; C – data analysis and interpretation;
D – writing the article; E – critical revision of the article; F – final approval of the article

Advances in Clinical and Experimental Medicine, ISSN 1899–5276 (print), ISSN 2451–2680 (online) *Adv Clin Exp Med*. 2019;28(2):263–270

Address for correspondence
Maciej Kempa
E-mail: kempa@gumed.edu.pl

Funding sources
None declared

Conflict of interest
None declared

Received on February 19, 2017
Reviewed on April 20, 2017
Accepted on November 20, 2017

Published online on July 26, 2018

Abstract

The increasing number of implantation procedures of implantable cardiac electronic devices (ICEDs) leads to a substantial growth of a cohort of patients in whom complications of such a therapy occur. Infective complications are among the most severe ones, as they are often associated with poor prognosis. Depending on the criteria applied, the incidence of cardiac device infection (CDI) is estimated at 0.5–2.2%. Many risk factors of CDIs have been identified, among which the most important are numerous previous cardiac electrotherapy procedures and their complexity, and the lack of perioperative antibiotic prophylaxis. Appropriate diagnosis of a suspected CDI is of utmost importance, as well as the correct classification of the infection, which leads to adequate treatment. Management of a CDI should include complete removal of the implanted device. Additionally, empirical and then targeted antibiotic therapy should be instituted. The prognosis of CDI may, nonetheless, be unfavorable. Despite appropriate treatment, the total mortality rate of such complication is estimated to be as high as 35%.

Key words: infective endocarditis, implantable cardioverter-defibrillator, implantable cardiac electronic device, cardiac pacemaker, infective complications

Cite as
Sławiński G, Lewicka E, Kempa M, Budrejko S, Raczak G. Infections of cardiac implantable electronic devices: Epidemiology, classification, treatment, and prognosis. *Adv Clin Exp Med*. 2019;28(2):263–270. doi:10.17219/acem/80665

DOI
10.17219/acem/80665

Introduction

Cardiac device infections (CDIs) of cardiac pacemakers, implantable cardioverters-defibrillators (ICDs) or resynchronization therapy devices (Cardiac Resynchronization Therapy Pacemaker or Cardiac Resynchronization Therapy Defibrillator: CRT-P or CRT-D) belong to the most significant clinical problems of contemporary cardiology. The increasing number of implantation procedures of implantable cardiac electronic devices (ICEDs) leads to a substantial growth of a cohort of patients in whom complications of such a therapy occur. Infective complications are among the most severe ones, as they are often associated with poor prognosis. CDIs create various clinical problems, including diagnosis, classification of infections and treatment.

Epidemiology

Depending on the criteria applied, the incidence of CDI is estimated at 0.5–2.2%.[1] Available research data shows that the infection rate increases along with the increasing complexity of the implantable device system; infection is least frequent in pacemaker patients, more frequent in patients with an ICD and most frequent in biventricular resynchronization therapy patients (with CRT-P or CRT-D devices). Most studies point to such a relationship, except one with contrary conclusions, which – according to the authors' opinion – may be due to the limited number of patients in the cohort with CRT systems.[2] Higher frequency of CDI in patients with more complex systems may be the consequence of longer procedural times in those patients, which was confirmed in some of the available studies.[3,4]

The incidence of CDIs is from 2-fold to 5-fold lower in the case of first-time procedures, as compared to subsequent revisions of the implanted system. It is estimated that infections complicate 0.5–0.8% of first-time implantations and 1–4% of system revisions.[5–7]

Risk factors

Cardiac device infections constitute a serious medical problem, but they also influence the economic balance of healthcare systems. Therefore, numerous studies have been undertaken to determine the risk factors of that complication. Among the most important factors mentioned is the number of previous cardiac electrotherapy procedures performed in a single patient,[2,5,8,9] the complexity of those procedures[3,6,10,11] and the lack of perioperative antibiotic prophylaxis.[4,5,8,11] Other important risk factors of infective complications (confirmed in at least 2 studies) comprise the following: male sex,[8,12] younger age,[8,10] anticoagulation,[2,12] chronic obstructive pulmonary disease,[9,13] chronic kidney disease,[2,12] and reoperation during the same hospitalization.[3,7] Additional CDI risk factors, though less documented, include: procedure performed before the year 1985,[8] fever during 24 h preceding the procedure,[5] temporary cardiac pacing before the procedure,[5] concomitant chronic heart failure,[12] chronic systemic glucocorticosteroid therapy,[11] hemodialysis,[3] prolonged duration of the procedure,[3] and pocket hematoma.[4]

Sohail et al. determined the risk factors of early infection after ICD implantation.[13] They showed that the risk of early ICD system infection is substantially increased by the presence of epicardial leads and perioperative ICD pocket complications – pocket hematoma, wound dehiscence and delayed wound healing.

The total mortality in the case of CDIs is estimated at 0–35%. Those numbers come from 19 studies, comprising at least 1,000 patients, with the follow-up period of up to 5.5 years.[11,14–26] The reported mortality in the course of CDIs increased along with the prolongation of the follow-up period. It was 2–15% during the first 30 days after implantation procedure,[14,21,24,27,28] 4–29% during 6 months,[14,19,21,26] 9–35% during the first year after implantation,[16,22–24,28] and 6–35% if at least 2 years of follow-up were taken into account.[15,17,20,22,29] It is of note that the data cited above included heterogeneous cohorts of patients with various manifestations of CDIs. Higher mortality was reported in studies where authors qualified only patients with a systemic form of CDI – 24.5–29% during 1-year follow-up,[14,21,24] as compared to studies reporting mortality in patients with only a local manifestation of the infection – 6% during 2-year follow-up.[17] Also, in studies of patient cohorts with any form of CDI, the reported mortality during 1-year follow-up was higher in systemic forms of CDI – 15.5–26%, as compared to local manifestations of CDI – 1.5–12.5%.[20,29]

Because of such an unfavorable course of CDI, many research teams have investigated risk factors of poor prognosis in patients with ICEDs. Among those, renal insufficiency has been most frequently reported.[20,26,30] Other risk factors of poor prognosis include the diagnosis of infective endocarditis (as well as peripheral thromboembolism or moderate/severe tricuspid regurgitation, indicating infective endocarditis)[26,30] and patients' older age.[20,30] Moreover, patients treated conservatively had a higher mortality rate than those in whom the complete removal of the previously implanted system was performed.[22,24,30]

Classification

In recent years, several classifications have been proposed to describe patients with CDIs. At present, it seems that the classification given by Sandoe et al. may be very useful in everyday clinical practice, and its use is advised also in Poland.[1] The authors propose to distinguish 4 basic clinical manifestations of CDIs, such as uncomplicated infection of the pulse generator, complicated infection of the

pulse generator, lead infection, and infective endocarditis in a patient with an ICED (Fig. 1).

In uncomplicated pulse generator infection, no signs or symptoms of a systemic infection may be found, and blood cultures are negative. Uncomplicated generator pocket infection (PI) may be diagnosed in the case of (Fig. 2):

– spreading cellulitis of the pocket;
– purulent exudate from the incision site;
– wound dehiscence or erosion through skin with the exposure of the generator or leads;
– pocket fistula or abscess formation.

Complicated pulse generator infection is diagnosed if the abovementioned PI signs are met, but with evidence of lead or endocardial involvement, systemic signs or symptoms of infection, or positive blood cultures.

Definite lead-related infective endocarditis (LRIE) is diagnosed in the case of:

– symptoms or signs of systemic infection, presence of vegetations attached to leads, as determined by echocardiography, and presence of major Duke microbiological criteria, with no signs of pulse generator PI; or
– symptoms or signs of systemic infection, and microbiological culture, histological or molecular evidence of infection of explanted lead, with no signs of pulse generator PI.

Possible LRIE may be diagnosed in the case of:

– symptoms or signs of systemic infection, presence of vegetations attached to leads, as determined by echocardiography, when major Duke microbiological criteria are not met; or
– symptoms or signs of systemic infection, presence of major Duke microbiological criteria, with no echocardiographic evidence of vegetations attached to leads.

Implantable cardiac electronic device-associated infective endocarditis (ICED-IE) may be diagnosed, if Duke criteria for infective endocarditis are met and infection

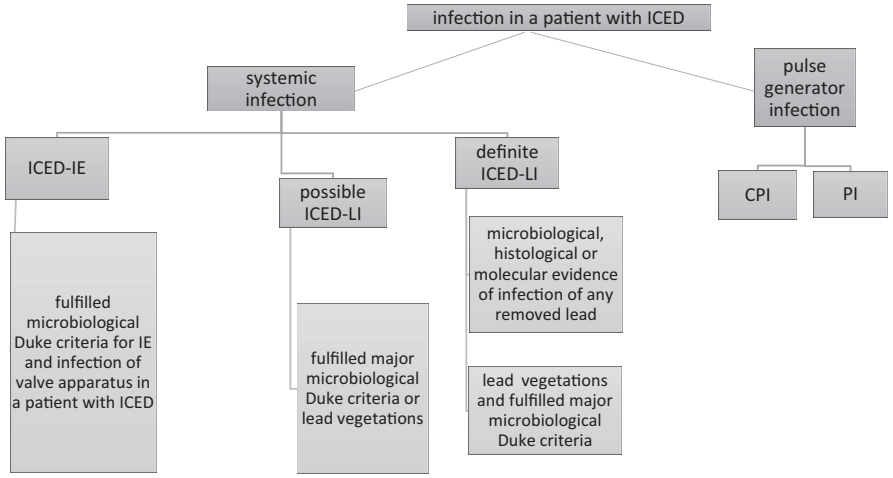

Fig. 1. Classification of implantable cardiac electronic device infections

PI – pocket infection; CPI – complicated pocket infection; ICED – implantable cardiac electronic device; ICED-IE – implantable cardiac electronic device-associated infective endocarditis; ICED-LI – implantable cardiac electronic device isolated lead infection.

Fig. 2. Examples of clinical manifestations of pocket infection (from Authors' archive)

of the valve apparatus is confirmed with echocardiography (Fig. 1).

Apart from the above definitions, it is proposed to include the following as the major diagnostic criteria of ICED isolated lead infection (ICED-LI) and ICED-IE:

– infection of the pulse generator pocket;

– vegetations revealed with fluorine-18-fluorodeoxyglucose positron emission tomography/computed tomography (18F-FDG-PET/CT) or radio-labeled leukocyte single-photon emission computed tomography combined with computed tomography (SPECT/CT), or vegetations in the pulmonary circulation demonstrated with angio-computed tomography (CT);

– recurrent pneumonia in a patient with an ICED (as a manifestation of septic pulmonary embolism).

Etiology

The main etiological factor of CDIs are Gram-positive bacteria, which are responsible for 67.2–92.5% of the total number of infections, while Gram-negative bacteria account for less than 18% of infections. Among Gram-positive bacteria, coagulase negative staphylococci (10–68% of infections) and *Staphylococcus aureus* (24–59%)[14,19,20,23,24,31–34] are most often involved in CDIs. Bacteria that are less frequently involved in CDIs are Gram-negative rods (1–17% of infections), enterococci (5–6%), streptococci (4–6%), propionibacteria and fungi (0.5–2%). Moreover, it is estimated that in 2–24.5% of cases, the CDI is caused by several species.[15–19,31,33] What is of importance is that in 12–49% of patients with clinical manifestations of CDI, blood cultures are negative.[7,14,15,19–21,24,26,31,33–35]

Clinical manifestation

Signs and symptoms of CDI depend on the clinical type of infection. In the case of isolated PI, they include redness, regional edema and tenderness of the pocket region. In more advanced types of infection, purulent exudate may appear, as well as wound dehiscence, fistula formation or erosion of the subcutaneous tissue over the pocket.[36] Spreading infection may affect the leads of the implanted system. Literature data shows that PI coexists with ICED-IE and ICED-LI in 6–58% of cases, depending on the methodology applied and the classification of infections.[7,15,26,37,38]

The diagnosis of ICED-LI or ICED-IE in patients in whom no signs of PI are present poses a great challenge. Patients with ICED-IE or ICED-LI often present non-specific signs and symptoms of systemic infection, such as fever, shivering, nocturnal sweat, and weakness. Laboratory tests show elevated C-reactive protein (CRP) levels, which are observed in up to 96% of patients, but it is not useful to differentiate PI, ICED-LI and ICED-IE.[24,36,39,40] In 9% of patients with ICED-LI and ICED-IE, signs of septic shock may occur, and 5% of patients present with symptoms of vascular involvement or pulmonary embolism.[41] Patients with ICED-LI and ICED-IE quite often report dyspnea and chest pain of pleural characteristics, with radiological features of pulmonary tissue involvement. Secondary infective foci, manifesting as vertebral body infection or intervertebral disc infection,[40] are additional signs of possible ICED-IE or ICED-LI.

Diagnostics

Patients with suspected CDI may require numerous imaging procedures before the final diagnosis is established. According to current guidelines, in every patient with suspected CDI, a chest X-ray is required to determine the pulse generator location, the number of leads and their location, the possible presence of a pulmonary inflammatory process, and pleural effusion.

Echocardiography should be performed as soon as possible in every patient with suspected CDI (the optimal time range is within the first 24 h of the diagnostic work-up). It has been shown that early system removal (within the first 3 days from the diagnosis) is associated with a significantly better prognosis.[42] Echocardiography is also essential in patients with PI due to the frequent coexistence with ICED-LI or ICED-IE. The purpose of echocardiographic examination is to search for possible endocardial or lead-associated vegetations, new valvular insufficiency or abscess formation. In the case of suspected ICED-LI or ICED-IE, transesophageal echocardiography (TEE) is indicated, as its sensitivity to reveal the abovementioned abnormalities is much higher, compared to transthoracic echocardiography (TTE). Observational studies have shown that TTE enables the detection of lead involvement in 22–43% of cases and TEE in 90–96% of cases.[21,39–41] However, one must remember that both methods are complementary. Transthoracic echocardiography enables a more precise evaluation of the left ventricle, the size of right heart chambers and right ventricular pressure, whereas TEE enables a more precise assessment of the intracardiac and extracardiac segments of implanted leads, left heart valvular involvement, and the number, size and mobility of vegetations. It is advised to repeat the echocardiography once the ICED has been removed to exclude the presence of remaining vegetations within the valvular apparatus.

It has been shown that FDG PET/CT may be a valuable imaging modality that is helpful in the diagnostic process of CDIs.[43] However, because of lacking evidence, it is not recommended as a clinical routine, but only as a complementary test in the case of infections of an atypical clinical course.

Diagnostics of suspected CDI comprises an appropriate number of blood cultures, sampled in proper time periods. It is vital to collect blood samples before antibiotic therapy

is instituted. According to the British recommendations, the number of blood samples depends on the clinical status of a patient with suspected CDI.[1] In a patient that is clinically stable, in whom subacute or chronic infection is suspected, it is recommended to collect 3 blood culture samples separated by at least 6-hour intervals. In a patient with CDI and severe sepsis or septical shock, to avoid any delay in empirical antibiotic therapy, it is recommended to collect 2 blood culture samples separated by 1-hour time interval before antibiotic therapy is started. Following the above recommendations allows obtaining positive blood cultures in 20–67% of patients with CDIs.[4,10,31,44]

Apart from blood cultures, it is recommended to perform a microbiological investigation of the removed lead or its fragments (optimally, both proximal and distal segments), vegetations collected from leads and pocket tissues, or purulent exudate from the pocket, if present.

Available data shows low accordance of blood culture results and cultures of removed lead fragments (35%). This should not be surprising, as blood cultures are collected before antibiotic therapy is started, and leads are removed and referred for a microbiological investigation after some period of antibiotic pharmacotherapy.[31]

Management

Management of any diagnosed infection (PI, ICED-LI or ICED-IE) comprises several common points. In each of the infection types, it is advised to remove totally, if possible, the infected system (i.e., the pulse generator and leads). The procedure should be performed as soon as possible and not later than 2 weeks from the diagnosis. Patients should receive antibiotics according to antibiograms obtained from blood cultures. Still, even if an appropriate management strategy is applied, CDI recurs in up to 7% of patients.[11,14–19] What is of note, infection recurrence is more likely if an ICED system is left in place. It is estimated that over a half of patients that has not undergone ICED system removal will develop the next CDI episode.[10,17,45]

Also, in the cases of pocket decubitus or the exposition of leads to extracorporeal environment, as bacterial contamination is inevitable, complete removal of the implanted system is recommended. If local and systemic signs and symptoms of infection are excluded, which means a diagnosis of the so-called "sterile decubitus", prolonged antibiotic treatment is not required, and only perioperative prophylaxis is applied.[1]

Transvenous lead extraction and pulse generator removal (Fig. 3) may be successfully performed in 98% of patients.[46] The risk of failure of such a procedure increases along with the prolongation of lead dwelling time in the venous system. In one of the studies, the authors found a linear correlation between the system dwelling time (from the initial implantation to the removal procedure) and the risk of the removal failure. In the case of leads implanted up to 3 years before, the risk of failure was 5%, and for the leads implanted from 9 to 12 years before, it was as high as 20%.[38] Cardiac surgical removal of an ICED is recommended in patients with large vegetations (>2 cm in diameter) and in those requiring valve replacement or repair because of infective endocarditis.

Complete removal of the implanted system may not always be possible. It may happen in the case of procedural failure, when some parts of leads remain in the patient's circulation, but also if a patient refuses the ICED removal[17] or if a patient is disqualified from the procedure because of poor prognosis due to severe concomitant diseases.[5,7] That may be the case in 3–15% of patients with CDI.[4,5,7,10,37,47] Management of such cases includes typical antibiotic therapy with leads left in situ, or alternatively the removal of the pulse generator in the case of confirmed PI. It has been shown that partial removal of an ICED system leads to infection cure in 13–71% of patients.[10,16,17,37,47]

If ICED extraction is planned, it is obligatory to reassess current indications for cardiac electrotherapy. It is estimated that up to 30% of patients do not require repeat implantation of the removed ICED.[47] In other cases, the repeat implantation procedure should be delayed (if possible) until general (fever) and local symptoms of infection have passed. Some authors suggest to maintain an arbitrary delay of 7–10 days from the system extraction to reimplantation.[7,37] The use of ipsilateral vascular access is discouraged. No part of the previously removed system is allowed to be reimplanted.

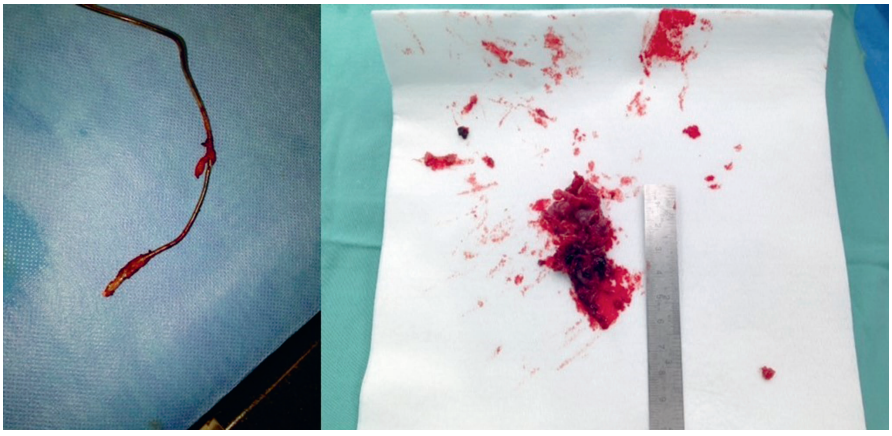

Fig. 3. The left panel pictures a pacing lead that was removed transvenously because of infection (ICED-LI); the right panel pictures vegetations removed during cardiac surgery (from Authors' archive)

ICED-LI – implantable cardiac electronic device isolated lead infection.

In exceptional situations, in the case of infection limited to the superficial tissue or skin incision only, after detailed exclusion of the infective involvement of the pocket, implanted leads and bacterial contamination of the above-mentioned structures, it is acceptable to apply conservative treatment, which means 7–10 days of oral antibiotic treatment (with an antistaphylococcal agent) with possible local surgical debridement. Nevertheless, in those exceptionally rare cases, the region of inflammatory involvement should be thoroughly inspected and monitored, and in the case of progression of the infection into deeper tissue layers, a typical treatment as for CDI should be instituted immediately, with complete removal of the implanted system.[48]

Antimicrobial therapy

Appropriate antimicrobial therapy is an indispensable part of the management strategy in patients with CDIs. The type of antibiotics used and the duration of treatment depend on the extent of infection and the clinical state of a patient. In the case of uncomplicated PI, empirical antibiotic therapy is necessary until the results of collected cultures may be obtained. Successful empirical antibiotic therapy usually includes vancomycin, daptomycin or teicoplanin. Local antibiotic treatment is not recommended. In the case of complicated PI, a typical treatment as for ICED-LI or ICED-IE should be implemented.

Obviously, the diagnosis of ICED-LI or ICED-IE also requires the initiation of appropriate empirical antibiotic therapy. Until blood culture results are available, and if the patient deteriorates (e.g., in severe sepsis), it is advised to use vancomycin with meropenem or daptomycin with meropenem. In patients with ICED-IE or ICED-LI with negative blood cultures, it is recommended to use vancomycin with gentamycin or daptomycin with gentamycin.

Empirical antibiotic therapy should include broad-spectrum agents; however, the efficacy of such a strategy was lower when compared to antibiogram-guided therapy. For example, flucloxacillin is far more effective as a therapy of *Staphylococcus aureus* infections than vancomycin. No randomized clinical trials have been conducted to assess the efficacy of each therapy regimen in the case of ICED-IE or ICED-LI. Moreover, many publications lack detailed information about the course of antibiotic treatment, such as the dosage, route of administration, duration of treatment, or the species of the pathogen responsible for infection.[5,7,8,37,44]

For the antimicrobial treatment of CDI, peripheral venous access is recommended. It is characterized by a lower risk of secondary infection and it does not result in the loss of a potential site for future reimplantation. Peripheral venous access is thus the best solution in the case of prolonged antibiotic administration, but it should be changed on a regular basis every 72 h.[25] Oral route of antibiotic administration is not recommended in CDIs. It was shown that oral antibiotics for PI not only did not cure the infection, but also increased the risk of infection dissemination and mortality.[27] Oral antibiotic therapy is allowed only in the case of persistent cellulitis after system extraction and in patients with no chance for ICED system extraction (subjects in the terminal phase of a chronic disease).

The duration of antibiotic treatment depends on several factors: type of CDI, management of the infected system, involvement of other cardiac structures, and extracardiac signs of infection. In the case of PI, experts' opinions are consistent and the recommended duration of antibiotic therapy is 10–14 days.[4,20,44]

In the case of ICED-LI or ICED-IE, antibiotic therapy is administered for 6 weeks[15,20,21,45]; however, an average of 5.4 weeks[35] and 2–4 weeks were also reported.[47] In patients with ICED-LI or ICED-IE with no ICED system extraction, the British recommendation is 6 weeks of antibiotic therapy.[1] It is generally recommended to stop the therapy after 6 weeks, with the following careful reassessment of the patient's clinical status, and to repeat blood cultures in the case of any suspicion of infection recurrence. There are no strict recommendations regarding the management of infection recurrences. It is advised to start with intravenous antibiotic therapy and subsequent long-lasting oral therapy.[7]

The duration of antibiotic treatment after the extraction of an infected ICED system is determined by several factors, such as the presence of extracardiac infective foci and the initial clinical response to treatment; it also depends on whether the valvular apparatus is involved. With good clinical response and no extracardiac foci, it seems sufficient to continue antibiotic therapy for 4 weeks after the extraction procedure. If CDI occurred in a patient with a mechanical valve prosthesis, a longer 6-week period is recommended. It should be underlined that every change of the treatment scheme (e.g., in case of inefficacy of the previous plan) should reset the time counter again for the complete period, as described above.

Prevention

Performing ICED system implantation or revision only by experienced electrophysiologists in appropriately equipped centers is very important in terms of CDIs prevention. Temporary transvenous cardiac pacing before ICED implantation is a risk factor of CDI. It is associated with 2–18% risk of sepsis[49] and a 2.5-fold increase of the risk of future CDI.[5]

Elective implantation procedures should be postponed until the complete regression of general symptoms (mainly fever) of any infection. It would be interesting to investigate the prognostic value of CRP concentration and white blood cells count before the implantation procedure for the prediction of future CDI.

Based on a meta-analysis of results from randomized clinical trials, it has been established that prophylactic antibiotic administration before the implantation procedure

is an effective method of prevention of CDI.[50,51] Cefazolin has best evidence as an effective antibiotic, preventing CDI.[4] Flucloxacillin compared to placebo did not show any clinical benefit.[52] It is recommended to administer the antibiotic before the implantation procedure, 1 h before skin incision.[50] This antibiotic scheme allows one to achieve tissue and plasma antibiotic concentration above minimal inhibitory concentration (MIC) for potential pathogens. It is not recommended to repeat the antibiotic after the procedure.[50,53]

A crucial part of CDI prevention is appropriate skin preparation in the region of the planned skin incision. Hair should be regionally removed with the use of electric clippers with a single-use head, because the use of razors is associated with a higher risk for infection of the tissue operated on. Hair should be removed on the day of the planned procedure. Recommended antiseptic agents include alcoholic 2% chlorhexidine solution or povidone iodine in alcohol, but notably the use of alcoholic 2% chlorhexidine is associated with higher antiseptic efficacy as compared to povidone iodine in alcohol.[54,55] Therefore, British recommendations postulate the use of alcoholic 2% chlorhexidine solution as the agent of choice for antiseptic preoperative skin preparation, and obeying the crucial rule to leave it on the skin until it dries, which usually takes approx. 30 s.[1]

Summary

CDIs still constitute a serious clinical problem. It is of particular difficulty to establish the final diagnosis in patients with a deceitful and chronic course of the disease. New imaging techniques, such as 18F-FDG-PET/CT or radio-labeled leukocyte SPECT/CT, show high sensitivity for CDI detection. Future studies are needed to assess whether laboratory tests (CRP, procalcitonin, leukocytosis) are useful in predicting CDI occurrence. With increasing resistance of pathogens to antibiotics, further studies are required to compare the efficacy of various therapeutic algorithms, as well as the search for new antimicrobial drugs.

References

1. Sandoe JA, Barlow G, Chambers JB, et al. Guidelines for the diagnosis, prevention and management of implantable cardiac electronic device infection. Report of a joint Working Party project on behalf of the British Society for Antimicrobial Chemotherapy (BSAC, host organization), British Heart Rhythm Society (BHRS), British Cardiovascular Society (BCS), British Heart Valve Society (BHVS) and British Society for Echocardiography (BSE). *J Antimicrob Chemother*. 2015;70:325–359.
2. Lekkerkerker JC, van Nieuwkoop C, Trines SA, et al. Heart rhythm disorders and pacemakers: Risk factors and time delay associated with cardiac device infections: Leiden device registry. *Heart*. 2009;95:715–720.
3. Romeyer-Bouchard C, Da Costa A, Dauphinot V, et al. Prevalence and risk factors related to infections of cardiac resynchronization therapy devices. *Eur Heart J*. 2010;31:203–210.
4. de Oliveira JC, Martinelli M, Nishioka SA, et al. Efficacy of antibiotic prophylaxis before the implantation of pacemakers and cardioverter-defibrillators: Results of a large, prospective, randomized, double-blinded, placebo-controlled trial. *Circ Arrhythm Electrophysiol*. 2009;2:29–34.
5. Klug D, Balde M, Pavin D, et al. Risk factors related to infections of implanted pacemakers and cardioverter-defibrillators: Results of a large prospective study. *Circulation*. 2007;116:1349–1355.
6. Nery PB, Fernandes R, Nair GM, et al. Device-related infection among patients with pacemakers and implantable defibrillators: Incidence, risk factors, and consequences. *J Cardiovasc Electrophysiol*. 2010;21:786–790.
7. Catanchin A, Murdock CJ, Athan E. Pacemaker infections: A 10-year experience. *Heart Lung Circ*. 2007;16:434–439.
8. Johansen JB, Jorgensen OD, Moller M, et al. Infection after pacemaker implantation: Infection rates and risk factors associated with infection in a population-based cohort study of 46,299 consecutive patients. *Eur Heart J*. 2011;32:991–998.
9. Landolina M, Gasparini M, Lunati M, et al. Long-term complications related to biventricular defibrillator implantation: Rate of surgical revisions and impact on survival: Insights from the Italian Clinical Service Database. *Circulation*. 2011;123:2526–2535.
10. Margey R, McCann H, Blake G, et al. Contemporary management of and outcomes from cardiac device related infections. *Europace*. 2010;12:64–70.
11. Sohail MR, Uslan DZ, Khan AH, et al. Risk factor analysis of permanent pacemaker infection. *Clin Infect Dis*. 2007;45:166–173.
12. Bloom H, Heeke B, Leon A, et al. Renal insufficiency and the risk of infection from pacemaker or defibrillator surgery. *Pacing Clin Electrophysiol* 2006;29:142–145.
13. Sohail MR, Hussain S, Le KY, et al. Risk factors associated with early- versus late-onset implantable cardioverter-defibrillator infections. *J Interv Card Electrophysiol*. 2011;31:171–183.
14. Grammes JA, Schulze CM, Al-Bataineh M, et al. Percutaneous pacemaker and implantable cardioverter-defibrillator lead extraction in 100 patients with intracardiac vegetations defined by transesophageal echocardiogram. *J Am Coll Cardiol*. 2010;55:886–894.
15. Knigina L, Kühn C, Kutschka I, et al. Treatment of patients with recurrent or persistent infection of cardiac implantable electronic devices. *Europace*. 2010;12:1275–1281.
16. Chua JD, Wilkoff BL, Lee I, et al. Diagnosis and management of infections involving implantable electrophysiologic cardiac devices. *Ann Intern Med*. 2000;133:604–608.
17. Klug D, Wallet F, Lacroix D, et al. Local symptoms at the site of pacemaker implantation indicate latent systemic infection. *Heart*. 2004;90:882–886.
18. Tascini C, Bongiorni MG, Gemignani G, et al. Management of cardiac device infections: A retrospective survey of a non-surgical approach combining antibiotic therapy with transvenous removal. *J Chemother*. 2006;18:157–163.
19. Viola GM, Awan LL, Darouiche RO. Nonstaphylococcal infections of cardiac implantable electronic devices. *Circulation*. 2010;121:2085–2091.
20. Deharo JC, Quatre A, Mancini J, et al. Long-term outcomes following infection of cardiac implantable electronic devices: A prospective matched cohort study. *Heart* 2012;98:724–731.
21. Greenspon AJ, Prutkin JM, Sohail MR, et al. Timing of the most recent device procedure influences the clinical outcome of lead-associated endocarditis results of the MEDIC (Multicenter Electrophysiologic Device Infection Cohort). *J Am Coll Cardiol*. 2012;59:681–687.
22. Le KY, Sohail MR, Friedman PA, et al. Impact of timing of device removal on mortality in patients with cardiovascular implantable electronic device infections. *Heart Rhythm*. 2011;8:1678–1685.
23. Tarakji KG, Chan EJ, Cantillon DJ, et al. Cardiac implantable electronic device infections: Presentation, management, and patient outcomes. *Heart Rhythm*. 2010;7:1043–1047.
24. Athan E, Chu VH, Tattevin P, et al. Clinical characteristics and outcome of infective endocarditis involving implantable cardiac devices. *JAMA*. 2012;307:1727–1735.
25. Voigt A, Shalaby A, Saba S. Continued rise in rates of cardiovascular implantable electronic device infections in the United States: Temporal trends and causative insights. *Pacing Clin Electrophysiol*. 2010;33:414–419.

26. Baman TS, Gupta SK, Valle JA, et al. Risk factors for mortality in patients with cardiac device-related infection. *Circ Arrhythm Electrophysiol.* 2009;2:129–134.
27. Corman LC, Levison ME. Sustained bacteremia and transvenous cardiac pacemakers. *JAMA.* 1975;233:264–266.
28. Sohail MR, Henrikson CA, Braid-Forbes MJ, et al. Mortality and cost associated with cardiovascular implantable electronic device infections. *Arch Intern Med.* 2011;171:1821–1828.
29. Kempa M, Budrejko S, Piepiorka-Broniecka M, et al. One-year follow-up of patients undergoing transvenous extraction of pacemaker and defibrillator leads. *PLoS One.* 2015;10(12):e0144915.
30. Habib A, Le KY, Baddour LM, et al. Predictors of mortality in patients with cardiovascular implantable electronic device infections. *Am J Cardiol.* 2013;111:874–879.
31. Bongiorni MG, Tascini C, Tagliaferri E, et al. Microbiology of cardiac implantable electronic device infections. *Europace.* 2012;14:1334–1339.
32. Kratz JM, Toole JM. Pacemaker and internal cardioverter defibrillator lead extraction: A safe and effective surgical approach. *Ann Thorac Surg.* 2010;90:1411–1417.
33. Jan E, Camou F, Texier-Maugein J, et al. Microbiologic characteristics and in vitro susceptibility to antimicrobials in a large population of patients with cardiovascular implantable electronic device infection. *J Cardiovasc Electrophysiol.* 2012;23:375–381.
34. Rodriguez DJ, Afzal A, Evonich R, et al. The prevalence of methicillin resistant organisms among pacemaker and defibrillator implant recipients. *Am J Cardiovasc Dis.* 2012;2:116–122.
35. Le Dolley Y, Thuny F, Mancini J, et al. Diagnosis of cardiac device-related infective endocarditis after device removal. *JACC Cardiovasc Imaging.* 2010;3:673–681.
36. Sohail MR, Uslan DZ, Khan AH, et al. Infective endocarditis complicating permanent pacemaker and implantable cardioverter-defibrillator infection. *Mayo Clin Proc.* 2008;83:46–53.
37. Ipek EG, Guray U, Demirkan B, et al. Infections of implantable cardiac rhythm devices: Predisposing factors and outcome. *Acta Cardiol.* 2012;67:303–310.
38. Rusanov A, Spotnitz HM. A 15-year experience with permanent pacemaker and defibrillator lead and patch extractions. *Ann Thorac Surg.* 2010;89:44–50.
39. Massoure PL, Reuter S, Lafitte S, et al. Pacemaker endocarditis: Clinical features and management of 60 consecutive cases. *Pacing Clin Electrophysiol.* 2007;30:12–19.
40. Klug D, Lacroix D, Savoye C, et al. Systemic infection related to endocarditis on pacemaker leads: Clinical presentation and management. *Circulation.* 1997;95:2098–2107.
41. Cacoub P, Leprince P, Nataf P, et al. Pacemaker infective endocarditis. *Am J Cardiol.* 1998;82:480–484.
42. Viganego F, O'Donoghue S, Eldadah Z, et al. Effect of early diagnosis and treatment with percutaneous lead extraction on survival in patients with cardiac device infections. *Am J Cardiol.* 2012;109:1466–1471.
43. Bensimhon L, Lavergne T, Hugonnet F, et al. Whole body [(18)F]fluorodeoxyglucose positron emission tomography imaging for the diagnosis of pacemaker or implantable cardioverter defibrillator infection: A preliminary prospective study. *Clin Microbiol Infect.* 2011;17:836–844.
44. Lakkireddy D, Valasareddi S, Ryschon K, et al. The impact of povidone-iodine pocket irrigation use on pacemaker and defibrillator infections. *Pacing Clin Electrophysiol.* 2005;28:789–794.
45. del Rio A, Anguera I, Miro JM, et al. Surgical treatment of pacemaker and defibrillator lead endocarditis: The impact of electrode lead extraction on outcome. *Chest.* 2003;124:1451–1459.
46. Seifert H, Wisplinghoff H, Schnabel P, et al. Small colony variants of *Staphylococcus aureus* and pacemaker-related infection. *Emerg Infect Dis.* 2003;9:1316–1318.
47. Sohail MR, Uslan DZ, Khan AH, et al. Management and outcome of permanent pacemaker and implantable cardioverter-defibrillator infections. *J Am Coll Cardiol.* 2007;49:1851–1859.
48. Baddour LM, Epstein AE, Erickson CC, et al. Update on cardiovascular implantable electronic device infections and their management: A scientific statement from the American Heart Association. *Circulation.* 2010;121:458–477.
49. McCann P. A review of temporary cardiac pacing wires. *Indian Pacing Electrophysiol J.* 2007;7:40–49.
50. Darouiche R, Mosier M, Voigt J. Antibiotics and antiseptics to prevent infection in cardiac rhythm management device implantation surgery. *Pacing Clin Electrophysiol.* 2012;35:1348–1360.
51. Da Costa A, Kirkorian G, Cucherat M, et al. Antibiotic prophylaxis for permanent pacemaker implantation: A meta-analysis. *Circulation.* 1998;97:1796–1801.
52. Bluhm G, Nordlander R, Ransjo U. Antibiotic prophylaxis in pacemaker surgery: A prospective double blind trial with systemic administration of antibiotic versus placebo at implantation of cardiac pacemakers. *Pacing Clin Electrophysiol.* 1986;9:720–726.
53. Bratzler DW, Dellinger EP, Olsen KM, et al. Clinical practice guidelines for antimicrobial prophylaxis in surgery. *Am J Health Syst Pharm.* 2013;70:195–283.
54. Lee I, Agarwal RK, Lee BY, et al. Systematic review and cost analysis comparing use of chlorhexidine with use of iodine for preoperative skin antisepsis to prevent surgical site infection. *Infect Control Hosp Epidemiol.* 2010;31:1219–1229.
55. Darouiche RO, Wall MJ, Itani KMF, et al. Chlorhexidine–alcohol versus povidone–iodine for surgical-site antisepsis. *N Engl J Med.* 2010;362:18–26.

The new perspectives of targeted therapy in acute myeloid leukemia

Angela Walasek[A–F]

Department and Clinic of Neoplasms and Bone Marrow Transplantation, Wroclaw Medical University, Poland

A – research concept and design; B – collection and/or assembly of data; C – data analysis and interpretation;
D – writing the article; E – critical revision of the article; F – final approval of the article

Advances in Clinical and Experimental Medicine, ISSN 1899–5276 (print), ISSN 2451–2680 (online) *Adv Clin Exp Med*. 2019;28(2):271–276

Address for correspondence
Angela Walasek
E-mail: angela.walasek@gmail.com

Funding sources
None declared

Conflict of interest
None declared

Received on November 27, 2017
Reviewed on December 12, 2017
Accepted on December 28, 2017

Published online on August 24, 2018

Abstract

Acute myeloid leukemia (AML) is a heterogeneous disease and the results of previous treatment with cytotoxic drugs have not been satisfactory. This situation has prompted investigations into novel approaches. The breakthrough in therapy brought by all-trans retinoic acid (ATRA) in acute promyelocytic leukemia (APL) and tyrosine kinase inhibitors in neoplasms with the Philadelphia chromosome has encouraged the search for other effective targeted therapies. Among the tested substances are higher molecular mass drugs such as antibodies and various small molecules: kinase inhibitors, cell pathway inhibitors and epigenetic modulators. So far, the U.S. Food and Drug Administration (FDA) has approved the antibody-drug conjugate gemtuzumab ozogamycin (GO), the tyrosine kinase inhibitor midostaurin and the IDH2 inhibitor enasidenib. These studies have led to a better understanding of the mechanisms of leukemogenesis and may soon allow for differentiating treatments depending on baseline mutational complements. Some innovative drugs described in this article have strong therapeutic potential, but there is still a long way to go before actual success in targeted treatment.

Key words: immunotherapy, target therapy, acute myeloid leukemia

Cite as
Walasek A. The new perspectives of targeted therapy in acute myeloid leukemia. *Adv Clin Exp Med*. 2019;28(2):271–276. doi:10.17219/acem/81610

DOI
10.17219/acem/81610

Acute myeloid leukemia (AML) occurs in 3–4 people out of 100,000 with a median age of 67 years. The 5-year survival rate is 20%.[1] The course of the disease depends on many factors, including cytogenetics, molecular genetics, comorbidity score, and the patient's age. Long-term survival rates for patients <65 years of age and >65 years of age are 40% and 5%, respectively.[2] Complete remission (CR) is achieved in 66% of elderly patients; in this group, the disease reoccurs in 16% of cases.[3] Allogenic stem cell transplantation provides a chance for recovery from AML and longer overall survival (OS). The unsatisfactory results of previous AML treatment have encouraged the study of intracellular mechanisms that prolong the survival of leukemic cells and their resistance to apoptotic stimuli. These genetic changes have inspired the search for an effective targeted therapy. The first drug of this kind was all-trans retinoid acid (ATRA) in acute promyelocytic leukemia (APL), directed against the fusion of the genes *PML* and *RARA* caused by t(15;17). The use of ATRA, especially with arsenic trioxide (ATO), has spectacularly improved OS and disease-free survival (DFS).[4,5] Another turning point was the discovery of BCR-ABL kinase inhibitors. BCR-ABL kinase is formed by t(9;22), which is the most common mutation for chronic myeloid leukemia (CML), but which also occurs in acute myeloid leukemia (ALL) and in AML. Philadelphia chromosome-positive acute myeloid leukemia (AML Ph+) comprises 0.5–3% of AML cases.

The experiments conducted on leukemic cell lines, animal models and in clinical trials have led to the discovery of substances that can be classified according to their structure as having high or low molecular mass.[6] The data is presented in Table 1.

Table 1. Targeted drugs in AML treatment

Target	Drug	Group	
CD33	gemtuzumab ozogamycin, lintuzumab, vadastuximab talirine	high molecular mass drugs	
CD33, CD3	AMG 330		
FLT3	1st-generation: sorafenib, midostaurin, lestaurtinib, sunitinib, tandutinib, pacritinib; 2nd-generation: quizartinib, crenolamid, ponatinib, PLX3397, gliteritinib, JH-IX-179	tyrosine kinase inhibitors	low molecular mass drugs
PLK1	volasertib		
CDK	flavopiridol		
AURK	alisertib, barasertib		
PIM	AZD1208, SGI-1776		
IDH	cenasidenib	cell pathway inhibitors	
GLI	GANT61		
BCL-2	navitoclax, venetoclax		
NAE	pevonedistat		
topoisomerase II	vosaroxin		
BET	OTX015, ARV-825		
LSD1	ORY-1001, GSK2879552	epigenetic modulators	
HDAC	pabinostat, vorinostat		
DOTL1L	pinometostat		
PD1/PDL1	nivolumab		
MDM2	RG7112, idasanutlin		

FLT3 – FMS-like tyrosine kinase-3; PLK1 – polo-like kinase 1; CDK – cyclin-dependent kinases; AURK – aurora kinase; PIM – proviral insertion in +murine; IDH – isocitrate dehydrogenase; GLI – glioma; BCL-2 – B-cell lymphoma 2; NAE – NEDD8 activating enzyme; BET – bromodomain and extraterminal; LSD1 – lysine-specific demethylase; HDAC – histone deacetylase; PD1/PDL1 – programmed death-1/programmed death-1 ligand.

High molecular mass drugs

Gemtuzumab ozogamicin (GO, Mylotarg) is an immunoconjugate compound created by the CD33 antibody, which is present on the surface of the myeloblasts in over 90% of AML cases and is toxic to DNA calicheamicin.[7] An epitope for GO, CD33 antigen, occurs in many expression and functional variants, and only some of these epitopes are sensitive to the cytotoxicity caused by GO.[8] Despite GO withdrawal caused by toxicity in early clinical trials, subsequent trials have renewed the interest in this drug. In a meta-analysis of prospective phase III trials, it was proven that the use of GO in inductive therapy in variable age groups prolongs relapse-free survival (RFS) with tolerable adverse effects. Overall survival elongation thanks to GO was proven in most clinical trials in age-differentiated groups, but the benefit for patients with adverse cytogenetics is controversial. Promising effects were observed among fit patients >50 years old and >60 years old not qualified for allogenic stem cell transplantation (alloSCT). The results of these trials suggest the advantage of using GO in bridge therapy before alloSCT with other cytostatics.[9,10] Promising results were achieved with GO applied in AML relapse after stem cell transplantation (SCT) therapy. On September 1, 2017, the U.S. Food and Drug Agency (FDA) approved GO for treatment in adults with newly diagnosed CD33+ AML.

BI 836858, lintuzumab (SGN-33; HuM195) and vadastuximab talirine are new anti-CD33 antibodies. Lintuzumab used with standard chemotherapy resulted in OS prolongation in a group of previously untreated patients who were unfit for intensive chemotherapy, aged 60–87 years, with an intermediate or adverse prognosis.[11,12] The use of vadastuximab talirine is undergoing a phase III trial in a group of elderly patients.

AMG 330 (bispecific T-cell engager antibody [BiTE]) is a new antibody directed against both CD33 and CD3, which are present on the surface of T lymphocytes. Bispecific T-cell engager antibody was created to engage the cytotoxic response of T cells against leukemic cells

in order to avert their immunological escape.[13] It showed the best results among previously untreated AML patients with standard prognosis. In addition, tetravalent bispecific anti-CD33/CD3, bispecific anti-CD3 and C-type lectin-like molecule-1 (CCL-1), which can be found on most leukemic cells, are being investigated in animals.[14]

Ulocuplumab (BMS-936564/MDX-1338) is a monoclonal antibody which inhibits the binding of the CXC chemokine receptor 4 (CXCR4) to stimulate migration from the bone marrow to peripheral blood stromal cell-derived chemokine CXC motif ligand 12 (CXCL12). CXCR4 is overexpressed on AML blasts, among others. CXCR4 inhibition restricts AML cell growth and induces their apoptosis. In the first clinical trial on patients with relapsed/refractory AML, ulocuplumab in combination with mitoxantrone, etoposide and cytarabine led to CR with incomplete marrow recovery (CRi) in 51% of the group of 73 patients.[15] In December 2015, the FDA decided to use ulocuplumab as an orphan drug.

Low molecular mass drugs

The *FMS-like tyrosine kinase-3* (*FLT3*) gene mutations *FLT3-ITD* and *FLT3-TDK* occur in 30% and 7% of AML cases, respectively. The FLT3 kinase inhibitors may be divided into 1st- and 2nd-generation drugs. The first group (1st-generation) are polykinase inhibitors, while the newer drugs are more selective molecules, which makes them safer and more effective.[16] The mutated *FLT3* gene has variable sensitivity to different drugs.[17]

Sorafenib is a multikinase inhibitor. It inhibits C-RAF, FLT3, VEGFR2, VEGFR3, and PDGFR family kinases. The action of sorafenib is amplified by the activation of p-AMPK by metformin, which potentiates the proapoptotic and antiproliferative effect. Glycolysis inhibition also plays a synergistic role, which has been proven in an animal model.[18] According to the National Comprehensive Cancer Network (NCCN) guidelines, sorafenib is used in the treatment of refractory/recurrent AML, in monotherapy or with other drugs. Despite a higher response rate in *FLT3*+ patients than in *FLT3*- patients, sorafenib does not influence OS. In addition, it is not effective in elderly patients. When added to standard chemotherapy in patients younger than 60 years, sorafenib prolongs DFS.[19] Moreover, sorafenib is effective before and after SCT it prolongs DFS and OS, maintains remission in sustained therapy after SCT in 100% of patients, and has a hematological response >90% in AML recurrence after SCT.[20–22] Promising effects have been reported from combining sorafenib with hypomethylating agents, ATRA or homoharringtonin, especially in refractory AML.[23–25] The greatest antiproliferative and proapoptotic accuracy in preclinical trials on human leukemic cell lines was demonstrated with a composite of 3 kinase inhibitors: FLT3 (sunitinib), PI3K (PF-04691502) and GLI1/2 (GANT61).[26] The use of sunitinib with standard inductive and life-sustaining therapy showed no benefits because of toxicity. The combination of FLT3 and AKT inhibitors is associated with the induction of resistance due to the protective effect of stroma on leukemia cells.

Lestaurtinib is a multikinase inhibitor whose targets include JAK-2. Added to a standard first-line *FLT3*+ AML therapy, it does not provide any benefits.[27]

Midostaurin used in monotherapy or in combination with different cytostatics in intensive chemotherapy has prolonged OS with tolerable toxicity in *FLT3*+ AML patients: studies include the addition of midostaurin in inductive or consolidative therapy, in sustaining therapy, in AML relapse, and in bridge therapy before SCT.[28–31] The greatest benefits were observed in a group of patients who did not qualify for SCT previously untreated with FLT3 inhibitors. A promising effect was achieved in preclinical trials by a combination of ATRA and midostaurin due to the synergic effect against leukemic cells. Midostaurin combined with other drugs was registered by the FDA in the treatment of refractory/relapsed AML with the *FLT3* mutation.[32]

Crenolamid represents a new, selective FLT3 kinase inhibitor group. It is currently in phase II trials. There is a possible synergy in using it with sorafenib against leukemic cells.

Quizartinib (AC220) has a high affinity for wild-type and mutated FLT3 kinase and has successfully completed phase I trials on a pediatric *FLT3*+ AML population.[33] Its activity was demonstrated in refractory/relapse AML. AKN 028, a dose-dependent FLT3 kinase inhibitor that stops the cell cycle, is still being investigated. Gliteritinib is a selective FLT3/ASXL1 inhibitor. Used in a group of 80 patients with refractory/relapse FLT3+ AML, it resulted in a 55% response rate and it doubled OS. Gliteritinib is currently under investigation in supportive care and rescue therapy. Kinase inhibitors may generate secondary mutations.[34] In trials on human leukemic cells, *FLT3* mutations resistant to AC220 and sorafenib succumbed to a new kinase inhibitor, TT-3002. New molecules are being investigated, for example, AMG 925.

Volasertib (BI6727) is a polo-like kinase (PLK) inhibitor. Polo-like kinases play a key role in mitosis. There is higher PLK expression in AML, Hodgkin lymphoma (HL), non-small-cell lung cancer (NSCLC), and breast cancer, and its concentration correlates with mortality.[35] In preclinical trials on leukemic cells acquired from patients, volasertib proved effective in monotherapy and with antimetabolites, hypomethylating agents and quizartinib. Associated with small doses of cytarabine, it increased CR and DFS in a previously untreated group of patients who, in the investigators' opinion, were unfit for intensive chemotherapy. In 2016, volasertib was called a breakthrough drug in the treatment of AML by the FDA.[36]

Flavopiridol (alvocidib) is a cyclin-dependent kinase (CDK), which induces cell cycle arrest and apoptosis

in leukemic cells. The latest studies show no benefits over standard chemotherapy in previously untreated AML patients with an intermediate or adverse prognosis.

Alisertib (MLN8237) is an orally taken aurora kinase A (AurKA) inhibitor. Its synergy with cytarabine has been proven in preclinical tests. In phase II studies on a group of refractory/relapsed AML patients who did not qualify for standard chemotherapy, the disease was stabilized in nearly half of the patients.

Barasertib is an aurora kinase B (AurKB) inhibitor. It is more effective in prolonging OS in patients >60 years of age, but is more toxic in comparison with cytarabine. AZD1208 is an inhibitor of all proviral insertion in +murine (PIM) kinases, which in correlation with PIM1 expression inhibits the growth of 5 of the 14 AML cell lines, including *FLT3-ITD*+. The PIM kinase inhibitors show synergy with mTOR and AKT inhibitors in suppressing leukemic cells and in sensitizing AML cells to topoisomerase II inhibitors.[37] SGI-1776 acts similarly; it has also been tested in NCL2 inhibition.

Cell pathway inhibitors

Isocitrate dehydrogenase (IDH) takes part in lipid metabolism and the Krebs cycle, and it catalyzes the transformation of isocitrate to α-ketoglutarate. The *IDH1* and *IDH2* gene mutations occur in 11% and 12% of AML cases, respectively. Enasidenib (AG-221/CC-90007) is the first selective IDH2 inhibitor to induce the differentiation of leukemic cells.[38–40] Enasidenib is taken orally and is active in monotherapy. It has been well-tolerated in phase II studies on patients with refractory/relapsed AML and has achieved an overall response rate (ORR) of 40% with a median response duration of 6 months.[41] On August 1, 2017, enasidenib was approved by the FDA for the treatment of adult patients with relapsed/refractory AML with the *IDH2* mutation.

The expression of the glioma (GLI) family transcription factors, which are the last part of the Hedgehog proliferative signal pathway, is a negative prognostic factor in AML. This finding has inspired the search for GLI inhibitors.[42] The small-molecule inhibitor GANT61 is currently being studied.[43]

Navitoclax (ABT-263) is a BCL-2, BCL-XL and BCL-W protein family inhibitor. Its antitumor activity is restricted by adverse effects. Venetoclax (ABT-199) is a small-molecule antiapoptotic BCL-2 protein inhibitor which is registered by the FDA for treating chronic lymphocytic leukemia (CLL) and AML.[44] In a high-risk recurrent/refractory AML patient group, a 38% response rate was achieved, half of these being complete responses according to the International Working Group (IWG) criteria.[45]

There have been studies on molecules influencing the suppressor protein p53 pathway, for instance, the HDM2 inhibitor CGM097, which neutralizes the p53-inhibiting effect of HDM2 on AML cells.

Tosedostat is an aminopeptidase inhibitor that blocks the destruction and rebuilding of intercellular proteins. It is undergoing phase II trials. It was demonstrated on a group of patients >60 years of age with relapsed/refractory AML that tosedostat is active in monotherapy, dose-independently. In the same group with a negative prognosis, tosedostat combined with cytarabine and azacitidine achieved a 30% ORR. Used on elderly patients in inductive therapy with cytarabine or decitabine, it resulted in a CR or CRi of more than 50%.[46]

Pevonedistat (MLN4924) is an NEDD8-activating enzyme (NAE) inhibitor that controls the destruction of many proteins taking part in the cell cycle, signal transduction, the destruction of DNA, or the stress response, for example, p53, p27, cyclin E, c-MYC, phospho-IκBα, CDT-1, NRF-2, and HIF-1α. In preclinical tests, pevonedistat was effective in monotherapy in amplifying cytarabine action, but there was only a 20% response rate.

Vosaroxin is a topoisomerase II inhibitor which is essential for cell survival. Vosaroxin induces DNA destruction and is most effective among elderly patients diagnosed with AML or myelodysplastic syndrome (MDS). Phase III trials showed that vosaroxin prolongs survival by about 6 weeks.[47]

OTX015 is a BRD2/3/4 inhibitor indispensable for leukemic clone survival of c-MYC. OTX015 used in conjunction with pabinostat and azacitidine showed synergic activity towards KASUMI AML cell lines. ARV-825 was more effective against AML post-myeloproliferative cell lines than OTX015. Both drugs are in phase I trials.[48]

Epigenetic modulators

Lysine-specific demethylase 1 (LSD1) is a histone demethylase.[49] Its expression has been demonstrated in many neoplasms and it plays a role in the self-renewal of AML stem cells. LSD1 inhibition leads to the inhibition of tumor growth and metastasis. ORY-1001 and GSK2879552 are tranylcypromine-derivative LSD1 inhibitors, both in phase I trials.[50,51]

Panobinostat (LBH589) induces AML cell apoptosis in vitro by inhibiting the expression of repair proteins (e.g., BRCA1, CHK1 and RAD51), increasing the efficiency of cytarabine and daunorubicin, and it is promising in t(8;21) AML due to the pathological AML1/ETO protein that recruits histone deacetylases.[52]

Vorinostat (suberoylanilidehydroxamic acid [SAHA]) promotes cell cycle inhibition and arrested growth, and induces differentiation and AML cell apoptosis. In phase II trials with cytarabine on AML/MDS patients with severe concomitant diseases, there was a median OS >7 months with acceptable toxicity.[53]

Histone deacetylase inhibitors, such as pracinostat and entinostat, are under investigation in AML patients.[54,55]

Rearranged mixed lineage leukemia (rMLL) is associated with an aggressive disease course and a poor response

to multidrug chemotherapy, which is caused by a higher expression of HOXA9 and MEIS1.[56] Pinometostat (EPZ-5676) is a histone methyltransferase DOT1L enzyme inhibitor. *DOT1L* is the rMLL target gene. Pinometostat is undergoing phase I trials.[57]

The programmed death-1 (PD-1) receptor occurs on activated T cells and after binding with its programmed death 1 or 2 ligand (PDL-1, PDL-2), it suppresses T cell cytotoxic activity. This immunological escape has been presented in many cell lines, including AML. High PDL-1 expression correlates with an unfavorable course. Nivolumab is a PDL-1 inhibitor which has been approved by the FDA for treating non-small-cell lung cancer, melanoma and renal cancer. Nivolumab with azacitidine is now in phase II studies in relapsed AML patients. A remission rate of 18% was achieved in elderly patients with tolerable side effects.[58]

The suppressor gene *p53* is called a genome warden due to its prevention of the replication of defective genome material and it leads to apoptosis. The destruction of the p53 protein is proceeded by ubiquitination after connecting with the MDM2 protein. A high MDM2 concentration with wild-type p53 appears in about 90% of AML types. RG 7112 is a 1st-generation MDM2 inhibitor. In phase I clinical studies, RG 7112 was effective in refractory/relapsed AML and in CLL.[59]

Idasanutlin (R7388) is a selective, next-generation MDM2 inhibitor. There were promising effects of phase I trials in refractory/relapsed AML: the higher the MDM2 expression was, the better the response to the drug was.[60] Idasanutlin is better tolerated than RG 7112.

Despite the growing interest awakened by targeted therapy in AML treatment, the current results are unsatisfactory. Undoubtedly, this is due to the complexity of leukemogenic mechanisms. There is potential for further investigations and clinical studies to improve AML therapy. All in all, each study brings us closer to achieving success in AML therapy.

References

1. Kell J. Considerations and challenges for patients with refractory and relapsed acute myeloid leukaemia. *Leuk Res*. 2016;47:149–160. doi:10.1016/j.leukres.2016.05.025
2. Almeida AM, Ramos F. Acute myeloid leukemia in the older adults. *Leuk Res Rep*. 2016;16(6):1–7. doi:10.1016/j.lrr.2016.06.001
3. von dem Borne PA, de Wreede LC, Halkes CJ, Marijt WA, Falkenburg JH, Veelken H. Effectivity of a strategy in elderly AML patients to reach allogeneic stem cell transplantation using intensive chemotherapy: Long-term survival is dependent on complete remission after first induction therapy. *Leuk Res*. 2016;46:45–50. doi:10.1016/j.leukres.2016.03.010
4. Kayser S, Krzykalla J, Elliott MA, et al. Characteristics and outcome of patients with therapy-related acute promyelocytic leukemia frontline treated with or without arsenic trioxide. *Leukemia*. 2017;31(11):2347–2354. doi:10.1038/leu.2017.92
5. Platzbecker U, Avvisati G, Cicconi L, et al. Improved outcomes with retinoic acid and arsenic trioxide compared with retinoic acid and chemotherapy in non-high-risk acute promyelocytic leukemia: Final results of the randomized Italian-German APL0406 trial. *J Clin Oncol*. 2017;35(6):605–612. doi:10.1200/JCO.2016.67.1982
6. Hołowiecki J, Hołowiecka A. Targeted therapy in acute myeloid leukemia [in Polish]. *Acta Haematol Pol*. 2013;44(2):85–92.
7. De Witte T, Amadori S. The optimal dosing of gemtuzumab ozagamicin: Where to go from here? *Haematologica*. 2016;101(6):653–654. doi:10.3324/haematol.2016.145763
8. Laszlo GS, Harrington KH, Gudgeon CJ, et al. Expression and functional characterization of CD33 transcript variants in human acute myeloid leukemia. *Oncotarget*. 2016;7(28):43281–43294. doi:10.18632/oncotarget.9674
9. Paubelle E, Ducastelle-Leprêtre S, Labussière-Wallet H, et al. Fractionated gemtuzumab ozogamicin combined with intermediate-dose cytarabine and daunorubicin as salvage therapy in very high-risk AML patients: A bridge to reduced intensity conditioning transplant? *Ann Hematol*. 2017;96(3):363–371. doi:10.1007/s00277-016-2899-0
10. Zahler S, Bhatia M, Ricci A, et al. A phase I study of reduced-intensity conditioning and allogeneic stem cell transplantation followed by dose escalation of targeted consolidation immunotherapy with gemtuzumab ozogamicin in children and adolescents with CD33+ acute myeloid leukemia. *Biol Blood Marrow Transplant*. 2016;22(4):698–704. doi:10.1016/j.bbmt.2016.01.019
11. Bixby DA, Fathi AT, Kovacsovics TJ, et al. Vadastuximab talirine monotherapy in older patients with treatment naive CD33-positive acute myeloid leukemia (AML) *Blood*. 2016;128(22):590.
12. Erba HP, Vasu S, Stein AS, et al. A phase 1b study of vadastuximab talirine in combination with 7+3 induction therapy for patients with newly diagnosed acute myeloid leukemia (AML). *Blood*. 2016;128 (22):211.
13. Masarova L, Kantarjian H, Garcia-Mannero G, Ravandi F, Sharma P, Daver N. Harnessing the immune system against leukemia: Monoclonal antibodies and checkpoint strategies for AML. *Adv Exp Med Biol*. 2017;995:73–95. doi:10.1007/978-3-319-53156-4_4
14. Leong SR, Sukumaran S, Hristopoulos M, et al. An anti-CD3/anti-CLL-1 bispecific antibody for the treatment of acute myeloid leukemia. *Blood*. 2017;129(5):609–618. doi:10.1182/blood-2016-08-735365
15. Cho BS, Kim HJ, Konopleva M. Targeting the CXCL12/CXCR4 axis in acute myeloid leukemia: From bench to bedside. *Korean J Intern Med*. 2017;32(2):248–257. doi:10.3904/kjim.2016.244
16. Hassanein M, Almahayni MH, Ahmed SO, Gaballa S, El Fakih R. FLT3 inhibitors for treating acute myeloid leukemia. *Clin Lymphoma Myeloma Leuk*. 2016;16(10):543–549. doi:10.1016/j.clml.2016.06.002
17. Nguyen B, Williams AB, Young DJ, et al. FLT3 activating mutations display differential sensitivity to multiple tyrosine kinase inhibitors. *Oncotarget*. 2017;8(7):10931–10944. doi:10.18632/oncotarget.14539
18. Ju HQ, Zhan G, Huang A, et al. ITD mutation in FLT3 tyrosine kinase promotes Warburg effect and renders therapeutic sensitivity to glycolytic inhibition. *Leukemia*. 2017;31(10):2143–2150. doi:10.1038/leu.2017.45
19. Roolf C, Dybowski N, Sekora A, et al. Phosphoproteome analysis reveals differential mode of action of sorafenib in wildtype and mutated FLT3 AML cells. *Mol Cell Proteomics*. 2017;16(7):1365–1376. doi:10.1074/mcp.M117.067462
20. Battipaglia G, Ruggeri A, Massoud R, et al. Efficacy and feasibility of sorafenib as a maintenance agent after allogeneic hematopoietic stem cell transplantation for Fms-like tyrosine kinase 3-mutated acute myeloid leukemia. *Cancer*. 2017;123(15):2867–2874. doi:10.1002/cncr.30680
21. De Freitas T, Marktel S, Piemontese S, et al. High rate of hematological responses to sorafenib in FLT3-ITD acute myeloid leukemia relapsed after allogeneic hematopoietic stem cell transplantation. *Eur J Haematol*. 2016;96(6):629–636. doi:10.1111/ejh.12647
22. Brunner AM, Li S, Fathi AT, et al. Haematopoietic cell transplantation with and without sorafenib maintenance for patients with FLT3-ITD acute myeloid leukaemia in first complete remission. *Br J Haematol*. 2016;175(3):496–504. doi:10.1111/bjh.14260
23. Ernst J, Schäfer V, Rinke J, et al. Continuous molecular remission and regression of side effects after discontinuation of salvage therapy with sorafenib and donor lymphocyte infusions in a young patient with relapsed AML. *Ann Hematol*. 2016;95(6):1027–1030. doi:10.1007/s00277-016-2637-7
24. Wang R, Xia L, Gabrilove J, Waxman S, Jing Y. Sorafenib inhibition of Mcl-1 accelerates ATRA-induced apoptosis in differentiation-responsive AML cells. *Clin Cancer Res*. 2016;22(5):1211–1221. doi:10.1158/1078-0432.CCR-15-0663

25. Lam SS, Ho ES, He BL, et al. Homoharringtonine (omacetaxine mepesuccinate) as an adjunct for FLT3-ITD acute myeloid leukemia. *Sci Transl Med.* 2016;8(359):359ra129.
26. Latuske EM, Stamm H, Klokow M, et al. Combined inhibition of GLI and FLT3 signaling leads to effective anti-leukemic effects in human acute myeloid leukemia. *Oncotarget.* 2017;8(17):29187–29201. doi:10.18632/oncotarget.16304
27. Knapper S, Russell N, Gilkes A, et al. A randomized assessment of adding the kinase inhibitor lestaurtinib to first-line chemotherapy for FLT3-mutated AML. *Blood.* 2017;129(9):1143–1154. doi:10.1182/blood-2016-07-730648
28. Gallogly MM, Lazarus HM. Midostaurin: An emerging treatment for acute myeloid leukemia patients. *J Blood Med.* 2016;7:73–83. doi:10.2147/JBM.S100283
29. Starr P. Midostaurin the first targeted therapy to improve survival in AML: Potentially practice-changing. *Am Health Drug Benefits*. 2016;9(Spec Issue):1–21.
30. Mazzarella L. Orlando Magic: Report from the 57th meeting of the American Society of Haematology, 5–7 December 2015, Orlando, USA. *Ecancermedicalscience.* 2016;10:612. doi:10.3332/ecancer. 2016.612.
31. Smuga-Otto K. Midostaurin + chemo ups AML survival. *Cancer Discov.* 2016;6(2):OF2. doi:10.1158/2159-8290.CD-NB2015-177
32. Levis M. Midostaurin approved for FLT3-mutated AML. *Blood.* 2017;129(26):3403-3406. doi:10.1182/blood-2017-05-782292
33. Cooper TM, Cassar J, Eckroth E, et al. A phase I study of quizartinib combined with chemotherapy in relapsed childhood leukemia: A Therapeutic Advances in Childhood Leukemia & Lymphoma (TACL) Study. *Clin Cancer Res*. 2016;22(16):4014–4022. doi:10.1158/1078-0432.CCR-15-1998
34. Kasi PM, Litzow MR, Patnaik MM, Hashmi SK, Gangat N. Clonal evolution of AML on novel FMS-like tyrosine kinase-3 (FLT3) inhibitor therapy with evolving actionable targets. *Leuk Res Rep.* 2016;5:7–10. doi:10.1016/j.lrr.2016.01.002
35. Talati C, Griffiths EA, Wetzler M, Wang ES. Polo-like kinase inhibitors in hematologic malignancies. *Crit Rev Oncol Hematol*. 2016;98:200–210. doi:10.1016/j.critrevonc.2015.10.013
36. van den Bossche J, Lardon F, Deschoolmeester V, et al. Spotlight on volasertib: Preclinical and clinical evaluation of a promising Plk1 inhibitor. *Med Res Rev.* 2016;36(4):749–786. doi:10.1002/med.21392
37. Doshi KA, Trotta R, Natarajan K, et al. Pim kinase inhibition sensitizes FLT3-ITD acute myeloid leukemia cells to topoisomerase 2 inhibitors through increased DNA damage and oxidative stress. *Oncotarget*. 2016;7(30):48280–48295. doi:10.18632/oncotarget.10209
38. Amatangelo MD, Quek L, Shih A, et al. Enasidenib induces acute myeloid leukemia cell differentiation to promote clinical response. *Blood.* 2017;130(6):732–741. doi:10.1182/blood-2017-04-779447
39. Travins J, Wang F, David MD, et al. AG-221, a first-in-class therapy targeting acute myeloid leukemia harboring oncogenic IDH2 mutations. *Cancer Discov.* 2017;7(5):478–493. doi:10.1158/2159-8290.CD-16-1034
40. Kats LM, Vervoort SJ, Cole R, et al. A pharmacogenomic approach validates AG-221 as an effective and on-target therapy in IDH2 mutant AML. *Leukemia.* 2017;31(6):1466–1470. doi:10.1038/leu.2017.84
41. Stein EM, DiNardo CD, Pollyea DA, et al. Enasidenib in mutant-IDH2 relapsed or refractory acute myeloid leukemia. *Blood.* 2017;130(6):722–731. doi:10.1182/blood-2017-04-779405
42. Long B, Wang LX, Zheng FM, et al. Targeting GLI1 suppresses cell growth and enhances chemosensitivity in CD34+ enriched acute myeloid leukemia progenitor cells. *Cell Physiol Biochem.* 2016;38(4):1288–1302. doi:10.1159/000443075
43. Masetti R, Bertuccio SN, Astolfi A, et al. Hh/Gli antagonist in acute myeloid leukemia with CBFA2T3-GLIS2 fusion gene. *J Hematol Oncol.* 2017;10(1):26. doi:10.1186/s13045-017-0396-0
44. Soderquist R, Eastman A. BCL2 Inhibitors as anticancer drugs: A plethora of misleading BH3 mimetics. *Mol Cancer Ther.* 2016;15(9):2011–2017. doi:10.1158/1535-7163.MCT-16-0031
45. Ruvolo PP, Ruvolo VR, Benton CB, et al. Combination of galectin inhibitor GCS-100 and BH3 mimetics eliminates both p53 wild type and p53 null AML cells. *Biochim Biophys Acta.* 2016;1863(4):562–571. doi:10.1016/j.bbamcr.2015.12.008
46. Mawad R, Becker PS, Hendrie P, et al. Phase II study of tosedostat with cytarabine or decitabine in newly diagnosed older patients with acute myeloid leukaemia or high-risk MDS. *Br J Haematol.* 2016;172(2):238–245. doi:10.1111/bjh.13829
47. Jamieson GC, Fox JA, Poi M, Strickland SA. Molecular and pharmacologic properties of the anticancer quinolone derivative vosaroxin: A new therapeutic agent for acute myeloid leukemia. *Drugs.* 2016;76(13):1245–1255. doi:10.1007/s40265-016-0614-z
48. Saenz DT, Fiskus W, Qian Y, et al. Novel BET protein proteolysis-targeting chimera exerts superior lethal activity than bromodomain inhibitor (BETi) against post-myeloproliferative neoplasm secondary (s) AML cells. *Leukemia.* 2017;31(9):1951–1961. doi:10.1038/leu.2016.393
49. Maiques-Diaz A, Somervaille TC. LSD1: Biologic roles and therapeutic targeting. *Epigenomics.* 2016;8(8):1103–1116. doi:10.2217/epi-2016-0009
50. Zheng YC, Yu B, Jiang GZ, et al. Irreversible LSD1 inhibitors: Application of tranylcypromine and its derivatives in cancer treatment. *Curr Top Med Chem.* 2016;16(19):2179–2188.
51. Przespolewski A, Wang ES. Inhibitors of LSD1 as a potential therapy for acute myeloid leukemia. *Expert Opin Investig Drugs*. 2016;25(7):771–780. doi:10.1080/13543784.2016.1175432
52. Zhao J, Xie C, Edwards H, Wang G, Taub JW, Ge Y. Histone deacetylases 1 and 2 cooperate in regulating BRCA1, CHK1, and RAD51 expression in acute myeloid leukemia cells. *Oncotarget.* 2017;8(4):6319–6329. doi:10.18632/oncotarget.14062
53. Montalban-Bravo G, Huang X, Jabbour E, et al. A clinical trial for patients with acute myeloid leukemia or myelodysplastic syndromes not eligible for standard clinical trials. *Leukemia.* 2017;31(2):318–324. doi:10.1038/leu.2016.303
54. Norsworthy KJ, Cho E, Arora J, et al. Differentiation therapy in poor risk myeloid malignancies: Results of companion phase II studies. *Leuk Res.* 2016;49:90–97. doi:10.1016/j.leukres.2016.09.003
55. Prebet T, Sun Z, Ketterling RP, et al.; Eastern Cooperative Oncology Group and North American Leukemia intergroup. Azacitidine with or without Entinostat for the treatment of therapy-related myeloid neoplasm: Further results of the E1905 North American Leukemia Intergroup study. *Br J Haematol.* 2016;172(3):384–391. doi:10.1111/bjh.13832
56. Waters NJ. Preclinical pharmacokinetics and pharmacodynamics of pinometostat (EPZ-5676), a first-in-class, small molecule s-adenosyl methionine competitive inhibitor of DOT1L. *Eur J Drug Metab Pharmacokinet.* 2017;42(6):891–901. doi:10.1007/s13318-017-0404-3
57. Smith SA, Gagnon S, Waters NJ. Mechanistic investigations into the species differences in pinometostat clearance: Impact of binding to alpha-1-acid glycoprotein and permeability-limited hepatic uptake. *Xenobiotica.* 2017;47(3):185–193. doi:10.3109/00498254.2016.1173265
58. Daver N, Basu S, Garcia-Manero G, et al. Phase Ib/II study of nivolumab in combination with azacitidine (AZA) in patients (pts) with relapsed acute myeloid leukemia (AML). Abstract #763. Presented at the ASH Annual Meeting and Exhibition, December 6, 2016; San Diego, CA.
59. Andreeff M, Kelly KR, Yee K, et al. Results of the phase I trial of RG 7112, a small-molecule MDM2 antagonist in leukemia. *Clin Cancer Res.* 2016;22(4):868–876. doi:10.1158/1078-0432.CCR-15-0481
60. Reis B, Jukofsky L, Chen G, et al. Acute myeloid leukemia patients' clinical response to idasanutlin (RG7388) is associated with pre-treatment MDM2 protein expression in leukemic blasts. *Haematologica.* 2016;101(5):e185–188. doi:10.3324/haematol.2015.139717

Interactions between platelets and leukocytes in pathogenesis of multiple sclerosis

Angela Dziedzic[A–E], Michał Bijak[A–F]

Department of General Biochemistry, Faculty of Biology and Environmental Protection, University of Lodz, Poland

A – research concept and design; B – collection and/or assembly of data; C – data analysis and interpretation;
D – writing the article; E – critical revision of the article; F – final approval of the article

Advances in Clinical and Experimental Medicine, ISSN 1899-5276 (print), ISSN 2451-2680 (online) *Adv Clin Exp Med*. 2019;28(2):277–285

Address for correspondence
Angela Dziedzic
E-mail: angela.dziedzic@unilodz.eu

Funding sources
This work was supported with funding from scientific research grant from the Polish National Science Centre (No. UMO-2016/21/B/NZ4/00543) as well as with University of Lodz grant (No. 506/1136).

Conflict of interest
None declared

Received on November 20, 2017
Reviewed on January 17, 2018
Accepted on January 18, 2018

Published online on September 6, 2018

Abstract

Neurodegenerative diseases are an increasing problem in the modern world. Multiple sclerosis (MS) is a major human demyelinating and degenerative disease of the central nervous system (CNS). There are many reports that point to the significant role of platelet–leukocyte interaction in neurodegenerative diseases and cardiovascular disturbances. Epidemiological studies confirm the high risk of cardiovascular diseases in patients with MS. The pathophysiology mechanisms of this multi-component disease are very complex and involve various types of cells. There is increasing evidence that some co-stimulatory pathways affect the function of inflammatory cells, both in the periphery and in the CNS. Interactions of leukocytes and endothelial cells (ECs) could be significantly modulated in the presence of activated blood platelets. The supposed role of activated platelets in the development of vessel inflammatory response is due to their ability to adhere to inflamed ECs or proteins included in the subendothelial layer of the blood vessel wall, as well as to the ability of platelets to form aggregates with leukocytes. Blood platelets are able to directly activate leukocytes through a receptor-dependent mechanism or, indirectly, by biologically active compounds secreted from their granules. Cell–cell interactions provide critical mechanisms by which platelets link thrombosis, inflammation and related processes, such as diapedesis and leukocyte infiltration, to the affected vessel. Determining the relationship between platelet–leukocyte interactions and the development of neuroinflammation in the course of MS may provide new therapeutic targets in the future.

Key words: blood platelets, multiple sclerosis, neuroinflammation, platelet-leukocyte aggregates

Cite as
Dziedzic A, Bijak M. Interactions between platelets and leukocytes in pathogenesis of multiple sclerosis. *Adv Clin Exp Med*. 2019;28(2):277–285. doi:10.17219/acem/83588

DOI
10.17219/acem/83588

Introduction

Neuroinflammation is an inflammation of the nervous tissue, whereas neurodegeneration is the progressive loss of structure and function of neurons in specific regions of the central nervous system (CNS), which is a significant microenvironment for the proper functioning of neurons.[1,2] The neurodegeneration is a term that embraces a broad range of clinical diseases with chronic inflammation, of which the most common are multiple sclerosis (MS), Alzheimer's disease (AD) and Parkinson's disease (PD). Multiple sclerosis is one of the most frequently occurring disorders of neurological disability among young adults, typically appearing between the age of 20 and 40. It affects around 2.3 million people worldwide, of whom roughly 600,000 live in Europe.[3] Multiple sclerosis is a chronic, demyelinating neurodegenerative disease of the CNS with a complex of different clinical courses and a number of pathophysiological mechanisms, such as axonal/neuronal damage, neuroinflammation, demyelination, gliosis, and remyelination. The pathomechanism of MS is based on alterations of the immune system together with biochemical disturbances and a disruption of blood–brain barrier (BBB). The blood–brain barrier is a structural complex composed of matrix components and several cell types (e.g., endothelial cells (ECs), pericytes, perivascular microglia, and astrocytes). These barriers are responsible for supporting metabolic homeostasis and immune regulation of CNS.[4]

Blood platelets are a key element in maintaining physiological hemostasis. Hemostasis is a complex of physiological processes that ensure vascular tightness and circulating blood flow, and inhibit bleeding after breaking the continuity of a blood vessel. Numerous interacting elements are involved in the maintenance of normal hemostasis, including blood vessel wall, blood platelets, coagulation cascade, fibrinolytic system, and phagocytic cells. Damage to ECs and exposure of the thrombogenic adhesion proteins lead to platelet activation and initiation of coagulation cascade. This is accomplished by forming a stable platelet plug via adhesion to the revealed subendothelial matrix proteins (e.g., von Willebrand factor (vWF) and collagen). The platelet membrane is rich in glycoproteins (GP Ia-IIa/$\alpha_2\beta_1$, GP Ib-V-IX, GP Ic-IIa/$\alpha_5\beta_1$, GP IIb-IIIa/$\alpha_{IIb}\beta_3$, and GP IV), which bind to activate platelets and serve a primarily adhesive function. Throughout the interaction with the ECs, platelets become partly active, accordingly changing their shape from a discoid to a pseudopodia state.[5] Activation results in platelet aggregation by binding GP IIb-IIIa to fibrinogen, which ultimately results in the formation of a stable platelet plug.[6]

Interestingly, epidemiological studies confirm that there is an increased risk of cardiovascular disease in patients with MS, especially of prothrombotic events fairly associated with decreased hemostatic platelet activity. Platelets have been recognized as the smallest blood cells that fulfill a complex role in hemostasis/thrombosis and also in inflammation. Platelets possess a large variety of molecules stored in their granules, including numerous membrane receptors, immunomodulatory mediators and cell adhesion molecules. There is a link between platelets and pathophysiology of MS, and these small cells may be a key player in neuroinflammation. Activated platelets are responsible for the interaction with leukocytes and initiate increased infiltration of autoreactive T cells, which form new neuroinflammatory lesions in CNS.[7]

Biological active substances derived from blood platelets

Platelets are one of the most abundant cells in the circulatory system, which contain numerous biologically active compounds that are stored in their granules and release them during activation. Those signaling substances play a key role in the continuous communication of platelets with other platelets, immune cells and ECs. The capacity of blood platelets to secrete from their storage vast amounts of cytokines, chemokines and other related molecules appears closely related to their role in hemostasis and inflammation. Circulating platelets are inactive until they adhere to exposed subendothelial matrix proteins or are stimulated by soluble agonists. Each activating event is associated with a change in platelet shape, cytoskeletal reorganization and the secretion of platelet granules.[8] Proteins involved in the behavior of physiological hemostasis include fibrinogen, vWF, vitronectin, fibronectin, thrombospondin, factor V, factor VIII, coagulation factors, fibrinolytic inhibitors, mitogens, adhesion molecules, and membrane glycoproteins (GP Ib, IIb and IIIa).[9] During activation, the platelets expose a vast number of surface-bound molecules stored in their α-granules, such as inflammatory cytokines (e.g., CD40L or interleukin (IL)–1β), resulting in endothelial activation and the secretion of chemoattractants, such as platelet activation factor (PAF), chemokines platelet factor (PF4) and RANTES/CCL5 (regulated on activation normal T-cells expressed and secreted). Furthermore, dense granule constituents, such as serotonin, adenosine 5'-triphosphate (ATP), adenosine 5'-diphosphate (ADP), polyphosphates, and glutamate, are known as modifiers of platelet activation and thrombus formation, but many have also immune cell-modifying effects.[10] PF4/CXCL4 is one of the most abundant proteins belonging to the CXC-subfamily of chemokines, synthesized in megakaryocytes, enclosed in vesicles and transferred to the α-granules from which it is secreted during platelet activation (it represents 25% of α-granule storage). Basal concentration of PF4 in human plasma is 2–20 ng/mL. The PF4 has many cell targets, such as neutrophils, monocytes/macrophages and T-cells. It has a wide scope of activities related to innate immunity, including effects on monocyte and neutrophil chemotaxis.[11] The PF4 initiates a signal transduction cascade in monocytes, leading to the induction of a wide spectrum of functions, including phagocytosis, respiratory burst, monocyte

survival, and the secretion of cytokines. It activates neutrophils by binding to the proteoglycan chondroitin sulfate on the surface of neutrophils. The PF4 can promote the release of neutrophil granules and enhanced adhesion neutrophils to ECs. It induces monocyte release of cytokines, such as CXCL3, CXCL8, IL-1α, IL-1β, IL-6, IL-19, tumor necrosis factor α (TNF-α), CCL2, CCL3, and CCL22.[12] Moreover, CXCL4 also expresses immunomodulatory activities, such as downregulation of interferon production by type 1 T-helper (Th1) cells, up-regulation of IL-4, IL-5, and IL-13 in type 2 T-helper (Th2) cells. The PF4 inhibits the production of Th1 cytokines and promotes the production of Th2 cytokines through the interaction with CXCR3-B receptor.[13] Chemokine (C-C motif) ligand 5 (CCL5), also known as RANTES (regulated on activation, normal T cell expressed and secreted), is a CC-subfamily of chemokines produced by extravascular cells. Chemotaxis induced by RANTES is dependent on the activation of p38 mitogen-activated protein kinase (MAPK) pathway. The RANTES and monocyte chemoattractant protein-1 (MCP-1/CCL2) induce tissue fibroblasts to produce IL-6 and IL-8. The RANTES can also promote IL-2 and IL-5 expression in T cells. The synthesis of IL-1, TNF-α, and IL-6 can be stimulated by macrophages-derived inflammatory protein-1 (MIP-1/CCL3).[14] Schober et al. observed that the blockade of RANTES is a powerful tool to inhibit monocyte recruitment on different ECs types, which impairs macrophage infiltration.[15]

Furthermore, platelet-derived IL-1α (but not IL-1β) stored in α-granules is capable of activating peripheral ECs, and mediates platelets-promoted leukocyte infiltration in peripheral tissues, which also enhances transendothelial migration of neutrophils (TEM). Measurements of platelet and leukocyte IL-1α level indicate that the expression of platelet-derived IL-1α was 3.6-fold higher compared with the levels expressed by leukocyte populations, suggesting that blood platelets are the main source of IL-1α. The study conducted by Thornton et al. showed that platelet-secreted IL-1α drives endothelial activation in a mouse brain, which can lead to the release of endothelial intercellular adhesion molecule 1 (ICAM-1), vascular cell adhesion protein 1 (VCAM-1) and CXCL1 chemokine. Low concentrations of IL-1α released from platelets during activation induce significant brain endothelium activation. Mouse brain endothelium is very sensitive to IL-1α, with concentrations as low as 1.5 pM being able to induce CXCL1 secretion and enhance CAM expression, which suggests that local release of platelet IL-1α could mediate cerebrovascular inflammation in vivo.[16]

Interactions between platelets and leukocytes in inflammation

The proinflammatory activity of blood platelets occurs through a variety of mechanisms, including receptor-ligand connection and activation of different cells, as well as through the release of severe biologically active molecules stored in their granules. This bidirectional process is called cellular cross-talk.[17] Platelets possess a wide array of glycoprotein membrane receptors that are crucial for their interactions with other platelets, leukocytes and ECs. Platelets are expressed by a few members of the β1-subfamily integrins ($\alpha_{II}\beta_1$ and $\alpha_v\beta_1$), and β3-subfamily integrins ($\alpha_v\beta_3$ and $\alpha_{IIb}\beta_3$), that support platelet adhesion to the endothelial cell-matrix proteins, such as collagen, fibronectin and laminin.[18] GP IIb-IIIa (also known as $\alpha_{IIb}\beta_3$) is a receptor for fibrinogen, vWF, fibronectin, and vitronectin, which is definitely a major initiator of platelet aggregation. The formation of hemostatic plug is determined, to a large extent, by the integrin GP IIb-IIIa-mediated interactions of platelets with their receptors.[19] There are several possible connections between platelets and leukocytes. The main interaction between platelets and leukocytes, which is responsible for the formation of platelet-leukocyte aggregates (PLAs), is the connection between platelet P-selectin (CD62P) and leukocyte P-selectin glycoprotein ligand-1 (PSGL-1). Platelets are a major source of CD62P in the circulatory system.[20] CD62P is a membrane glycoprotein heavily present in platelet α-granules and Weibel-Palade bodies in ECs that is exposed on the platelet surface during activation. CD62P/PSGL-1 interaction has a functionally key role in leukocyte rolling and adhesion to platelets and endothelium, which are the main step in the process of leukocyte recruitment and extravasation.[21] PSGL-1 protein is also expressed on all T-cells types. In murine models, CD62P-positive platelets mediate adhesion of leukocytes into endothelium leading to the recruitment of T-cells to the place of inflammation/injury.[22] Individual leukocyte subpopulation demonstrates different affinity for CD62P present on platelets surface. From all leukocytes, monocytes show the greatest affinity for platelet CD62P, and thus to the formation of platelet-leukocyte aggregates.[23] It is known that PSGL-1 is likely to be a prevailing ligand for CD62P. Interestingly, Hirata et al. have confirmed that PSGL-1 on Th1 cells functions is the only ligand for CD62P and E-selectin in vivo.[24] It is worth noticing that most lymphocytes express PSGL-1 on their surface, but only 10–20% of them are actually able to bind platelet CD62P. To make a connection with P-selectin, PSGL-1 ligand needs to be post-translationally modified by protein glycosylation and tyrosine sulfation.[25] Abundant adhesion connections have been identified and implicated in the leukocyte transmigration process. Leukocyte recruitment occurs at the sites of vascular injury, where the subendothelial proteins have been externalized and activated platelets have been deposited. The initial tethering and rolling of leukocytes are followed by their strong adhesion and platelet migration, which depends on macrophage antigen 1 (Mac-1,$\alpha_M\beta_2$, CD11b/CD18). The initial link between platelets and leukocytes (CD62P/PSGL-1) leads to increased expression of Mac-1 on leukocytes, which itself supports interactions with platelets. Mac-1 can also interact with GP IbA present on platelets, which mediate adhesive

interactions between leukocytes and platelets. Wang et al. had observed that leukocyte recruitment markedly had been decreased by 73% in the case of CD62P deficiency on the platelet surface and 67% in the lack of Mac-1, suggesting that leukocyte recruitment is largely dependent on the aforementioned interactions.[26] Simon et al. observed that the binding of neutrophils from wild-type (Mac-$1^{+/+}$) and Mac-1-deficient (Mac-$1^{-/-}$) mice to GP IbA. Mac-$1^{+/+}$ neutrophils bound to adherent platelet; however, Mac-$1^{-/-}$ neutrophils demonstrated markedly reduced adhesion to platelets, which implies that the predominant interaction between neutrophils and platelets occurs between Mac-1 and GP IbA. The specificity of the interaction was that neutrophils from wild-type mice (but not from Mac-$1^{-/-}$ mice) bound to adherent platelet GP IbA. These studies demonstrate that GPIbA is a physiologically relevant ligand for Mac-1 and is critical to leukocyte function in vivo.[27] Binding of platelet endothelial cell adhesion molecule-1 (PECAM-1/CD31), ICAM-2/CD102, CD99, and members of the junctional adhesion molecule (JAM) family (e.g., JAM-A and JAM-C) with leukocyte ligands may assist in leukocyte transendothelial migration. ICAM-2, JAM-A and PECAM-1 are all members of the immunoglobulin superfamily of adhesion molecules. Woodfin et al. have observed that the lack of ICAM-2 in a murine asthma model has delayed the increase in eosinophil infiltration. Those findings indicate that the adhesion molecules ICAM-2, JAM-A and PECAM-1 can support neutrophil emigration through venular walls in a highly organized and regulated manner after local ECs activation. These studies may suggest that adhesion molecules may play a crucial role in mediating physiologic leukocyte infiltration as part of the immune response. There is a vast number of evidence demonstrating that the EC molecules support neutrophil transmigration in vivo in a stimulus-dependent way.[28]

Despite the lack of cell nucleus, the platelets contain stable mRNA transcripts that can synthesize de novo the proteins involved in maintaining physiological hemostasis and inflammatory process. For hemostasis, platelets synthesized proteins, including coagulation factor XI, tissue factor (TF), GP Iib-IIIa,[29] and cyclooxygenase (COX).[29,30] Proteins involved in inflammation, synthesized by platelets, are IL-1β and chemokine RANTES.[31] The mRNA transcript for IL-1β are constitutively present in platelet polysomes. Platelet activation induces a rapid and sustained synthesis of pro-IL-1β protein. A portion of the IL-1β is shed in its mature form in membrane microvesicles and induces adhesiveness of human ECs for neutrophils. Lindeman et al. recently found that IL-1β acts in concert with CD62P to induce expression of COX-2, when human monocytes interact with activated platelets.[32] Interleukin 1-β and IL1R1 are associated with the innate immune system and can regulate both megakaryocyte and platelet functions in human models. Platelet IL-1β through IL1R1 can stimulate megakaryocyte maturation and modify the RNA profiles in the evolving platelets to be prothrombotic and proinflammatory. The presence of IL-1β stimulates ECs to secrete their chemotactic proteins. Interleukin 1β affects the endothelium layer and smooth muscle cells by stimulating inflammation, and initiates platelet adhesion to ECs. NFκB pathway can be activated by myeloid differentiation primary response gene 88 (*MYD88*), which stimulates it through IL1R1 and its ligand IL-1β. This process also enhances the expression of other immune-related cytokines, growth factors and adhesion molecules.[33] Studies conducted by Dixon et al. show that activated platelet interactions with PSGL-1 on the monocytes enhance COX-2 expression and increase synthesis of prostaglandin E2 by monocytes via molecular mechanisms involving cellular adhesion and cytokine signaling.[30]

Role of blood platelets in neuro-inflammation and neurodegenerative diseases

One of the major hallmarks of MS is chronic inflammation. There are a vast number of different inflammatory effectors, which can be responsible for the neuronal/axonal pathology in MS.[34] Multiple sclerosis is a chronic inflammatory disease of the CNS. The association between chronic inflammation and subsequent cancer is well-established, and chronic inflammation is thought to have a role in both the initiation and promotion of neoplasms. Chronic inflammation has been hypothesized to play a role in triggering clonal evolution in myeloproliferative neoplasms (MPNs) which are stem-cell-derived disorders causing overproduction of 1 or more of blood elements, including essential thrombocythemia. In this context, it is important to note the unusual concurrence of MS and MPNs in 5 patients from a localized geographic area in Denmark. It is highly interesting to recognize the potentially common factors predisposing patients to both MS and MPNs.[35] Further studies are needed to clarify if any association between MS and MPNs indeed exists, especially that essential thrombocythemia may contribute to the increased risk of cardiovascular disease, especially ischemic stroke, myocardial infarction and thrombosis observed in MS.[36–38] Symptoms of MPNs associated with essential thrombocythemia may be underdiagnosed in MS patients, since many different possible reasons of high risk of tromboembolism events have inclinations in MS. Multiple sclerosis patients lead a more sedentary lifestyle, which promotes the occurrence of stroke,[39] and, above all, is associated with the risk of venous thrombosis.[40,41] Treatments for MS may also increase the risk for cardiovascular diseases.[42]

There are a number of studies which indicate that platelets, apart from their major role in cellular hemostasis, also participate in the development of autoimmune

mechanisms, neurodegeneration and neuroinflammation.[43,44] There are many reports suggesting that platelets are chronically activated in neurodegenerative diseases. Platelet activation, degranulation and platelet-leukocyte interactions may affect the pathophysiology of neurodegenerative diseases, including MS.

There is quite a long history of studies conducted on the pathogenesis of MS, dating back to the middle of the previous century. Nathanson and Savitsky were the first to indicate increased platelet adhesiveness in patients suffering from MS.[45] In the following years, platelet overactivation in MS was confirmed. Sheremata et al., using a flow cytometer, showed increased platelet activation in MS, expressed in a high percentage of microparticles and platelet aggregates, and increased surface exposure of P-selectin, a platelet activation marker that plays an important role in their interaction with ECs and leukocytes.[46] The latest research also confirms that MS patients displayed higher levels of platelet activation parameters in the circulation.[47,48] Moreover, cyclooxygenase-dependent arachidonic acid metabolism (a key pathway of platelet activation) is significantly increased in blood platelets of patients with MS.[49]

The chronic activation of platelets in MS has been proven, although their role in this pathology still needs to be clarified. Patients with MS experience various generalized disruptions, depending on the number and placement of active lesions in the CNS. In physiological conditions, there is an extremely low level of immune cells, such as neutrophils and lymphocytes, in CNS. Platelets may contribute to inflammation by enhancing leukocytes adhesion to ECs and promote CNS inflammation. Moreover, Langer et al. proved that platelets are trapped in chronic active demyelinating MS lesion. They also observed that after inhibiting the main platelets receptors – GP IIb/IIIa (responsible for binding of Fg and aggregation), the paralysis and experimental autoimmune encephalomyelitis (EAE) were respectively ameliorated and reduced. Similarly, reduction of platelet count markedly alleviated the symptoms and inhibited the inflammation process.[50,51] The hematological profile of patients with MS indicates an increased number of platelets in the circulation of patients, which may suggest their immunological involvement.[52] Therefore, the decrease in platelet count in MS patients may be a positive force for protecting against the development of the disease. Farrokhi et al. showed a statistically significant decrease in platelet level for patients taking fingolimod oral medication (reducing classic autoimmune cells). Platelet count was decreased in the entire cohort taking fingolimod for 1 month.[53] Probably, a similar thrombocytopenia effect may be demonstrated by the treatment with alemtuzumab.[54]

The direct interaction of platelets with ECs and inflammatory cells promotes leukocyte recruitment to the inflamed tissue through platelet receptors. The pathomechanism of MS involved alterations of the immune cells together with biochemical disturbances and a disruption of the BBB.[1] Enormous influx of inflammatory cells (lymphocytes, neutrophils, monocytes, and macrophages) recruitment, along with the proinflammatory stimulation of microglia cells, altogether result in the destruction of the myelin sheath, which accelerates demyelinating lesions.[50]

CD40 ligand (CD40L; CD154) and its receptor CD40, co-stimulatory molecules of the TNF-family receptor, have an important role in inflammation. CD40L is expressed in many cell types, such as platelets, T-cells, macrophages, neutrophils, smooth muscle cells, and ECs. CD40L affect platelet–platelet, platelet–leukocyte and leukocyte–endothelium interactions. CD40L is responsible for transferring adhesion signals into the cell "outside-in" signaling by reaction within ECs, and integrins that mediate platelet-endothelium adhesion. Platelet CD40L enhances the expression of endothelial adhesion receptors, including E-selectin, VCAM-1, ICAM-1, as well as chemokines (e.g. CCL2, CXCL4 and CCL5) and MMPs (MMP-1, MMP-2, MMP-9, and MMP-14).[55] All these molecules can mediate the attachment of neutrophils, monocytes and lymphocytes to the inflamed vessel wall. Ligation of CD40 on ECs by CD40L, expressed on the surface of activated platelets, increases the release of IL-8 and MCP-1, which is the principal chemo-attractants for neutrophils and monocytes recruitment.[56] The CD40/CD40L pathway at sites of immune reactivity in chronic inflammatory and autoimmune disorders is constantly activated, as shown by the presence of abundant CD40-positive and CD40L-positive cells. This pathway is designed to generate signals for the recruitment of leukocytes at the site of inflammation. CD40L molecules are highly expressed in activated T-cells and active platelets, and they induce ECs to secrete chemokines and to express adhesion molecules. CD40 is present in B cells, monocytes, macrophages and ECs. Firstly, platelets are activated through binding with CD40L-positive T-cells. Secondly, through the release of RANTES, platelets can recruit more T-cells to create an amplification loop promoting leukocytes' recruitment to the site of inflammation. CD40L-positive T-cells induced platelet activation resulting in RANTES release, which binds to ECs and mediates T-cell recruitment. Furthermore, CD62P/PSGL-1 connection could increase the intensification and maintenance of immune and inflammatory responses.[17] Lievens et al. have demonstrated that platelet CD40L promotes platelet and leukocyte adhesion to the endothelium and stimulates the formation of PLAs. Activated platelets can indirectly support leukocyte recruitment via formation of PLAs. The lowest numbers of PLAs were detected with both platelets and leukocytes lacking CD40L, which indicates that the interaction between platelet CD40L and leukocyte CD40 facilitates PLAs formation. Repeated intravenous injection of activated CD40L-negative platelets into ApoE-negative mice prevented the increase of atherosclerosis and the disruption of T-cell homeostasis that was observed after injection of activated CD40L-positive platelets.

This study suggests that CD40L plays an important role in hemostasis/thrombosis and in modulating immune responses.[57]

Active tissue injury in MS lesions is associated with activated microglia and massive infiltration of macrophages. Th cells are a type of T-cell that plays a major role in the immune system, especially in the adaptive immune system. These cells secrete a number cytokines, such as interferon γ (IFN-γ) and IL-2, which activate other immune cells and enhance vascular inflammation. Th cells are well-known to potentiate atherogenesis, while regulatory T-cells (Tregs) display atheroprotective effects. Platelets can form PLAs, which may facilitate lymphocyte into arterial thrombi, and gatheringon ECs. Platelets enhance Thcell cytokine production through CD40–CD40L binding. Platelets may promote CD4-positive T-cell differentiation by inhibiting their proliferation. Platelets enhance the production of Th1 and promote both Tregs and Th17 differentiation, as evidenced by elevated level of IL-10 and IL-17 production. Th1 and Th17 are 2 basically counteracting pathways of CD4-positive T-cell differentiation.[58,59] In most EAE models, which are driven by Th1 or Th17 cells, inflammation starts with profound infiltration of the tissue by the major histocompatibility complex (MHC) Class II restricted CD4-positive T-cells, which is followed by microglia activation and macrophage recruitment into the lesions.[43] In EAE and MS, Th1 and Th17 cells infiltrate into the CNS through the BBB, where they become reactivated and initiate the destruction of myelin sheath (demyelination) and axonal/neuronal degeneration in MS.[2,60] It has also been demonstrated that IL-1β, IL-6, IL-23, and the transforming growth factor (TGF-β) are crucial for human Th17 differentiation from naive CD4-positive and CD45-positive peripheral blood lymphocytes. The TGF-β and IL-21 promote the polarization of Th17 cells from human naive CD4-positive T-cells.[61] Th1 cells also secrete proinflammatory cytokines, such as IL-2 and TNF-α, which can activate other lesional cells. Th17 cell secrets cytokine, including IL-17, TNF-α and IL-6, which have both overlapping and distinct roles in neuroinflammation.[62] Interleukin 17 enhances the production of proinflammatory cytokines and chemokines by other cells via activating the nuclear factor kappa B (NFkB) pathway. Interleukin 17 appears to play an essential role in the pathogenesis of chronic inflammatory disorders and in many autoimmune diseases, including MS.[63] T-effector-cell responses and cytokine production is modulated by platelet-derived soluble mediators, such as IL-1β, PAF and PF4, which can stimulate the differentiation of T-cells into pathogenic Th1, Th17 and IFN-γ/IL-17-producing CD4-positive T cells. At the later stages of these neurodegenerative diseases, platelets became exhausted in their capacity to produce proinflammatory factors and to stimulate CD4-positive T-cells, but strongly increase their ability to form complexes with CD4-positive T-cells. Formation of platelet-CD4-positive T-cell complexes involve the interaction of CD62P in activated platelets with the adhesion molecule CD166 in activated CD4-positive T-cells, contributing to the downmodulation of CD4-positive T-cell activation, the proliferation and production of IFN-γ.[47]

Patients with MS displayed increased numbers of proinflammatory cytokine producing Tregs. Furthermore, Forkhead box P3 (FOXP3) Tregs are fundamental for immunity and homeostasis. FOXP3 expression is essential for Treg suppressor function and Treg stability. The human peripheral blood CD4-positive T-cells comprise 5% of expression of naturally occurring FOXP3 in Tregs.[64]

Activated platelets release plasma membrane platelet-derived microparticles (PMPs) into the circulatory system. Platelet-derived microparticles play an important role in the regulation of immunity by transferring membrane receptors and microRNA to other circulatory cells. These platelets and megakaryocyte-derived microparticles are identified by the expression of platelet activation markers, such as CD62P and/or CD63. Thus, cell proliferation may be one of the mechanisms, whereby PMPs prevent IL-17 production by Tregs.[64]

During circulation, platelets become reactive and release different types of constituents stored in their granules. An increased level of platelet-derived active compounds (PF4, CD40L, PAF, MMPs, serotonin, RANTES, and 5HT) has been taken as a marker of platelet activation in MS.[56,65] Duerschmied et al. hypothesized that peripheral serotonin/5-hydroxytryptamine (5HT) may be involved in the migration of leukocytes during acute inflammatory processes. They report that the targeted recruitment of neutrophils into inflammation site is promoted probably by platelet-derived 5HT. Thus, they play an important role in neutrophil homeostasis that is reminiscent of the phenotype of CD62P-deficient mice.[66] Blood platelets are the exclusive source of 5HT, which is a main neurotransmitter that can directly affect the functions of neurons in the CNS and can modulate the functions of the immune cells. It has an important role in neutrophil rolling and adhesion to the endothelium; therefore, it can recruit neutrophils at the site of inflammation. It can enhance the stimulation of CD4-positive T-cells by a monocyte.[21] Adenosine 5'-triphosphate can modulate inflammatory pathways by activating dendritic cells. The ATP signaling through T cell P2X7 receptor can increase the differentiation of CD4-positive Th cells toward a proinflammatory Th17 cell type. Polyphosphates may induce NFκB pathway activation and the expression of endothelial adhesion molecules.[67] The glutamate transmission in the striatum and dendritic spine loss lead to the chronic inflammation in experimental autoimmune encephalomyelitis (EAE) and murine model of MS. It is strongly independent of demyelination and associated with a huge release of TNF-α from activated microglia cells. Excitotoxicity mediated from glutamate is emerging as a critical determinant of axonal/neuronal injury in MS, and T-cell migration. The level

of glutamate have been found to be meaningfully higher in the brains of MS patients.[68]

Matrix metalloproteinases (MMPs) are enzymes that play a major role in basic cell behaviors, such as cell proliferation, migration, differentiation, angiogenesis, apoptosis, and host defense. There are 3 different mechanisms of directing MMPs activity to specific target sites. Firstly, platelets can concentrate the proteolytic activity of inflammatory cells at the site of a vascular injury. Secondly, by forming cellular aggregates with leukocytes, platelets may stimulate the production of MMPs in these cells. Lastly, a great deal of evidence indicates direct platelet expression of couple MMPs, including MMP-1, MMP-2, MMP-3, and MMP-14.[69] All protein components of extracellular matrix (ECM) can be degraded by MMPs. Another negative function of MMPs in MS is thought to include the disruption of the BBB. In vitro, inhibitors of MMPs block the transmigration of T-cells across basement membrane matrices. The abundance of MMPs expression occurs in monocytes, which emphasizes the key role of monocytes, crucial for evolving the neuroinflammatory process in MS. Bar-Or et al. have reported an increased level of MMP-2, MMP-7, MMP-9, and MMP-12 in MS brain tissue. Young mice that are genetically deficient in MMP-9 are relatively resistant to EAE induction compared with wild-type mice.[70]

Experimental studies conducted by Saluk-Juszczak et al. showed that platelets are a source of reactive oxygen species (ROS). Platelet activation by the typical agonists leads to the production and/or release of TXA_2, ADP and ROS, which activates unstimulated platelets. For example, the burst of H_2O_2 enhances the formation of platelet aggregates by phospholipid-derived arachidonate pathway.[71] Reactive oxygen species are natural products of oxidative phosphorylation, but can also be generated by activated inflammatory cells, including macrophages and microglia. Markers of oxidative stress may be different across MS lesions. Many studies suggest that antioxidant enzymes activity is correlated with the presence of oxidative damage and neuroinflammation.[72]

Conclusions

Chronic neurodegeneration diseases are a serious problem, despite the advanced development of medicine. Multiple sclerosis is one of the most common causes of neurological disability among young adults. Knowledge about the pathophysiology of this disease is insufficient and still needs to be clarified. There is a great deal of evidence to support the significant interaction between platelets and leukocytes in neurodegenerative diseases, including MS. There are many studies which indicate that platelets are highly activated in some patients with MS. Platelets are a rich source of proinflammatory agents and are capable of interacting with leukocytes. The interaction between platelets and leukocytes is based on increased leukocyte recruitment through BBB, and enhanced release of proinflammatory molecules from leukocyte and platelet granules. On the MS example, the major migration of leukocytes to the CNS can cause a temporary loss of integrity by BBB, which contributes to damage and neuronal death. Accurate knowledge and determination of the relationship between platelet interaction in immune cells and the mediators of inflammation in neurodegenerative diseases is a challenge for modern research, which may provide new therapeutic targets in the future. Understanding platelet physiology in the pathobiological processes associated with venules in the inflamed brain will provide new targets for therapy in MS.

References

1. Waubant E. Biomarkers indicative of blood-brain barrier disruption in multiple sclerosis. *Dis Markers*. 2006;22(4):235–244.
2. Chen W, Zhang X, Huang W. Role of neuroinflammation in neurodegenerative diseases (review). *Mol Med Rep*. 2016;13(4):3391–3396.
3. Brola W, Sobolewski P, Flaga S, et al. Prevalence and incidence of multiple sclerosis in central Poland, 2010–2014. *BMC Neurol*. 2016;16:134.
4. Wachowicz B, Morel A, Miller E, Saluk J. The physiology of blood platelets and changes of their biological activities in multiple sclerosis. *Acta Neurobiol Exp (Wars)*. 2016;76(4):269–281.
5. Dziedzic A, Idzikowska K, Saluk J. Tworzenie się kompleksów płytkowo-leukocytarnych we krwi obwodowej u pacjentów z ostrym zespołem wieńcowym. In: Szklarczyk M, Bajek E, eds. *Diagnostyka, profilaktyka, leczenie – najnowsze doniesienia*. Vol. II. Lublin, Poland: Wydawnictwo Naukowe Tygiel; 2017:42–50.
6. Drelich DA, Bray PF. The traditional role of platelets in hemostasis (Chapter 2). In: Kerrigan S, Moran N, eds. *The Non-Thrombotic Role of Platelets in Health and Disease*. London, UK: IntechOpen Ltd.; 2015. doi:10.5772/58357
7. Morel A, Rywaniak J, Bijak M, Miller E, Niwald M, Saluk J. Flow cytometric analysis reveals the high levels of platelet activation parameters in circulation of multiple sclerosis patients. *Mol Cell Biochem*. 2017;430(1–2):69–80.
8. Elzey BD, Tian J, Jensen RJ, et al. Platelet-mediated modulation of adaptive immunity: A communication link between innate and adaptive immune compartments. *Immunity*. 2003;19(1):9–19.
9. Bijak M, Saluk J, Ponczek M, Nowak P, Wachowicz B. The synthesis of proteins in unnucleated blood platelets [in Polish]. *Postepy Hig Med Dosw*. 2013;67:672–679.
10. King SM, McNamee RA, Houng AK, Patel R, Brands M, Reed GL. Platelet dense granule secretion plays a critical role in thrombosis and subsequent vascular remodeling in atherosclerotic mice. *Circulation*. 2009;120(9):785–791.
11. Srivastava K, Cockburn IA, Swaim AM, et al. Platelet factor 4 mediates inflammation in cerebral malaria. *Cell Host Microbe*. 2008;4(2):179–187.
12. Kasper B, Brandt E, Brandau S, Petersen F. Platelet factor 4 (CXC chemokine ligand 4) differentially regulates respiratory burst, survival, and cytokine expression of human monocytes by using distinct signaling pathways. *J Immunol*. 2007;179(4):2584–2591.
13. Lasagni L, Grepin R, Mazzinghi B, et al. PF-4/CXCL4 and CXCL41 exhibit distinct subcellular localization and a differentially regulated mechanism of secretion. *Blood*. 2007;109(10):4127–4134.
14. Shahrara S, Park CC, Temkin V, Jarvis JW, Volin MV, Pope RM. RANTES modulates TLR-4-induced cytokine secretion in human peripheral blood monocytes. *J Immunol*. 2006;177(8):5077–5087.
15. Schober A, Manka D, von Hundelshausen P, et al. Deposition of platelet RANTES triggering monocyte recruitment requires P-selectin and is involved in neointima formation after arterial injury. *Circulation*. 2002;106(12):1523–1529.
16. Thornton P, McColl BW, Greenhalgh A, Denes A, Allan SM, Rothwell NJ. Platelet interleukin-1alpha drives cerebrovascular inflammation. *Blood*. 2010;115(17):3632–3639.

17. Danese S, de la Motte C, Rivera Reyes BM, Sans M, Levine AD, Fiocchi C. Cutting edge: T cells trigger CD40-dependent platelet activation and granular RANTES release: A novel pathway for immune response amplification. *J Immunol*. 2004;172(4):2011–2015.
18. Bennett JS. Structure and function of the platelet integrin αIIbβ3. *J Clin Invest*. 2005;115(12):3363–3369.
19. Höök P, Litvinov RI, Kim OV, et al. Strong binding of platelet integrin αIIbβ3 to fibrin clots: Potential target to destabilize thrombi. *Sci Rep*. 2017;7(1):13001. doi:10.1038/s41598-017-12615-w
20. von Hundelshausen P, Weber C. Platelets as immune cells: Bridging inflammation and cardiovascular disease. *Circ Res*. 2007;100(1):27–40.
21. Lam FW, Vijayan KV, Rumbaut RE. Platelets and their interactions with other immune cells. *Compr Physiol*. 2015;5(3):1265–1280.
22. Green SA, Smith M, Hasley RB, et al. Activated platelet–T-cell conjugates in peripheral blood of patients with HIV infection: Coupling coagulation/inflammation and T cells. *AIDS*. 2015;29(11):1297–1308.
23. Schrottmaier WC, Kral JB, Badrnya S, Assinger A. Aspirin and P2Y12 inhibitors in platelet-mediated activation of neutrophils and monocytes. *Thromb Haemost*. 2015;114(3):478–489.
24. Hirata T, Merrill-Skoloff G, Aab M, Yang J, Furie BC, Furie B. P-selectin glycoprotein ligand 1 (PSGL-1) is a physiological ligand for E-selectin in mediating T helper 1 lymphocyte migration. *J Exp Med*. 2000; 192(11):1669–1675.
25. Frenette PS, Denis CV, Weiss L, et al. P-selectin glycoprotein ligand 1 (PSGL-1) is expressed on platelets and can mediate platelet–endothelial interactions in vivo. *J Exp Med*. 2000;191(8):1413–1422.
26. Wang Y, Sakuma M, Chen Z, et al. Leukocyte engagement of platelet glycoprotein Ib via integrin Mac-1 is critical for the biological response to vascular injury. *Circulation*. 2005;112(19):2993–3000.
27. Simon DI, Chen Z, Xu H, et al. Platelet glycoprotein Iba is a counterreceptor for the leukocyte integrin Mac-1 (CD11b/CD18). *J Exp Med*. 2000;192(2):193–204.
28. Woodfin A, Voisin M, Imhof BA, Dejana E, Engelhardt B, Nourshargh S. Endothelial cell activation leads to neutrophil transmigration as supported by the sequential roles of ICAM-2, JAM-A and PECAM-1. *Blood*. 2009;113(24):6246–6257.
29. Weber A, Przytulski B, Schumacher M, et al. Flow cytometry analysis of platelet cyclooxygenase-2 expression: Induction of platelet cyclooxygenase-2 in patients undergoing coronary artery bypass grafting. *Br J Haematol*. 2002;117(2):424–426.
30. Dixon DA, Tolley ND, Bemis-Standoli K, et al. Expression of COX-2 in platelet-monocyte interactions occurs via combinatorial regulation involving adhesion and cytokine signaling. *Clin Invest*. 2006; 116(10):2727–2738.
31. Glenister KM, Payne KA, Sparrow RL. Proteomic analysis of supernatant from pooled buffy-coat platelet concentrates throughout 7-day storage. *Transfusion*. 2008;48(1):99–107.
32. Lindemann S, Tolley ND, Dixon DA, et al. Activated platelets mediate inflammatory signaling by regulated interleukin 1β synthesis. *J Cell Biol*. 2001;154(3):485–490.
33. Beaulieu LM, Lin E, Mick E, et al. Interleukin 1 receptor 1 and interleukin 1β regulated megakaryocyte maturation, platelet activation and transcript profile during inflammation in mice and humans. *Arterioscler Thromb Vasc Biol*. 2014;34(3):552–564.
34. Neumann H. Molecular mechanisms of axonal damage in inflammatory central nervous system diseases. *Curr Opin Neurol*. 2003;16(3): 267–273.
35. Thorsteinsdottir S, Bjerrum OW, Hasselbach HC. Myeloproliferative neoplasms in five multiple sclerosis patients. *Leuk Res Rep*. 2013;2(2): 61–63.
36. Christiansen CF, Christensen S, Farkas DK, Miret M, Sørensen HT, Pedersen L. Risk of arterial cardiovascular diseases in patients with multiple sclerosis: A population-based cohort study. *Neuroepidemiology*. 2010;35(4):267–274.
37. Jadidi E, Mohammadi M, Moradi T. High risk of cardiovascular diseases after diagnosis of multiple sclerosis. *Mult Scler*. 2013;19(10):1336–1340.
38. Brønnum-Hansen H, Koch-Henriksen N, Stenager E. Trends in survival and cause of death in Danish patients with multiple sclerosis. *Brain*. 2004;127(Pt 4):844–850.
39. Shah SM, Khan S, Rehman SU, Khan ZA, Wisal A, Wisal Z. Addressing the impact of stroke risk factors in a case control study in tertiary care hospitals: A case-control study in Tertiary Care Hospitals of Peshawar, Khyber Phukhtoonkhwa (KPK), Pakistan. *BMC Res Notes*. 2013;6:268.
40. Ocak G, Vossen CY, Verduijn M, et al. Risk of venous thrombosis in patients with major illnesses: Results from the MEGA study. *J Thromb Haemost*. 2013;11(1):116–123.
41. Arpaia G, Bavera PM, Caputo D, et al. Risk of deep venous thrombosis (DVT) in bedridden or wheelchair-bound multiple sclerosis patients: A prospective study. *Thromb Res*. 2010;125(4):315–317.
42. Sternberg Z, Leung C, Sternberg D, Yu J, Hojnacki D. Disease-modifying therapies modulate cardiovascular risk factors in patients with multiple sclerosis. *Cardiovasc Ther*. 2014;32(2):33–39.
43. Pankratz S, Bittner S, Kehrel BE, et al. The inflammatory role of platelets: Translational insights from experimental studies of autoimmune disorders. *Int J Mol Sci*. 2016;17(10):1723.
44. Behari M, Shrivastava M. Role of platelets in neurodegenerative diseases: A universal pathophysiology. *Int J Neurosci*. 2013;123(5):287–299. doi:10.3109/00207454.2012.751534
45. Nathanson M, Savitsky JP. Platelet adhesive index studies in multiple sclerosis and other neurologic disorders. *Bull N Y Acad Med*. 1952;28(7):462–468.
46. Sheremata WA, Jy W, Horstman LL, Ahn YS, Alexander JS, Minagar A. Evidence of platelet activation in multiple sclerosis. *J Neuroinflammation*. 2008;5:27. doi:10.1186/1742-2094-5-27
47. Starossom SC, Veremeyko T, Yung AW, et al. Platelets play differential role during the initiation and progression of autoimmune neuroinflammation. *Circ Res*. 2015;117(9):779–792.
48. Morel A, Bijak M, Miller E, Rywaniak J, Miller S, Saluk J. Relationship between the increased haemostatic properties of blood platelets and oxidative stress level in multiple sclerosis patients with the secondary progressive stage. *Oxid Med Cell Longev*. 2015;2015:240918. doi:10.1155/2015/240918
49. Morel A, Miller E, Bijak M, Saluk J. The increased level of COX-dependent arachidonic acid metabolism in blood platelets from secondary progressive multiple sclerosis patients. *Mol Cell Biochem*. 2016;420(1–2): 85–94. doi:10.1007/s11010-016-2770-6
50. Langer HF, Chavakis T. Platelets and neurovascular inflammation. *Thromb Haemost*. 2013;110(5):888–893.
51. Langer HF, Choi EY, Zhou H, et al. Platelets contribute to the pathogenesis of experimental autoimmune encephalomyelitis. *Circ Res*. 2012;110(9):1202–1210. doi:10.1161/CIRCRESAHA.111.256370
52. Hon GM, Hassan MS, van Rensburg SJ, Erasmus RT, Matsha T. The haematological profile of patients with multiple sclerosis. *Open J Mod Neurosurg*. 2012;2(3):36–44.
53. Farrokhi M, Beni AA, Etemadifar M, et al. Effect of fingolimod on platelet count among multiple sclerosis patients. *Int J Prev Med*. 2015; 6:125. doi:10.4103/2008-7802.172539
54. Obermann M, Ruck T, Pfeuffer S, Baum J, Wiendl H, Meuth SG. Simultaneous early-onset immune thrombocytopenia and autoimmune thyroid disease following alemtuzumab treatment in relapsing-remitting multiple sclerosis. *Mult Scler*. 2016;22(9):1235–1241. doi:10.1177/1352458516638558
55. May AE, Kälsch T, Massberg S, Schmidt R, Gawaz M. Engagement of glycoprotein IIb/IIIa (αIIbβ3) on platelets upregulates CD40L and triggers CD40L-dependent matrix degradation by endothelial cells. *Circulation*. 2002;106(16):2111–2117.
56. Gawaz M, Langer H, May AE. Platelets in inflammation and atherogenesis. *J Clin Invest*. 2005;115(12):3378–3384.
57. Lievens D, Zernecke A, Seijkens T, et al. Platelet CD40L mediates thrombotic and inflammatory processes in atherosclerosis. *Blood*. 2010;116(20):4317–4327.
58. Gerdes N, Zhu L, Ersoy M, et al. Platelets regulate $CD4^+$ T-cell differentiation via multiple chemokines in humans. *Thromb Haemost*. 2011;106(2):353–362.
59. Fletcher JM, Lalor SJ, Sweeney CM, Tubridy N, Mills KH. T cells in multiple sclerosis and experimental autoimmune encephalomyelitis. *Clin Exp Immunol*. 2010;162(1):1–11.
60. Kempuraj D, Thangavel R, Natteru PA, et al. Neuroinflammation induces neurodegeneration. *J Neurol Neurosurg Spine*. 2016;1(1):1003.
61. Shahrara S, Pickens SR, Mandelin AM, et al. IL-17-mediated monocyte migration occurs partially through CCL2/MCP-1 induction. *J Immunol*. 2010;184(8):4479–4487.
62. Drolet AM, Thivierge M, Turcotte S, et al. Platelet-activating factor induces Th17 cell differentiation. *Mediators Inflamm*. 2011;2011: 913802.

63. Li N. CD4+ T cells in atherosclerosis: Regulation by platelets. *Thromb Haemost*. 2013;109(6):980–990.
64. Dinkla S, van Cranenbroek B, van der Heijden W, et al. Platelet microparticles inhibit IL 17 production by regulatory T cells through P-selectin. *Blood*. 2016;127(16):1976–1986.
65. Horstman LL, Jy W, Ahn YS, et al. Role of platelets in neuroinflammation: A wide-angle perspective. *J Neuroinflammation*. 2010;7:10.
66. Duerschmied D, Suidan GL, Demers M, et al. Platelet serotonin promotes the recruitment of neutrophils to sites of acute inflammation in mice. *Blood*. 2013;121(6):1008–1015.
67. Morrell CN, Aggrey AA, Chapman LM, Modjeski KL. Emerging roles for platelets as immune and inflammatory cells. *Blood*. 2014;123(18): 2759–2767.
68. Centonze D, Muzio L, Rossi S, et al. Inflammation triggers synaptic alteration and degeneration in experimental autoimmune encephalomyelitis. *J Neurosci*. 2009;29(11):3442–3452.
69. Seizer P, May AE. Platelets and matrix metalloproteinases. *Thromb Haemost*. 2013;110(5):903–909.
70. Bar-Or A, Nuttall RK, Duddy M, et al. Analyses of all matrix metalloproteinase members in leukocytes emphasize monocytes as major inflammatory mediators in multiple sclerosis. *Brain*. 2003;126(Pt 12): 2738–2749.
71. Saluk-Juszczak J, Wachowicz B, Kaca W. Endotoxins stimulate generation of superoxide radicals and lipid peroxidation in blood platelets. *Microbios*. 2000;103(404):17–25.
72. Gironi M, Borgiani B, Mariani E, et al. Oxidative stress is differentially present in multiple sclerosis courses, early evident and unrelated to treatment. *J Immunol Res*. 2014;2014:961863. doi:10.1155/2014/961863